Passive Protection of Structures using Innovative Rotational Inertia Dampers and Rotational Energy Conversion Devices

A Dissertation Presented for the

Doctor of Philosophy

Degree

The University of Tennessee, Knoxville

Abdollah Javidialesaadi

May 2020

DEDICATION

I dedicate this dissertation to my sister Dr. Roya Javidialessadi

ACKNOWLEDGEMENTS

I would like to express the deepest appreciation to my committee chair and my advisor, Dr. Nicholas Edward Wierschem. Nicholas is one of the smartest people I know. He is a perfect advisor, professional and nice person. He is my primary resource for getting my questions answered and without his guidance and supports this dissertation would not have been possible.

I would like to express my appreciation to my committee members Dr. Mark Deviant, Dr. Brian Philips, and Dr. Eric Wade for their guidance and support during my PhD studies.

In addition, I would like to thank my family and friend for their support and patience during my PhD studies.

Finally, I would like to thank all the faculty members and staff of the Department of Civil and Environmental Engineering department at the University of Tennessee, Knoxville.

ABSTRACT

Civil structures, including bridges, buildings, roads, railways, and utility networks, are vital parts of modern life; therefore, it is essential to protect these structures and systems against natural and artificial hazards. Some hazards, such as earthquake or extreme winds, can put structures in danger of damage or destruction. In some cases, even moderate amplitude vibrations decrease the serviceability of structures. Considerable research has been conducted for the purpose of reducing the effects of dynamic loads on structures due to external natural and artificial excitations. Accordingly, many different structural control technologies have been developed and utilized in civil structures in recent decades. Active, semi–active, and passive control strategies have been proposed, developed, and utilized for the purpose of protecting structures against various types of excitations and ensuring occupant safety and structural serviceability.

Unlike semi-active and active control devices, passive control devices can adjust the dynamic properties of a structure and improve its energy dissipation potential without relying on a controller, sensor, and power. Because of these advantages, passive control systems are, in general, more accepted by the construction industry and have been increasingly utilized by practicing structural engineers. Significant research efforts have been made in the past and are currently ongoing to develop and improve these passive control systems including systems exploiting rotational inertial devices.

There is significant potential for the further development and advancement of rotational inertial devices such that their effectiveness is increased and they are brought closer to commercial implementation. Inerter-based passive control devices have begun to receive a significant amount of attention in the field of passive control in the past few years; however, there is still significant room for

advancement. These advances include contributions to the closed-form and numerical optimization of these devices, the evaluation of the performance of these devices for loading scenarios not yet considered, and the proposal of novel rotational inertia devices for passive control.

TABLE OF CONTENTS

LIST OF TABLES

LIST OF FIGURES

CHAPTER ONE:INTRODUCTION

Structural control is considered one of the most effective approaches for protection of structures against external loads. Passive, active, semi-active, and hybrid [1] are the most common types of control strategies used in structural engineering [2]. These control strategies can be summarized as follows:

- Passive control systems: This type of control system does not need external power sources, sensors, or controllers. Passive systems include simple mechanical devices or other mechanisms that are attached to the structure and alter the structure's dynamics. The force developed in passive systems is a function of the motion of the structure.
- Active control systems: These systems require a reliable power source that is relatively large for civil applications, sensors, and a controller. Furthermore, these systems require a mechanism, such as actuators, for delivering a control force. The control force is developed based on the feedback information from sensors and the implemented control algorithm.
- Hybrid control systems: Hybrid control systems combine active and passive control systems. Utilizing a combination of viscous dampers and an active mass damper is an example of a hybrid control system.
- Semi-active systems: Semi-active control systems require sensors, a controller, and a power source; however, this power source typically needs to be much smaller than that required for active control. These systems, also called controllable passive, are adaptive. This means that, instead of having a controller directly applying a control force, in semi-active systems a controller is used to modify the properties of an otherwise passive system. An example of a semi-active system is a tuned mass damper that can adjust its tuning with a computer controlled variable stiffness element [3].

As civil structures are large, huge control forces are needed in most active, semi active, and hybrid control strategies. Furthermore, the requirements of feedback loops make these devices complicated. Contrarily, passive control devices do not need a controller, sensors and a power source, which makes them less complicated in comparison to active and semi-active devices. These devices modify the dynamics of systems and enhance their energy dissipation potential through the conversion of kinetic energy to heat or transferring energy between the vibration modes [1]. Having said that, passive control devices are one of the more desirable control strategies in civil engineering. There is a rich literature on passive control devices such as tuned mass dampers (TMDs) metallic yielding dampers, friction dampers, viscoelastic dampers, viscous fluid dampers and tuned liquid dampers.

TMDs are one of the most popular devices for the passive control of structures. TMDs are simple mechanical devices consisting of a mass, spring, and damper. When the properties of the TMD are properly tuned, a critical mode of vibration of the structure is replaced with a pair of modes that feature the response of the system concentrated in the relative motion of the TMD.

TMDs have been installed in building structures throughout the world including skyscrapers such as the City Corp Center in New York, the Sydney Tower in Australia, Taipei 101 in Taipei, and Shanghai World Financial Center in Shanghai China [4,5]. For TMDs to be effective at controlling the response of structures subjected to stationary loads, such as wind, they must be relatively large. For example, the TMDs designed to control the response to wind loading of the City Corp Center Tower in New York and the Sydney tower are 370,000 kg and 220,000 kg, respectively [4]. However, to be effective at controlling the response due to transient loads, such as earthquakes, TMDs must be even larger [6,7].

Recently, in order to address this issue and provide effective passive control devices which are either more effective or smaller than the presently utilized TMDs, inerter-based passive control devices have been proposed and developed [8–10]. The key benefits of inerter-based passive control devices are that they can utilize a relatively small physical mass and provide a large effective mass. These devices exploit mechanisms like the ball-screw or the rack and pinion, which transfer translational motion to the rotational motion of a small mass that has been designed to have a large rotational inertia. Well-designed inerters can amplify small physical mass between 7000-9000 times [11,12]. This significant amplification of mass can lead to devices with small physical mass, that are less expensive and easier to install, which can be effective structural control devices able to mitigate the response of the structure to wind and earthquakes.

To date, inerter-based passive control devices have been primarily utilized in structural control in two different ways:

Inerter-based mass dampers: These devices consist physical mass and inerter. In another word, this type of devices is development of mass dampers such as TMDs.

Inerter-based dampers: These devices consist of inerter, spring, and dashpot with different configurations in connection. The values of the spring and dashpot can be equal to zero or nonzero.

Despite the benefits of the recently developed inerter-based passive control devices, there is significantly more potential for the development of this field. Therefore, the primary goal of this dissertation is extending the state of the art in inerter-based passive control devices by pursuing the following objectives:

- Development and implementation of optimum design methods for inerter-based mass dampers.
- Design, evaluation, and performance evaluation of inerter-based mass dampers for the control of structures subjected to seismic excitation.
- The proposal and evaluation of new inerter-based mass dampers that incorporate inerters into and improve upon existing passive control devices.

- The proposal and evaluation of innovative inerter-based passive control devices that exploit phenomenon that are related to inertance, but are nonlinear.

The main body of this dissertation (Chapters 3– 9) consists of the individual manuscripts that have been produced in the pursuit of developing this field. In addition, Chapter 2 provides an overall literature review and Chapter 9 provides the conclusions resulting from this work. A brief description of the content of each chapter of this dissertation is presented below.

The literature review chapter includes the background and an overall review of research works related to the topic of this dissertation. Included in this chapter is a discussion of the tuned mass damper, ways to produce inertance, various types of inerter-based mass dampers, various types of other inerter-based dampers, and initial work on state switching inertance devices.

Chapter 3 proposes an analytical exact optimization solution for the rotational inertia double tuned mass damper, which is one type of inerter-based mass damper. In addition, the performance of the device in comparison to the TMD is also investigated in this chapter.

In Chapter 4, the performance evaluation of a set of different types of inerter-based mass dampers is presented. These inerter-based mass dampers have been previously examined for random and harmonic excitation, however, the performance of these devices considering seismic ground acceleration has not been studied before. Furthermore, the effectiveness of different optimization techniques is compared considering this loading.

In Chapter 5, a new inerter-based mass damper called the “Three element vibration absorber inerter’ is proposed. The design and performance evaluation of this proposed device is presented in this chapter and comparisons are made to the tuned mass damper inerter and the three-element vibration absorber.

Chapter 6 introduces a new nonlinear inerter-based mass damper called the “nonlinear energy sink inerter”. Unlike the TMD, the nonlinear energy sink is a more robust device and, due to the essential nonlinearity, is capable of coupling with a broad range of frequencies. The proposed device is designed to increase the performance of the nonlinear energy sink by increasing the effective mass of the absorber through inertia mass.

Chapter 7 proposes the multiple tuned mass damper inerter (MTMDI), which is a development based on the multiple tuned mass damper and the tuned mass damper inerter. In this chapter, the MTMDI is formulated, design philosophies are presented, and its performance is investigated. Furthermore, this chapter investigates the effect of the distribution of inertance in this device.

Chapter 8 proposes an innovative inerter-based passive control device with a state switching mechanism. In traditional inerter-based dampers, energy transferred to the device transfers back to the structure during the response cycles of the device because the inerter will slow down and reverse its rotation direction during changes in the direction of the system response. In the proposed device investigated in this chapter, a state switching rotational inertial mechanism allows energy to transfer to the damper in a one-directional fashion without the ability to transfer that energy back to the structure.

In Chapter 9, a summary of the contributions found in this dissertation are presented, major conclusions from this work are listed, and directions for future work on this subject are outlined and discussed.

CHAPTER TWO:LITERATURE REVIEW

Introduction

This chapter covers background and recent developments of inerter-based passive control devices. The focus of the first section is on the background of tuned mass dampers (TMDs) and its recent developments. After introducing the inerter, inerter-based mass dampers presented. In continuation, background and recent development of inerter-based damper, tuned mass inerter damper, tuned viscous inerter damper, and inerter tuned damper are presented in detail.

Much of the information presented in this chapter will be duplicated in the subsequent chapters of this document that are based on journal manuscripts; however, this information is presented in this literature review chapter in order to give the reader a complete and distinct review of the state of the art.

Tuned mass damper

Conventional tuned mass dampers (TMDs), which are designed to damp the vibrations of a primary mass [13], are composed of a secondary mass, spring, and viscous damper (Figure 2-1).

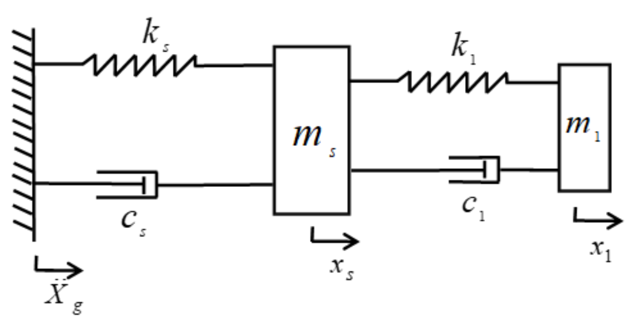

Figure 2-1: Tuned mass damper (TMD)

TMDs have been proposed originally as a device for damping motion of rigid bodies [13]. Since TMDs performance in reduction the dynamic response is rely on the spring and damping values, it is crucial to find the optimum design values in TMDs. Optimum design values can be obtained through optimization procedure; however, type of the excitation and goal of the optimization leads to different optimum design values.

One of the most important methods for optimum design of TMDs, which is called the" fixed point method" [14]. The first version of the method is limited to the force excitation and undamped primary structure. The fixed-points method is based on the existence of fixed points on the frequency response curve for a primary structure with a TMD that are independent of the damping level of the absorber and are thus at the same location during both the zero, optimum and infinite damping conditions. Optimum tuning parameters for tuned mass dampers (TMDs) have been obtained by equalizing the magnitude of the response at these fixed-points. Despite the approximation, this method provides acceptable design values when the goal is minimizing the maximum response; thus, this method has been used for H_∞ optimization. In continuation, this method has been developed for the optimum design of nonlinear TMDs vibration absorbers [15], undamped primary structure [16], and MDOF primary structure [17]. As the fixed-point method is an approximation method, some works have been done in order to provide exact solution optimization of the TMDs when the objective function is minimizing the maximum displacement [18,19].

When the primary structure is subjected to random excitation, it is typically more desirable to minimize the variance of the output in the frequency domain [20]. This type of optimization, called “H2 optimization”, has been proposed for TMDs [18–21]. Solutions for exact H2 optimization require obtaining the H2 norm of the response in closed form, finding the derivative of the response function, and solving a nonlinear set of equations [18,22]. In exact solution methods, the global optimum can be achieved and guaranteed; however, numerical optimizations may lead to local optimum design values. Numerical optimization methods including metaheuristic methods, harmony search particle swarm, and gradient based methods have also been proposed and investigated for design of TMDs [23–25].

The effectiveness of TMDs when the structure is subjected to random or harmonic excitation has been broadly demonstrated. However, the effectiveness of TMDs against seismic load is still under investigation and a point of controversy. While some studies have shown that TMDs cannot reduce the displacement response of the structure[26], others have suggested that, through new design approaches, TMDs can be effective during earthquake [6,7]. Having said that, even when TMDs can be effective in reducing the dynamic response during earthquake, their performance during earthquakes is not as effective as when harmonic loads are considered.

By adding a viscous damper in series with the spring in TMDs, the three-element vibration absorber (Figure 2-2) was introduced [27,28]. When introduced, the three-element vibration absorber showed superior performance in the reduction of dynamic responses; however, this device has not been investigated more recently. The three-element vibration absorber can provide a 6% reduction in the maximum response as well as variance of the response in comparison to the TMD with the same mass ratio.

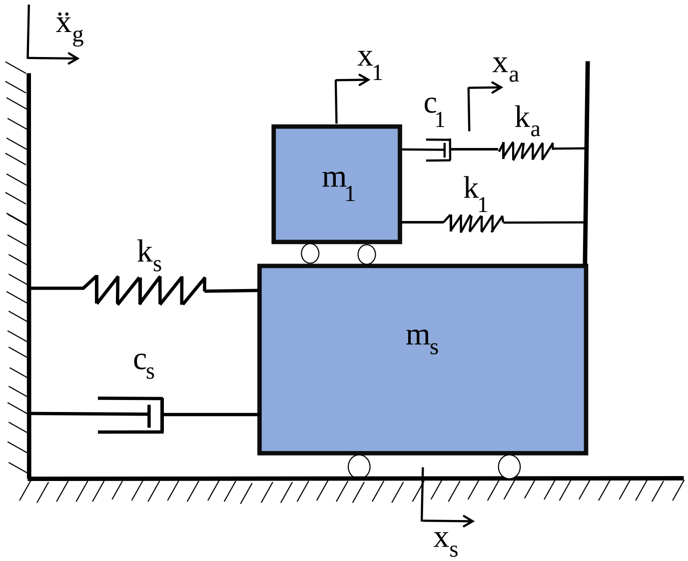

Figure 2-2: Three element vibration absorber (TEVA)

Non-traditional tuned mass dampers have been proposed and investigated by connecting the dashpot between the secondary mass and ground [29]. Recently, more extensive investigation on this type of TMD has been published with these results supported by experimental validation [30]. Considering the spring of TMDs as a combination of linear and cubic springs, nonlinear TMDs have been studied, but the results have shown insignificant improvement to performance [31]. In context of nonlinearity, design and performance of the TMDs when the primary structure oscillate in a nonlinear range has been studied extensively [32,33].

TMDs are installed in some structures, including a significant number of tall buildings [4]; however, a number of issues exist that limit their more widespread adoption. One of these issues is that TMDs need a large ratio of secondary mass to the main structure's mass to be effective [6,7], which may not be practical and often dominates the budget of the TMD [34]. Another issue is that TMDs are very sensitive to the detuning that might occur due to errors in the design and fabrication [13] or due to stiffness changes in the structure that may occur over time or because of dynamic loads [2]. In addition, TMDs are mostly tuned to the first mode of the structure and cannot be highly effective in reduction of the response in higher modes [1]. To provide more effective dynamic response reduction in different modes and protect against detuning, the multiple tuned mass damper (MTMD) has been proposed and investigated [35–37].

MTMDs consist of two or more interdependently designed TMDs connected to a main structure through springs and dampers. To date, various types of MTMD design philosophies have been proposed and investigated [36]. One of the most common of these philosophies is one where identical spring and dampers are used for each of the MTMD's TMDs along with different masses to produce a MTMD with a prescribed distribution of individual TMD frequencies [35,37–39]. The other most common design philosophy is one where the MTMD's TMDs have equal masses, but nonidentical springs and dampers [37,38]. As the manufacturing of MTMDs with the same damping and stiffness elements is typically simpler, this type of MTMD are often more desirable in structural engineering applications [38]; however, MTMD with nonidentical stiffness and damping can be more effective [40]. Despite these differences, for all of the major MTMD design philosophies considered, it has been found that MTMDs are generally more robust against detuning and can more effectively reduce dynamic responses [37,38,40–44].

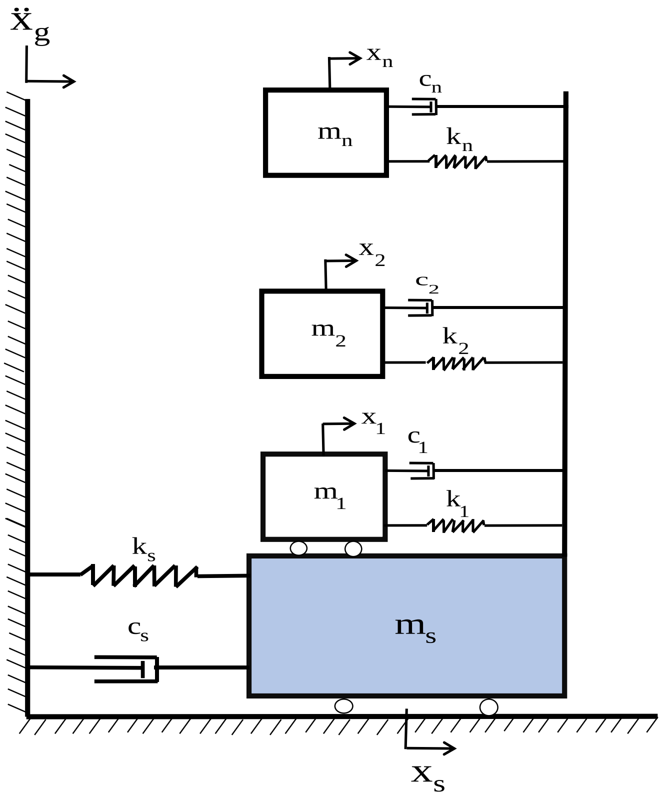

Figure 2-3: Multiple tuned mass damper

As the TMD is a linear vibration absorber and cannot transfer energy within a structure nonlinear energy sinks (NESs) have been investigated as passive control devices for the past two decades [45–50]. The traditional NES design, which consists of a small mass connected to a primary structure through a linear dashpot and an essentially nonlinear spring with a cubic stiffness, has been studied for passive structural control and demonstrated robustness and effectiveness [51] . Unlike tuned mass dampers (TMDs), which have a particular resonance frequency, the essential nonlinearity of the NES stiffness element allows the NES to vibrate in a broadband fashion and transfer energy to higher modes of a structure [49,51].

Inerter

In an effort to improve the effectiveness of TMDs, the utilization of supplemental rotational masses in TMDs has recently been studied. One of the most important benefit of rotational devices is that they are able to produce a large effective mass by using a relatively small rotational physical mass; therefore, these devices potentially require a smaller physical mass than a conventional TMD to be effective [8–10,52,53].

Inerter-based passive control devices have been proposed as part of a new generation of passive control devices [8,54].The key component of many of these devices is referred to as an inerter and it enables the transfer of translational motion to rotational motion. One of the main benefits of the inerter is that it is capable of providing a large amount of effective mass by utilizing a physically small rotational mass. Many mechanisms could potentially be used to produce this conversion to rotational motion; however, two alternatives have been primarily considered in the literature: the rack and pinion mechanism and the ball screw mechanism (see Figure 2-4).

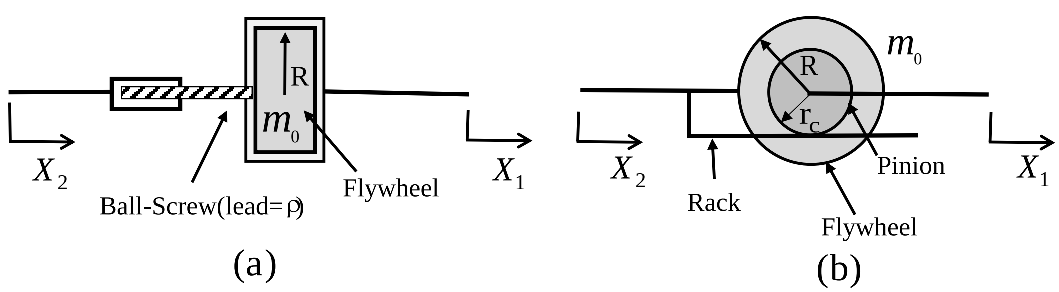

Figure 2-4: Example physical inerter realizations (a) ball screw mechanism, (b) rack and pinion mechanism

The schematic representation of the inerter is presented in

Figure 2-5, where F is the equal force at the two nodes of the device and b is effective rotational mass or “inertance” of the device. The relationship between the equal force at the nodes and the relative acceleration in the inerter can be express as the following:

$$F = b\left(\ddot{u}_1 - \ddot{u}_2\right) \tag{2.1}$$

Considering $\omega_s = \sqrt{k_s / m_s}$ as the frequency of the uncontrolled SDOF structure with k_s and m_s , the frequency of the structure attached to an inerter with inertance (b), the frequency of the structure (ω_c) can be expressed as follows :

$$\omega_c = \sqrt{\frac{k_s}{m_s + b}} = \omega_s \sqrt{\frac{m_s}{m_s + b}} \tag{2.2}$$

Eq. (2.2) demonstrates the influence of the inertia mass in the reduction of the frequency of the system with increases in the effective mass [55].

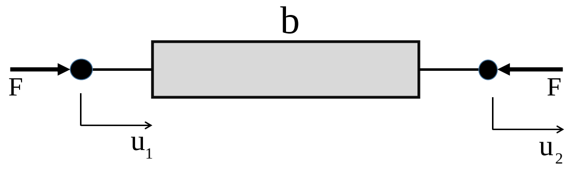

Figure 2-5: Schematic representation of an inerter as a two-terminal device with inertance (equivalent rotational mass) equal to b

In addition to the traditional inerter discussed above, a hydraulic mechanism has been proposed as fluid-based inerter. This type of inerter consist of a piston and cylinder driving through a helical tube surrounding the cylinder [56,57]. The size of the device is comparable to traditional inerter mechanisms and it was shown the fluid damper can be modeled as a traditional inerter in parallel with a nonlinear damping component.

Inerter-based mass dampers

The rotational inertial double tuned mass damper (RIDTMD) is a type of inerter-based mass dampers which has been proposed recently [9]. The RIDTMD consists of a conventional TMD, but the typical viscous damper has been replaced with a tuned viscous damper (Figure 2-6). The tuned viscous damper consists of a spring, axial dashpot, and an inerter. While the rack and pinion mechanism has been proposed for use in the RIDTMD, different alternative mechanisms for transferring translational motion to rotation, such as a ball screw mechanism, could be utilized. The RIDTMD, with a small added rotational mass, has demonstrated effective results compared to the TMD [9]. Since the RIDTMD has one more degree of freedom in comparison to TMDs, the frequency response curve is broader and has three peaks instead of two.

The RIDTMD is one particular configuration from a group of inerter-base devices that have been considered and, most prominently, optimally design for random force excitation on the primary system using a numerical optimization method [5]. This category of devices is classified as “Inerter-based mass damper”. Six inerter-based mass dampers were optimally designed for minimizing the response’s variance and maximum amplitude when the primary structure was subjected to a random excitation [10]. Thus far, these optimum designs have been performed utilizing numerical methods, which may not lead to the global optimum design. Three of the six configurations have been shown to have more effective performance, compared to the TMD, including the RIDTMD (also known as C1, Figure 2-6), C1 (Figure 2-7), and C2 (Figure 2-8) configurations.

The goal of the design of these devices is to find the device stiffness, damping, and rotational inertia mass to achieve an objective function. Common objective functions include the minimization of the maximum or RMS response of the primary structure. The previous design and performance evaluation of the RIDTMD, C1, and C2 inerter-based mass dampers are limited to numerical optimizations and only consider when the primary structure is subjected to harmonic or random excitation.

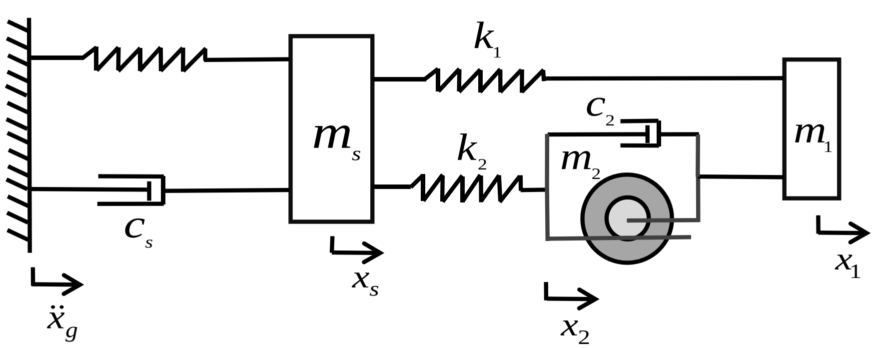

Figure 2-6: Rotational inertial double tuned mass damper (RIDTMD)

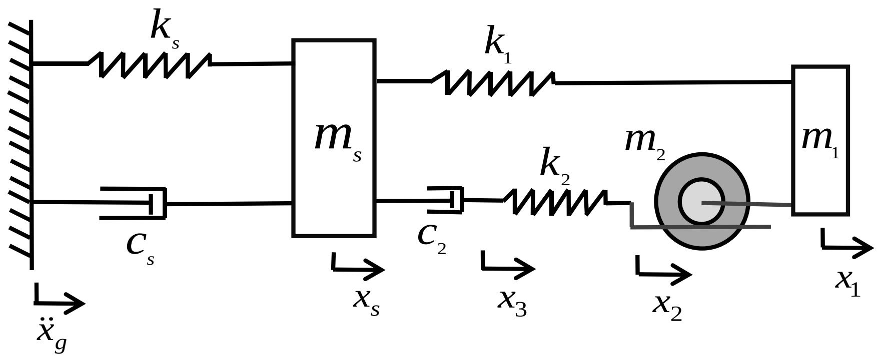

Figure 2-7: Inerter-baesd mass damper (C1 configuration)

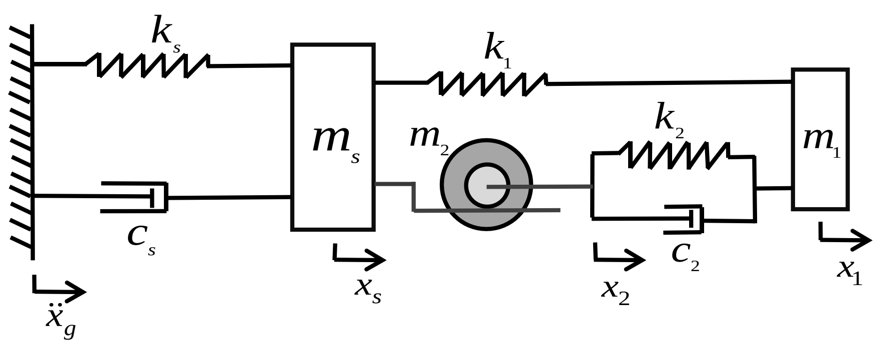

Figure 2-8: : Inerter-based mass damper (C2 configuration)

Furthermore, no exact optimum design solution for the three configurations exist when the main structure is subjected to random base excitation. In most inerter-based mass dampers, the inerter is embedded between the primary structure and the secondary mass. This type of device has limitations regarding its performance and adding additional effective mass does not necessarily increase the device's effectiveness [58]. As an alternative, the tuned mass damper-inerter (TMDI) has been proposed, developed and optimized [53]. Figure 2-9 depicts the TMDI which consists of a traditional TMD, which has an inerter attached between the TMD mass and the ground.

Minimization of the variance (H_2 norm) of the structural response with a TMDI has demonstrated the device's capacity for enhanced performance, in comparison to TMDs with similar secondary mass ratio [53]. Additionally, studies have considered utilizing the TMDI for the control of tall building subjected to wind [59], the transient response of systems with TMDI subject to nonstationary stochastic excitation [60,61], and the optimum design and performance evaluation of TMDIs in systems subjected to seismic loading [62–64]. In addition, recent studies of the TMDI have included investigating the efficiency of the TMDI to harvest kinetic energy in wind excited systems [62], the effect of the location of the TMDI on control of structures subjected to wind excitation [65], and the TMDI in base isolation applications [66].

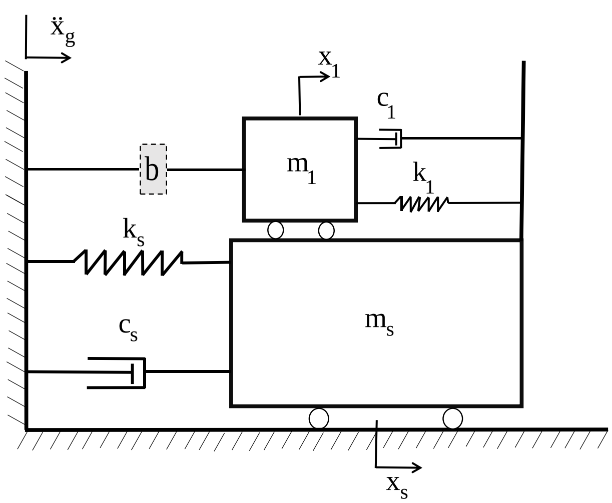

Figure 2-9: Tuned mass damper-inerter (TMDI)

Inerter-based dampers

Inerter-based dampers that do not have a significant physical mass as a part of their configuration have also been studied. The rotational inertia viscous damper (RIVD), which has been investigated as part of a toggle bracing system [8], is one of the first generation of inerter-based devices proposed for the passive control of SDOF systems. Figure 2-10 [67] shows the RIVD, which can provide a large inertial mass for a system and is designed for the control of structures by coupling the structure's motion to the rotational motion of a rotary mass and transferring kinetic energy to that rotary mass. Part of the transferred energy also can be dissipated through the deformation of a viscous material in a rotational cylinder. In the same context, but utilizing a rack and pinion mechanism, the gyro-mass damper (GMD) with linear and nonlinear viscous damping has been experimentally examined for use in the control of structures [68]. The GMD has been used and demonstrated effectiveness at reducing the large lateral displacements that can be found in base isolated SDOF systems [69].

In addition, effect of inerter on the frequency of the structures and mode shapes also have been studied explicitly. It was shown utilizing the inerter in SDOF and MDOF structures leads to a reduction of natural frequencies, however, the amount of reduction and mode shape depends on the location, number and amount of inerter. For example, it is shown that a 47 percent reduction in the fundamental frequency of a six degree of freedom structure can be obtained by using 5 inerters [55,70].

By adding a tuning spring to the RIVD, the tuned viscous mass damper (TVMD) has been proposed for the control of frames [52] (see Figure 2-11).

The tuned inerter damper (TID) (see Figure 2-12), which consists of an inerter attached in series to a parallel spring and dashpot, has been proposed for the vibration suppression of multi-degree-of-freedom (MDOF) structures [71].

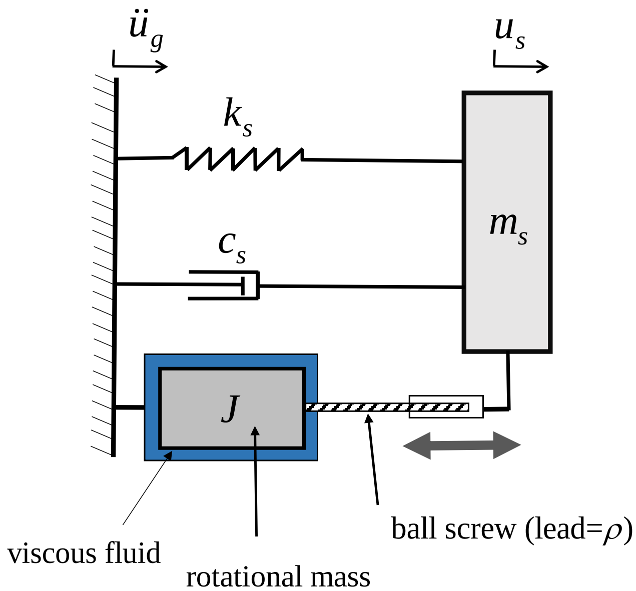

Figure 2-10: Rotational inertia viscous damper (RIVD) [67]

The influence of the inerter on the frequency of MDOF structures [55] and the effect of inter-story inerters on the response of MDOF structures subjected to earthquake [70] have been studied. Recently, the performance evaluation of the TID and the TVMD for seismic control of MDOF structures has been investigated [72]. However, these investigations have been limited and have only considered linear shear buildings. performance based design of TID for seismic application of SDOF structures [75], control of cables utilizing TID and TVMD [73–75], base isolation application of TID [76], and performance of TVMD when the damping is nonlinear [77] are some recent works regarding these devices.

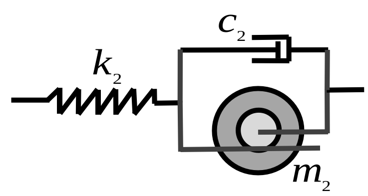

Figure 2-11: Tuned viscous mass damper (TVMD)

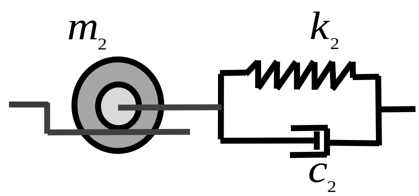

Figure 2-12: Tuned inerter damper (TID)

The performance evaluation of TVMD and TID incorporated into simplified linear MDOF structures against seismic load demonstrated the effectiveness of these devices compared to the viscous damper [72]. In the specific context of building structures and the control of their dynamic response, the evaluation and optimum design of VMD, TVMD and TID as inter-story control devices has been investigated considering linear spring-mass-damper models of MDOF structures [72]. The results of this study show the superiority of the considered inerter-based dampers compared to viscous dampers in reducing the structures' drift and acceleration response. Utilizing inerter-based dampers on the first and second story of frames for the suppression of the response of multistory buildings has also been considered [81]. The optimal configurations for structural control of using inerter-based dampers located in the first story of multi-story buildings has also been investigated recently [79].

With the goal of improving rotational inertia mass dampers, a new type of inerter-based passive control device featuring state switching has been proposed [80]. This proposed device consists of two flywheels and a passive clutch system. With this clutch, the rotational inertia mass is engaged with the SDOF system it is attached to when the velocity and acceleration of the structural mass have the same sign. When the acceleration and velocity have different signs, the device is not engaged with the primary system. In other words, the inerter is engaged while the absolute value of the velocity of the system is increasing and after this absolute velocity peaks, when the acceleration of the system reverses, the device is no longer engaged. The benefit of this state switching configuration is that the kinetic energy contained within the device cannot be transferred back and drive the system. The displacement reduction effect of this clutch inerter for SDOF systems have been investigated and evaluated recently [81]. In addition., seismic assessment, optimum design, and performance evaluation of clutch inerter damper on steel frames can be mention as most recent studies [82,83]

While the device proposed by [80] does consider one-directional behavior, the energy in the flywheels is not accounted for after the flywheels stop being engaged. This assumption allows this device to be always able to be engaged with a flywheel after a change in the sign of the device's velocity. In addition, as the rotational inertia mass in this device is an inerter, it leads to changes in the frequency of the structure [55,81]

CHAPTER THREE: OPTIMAL DESIGN OF ROTATIONAL INERTIAL DOUBLE TUNED MASS DAMPERS UNDER RANDOM EXCITATION

A version of this chapter was originally published by Abdollah Javidialesaadi and Nicholas Wierschem:

A. Javidialesaadi, N.E. Wierschem, Optimal design of rotational inertial double tuned mass dampers under random excitation, Engineering Structures. 165 (2018) 412–421. https://doi.org/10.1016/j.engstruct.2018.03.033.

This paper is part of the development of state of the art in inerter-based mass dampers. This work is more focused on analytical design solution methods of inerter-based mass dampers.

Abstract

The rotational inertial double tuned mass damper (RIDTMD) is a type of passive mass damper which includes a physical mass as well as a rotational mass. This rotational mass is produced by an inerter which is capable of providing large effective mass utilizing very little physical mass. By selecting the proper design parameters, the RIDTMD show promise at more effective response reduction of underlying primary systems in comparison to conventional tuned mass dampers (TMDs). However, when the primary system is subjected to random loads, the previously considered optimum design values for harmonic excitation are not effective. This motivates an investigation to determine the exact analytical optimum solution for selecting the stiffness and damping design values of RIDTMD when the primary structure is subjected to random force and base excitation. In this paper, an exact optimization solution procedure is presented with the goal of finding the optimum design values of the RIDTMD when mitigating the response of a structure subjected to random force and base excitation. Utilizing the obtained optimum design values, the effectiveness of RIDTMD is also studied in comparison to conventional TMDs. The results of this study show that the RIDTMD with optimized stiffness and damping values outperforms the optimized conventional TMD; however, the degree of its increased effectiveness in reducing the main

mass response is reliant upon the selection of appropriate pairs of secondary and rotational mass.

Introduction

Structures are subjected to various types of dynamic excitations. Of particular interest to structural engineers are wind, which directly loads a structure, and earthquakes, which load the structure as a result of base excitation. Reducing the effects of dynamic loads has motivated many researchers to study the use of supplemental mechanical vibration absorbers. Conventional tuned mass dampers (TMDs), which are designed to damp the vibration of a primary mass [13], are composed of a secondary mass, spring, and viscous damper. TMDs have been developed and used as a reliable device for structural vibration control of loads which can be modeled as a stationary process. The performance of a TMD is highly dependent on three parameters: 1) the ratio of the mass of the TMD to the main mass, 2) the frequency ratio of the TMD to the main mass, and 3) the TMD damping ratio. It has been found that by utilizing optimized parameters, the TMD can be effective at reducing the response of the main mass it is attached to [14].

Design parameters of TMDs have been obtained through the use of the H_∞ optimization criterion, which minimizes the maximum displacement response of the main mass in the frequency domain. The fixed-points theory, which approximates the H_∞ method [14] , is commonly used for TMD optimization. This method is based on the existence of two equal magnitude fixed points on the system's frequency response curve that do not depend on the system's damping level and are thus at the same location in either the zero or infinite damping condition. TMD optimum design parameters under harmonic force and base excitation for undamped primary systems have been obtained by applying the fixed points method [84]. In addition, analytical exact solutions for H_∞ optimization of the TMD for damped and undamped primary systems have been developed [18,85].

However, when the main system is subjected to random vibration, it is often the minimization of the mean square of the response that is considered [20]. In the literature, the minimization of the mean square response of the primary structure over all frequencies is called the H_2 optimization criterion. Utilizing this criterion, design formulas have been proposed for random force and base excited systems utilizing a TMD when the main system is undamped [84]. Using residue theory from complex analysis, exact solutions for TMD parameter optimization considering random force and base excitation have been proposed for a TMD attached to a damped single-degree-of-freedom (SDOF) system [18,28]. Furthermore, robust H_2 optimization using a numerical approach has been proposed [86] and a mixed analytical and numerical curve fitting approach has been utilized [87].

Variant types of TMD have been proposed, formulated, and investigated to determine optimum design values. Non-traditional vibration absorbers for random force vibration attached to an undamped single-degree-of-freedom primary system have been optimized utilizing an analytical solution [29]. Three-element type TMD [89], which have an additional spring in series with the viscous damper, have been proposed and optimized considering a random force excitation [88]. Another variant of the TMD is the multiple tuned mass dampers (MTMD) system which utilizes multiple separately tuned TMDs attached to a primary system. H_2 optimum parameters for the MTMD have been investigated using numerical methods for single [36] and multi-degree-of-freedom primary systems [89]. In addition, numerical approaches implemented for minimax optimization of MTMD attached to multi-degree-of-freedom primary systems have also been developed [19].

In an effort to improve the effectiveness of TMDs, the utilization of supplemental rotational masses in TMDs has recently been studied [8–10,52]. The most important benefit of rotational devices is that they are able to produce a large effective mass by using a relatively small rotational physical mass; therefore, these devices potentially need smaller physical mass than a conventional TMD to be effective. Using the ball screw mechanism concept, the rotational inertial viscous damper (RIVD) was proposed and evaluated for use with toggle bracing for control of a single-degree-of-freedom system [8]. The tuned viscous mass damper (TVMD), which consists of a tuning spring connected to a viscous mass damper that contains a rotational inertial mass, has also been proposed [52] .The results of this study showed that the TVMD attached to a single-degree-of-freedom system was effective under harmonic and seismic loading. The authors of this work also designed and produced a ball screw mechanism, which provides 350 kg of effective mass utilizing only 2 kg of physical mass.

The rotational inertial double tuned mass damper (RIDTMD) is another type of rotational device which has been proposed recently [9]. The RIDTMD consists of a conventional TMD, but the typical viscous damper has been replaced with a tuned viscous damper [9].The tuned viscous damper consists of a spring, axial dashpot, and a rotational mass, known as an inerter. While the rack and pinion mechanism has been proposed for use in the RIDTMD [9], different alternative mechanisms for transferring translational motion to rotation, such as a ball screw mechanism, could be utilize. The RIDTMD, with a small added rotational mass, has demonstrated effective results compared to the TMD under force harmonic excitation.

Optimum design values of RIDTMD have been obtain using a numerical method optimization for force harmonic excitation [9]. Furthermore, the RIDTMD is a special case of inerter-base devices which have been optimally design only for random force excitation on the primary system using a numerical optimization method [10]. In addition, compared to other inerter-base devices with the same number of degrees of freedom, RIDTMD shows better performance in the reduction of the dynamic magnification factor [10]. Because the investigation of optimum design values for this device have been limited to force excitation using numerical methods [9,10], it is important to develop the optimum design of this device through the exact analytical solution for both force and base excitations.

In this study, an analytical exact solution procedure for selecting the optimum values for the RIDTMD under random force and base excitation attached to an undamped primary system is provided. The rotational device, attached to a single-degree-of-freedom primary system, is formulated considering a general mechanism, not specifically a rack and pinion system, for transferring the linear motion to the rotational part of the RIDTMD. The analytical solution is performed based on H_2 optimization criterion and the variance of the output equations are derived and presented analytically. Using the optimum values for different mass ratio combinations, the performance of the device at controlling an undamped primary system under random force and base excitation is compared to the TMD. The optimized system response for different mass ratio combinations are also presented to evaluate the optimum mass ratio of this type of device when subjected to random vibration.

In the next section, dynamic modeling and explicit formulation of the RIDTMD is presented. Section 3 presents the optimum design formulas for TMD under random force and base excitation. Section 4 and 5 present the H_2 optimum design of RIDTMD under random force and base excitation, respectively. Curves showing the optimal RIDTMD parameter design values for both cases are presented in Section 6. Section 7 covers the evaluation of the performance of the device with respect to the H_2 norm and the reduction of the dynamic magnification factor. Comparisons between the performance of the optimal RIDTMD and optimal TMD are also made in Section 7. Section 8 presents a summary and the conclusions of this study.

Rotational inertial double tuned mass damper (RIDTMD)

The primary physical difference between TMDs (Figure 3-1) and rotational inertial double tuned mass dampers (RIDTMDs) (Figure 3-2) is the replacement of the TMD's damper with a parallel rotational mass and viscous damper, often referred to as a rotational inertial device, which is in series with a tuning spring. The rotational mass works by transforming relative translation motion into the localized rotation of a small mass. While many mechanisms could potentially be used to produce this rotation, two alternatives have been primarily considered in the literature: the rack and pinion mechanism [9] and the ball screw mechanism [8,52] (Figure 3-3).

The rotational velocity of this rotational mass, usually a flywheel, (ω) is based on the derivative of relative displacement between the two terminal ends of the device and α, a coefficient related to the mechanism's physics.

$$\omega = \alpha(\dot{x}_1 - \dot{x}_2) \tag{3.1}$$

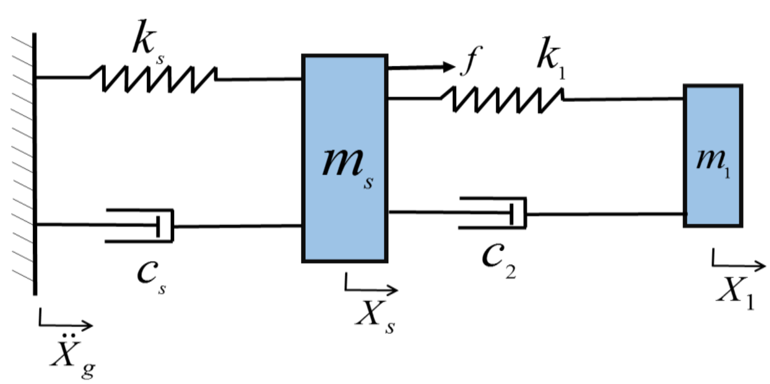

Figure 3-1: Traditional TMD

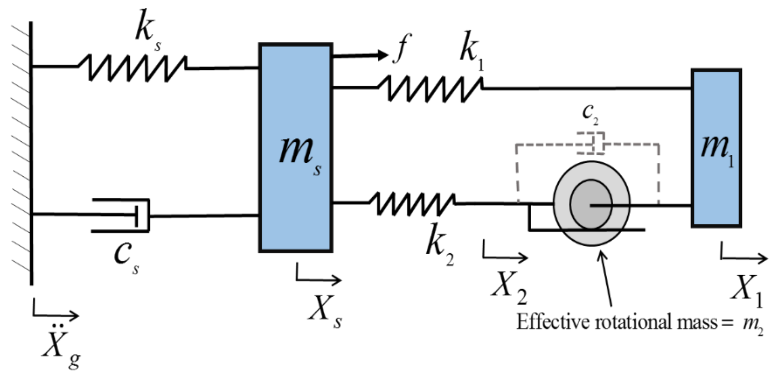

Figure 3-2: Rotational inertial double tuned mass damper (RIDTMD)

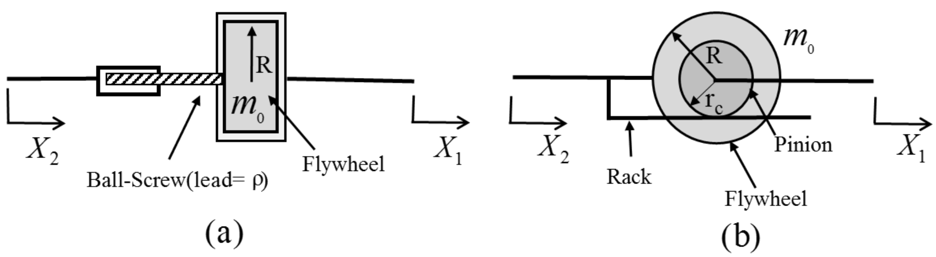

Figure 3-3: Rotational inertial devices for transferring translation motion to rotational motion (a) ball and screw mechanism, (b) rack and pinion mechanism

For the ball screw mechanism,

$$\alpha = 2\pi/\rho \tag{3.2}$$

where ρ is the ball screw lead. For the rack and pinion mechanism,

$$\alpha = 1/r_c \tag{3.3}$$

Where r_c is the pinion radius.

Utilizing Eq. (3.1)in calculating the kinetic energy of the rotational body, the contribution of the rotational mass to the kinetic energy of the system can be written as:

$$T = \frac{1}{2} J\omega^2 \tag{3.4}$$

In this expression, the kinetic energy related to translation of the rotational mass is neglected because of the small physical mass assumed to be used for this portion of the device. If the flywheel is assumed to be a hollow cylinder, $J = m_0 R^2$, where m_0 and R are the flywheel mass and radius. Substituting Eq. (3.1) into Eq. (3.4), the kinetic energy of the rotational body can be rewritten as:

$$T = \frac{1}{2} m_0 R^2 \alpha^2 (\dot{x}_1 - \dot{x}_2)^2 \tag{3.5}$$

Based on this kinetic energy, the effective inertial contribution to the system can be written as:

$$\frac{\mathrm{d}}{\mathrm{dt}}\left(\frac{\partial T}{\partial \dot{x}_i}\right) = m_0 R^2 \alpha^2 (\ddot{x}_1 - \ddot{x}_2) \tag{3.6}$$

Eq. (3.6) shows that by utilizing a small physical mass in the rotational mechanism mentioned, the effective mass can be amplified by the coefficient $R^2\alpha^2$. By setting $m_0 R^2 \alpha^2 = m_2$, and considering a damped SDOF primary system, the equation of motion of the system can be written as:

$$\begin{aligned}
&m_s \ddot{x}_s + c_s \dot{x}_s + k_s x_s + k_1 (x_s - x_1) + k_2 (x_s - x_2) = -m_s \ddot{x}_0(t) + f \\
&\ddot{x}_1 m_1 + m_2 (\ddot{x}_1 - \ddot{x}_2) + c_2 (\dot{x}_1 - \dot{x}_2) + k_1 (x_1 - x_s) = -m_1 \ddot{x}_0(t) \\
&m_2 (\ddot{x}_2 - \ddot{x}_1) + c_2 (\dot{x}_2 - \dot{x}_1) + k_2 (x_2 - x_s) = 0
\end{aligned} \tag{3.7}$$

where

m_s : Primary structure mass, m_1 : Main system mass

m_2 : Secondary system mass (effective rotational mass)

c_s : Primary structure damping, c_2 : Secondary system damping,

k_s : Primary structure stiffness, k_1 : Main system stiffness, k_2 : Secondary system stiffness

As the displacement of the primary system is of primary concern in this study, it is more convenient to write the equation of motion using the state space representation with the primary system displacement relative to the ground as the only output.

$$\begin{aligned} \dot{\mathbf{X}}(t) &= \mathbf{AX}(t) + \mathbf{B}u(t) \\ \mathbf{y}(t) &= \mathbf{CX}(t) \end{aligned} \tag{3.8}$$

where

$$\mathbf{X} = [\mathbf{x}\ \ \dot{\mathbf{x}}]^{\mathbf{T}};\ \ \mathbf{x} = \begin{bmatrix} x_s & x_1 & x_2 \end{bmatrix}^{\mathbf{T}};\ \ \mathbf{A} = \begin{bmatrix} \mathbf{0}_{3\times 3} & \mathbf{I}_3 \\ \mathbf{-M}^{-1}\mathbf{K} & \mathbf{-M}^{-1}\mathbf{C}_\mathbf{d} \end{bmatrix};\ \ \mathbf{C} = \begin{bmatrix} 1 & 0 & 0 & 0 & 0 & 0 \end{bmatrix} \tag{3.9}$$

The input matrix, $\mathbf{B}$, is dependent on the type of loading on the structure. As shown in Eq. (3.10), $\mathbf{B}_f$ is the input matrix for force loading on the primary structure, and $\mathbf{B}_{\ddot{x}}$ is the input matrix for base excitation.

$$\mathbf{B}_f = \begin{bmatrix} \mathbf{0}_{3\times 1} \\ \mathbf{-M}^{-1}\begin{bmatrix} 1 \\ 0 \\ 0 \end{bmatrix} \end{bmatrix};\quad \mathbf{B}_{\ddot{x}} = \begin{bmatrix} \mathbf{0}_{3\times 1} \\ \mathbf{M}^{-1}\begin{bmatrix} m_s \\ m_1 \\ 0 \end{bmatrix} \end{bmatrix}; \tag{3.10}$$

The mass matrix $(\mathbf{M})$, damping matrix $(\mathbf{C_d})$, and stiffness matrix $(\mathbf{K})$ can be written as follows:

$$\mathbf{M}=\begin{bmatrix} m_s & 0 & 0 \\ 0 & m_1+m_2 & -m_2 \\ 0 & -m_2 & m_2 \end{bmatrix};\ \mathbf{C_d}=\begin{bmatrix} c_s & 0 & 0 \\ 0 & c_2 & -c_2 \\ 0 & -c_2 & c_2 \end{bmatrix};\ \mathbf{K}=\begin{bmatrix} k_s+k_1+k_2 & -k_1 & -k_2 \\ -k_1 & k_1 & 0 \\ -k_2 & 0 & k_2 \end{bmatrix} \tag{3.11}$$

It should be noted that when the effective rotational mass of the RIDTMD is zero, the device is not the same as a TMD. Rather when the effective rotational mass is zero, the device works as a three-element vibration absorber, which is a modified version of a TMD with an additional spring in series with its damper [89].

For more convenience, the following dimensionless parameters are defined and will be used throughout this paper.

$\mu_1=\dfrac{m_1}{m_s}$: Main mass ratio; $\mu_2=\dfrac{m_2}{m_1}$: Secondary mass ratio

$\omega_s=\sqrt{k_s/m_s}$: Primary system frequency; $\omega_1=\sqrt{k_1/m_1}$: Main system frequency

$\omega_2=\sqrt{k_2/m_2}$ Secondary system frequency; $\beta_1=\dfrac{\omega_1}{\omega_s}$: Main tuning frequency ratio

$\beta_2=\dfrac{\omega_2}{\omega_s}$: Secondary tuning frequency ratio; $\lambda=\dfrac{\omega}{\omega_s}$: Input frequency ratio

$\xi_s=\dfrac{c_s}{2\omega_s m_s}$: Primary structure damping ratio; $\xi_2=\dfrac{c_2}{2\omega_2 m_2}$: Secondary damping ratio

TMD Optimization

The exact optimization solutions for conventional TMDs attached to an undamped SDOF system are presented by Warburton [84]. The same optimization goal is shared in this work, the minimization of the variance of the main mass displacement response, and both loading via random force and base excitation are considered. By considering $\mu = \frac{m_1}{m_s}$ as the mass ratio for TMDs, the optimum frequency β_{opt} and damping ratio ξ_{opt} for the main mass random force excitation can be written as follows:

$$\beta_{opt} = \frac{\sqrt{(1+\mu/2)}}{1+\mu} \tag{3.12}$$

$$\xi_{opt}{}^{2} = \frac{\mu(1+3\mu/4)}{4(1+\mu)(1+\mu/2)} \tag{3.13}$$

And for the random base excitation case:

$$\beta_{opt} = \frac{\sqrt{(1-\mu/2)}}{1+\mu} \tag{3.14}$$

$$\xi_{opt}{}^{2} = \frac{\mu(1-\mu/4)}{4(1+\mu)(1-\mu/2)} \tag{3.15}$$

RIDTMD Optimum Design: Force Excitation Case

In this section, the goal is to find β_1, β_2, and ξ_2 to provide the minimum variance of the RIDTMD's output under the random force excitation case. Considering the SDOF system with a RIDTMD attached, the force excitation load case, and the output of the system as the primary structure mass displacement, a generic transfer function of the system in the frequency domain can be written as:

$$H_{\mathrm{f}}(i\omega) = \mathbf{C}(i\omega\mathbf{I_6} - \mathbf{A})^{-1}\mathbf{B_f} \tag{3.16}$$

When the system is excited by random white noise input, the non-dimensional variance of the output [10,21,84] can be written as:

$$\bar{\sigma}_f^{\,2} = \frac{1}{2\pi}\int_{-\infty}^{\infty}\left|H_f(i\lambda)\right|^2 d\lambda \tag{3.17}$$

where

$$\left|H_f(i\lambda)\right|^2 = \frac{\mathrm{Im}\left(H(i\lambda)_f\right)_n^2 + \mathrm{Re}(H(i\lambda)_f)_n^2}{\mathrm{Im}\left(H(i\lambda)_f\right)_d^2 + \mathrm{Re}\left(H(i\lambda)_f\right)_d^2} \tag{3.18}$$

In Eq. (3.18), Im and Re represents the imaginary and real parts of the transfer function and the subscripts n and d represent the numerator and denominator, respectively. By multiplying both the numerator and denominator by the complex conjugate and performing algebraic manipulations, Eq. (3.18) can be rewritten as Eq. (3.19).

$$\left|H_f(i\lambda)\right|^2 = \frac{g_f(\lambda)}{h_f(\lambda)h_f(-\lambda)} \tag{3.19}$$

The numerator of Eq. (3.19) can be written in the polynomial form presented in Eq. (3.20).

$$g_f(\lambda) = \lambda^8 + b_1\lambda^6 + b_2\lambda^4 + b_3\lambda^2 + b_4 \tag{3.20}$$

where

$$
\begin{aligned}
b_1 &= \left(4\xi_2^{\,2}\beta_2^{\,2} - 2\beta_2^{\,2}\mu_2 - 2\beta_1^{\,2} - 2\beta_2^{\,2}\right) \\
b_2 &= \left(-4\left(2\beta_2^{\,3}\mu_2 + 2\beta_1^{\,2}\beta_2\right)\beta_2\xi_2^{\,2} + 2\beta_1^{\,2}\beta_2^{\,2} + \left(-\beta_2^{\,2}\mu_2 - \beta_1^{\,2} - \beta_2^{\,2}\right)^2\right) \\
b_3 &= \left(\left(2\beta_2^{\,3}\mu_2 + 2\beta_1^{\,2}\beta_2\right)^2\xi_2^{\,2} + 2\beta_1^{\,2}\beta_2^{\,2}\left(-\beta_2^{\,2}\mu_2 - \beta_1^{\,2} - \beta_2^{\,2}\right)\right) \\
b_4 &= \beta_1^{\,4}\beta_2^{\,4}
\end{aligned}
$$

Utilizing the complex conjugate of the function and considering $\mathrm{i} = \sqrt{-1}$, the denominator of Eq. (3.21) can be rewritten as

$$
h_f(\lambda) = \lambda^6 + a_1\mathrm{i}\lambda^5 + a_2\lambda^4 + a_3\mathrm{i}\lambda^3 + a_4\lambda^2 + a_5\mathrm{i}\lambda + a_6 \tag{3.21}
$$

where

$$
\begin{aligned}
a_1 &= -2\xi_2\beta_2 \\
a_2 &= -\beta_2^{\,2}\mu_1\mu_2 - \beta_1^{\,2}\mu_1 - \beta_2^{\,2}\mu_2 - \beta_1^{\,2} - \beta_2^{\,2} - 1 \\
a_3 &= 2\beta_2\xi_2\left(\mu_2(\mu_1+1)\beta_2^{\,2} + 1 + (\mu_1+1)\beta_1^{\,2}\right) \\
a_4 &= \beta_1^{\,2}\beta_2^{\,2}\mu_1 + \beta_1^{\,2}\beta_2^{\,2} + \beta_2^{\,2}\mu_2 + \beta_2^{\,2} + \beta_1^{\,2} \\
a_5 &= \beta_2\left(\mu_2(\mu_1+1)\beta_2^{\,2} + 1 + (\mu_1+1)\beta_1^{\,2}\right)\xi_2 \\
a_5 &= 2\left(\beta_2^{\,2}\mu_2 + \beta_1^{\,2}\right)\beta_2\xi_2 \\
a_6 &= -\beta_1^{\,2}\beta_2^{\,2}
\end{aligned}
$$

Writing the variance of the output in the form shown in Eq. (3.19) is beneficial for determining the exact solution of the integral. This type of integration can be evaluated directly by utilizing Cauchy's residue theorem, which has been previously performed for a damped primary system with a TMD [18,21] and recently for optimum design of double series and parallel TMDs [90]. However, integration of Eq. (3.17) with the form shown in Eq. (3.19) can also be performed using integral tables [99]. This approach has been used for the optimization of non-traditional TMDs [29]. Both of these solution techniques are based on Cauchy's residue theorem, which can be found in explicit form in [91].

To aid in accurately and efficiently implementing the integral method presented in [91], Maple [92], a computational software package for symbolic mathematics, was used to perform the following mathematical manipulations. In the first step, the variance of the output of the system loaded with the force excitation can be written as:

$$\overline{\sigma_f}^2 = \frac{\nu_0 \beta_2^{\,6} + \nu_1 \beta_2^{\,4} + \nu_2 \beta_2^{\,2} + \nu_3}{4\xi_2 \beta_2^{\,5} \mu_2 \mu_1} \tag{3.22}$$

where

$$\begin{aligned}
\nu_0 &= 4\xi_2^{\,2}\mu_2^{\,2}\left(\mu_1+1\right)\\
\nu_1 &= \left(\mu_1+1\right)^2 \beta_1^4 + \left(\left(8\xi_2\mu_1 + 8\xi_2^{\,2} - 2\mu_1 - 2\right)\mu_2 - \mu_1 - 2\right)\beta_1^2 - 8\xi_2^{\,2}\mu_2 + \mu_2^{\,2} + 2\mu_2 + 1\\
\nu_2 &= \left(4\xi_2^{\,2}\mu_1 + 4\xi_2^{\,2} - 2\mu_1 - 2\right)\beta_1^4 + \left(-8\xi_2^{\,2} + 2\mu_2 + 4\right)\beta_1^2 + \left(\mu_1 - 2\right)\mu_2 + 4\xi_2^{\,2} - 2\\
\nu_3 &= 1 + \beta_1^4 + \left(\mu_1 - 2\right)\beta_1^2
\end{aligned}$$

For the optimization of TMDs, the optimization condition needs to satisfy two equations; the partial derivatives of the output variance with respect to the damping coefficient and the frequency ratio must be both equal to zero. However, assuming given mass ratios, the rotational tuned mass damper is a three-parameter device, (β_1, β_2, ξ_2); thus, three equations are needed. Because the optimum condition is a minimum, the following necessary conditions must be satisfied:

$$\frac{\partial(\bar{\sigma}_f^{\,2})}{\partial(\beta_1)} = 0 \tag{3.23}$$

$$\frac{\partial(\bar{\sigma}_f^{\,2})}{\partial(\beta_2)} = 0 \tag{3.24}$$

$$\frac{\partial(\bar{\sigma}_f^{\,2})}{\partial(\xi_2)} = 0 \tag{3.25}$$

Eq. (3.23) to (3.25) are presented in explicit form in Appendix A.

All roots of Eq. (3.23) to (3.25) can be solved using Maple with given μ_1 and μ_2. However, only real positive solutions are meaningful; thus, the considered solutions can be limited to real domain and positive values. It is found using Maple that there are a maximum of four real positive roots for a given combination of μ_1 and μ_2 considering $0.01 \le \mu_1 \le 0.05$ and $0.001 \le \mu_2 \le 1$. These ranges of mass ratios are used because the main mass ratio of this device in a real structure would likely be limited in practice to less than 5% of the structure's mass, while the range of possible secondary mass ratios possible would be greater due to the small physical mass used in the inerter. Once all four roots have been considered and all possible values of Eq. (3.22) calculated, the solution which provides the minimum value of Eq. (3.22) is considered as the final solution. In addition, the eigenvalues of the hessian matrix of the Eq. (3.22) are calculated and checked to be positive. Finding the solution which provides the minimum value and positive hessian's matrix eigenvalues, guarantees finding the global minimum instead of a local minimum.

RIDTMD Optimum Design: Base Excitation Case

In a manner similar to the optimization performed in Section 4, the optimization of the RIDTMD attached to a SDOF base structure can be performed when the system is subjected to a random base excitation. As a first step, the generic transfer function of the system in the frequency domain considering an output of the main mass displacement and an input of the base excitation can be written as:

$$H_b(i\omega) = \mathbf{C}(i\omega\mathbf{I_6} - \mathbf{A})^{-1}\mathbf{B}_{\ddot{\mathbf{x}}} \tag{3.26}$$

The non-dimensional variance of the output [22,28,84] can be written as:

$$\bar{\sigma}_b{}^2 = \frac{1}{2\pi}\int_{-\infty}^{\infty} |H_b(i\lambda)|^2 d\lambda \tag{3.27}$$

Then, the variance of the output can be written as:

$$\left|H_b(i\lambda)\right|^2 = \frac{g_b(\lambda)}{h_b(\lambda)h_b(-\lambda)} \tag{3.28}$$

The numerator of Eq. (3.28) can be expressed as a polynomial

$$g_b(\lambda) = \lambda^8 + b_1\lambda^6 + b_2\lambda^4 + b_3\lambda^2 + b_4 \tag{3.29}$$

where

$$b_1 = \left(4\xi_2{}^2 - 2\mu_1\mu_2 - 2\mu_2 - 2\right)\beta_2{}^2 - 2\beta_1^2\left(\mu_1+1\right)$$
$$b_2 = \left(\mu_1^2\mu_2{}^2 + \left(-8\xi_2{}^2\mu_2 + 2\mu_2{}^2 + 2\mu_2\right)\mu_1 - 8\xi_2{}^2\mu_2 + \mu_2{}^2 + 2\mu_2 + 1\right)\beta_2{}^4 + ..$$
$$..2\beta_1^2\left(\mu_1+1\right)\left(-4\xi_2{}^2 + \mu_1\mu_2 + \mu_2 + 2\right)\beta_2{}^2 + \beta_1^4\left(\mu_1+1\right)^2$$
$$b_3 = 4\left(\mu_1+1\right)\begin{pmatrix} \xi_2{}^2\mu_2{}^2\left(\mu_1+1\right)\beta_2{}^4 + 2\left(\mu_2\left(\xi_2{}^2 - \frac{1}{4}\right)\mu_1 + \xi_2{}^2\mu_2 - \frac{1}{4}\mu_2 - \frac{1}{4}\right)\beta_1^2\beta_2{}^2 + ... \\ +\left(\xi_2{}^2 - \frac{1}{2}\right)\left(\mu_1+1\right)\beta_1^4 \end{pmatrix}\beta_2{}^2$$
$$b_4 = \beta_1^4\beta_2{}^4\left(\mu_1+1\right)^2$$

Utilizing the complex conjugate of the function and considering $\mathrm{i} = \sqrt{-1}$, the denominator of Eq. (3.28) can be rewritten as

$$h_b(\lambda) = \lambda^6 + a_1\mathrm{i}\lambda^5 + a_2\lambda^4 + a_3\mathrm{i}\lambda^3 + a_4\lambda^2 + a_5\mathrm{i}\lambda + a_6 \tag{3.30}$$

where

$$a_1 = -2\xi_2\beta_2$$
$$a_2 = \left(-1+\left(-\mu_1-1\right)\mu_2\right)\beta_2{}^2 - 1 + \left(-\mu_1-1\right)\beta_1{}^2$$
$$a_3 = 2\xi_2\beta_2\left(\left(\mu_1+1\right)\mu_2\beta_2{}^2 + 1 + \beta_1{}^2\left(\mu_1+1\right)\right)$$
$$a_4 = \left(\beta_1{}^2\left(\mu_1+1\right) + \mu_2 + 1\right)\beta_2{}^2 + \beta_1{}^2$$
$$a_5 = -2\xi_2\beta_2\left(\beta_2{}^2\mu_2 + \beta_1{}^2\right)$$
$$a_6 = -\beta_1{}^2\beta_2{}^2$$

The variance of the output is calculated by performing the process outlined in [91] and utilizing Maple [92]. The resulting variance is

$$\bar{\sigma}_b{}^2 = \frac{\nu_0\beta_2{}^6 + \nu_1\beta_2{}^4 + \nu_2\beta_2{}^2 + \nu_3}{4\xi_2\beta_2{}^5\mu_2\mu_1} \tag{3.31}$$

where

$$\nu_0 = 4\xi_2{}^2\mu_2{}^2\left(\mu_1+1\right)^3$$
$$\nu_1 = \begin{pmatrix} \left(\mu_1+1\right)^4\beta_1^4 + 8\left(\left(\xi_2{}^2\mu_2 - \frac{1}{4}\mu_2 + \frac{1}{8}\right)\mu_1 + \xi_2{}^2\mu_2 - \frac{1}{4}\mu_2 - \frac{1}{4}\right)\left(\mu_1+1\right)^2\beta_1^2 + \ldots \\ \ldots. + \mu_1^2\mu_2{}^2 + \left(-8\xi_2{}^2\mu_2 + 2\mu_2{}^2 + 2\mu_2\right)\mu_1 - 8\xi_2{}^2\mu_2 + \mu_2{}^2 + 2\mu_2 + 1 \end{pmatrix}$$
$$\nu_2 = 4\left(\mu_1+1\right)^3\left(\xi_2{}^2 - \frac{1}{2}\right)\beta_1^4 + 2\left(\mu_1+1\right)\left(-4\xi_2{}^2 + \mu_1\mu_2 + \mu_2 + 2\right)\beta_1^2 - \mu_1\mu_2 + 4\xi_2{}^2 - 2\mu_2 - 2$$
$$\nu_3 = 1 + \beta_1^4\left(\mu_1+1\right)^2 + \left(-\mu_1-2\right)\beta_1^2$$

Assuming given mass ratios, the rotational tuned mass damper is a three parameters device, (β_1, β_2, ξ_2); thus, three equations are needed. Because the optimum condition is a minimum, the following necessary conditions must be satisfied:

$$\frac{\partial(\bar{\sigma}_b{}^2)}{\partial(\beta_1)} = 0 \tag{3.32}$$

$$\frac{\partial(\bar{\sigma}_b{}^2)}{\partial(\beta_2)} = 0 \tag{3.33}$$

$$\frac{\partial(\bar{\sigma}_b{}^2)}{\partial(\xi_2)} = 0 \tag{3.34}$$

Eq. (3.32) to (3.34) are presented in explicit form in Appendix B.

The same solution procedure used when considering the force excitation case is once again implemented here to determine the optimum design values.

Optimum design values

In this section, the optimum design values for the design of RIDTMD subjected to random force and base excitation are presented. Optimum design values of the RIDTMD damping and stiffness elements for the force excitation are obtained from the solution of Eq. (3.23) to Eq. (3.25), while the optimum values are obtained in the base excitation case from the solution of Eq. (3.32) to (3.34).

Once again, this optimization is performed for all mass ratios over the range $0.01 \le \mu_1 \le 0.05$ (with a step of 0.01) and $0.001 \le \mu_2 \le 1$ (with a step of .001).

The resulting optimum main tuning frequency ratios ($\beta_1 = \frac{\omega_1}{\omega_s}$) for force and base excitation case are presented in Figure 3-4. For each μ_1 value considered, it was found that increasing μ_2 resulted in small changes in β_1 until a point is reached and a jump in optimal β_1 is observed. After this jump, the optimal β_1 steadily decreases with increased μ_2. While this behavior is observed for each value of μ_1 considered, the jump occurs at higher values of μ_2 when μ_1 is higher. While the optimal β_1 values and point at which they jump are different in the base excitation and force excitation cases, the basic shape of the optimal β_1 curves are the same in both cases. The optimum secondary tuning frequency ratios ($\beta_2 = \frac{\omega_2}{\omega_s}$) for $0.01 \le \mu_1 \le 0.05$ and $0.001 \le \mu_2 \le 1$ are presented in Figure 3-5. From these results, it was found that for each μ_1 value considered, β_2 decreases with increasing μ_2. However, this decrease is not uniform. For small values of μ_2, increases in μ_2 result in large decreases in optimal β_2 until a point is reached and a jump lower in optimal β_2 results. After this jump downward, the optimal β_2 only changes very little with increased μ_2. As will be shown in this section, for a given μ_1, this jump is observed to occur at the same μ_2 for all optimized parameters. This can be seen as the point that the behavior of the device changes and is more influenced by the effect of the secondary mass. As will be discussed in Section 7, at secondary mass ratios before the jump, the effect of increasing the secondary mass is insignificant; however, after the jump, increases in secondary mass ratio have a large effect on the effectiveness of the device.

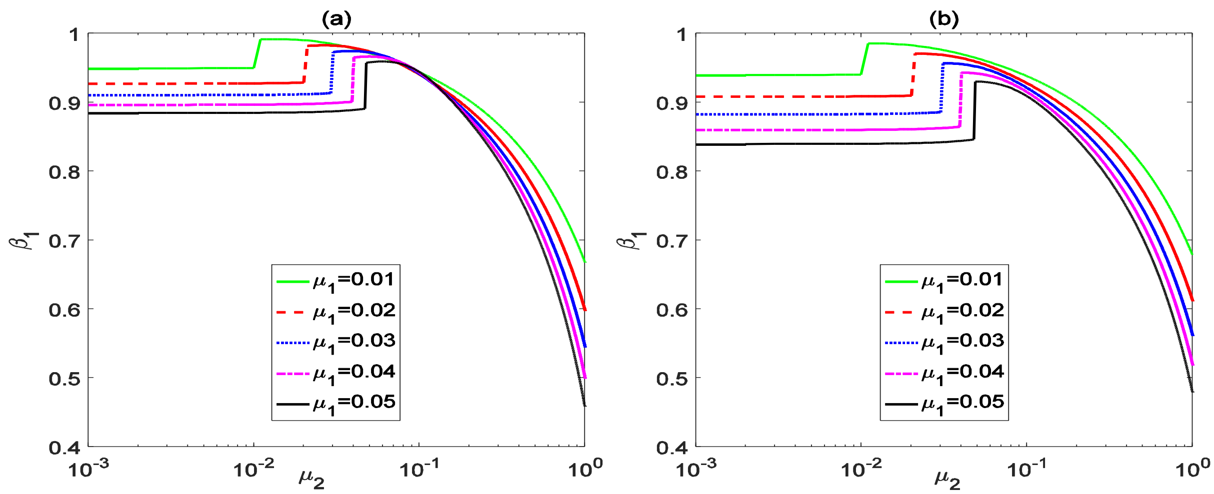

Figure 3-4: Optimum main tuning frequency ratio (β_1) (a) random force excitation, (b) random base excitation

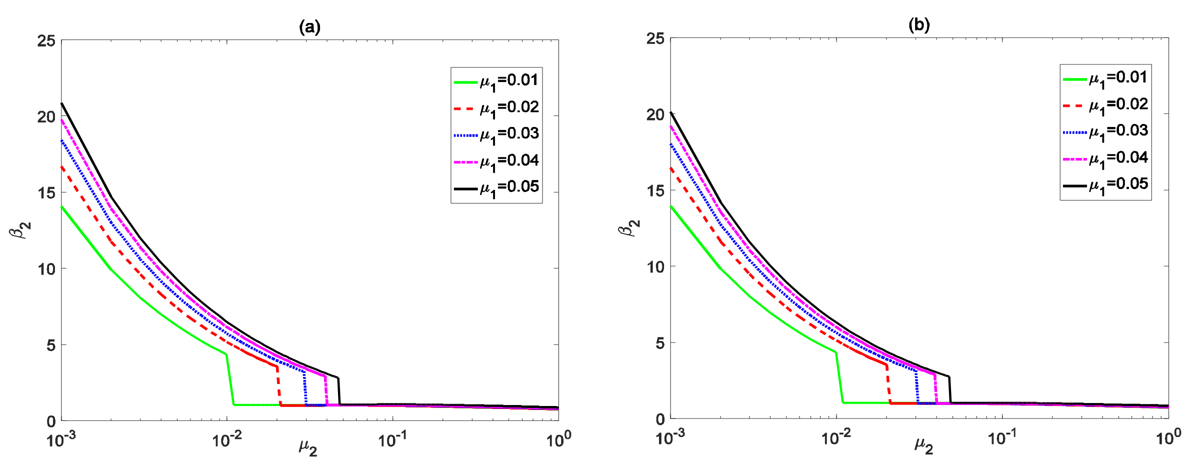

Figure 3-5: Optimum secondary tuning frequency ratio (β_2) (a) random force excitation, (b) random base excitation

It can be observed with an investigation of the locations of the poles of an RIDTMD that when $\mu_2 < \mu_1$ there are two poles that are located on the real axis: one near the imaginary axis and one to the far left side of the plot. When μ_2 grows larger, but is still less than μ_1, the location of this far left pole drifts towards the imaginary axis. When μ_2 is approximately equal to μ_1, the two poles on the real axis meet up; this is the point on the parameter optimization plots where the sharp change in behavior is located. When μ_2 grows larger than μ_1, one of the poles again eventually drifts to the far left side of the pole zero plot.The optimum secondary damping ratio (ζ_2) is also calculated for force and base random excitation and presented in Figure 3-6, respectively. For both of these cases, it is observed that the optimal value decreases smoothly with increasing until a point is reached and a jump to a lower optimal is observed. After this point, the optimal will then increase with increasing.

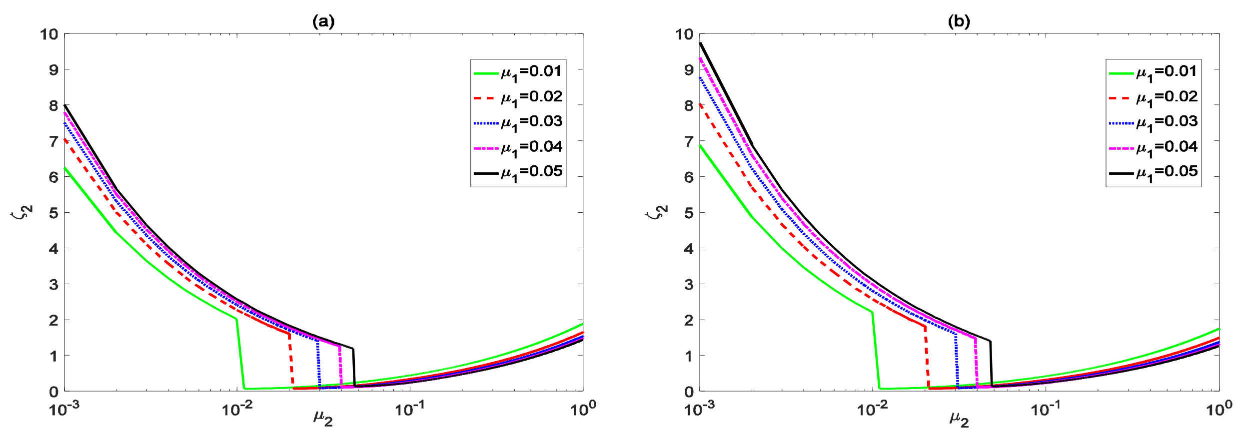

Figure 3-6: Optimum secondary damping ratio (ζ_2) (a) random force excitation, (b) random base excitation

Optimum secondary mass ratio and H_2 performance

Even though the optimum design procedure through exact solution can be utilized for any given combination of μ_1 and μ_2, the effect of the secondary mass ratio (μ_2) on the H_2 norm is the primary subject of the investigation in this section. The investigation of the optimum μ_2 is important because, as will be shown in this section, the overall effectiveness of the RIDTMD is dependent on μ_2 and its effectiveness does not monotonically increase with increased μ_2.

To evaluate the effect of μ_2 on the H_2 norm of the primary structure, the H_2 norm is calculated for $0.01 \le \mu_1 \le 0.05$ and $0.001 \le \mu_2 \le 1$ utilizing the optimum design values $(\beta_1, \beta_2, \zeta_2)$ presented in the previous section. Since the optimum design values provides the optimum RMS, then the presented system H_2 norm is also optimum [102]. Figure 3-7 shows the calculated H_2 norm of the RIDTMD for random force and base excitation.

From these figures, it is observed that for the force and base excitation cases, the variation of the primary structure H_2 norm is small around $\mu_2 < .01$, and then a smooth reduction in H_2 norm is observed with higher values of μ_2 until a minimum H_2 norm is reached and the H_2 norm starts to increase with higher values of μ_2. Additionally, for higher values of μ_1, the μ_2 value corresponding to the minimum H_2 norm increases. In other words, for every value of μ_1, there is a distinct μ_2 which provides the optimum H_2 norm of the RIDTMD.

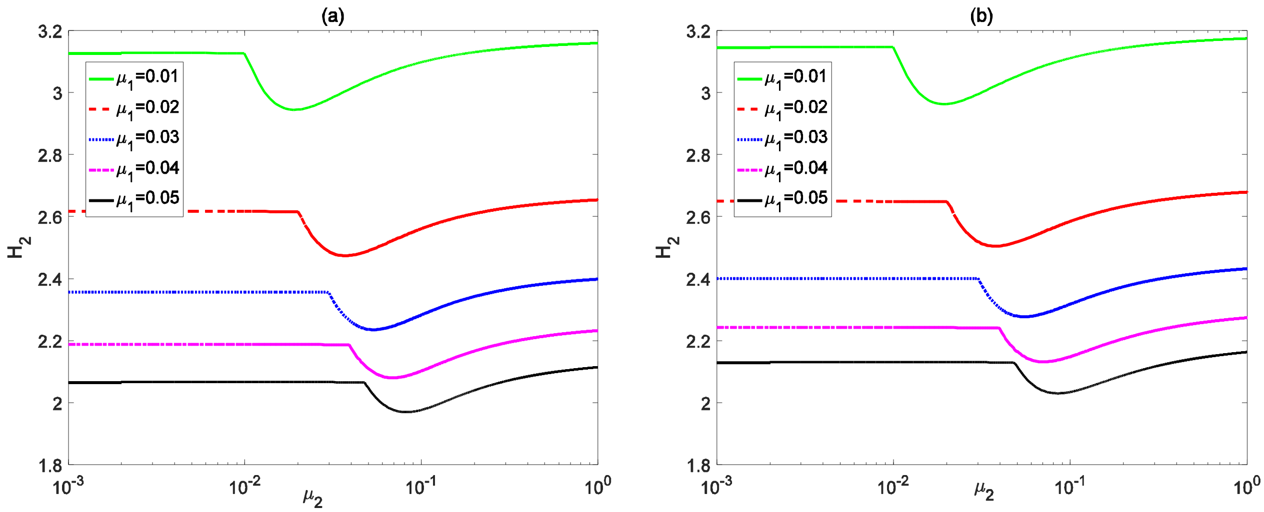

Figure 3-7: Optimum H_2 norm of RIDTMD (a) random force excitation, (b) random base excitation

The optimum μ_2 for different μ_1 and the corresponding optimum design values are presented in Table 1 for the force and base excitation cases, respectively.

In order to evaluate the H_2 norm performance of the RIDTMD in comparison to the TMD, the following index is defined:

$$R = \frac{\|H_2\|_{RIDTMD}}{\|H_2\|_{TMD}} \tag{3.35}$$

The index R is calculated for RIDTMD and TMD with the same μ_1 over the range of values for and μ_2 ($0.001 \le \mu_2 \le 1$) considered for RIDTMD.

Table 1. Optimum secondary mass and optimum design values (a) random force excitation, (b) for random base excitation

(a)					(b)				
μ_1	μ_2	β_1	β_2	ζ_2	μ_1	μ_2	β_1	β_2	ζ_2
0.01	0.019	0.9828	1.002	0.0847	0.01	0.019	0.9828	1.002	0.0845
0.02	0.031	0.9824	1.01738	0.1011	0.02	0.038	0.9655	1.005	0.1228
0.03	0.053	0.9714	1.02940	0.1445	0.03	0.055	0.9490	1.007	0.1491
0.04	0.069	0.9620	1.0394	0.1677	0.04	0.07	0.9334	1.009	0.1687
0.05	0.083	0.9177	1.01206	0.18812	0.05	0.085	0.9177	1.0120	0.1881

Figure 3-8 shows the R variation with respect to μ_2 for different values of μ_1. It is observed that the RIDTMD utilizing the optimum secondary mass ratio values can provide about a 7% reduction in the H_2 norm in comparison to the TMD with the same μ_1 in both force and base excitation. Additionally, these figures show that for the vast majority of μ_2 considered, R is under 1, meaning that the RIDTMD roved the performance of the system compared to the TMD. It should be noted that when the rotational effective mass μ_2, approaches zero, the RIDTMD works as a three-element vibration absorber with more effective performance than the TMD in the reduction of the H_2 norm [89].

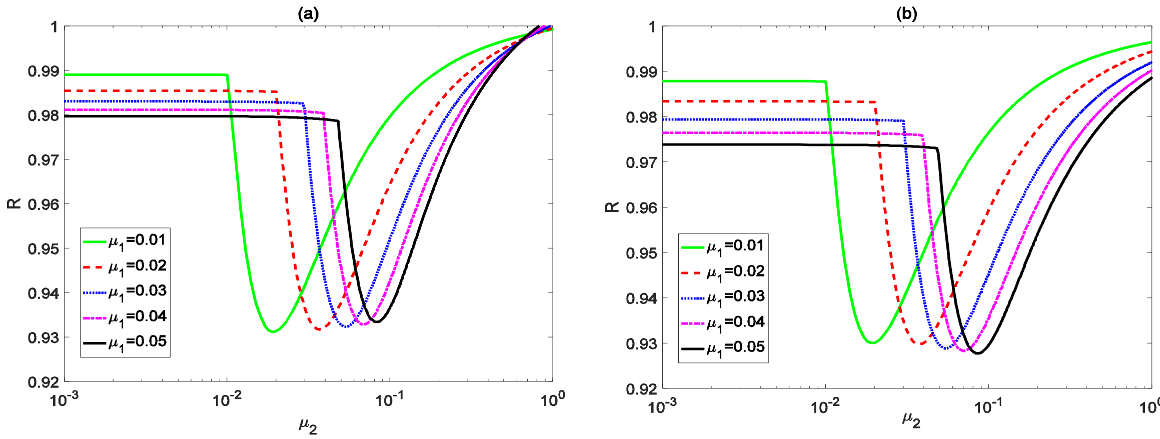

Figure 3-8: Ratio of RIDTMD to TMD H_2 norm (a) random force excitation, (b) random base excitation

Besides the H_2 norm, the frequency response of the optimum RIDTMD with optimum values is presented in Figure 3-9 and the frequency response of the H_2 optimized TMD is presented in Figure 3-10. The dynamic magnification factor (DMF) featured in these figures is define as the normalized displacement of the primary structure in the frequency domain. It is observed that the H_2 optimized RIDTMD frequency response curves have three peaks, unlike the TMD curves which have two peaks. This extra peak appears due to the additional DOF present in the RIDTMD and has the effect of broadening the frequency response curves of the RIDTMD.

Even though the system is optimized for minimizing the H_2 norm, the DMF of the H_2 optimized system is an indicator of the displacement response of the primary structure under random excitation; therefore, it is important for the evaluation of the performance of the vibration absorber. From results which are used to plot Figure 3-9, it is calculated that, for the force excitation case, the H_2 optimum RIDTMD provides a 23%, 16%, 25%, 24%, and 24% reduction in the maximum DMF compare to the optimum TMD for $\mu_1 = 0.01, 0.02, 0.03, 0.04, 0.05$, respectively. In the base excitation case, it is found that the optimum H_2 RIDTMD provides a 22%, 22%, 28%, 30%, and 24% reduction in the maximum DMF compare to the optimum TMD for $\mu_1 = 0.01, 0.02, 0.03, 0.04, 0.05$, respectively. It should be noted that these reduction improvements are obtained by utilizing small values of secondary mass ratio, which are presented in Table 1.

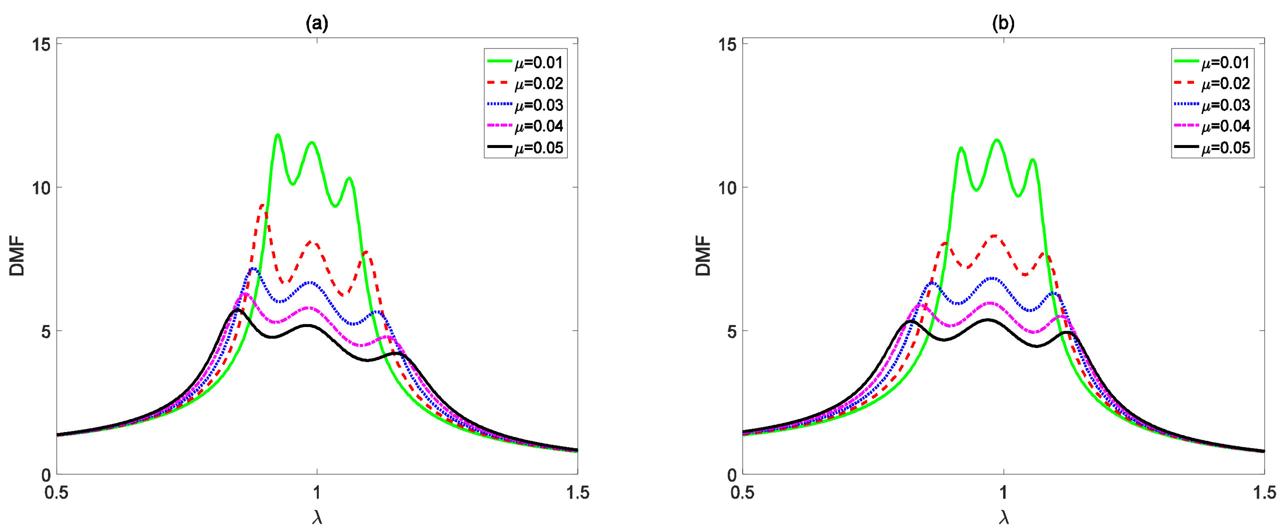

Figure 3-9: H2 optimum RIDTMD frequency response with optimum secondary mass (a) random force excitation, (b) random base excitation

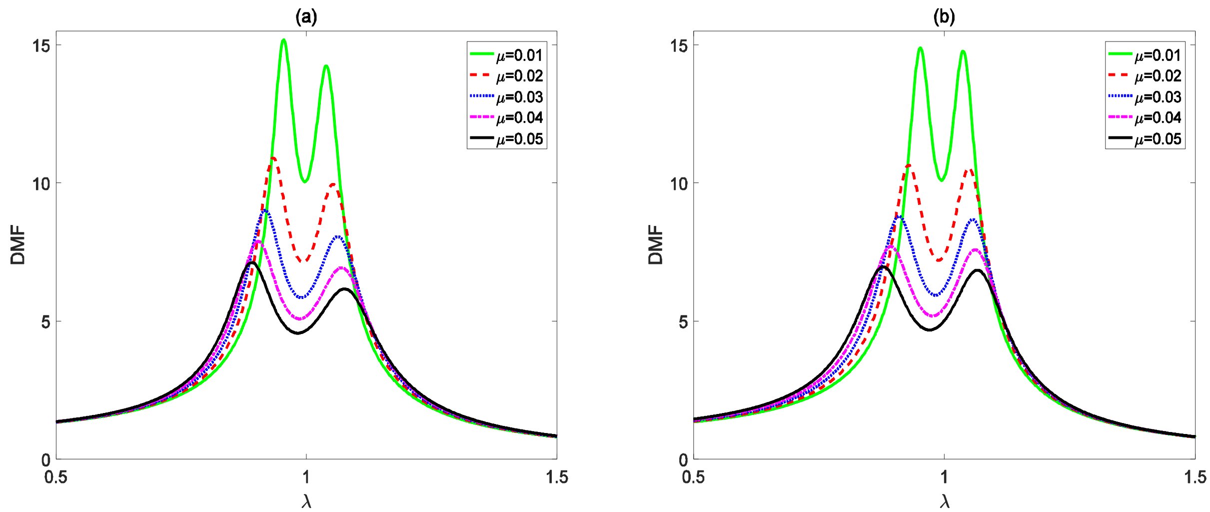

Figure 3-10: H2 optimum TMD frequency response (a) random force excitation, (b) random base excitation

Conclusions

The rotational inertial double tuned mass damper (RIDTMD) is a type of passive mass damper which includes a physical mass as well as a rotational mass. This rotational mass is produced by an inerter which is capable of providing large effective mass utilizing very little physical mass. This paper presents an exact algebraic procedure for the design of the optimum values of stiffness and damping for RIDTMD devices attached to an undamped SDOF system subjected to random force or random base excitation. Expressions for the variance in the displacement response of the structure the RIDTMD is attached to for both force and base excitation are derived in closed-form and conditions for optimization of this response are satisfied mathematically. The proposed method provides a set of closed-form equations for the optimal main tuning frequency ratio, the secondary tuning frequency ratio, and damping ratio for given arbitrary mass ratios. While these results show that the value of the optimum parameters have substantial differences for the force and base excitation cases, the trends observed with changes in the mass ratios are the same for each loading case.

Utilizing optimum design values from the proposed exact solution method, the optimum secondary mass ratio and the effectiveness of the RIDTMD was investigated. Based on this investigation, some conclusions regarding the performance of the RIDTMD can be drawn.

For both force and base excitation, the optimum RIDTMD with appropriate main and secondary mass ratios shows more effective performance in reducing the response of the primary structure, as measured by the dynamic magnification factor and H_2 norm, in comparison to the optimal TMD with the same main mass ratio.

The secondary effective mass plays a significant role in the RIDTMD behavior and performance. The results presented here demonstrate that there is not a linear trend between the amplitude of the secondary mass ratio and the reduction in the magnification factor. Rather, it was found that for each main mass ratio, there is a particular optimum secondary mass ratio which provides a minimum H_2 norm.

RIDTMD performance advantage, compared to the TMD, is substantial when the secondary mass is optimum; around a 7% reduction in H_2 norm and 16%-30% reduction of the DMF observed by utilizing optimum secondary mass.

For the mass ratios considered in this investigation, the addition of the secondary mass never resulted in an optimal RIDTMD that was appreciably less effective than an optimal TMD with the same main mass ratio.

The secondary mass in the RIDTMD is effective mass, which can be provided by utilizing a rotational device with a small physical mass. In a previous study, a 350 kg effective mass was obtained by utilizing 2 kg physical mass [52]; resulting in an effective mass amplification of 17500%. Considering that the optimum secondary mass found in this study are small with secondary mass ratios between 0.019 and 0.084, the physical mass of this secondary mass will be very small. As a result, the addition of a small rotational mass in the RIDTMD has great promise to be a cost-effective way to create a device with superior performance in comparison to the TMD.

CHAPTER FOUR:DESIGN AND PERFORMANCE EVALUATION OF INERTER-BASED TUNED MASS DAMPERS FOR A PASSIVE CONTROL OF STRUCTURE UNDER THE GROUND ACCELERATION

This Chapter is part of the development of state of the art in inerter-based mass dampers. This work covers analytical design solution methods and performance evaluation of the inerter-based mass dampers when the structure is subjected to the ground acceleration and seismic load. This paper is under preparation and will be submitted by the end of May 2020.

Abstract

This paper investigates the design and performance evaluation of inerter (rotational inertia) –based tuned mass dampers for the passive control of undamped single-degree-of-freedom (SDOF) structures subjected to ground acceleration. Inerter-based tuned mass dampers (TMDs) have been developed recently by utilizing an inerter combined with spring and damping elements in otherwise conventional tuned mass dampers (TMDs). The inerter is a mechanical device that can provide mass effects (inertance) by converting linear motion to the rotational motion of a rotational inertia mass. The optimum design and performance evaluation of different types of inerter-based devices when the primary structure is subjected to harmonic or random load has been studied previously. However, optimum design and performance evaluation of civil structures subjected to ground acceleration has not received much attention. In this study, three recently developed cases of inerter-based TMDs attached to an undamped SDOF structure subjected to ground acceleration are studied. In the first step, by considering the ground acceleration as white noise and the minimization of the mean square of the response, H2 optimum design values are presented through an exact optimization procedure. Then, in the case of harmonic pulse ground motion, where the minimization of the maximum dynamic magnification factor is considered, a numerical optimization procedure is proposed to find the H_infinity optimum design values. Considering 44 earthquake records, each device is optimally designed to reduce the resulting dynamic response of the system to each individual record. Then, utilizing these individual designs, average designs, H2 designs, and H-infinity designs, the performance evaluation of the

devices is presented, including comparisons to the conventional TMD. This study found similar performance in the different inerter-based TMDs considered. Compared to the TMD, the inerter-based TMDs can provide a 7% reduction in RMS response to a white noise ground motion, a 20% reduction in the maximum dynamic magnification factor, and a 5%-8% reduction in the RMS of the primary structure’s displacement subjected to real earthquake records.

Introduction

Tuned mass dampers have been proposed since 1909 and are designed to mitigate the effects of resonance [13]. Conventional TMDs consist of a small secondary or auxiliary mass, connected to a primary structure through a spring and dashpot. When the TMD is optimally designed (tuned), it can lessen the maximum amplitude and variance related to the response of a structure in the mode the TMD is tuned to [14]. The purpose of the design of TMDs is to find the stiffness and damping values that optimizes the response of the system they are incorporated in to that results from dynamic loads. There have been many studies on the optimum design of TMDs, including ones that have a goal to minimize the maximum amplitude of the dynamic response of single- and multi-degree of freedom primary structures [14,84,93,94]. In the case of random excitation, it is more common to find the optimum design values by minimizing the resulting variance of the primary structure’s response [18,20,21,36,84] . As TMDs are typically tuned to the first mode of the structure and are sensitive to detuning [106], multi tuned mass damper in parallel and series connection have been proposed and investigated [36–38,41,95].

TMDs are typically more effective for the passive control of structures when large secondary mass ratios are utilized [6,7]. Thus, the improvement of the TMD, and other structural control devices, by utilizing the inerter to produce large effective inertia mass has been recently proposed. The inerter, also described as a rotational inertial mass, is a two terminal mechanical device that produces resistive forces at its terminals that are equal and proportionally related to the relative acceleration between its terminals [54,96]. Through applying an inerter with a ball-screw mechanism rotating in a viscous fluid, the rotational inertia viscous damper (RIVD) has been introduced and studied for the passive control of structures when incorporated into toggle bracing systems [8]. The tuned viscous mass damper (TVMD) has been proposed in the same context by adding a spring to the RIVD and has shown promising performance for the control of SDOF and MDOF structures against seismic loads [52,97]. Similarly, the tuned inerter damper (TID), which consists of an inerter connected to a parallel spring and damper was proposed for the vibration suppression of frame structures [71]. The performance evaluation and optimum design of RIVD, TVMD, and TID as interstory control devices for MDOF structures, has been investigated [72] and the results show the superiority of the inerter-based devices compared to viscous dampers. In addition, the effect of inerters on the frequency, mode shapes, and displacement of MDOF structures has been studied through analytical approaches [55,70]. Research on inerter-based devices are not limited to building structures and has recently been extended to the passive control of cables and beams [73,75].

Studies on the improvement of TMDs by utilizing inerters can be divided into two categories of enhanced TMDs. In the first category, which most prominently features the tuned mass damper-inerter (TMDI), the inerter is attached between the secondary mass of a TMD and a support [63]. Studies on the TMDI for seismic applications, wind and non-stationary excitation show significant effectiveness compared to conventional TMDs. To further enhance the TMDI performance, the three-element vibration absorber-inerter (TEVAI) has been proposed [98]. Despite the high effectiveness of the TMDI and TEVAI, the need for the inerter to be connected between the secondary mass and an external support leads to significant questions over the feasibility of this category of devices for many applications.

In the second category of enhanced TMDs, the dashpot of the TMD is substituted with an inerter-based device. This category of devices is classified as “inerter-based dynamic vibration absorbers"[10], and designated herein as "inerter-based tuned mass dampers". The rotational inertia double tuned mass damper (RIDTMD) has been proposed through substituting the dashpot of a TMD with a TVMD. Accordingly, optimum designs of RIDTMD for harmonic and random vibration have been investigated and shows superior performance compared to TMDs [9,58,99] In the same context and by replacing the dashpot in TMDs with six different arrangements of inerter-based devices, six configurations of inerter-based tuned mass dampers were introduced [10]. All six inerter-based TMDs were optimally designed for minimizing the response's variance and maximum amplitude when the primary structure was subjected to a force excitation.

Previous designs for minimizing the response of structures to ground excitations with inerter-based TMDs are limited to ones that have considered only white noise and harmonic loads [10,100]. In addition, the design for random ground excitation proposed in [101] utilized an exact optimum design method that considered four design values and needed high computational effort. Despite these recent studies, the design of inerter-based TMDs considering ground excitation has not been comprehensively investigated yet, particularly when considering seismic ground motion and alternative optimum design methodologies.

The present study focuses on the optimum design and performance evaluation of three recently developed configurations of inerter-based TMDs [9,10]. This study is organized as follows. In Section 2, the inerter-based TMDs considered are formulated. Section 3 presents the analytical optimum design procedure and performance evaluation of the three configurations of inerter-based TMDs for the case of random ground excitation. In Section 4, optimization and performance evaluation of the three configurations of inerter-based TMDs is presented for the case of harmonic ground acceleration. In Section 5, the capabilities of the inerter-based TMDs for reducing the RMS of the response considering seismic ground excitation is presented and comparisons are made with the performance of conventional TMDs. Finally, in Section 6, the major findings of this work are outlined and potential future research directions are presented.

Inerter –based tuned mass dampers

This section provides the formulation for the TMD, the inerter, and the three configurations of inerter-based TMDs considered. These configurations feature the parallel or series connection of an inerter, damper, and spring [10] and their design and optimization under force excitation scenarios has been previously considered [101].

Figure 4-1 depicts depicts a TMD attached to a SDOF structure subjected to a ground acceleration, $\ddot{x}_g$, and with the structure's mass, damping and stiffness equal to m_s , c_s , and k_s , respectively. The TMD's mass m_1 is connected to the structure through a spring with stiffness equal to k_1 and dashpot with viscous damping coefficient equal to c_1 .

In order to find the equation of motion and transfer function of inerter-based tuned mass dampers, the inerter will first be briefly introduced. The inerter is a two terminal mechanical device that transfers translational motion to the rotational motion of a flywheel. The terminals of the inerter develop equal and opposite forces proportional to the relative acceleration at the terminals [54,96]. By this definition, an ideal inerter holds the following relationship:

$$F = b\left(\ddot{x}_j - \ddot{x}_i\right) \tag{4.1}$$

where, $\ddot{x}_j$ and $\ddot{x}_i$ denote the acceleration of the node j and i respectively and b is the constant referred to as the inertance or effective inertia mass. The rack and pinion mechanism (see Figure 4-2 and ball screw mechanism are two of the most common mechanisms that have been used to form an inerter [8,9,52]. Considering the equilibrium of the inerter shown in Figure 4-2, the following equation holds:

$$Fr = J\ddot{\theta} \tag{4.2}$$

In Eq. (4.2), F , J , and stands for force, moment of inertia of the flywheel ($\frac{1}{2}m_0R^2$), and rotational acceleration of the flywheel. Furthermore, the relationship between the relative displacement and the rotation of the flywheel holds as:

$$\theta = \frac{x_j - x_i}{r} \tag{4.3}$$

Substituting Eq. (4.3) into Eq. (4.2) gives the following equation of motion for the inerter with rack and pinion mechanism:

$$\frac{R^2}{2r^2} m_0 \left(\ddot{x}_j - \ddot{x}_i \right) = F \tag{4.4}$$

From Eq. (4.1) and Eq. (4.4), the inertance, $b = \frac{R^2}{2r^2} m_0$, is shown to be a function of the geometry of the inerter and the physical mass of the flywheel, m_0 . This, perhaps small, physical mass is amplified by the coefficient $\frac{R^2}{2r^2}$. By configuring the parameters of the device, a wide range of mass amplification is possible; for example, mass amplification equal to 175 and 3300 times have been reported in experimental studies [52,102].

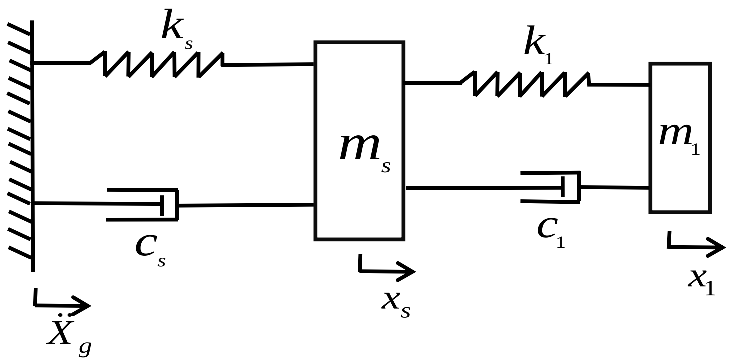

Figure 4-1: Traditional tuned mass damper (TMD)

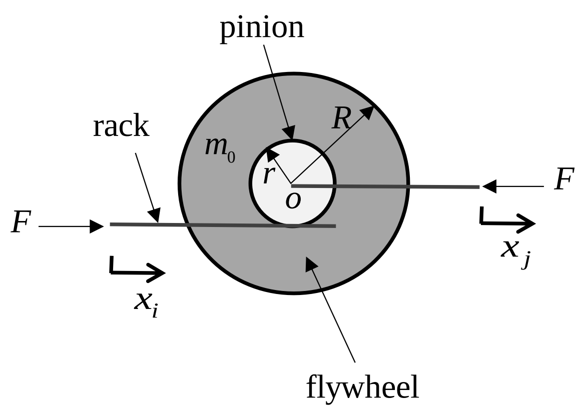

Figure 4-2: Inerter device with rack and pinion mechanism

Inerter –based tuned mass dampers (C1)

Figure 4-3 shows the inerter-based tuned mass dampers (C1) attached to a SDOF system. The addition of C1, with a dashpot, spring and inerter connected in series, makes the system a three-degree-of-freedom system

The equation of motion for this system can be written as follow:

$$
\begin{aligned}
&m_s\ddot{x}_s + c_s\dot{x}_s + k_s x_s + k_1(x_s - x_1) + c_2(\dot{x}_s - \dot{x}_3) = -m_s\ddot{x}_g(t) \\
&m_1\ddot{x}_1 + k_1(x_1 - x_s) + b(\ddot{x}_1 - \ddot{x}_2) = -m_1\ddot{x}_g(t) \\
&b(\ddot{x}_2 - \ddot{x}_1) + k_2(x_2 - x_3) = 0 \\
&c_2(\dot{x}_3 - \dot{x}_s) + k_2(x_3 - x_2) = 0
\end{aligned} \tag{4.5}
$$

In this case, and throughout this paper, $m_2 = \frac{R^2}{2r^2} m_0$, which is the inertance mass. k_2 and c_2 are the damping and stiffness of the inerter-based device and $\ddot{x}_g$ denotes the ground acceleration of the primary structure.

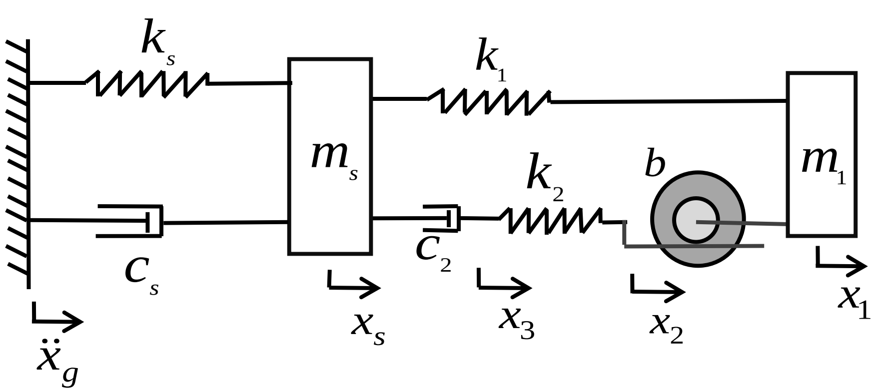

Figure 4-3 : Inerter based tuned mass dampers (C1)

Inerter –based tuned mass dampers (C2)

Substituting the dashpot in TMDs with an inerter connected in series with a parallel spring and dashpot, gives inerter-based TMD C2 (see Figure 4-4).

The equation of motion for this system can be written as follows:

$$\begin{aligned} &m_s\ddot{x}_s + b(\ddot{x}_s - \ddot{x}_2) + c_s\dot{x}_s + k_s x_s + k_1(x_s - x_1) = -m_s\ddot{x}_g(t) \\ &m_1\ddot{x}_1 + c_2(\dot{x}_1 - \dot{x}_2) + k_2(x_1 - x_2) + k_1(x_1 - x_s) = -m_1\ddot{x}_g(t) \\ &b(\ddot{x}_2 - \ddot{x}_s) + c_2(\dot{x}_2 - \dot{x}_1) + k_2(x_2 - x_1) = 0 \end{aligned} \tag{4.6}$$

Inerter –based tuned mass dampers (C3)

Figure 4-4 depicts the third inerter-based TMD (C3), where the dashpot in the TMD is substituted with a spring in series with a parallel dashpot and inerter.

This configuration is also called the RIDTMD and has been investigated recently when the primary structure is subjected to force and ground random excitation [58]. However, the design for minimization of the maximum amplitude and the performance evaluation considering the reduction of the maximum amplitude have not been considered in the previous studies. Eq. (4.7) presents the equations of motion for this inerter-based TMD.

$$\begin{aligned} &m_s\ddot{x}_s + c_s\dot{x}_s + k_s x_s + k_1(x_s - x_1) + k_2(x_s - x_2) = -m_s\ddot{x}_g(t) \\ &\ddot{x}_1 m_1 + m_2(\ddot{x}_1 - \ddot{x}_2) + c_2(\dot{x}_1 - \dot{x}_2) + k_1(x_1 - x_s) = -m_1\ddot{x}_g(t) \\ &m_2(\ddot{x}_2 - \ddot{x}_1) + c_2(\dot{x}_2 - \dot{x}_1) + k_2(x_2 - x_s) = 0 \end{aligned} \tag{4.7}$$

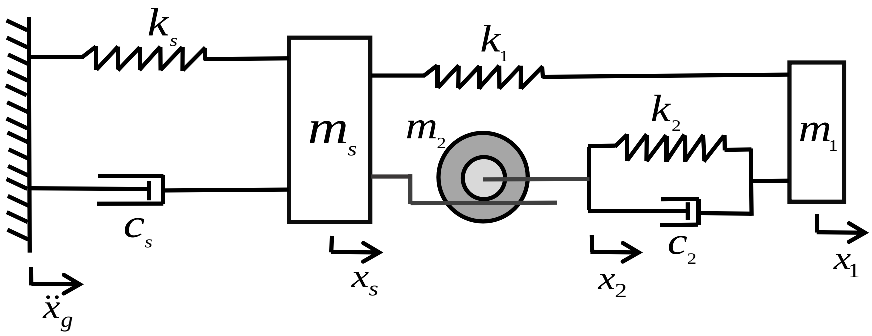

Figure 4-4: Inerter based tuned mass dampers (C2)

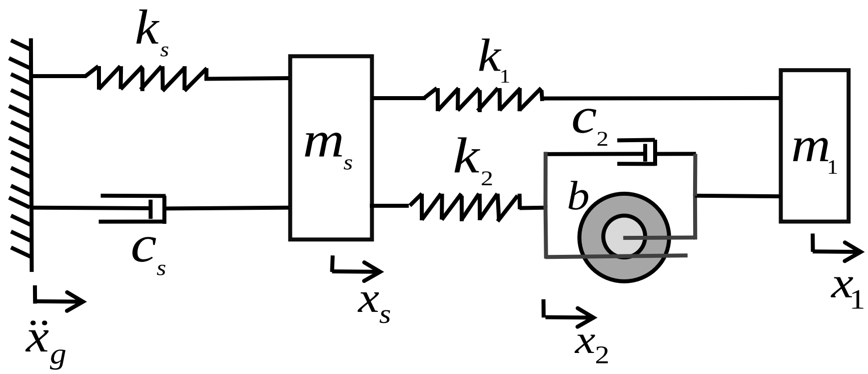

Figure 4-5: Inerter based tuned mass dampers (C3)

Transfer functions of C1, C2, and C3

In In order to determine generic transfer functions for the inerter-TMDs in the frequency domain, the following parameters are defined and used throughout this study for inerter-based TMDs C1, C2, and C3:

$\omega_s = \sqrt{\dfrac{m_s}{k_s}}$: The primary structure frequency, $\omega_1 = \sqrt{\dfrac{m_1}{k_1}}$: The main system frequency

$\omega_2 = \sqrt{\dfrac{m_2}{k_2}}$: The secondary system frequency, $\zeta = \dfrac{c_2}{2m_2\omega_2}$: The secondary damping ratio

$\mu_1 = \dfrac{m_1}{m_s}$: Main mass ratio; $\mu_2 = \dfrac{m_2}{m_1}$: Inertance mass ratio

$\lambda = \dfrac{\omega}{\omega_s}$: Input frequency ratio; $\alpha_1 = \dfrac{\omega_1}{\omega_s}$: first frequency ratio; $\alpha_2 = \dfrac{\omega_2}{\omega_s}$: secondary frequency ratio

Note that for the TMD the parameters are:

$\alpha = \dfrac{\omega_1}{\omega_s}$: Frequency ratio, $\zeta = \dfrac{c_1}{2m_1\omega_1}$: the TMD damping ratio , $\mu_1 = \dfrac{m_1}{m_s}$: Main mass ratio

Transfer functions for the C1, C2, and C3 can be achieved by considering $x_s = X_s e^{i\omega t}$, $x_a = X_a e^{i\omega t}\left(a = 1,2,3\right)$, $\ddot{x}_g = A_0 e^{i\omega t}$, and ($c_s = 0$) as follows:

$$H\left(i\lambda\right) = \frac{X_S}{A_0} = \frac{p_4\lambda^4 + p_3\lambda^3 + p_2\lambda^2 + p_1\lambda + p_0}{q_6\lambda^6 + q_4\lambda^4 + q_2\lambda^2 + q_0} \tag{4.8}$$

The coefficients of the Eq (4.8) in case of C1 can be express as following:

$$p_4 = 2\zeta;\, p_3 = -i\alpha_2;\, p_2 = -2\left(\left(\mu_2\mu_1 + \mu_2 + 1\right)\alpha_2^{\,2} + \alpha_1^{\,2}(\mu_1 + 1)\right)\zeta;$$
$$p_1 = i\alpha_1^{\,2}\alpha_2(\mu_1 + 1);\, p_0 = +2\zeta\alpha_1^{\,2}\alpha_2^{\,2}(\mu_1 + 1)$$
$$q_6 = 2\zeta;\, q_5 = -i\alpha_2;\, q_4 = -2\left(\left(\mu_2\mu_1 + \mu_2 + 1\right)\alpha_2^{\,2} + 1 + \alpha_1^{\,2}(\mu_1 + 1)\right)\zeta;$$
$$q_3 = i\alpha_2\left(1 + \alpha_1^{\,2}\left(\mu_1 + 1\right)\right);\, q_2 = 2\left(\left(\alpha_1^{\,2}\left(\mu_1 + 1\right) + \mu_2 + 1\right)\alpha_2^{\,2} + \alpha_1^{\,2}\right)\zeta;$$
$$q_1 = -i\alpha_1^{\,2}\alpha_2;\, q_0 = -2\zeta\alpha_1^{\,2}\alpha_2^{\,2} \tag{4.9}$$

The coefficients of the Eq. (4.8) in the case C2 are:

$$p_4 = 1;\, p_3 = -2i\zeta\alpha_2\left(\mu_2\mu_1 + \mu_2 + 1\right);\, p_2 = \left(\left(\mu_2\mu_1 + \mu_2 + 1\right)\alpha_2^{\,2} + \alpha_1^{\,2}\left(\mu_1 + 1\right)\right);$$
$$p_1 = -2i\zeta\alpha_2\alpha_1^{\,2}\left(\mu_1 + 1\right);\, p_0 = +2\zeta\alpha_1^{\,2}\alpha_2^{\,2}(\mu_1 + 1)$$
$$q_6 = 2\zeta;\, q_5 = -2i\zeta\alpha_2\left(\mu_2\mu_1 + \mu_2 + 1\right);\, q_4 = -\left(\left(\mu_2\mu_1 + \mu_2 + 1\right)\alpha_2^{\,2} + 1 + \alpha_1^{\,2}\left(\mu_1 + 1\right)\right);$$
$$q_3 = 2i\zeta\alpha_2\left(\alpha_1^{\,2}\left(\mu_1 + 1\right) + \mu_2 + 1\right);\, q_2 = -\left(\left(\left(-\mu_1 - 1\right)\alpha_1^{\,2} - \mu_2 - 1\right)\alpha_2^{\,2} - \alpha_1^{\,2}\right);$$
$$q_1 = -2i\zeta\alpha_1^{\,2}\alpha_2;\, q_0 = -\alpha_1^{\,2}\alpha_2^{\,2} \tag{4.10}$$

The coefficients of the Eq. (4.8) in the case C3 are:

$$p_4 = 1;\, p_3 = -2i\zeta\alpha_2;\, p_2 = \left(\left(-\mu_2\mu_1 - \mu_2 + 1\right)\alpha_2^{\,2} - \alpha_1^{\,2}\left(\mu_1 + 1\right)\right);$$
$$p_1 = 2i\zeta\alpha_2\alpha_1\left(\mu_1 + 1\right)\left(\alpha_2^{\,2}\mu_2 + \mu_1^{\,2}\right);\, p_0 = +\alpha_1^{\,2}\alpha_2^{\,2}\left(\mu_1 + 1\right)$$
$$q_6 = 1;\, q_5 = +2i\zeta\alpha_2;\, q_4 = \left(\left(-1 + \left(-\mu_1 - 1\right)\mu_2\right)\mu_2^{\,2} - 1 + \left(-\mu_1 - 1\right)\alpha_1^{\,2}\right);$$
$$q_3 = 2i\zeta\alpha_2\left(\left(\mu_1 + 1\right)\mu_2\alpha_2^{\,2} + 1 + \alpha_1^{\,2}\left(\mu_1 + 1\right)\right);\, q_2 = \left(\left(\alpha_1^{\,2}\left(\mu_1 + 1\right) + \mu_2 + 1\right)\alpha_2^{\,2} + \alpha_1^{\,2}\right);$$
$$q_1 = -2i\zeta\left(\alpha_2^{\,2}\mu_2 + \alpha_1^{\,2}\right)\alpha_2;\, q_0 = -\alpha_1^{\,2}\alpha_2^{\,2} \tag{4.11}$$

In these equations, $i = \sqrt{-1}$ denotes the complex number.

The next two sections cover the optimum design and performance evaluation of inerter-based TMDs under different ground acceleration conditions utilizing the transfer functions for the inerter-based TMDs presented in this section.

Random Ground Excitation and H2 Optimum Designs

In this section, the analytical optimum design and performance evaluation of the inerter-based TMDs when the primary structure is subjected to random ground excitation is presented.

The goal of the optimum design of inerter-based TMDs is to find the damping, stiffness, and the inertance mass ratio of the absorber (c_2, k_1, k_2, b) to satisfy the optimization criterion. When the primary structure is subjected to random excitation, it is often more desirable to optimize the mean square of the primary structure response, which is also called H2 optimization in the literature [21,29,41,53,84,94]. In addition to the optimum design of the case C3 (RIDTMD) [58], another exact solution optimization of these devices have been proposed [101] recently. However, the method proposed in [101] is prohibitively complex. [101] While the previous optimization in [101], considers 4 parameters (c_2, k_1, k_2, b) as the optimum design values, the proposed method considers three design values (c_2, k_1, k_2) in the optimization and a sweep over b to reduce the computational cost and complexity of the optimization.

Considering unit white noise as input, the H2 norm and variance of the primary structure displacement response are equivalent [103]. Therefore, the H2 optimization problem can be express as the optimization of the variance of the response as follows [84]:

$$\bar{\sigma}^2 = \frac{1}{2\pi}\int_{-\infty}^{\infty} \left|H(i\lambda)\right|^2 d\lambda \tag{4.12}$$

where $\left|H(i\lambda)\right|$ is the magnitude of the transfer function. In order to solve the integration, it is more convenient to write $\left|H(i\lambda)\right|^2$ as follows:

$$\left|H(i\lambda)\right|^2 = \frac{\left(\mathrm{Im}\left|H(i\lambda)_n\right|\right)^2 + \left(\mathrm{Re}\left|H(i\lambda)_n\right|\right)^2}{\left(\mathrm{Im}\left|H(i\lambda)_d\right|\right)^2 + \left(\mathrm{Re}\left|H(i\lambda)_d\right|\right)^2} \tag{4.13}$$

Note that in Eq. (4.13), $\mathrm{Im}\left|H(i\lambda)_n\right|$ and $\mathrm{Im}\left|H(i\lambda)_d\right|$ are the imaginary part of the numerator and denominator of the transfer function, respectively, and $\mathrm{Re}\left|H(i\lambda)_n\right|$ and $\mathrm{Re}\left|H(i\lambda)_d\right|$ represent the real part of the numerator and denominator of the transfer function, respectively.

Eq. (4.13) can be rewritten in the following form:

$$\left|H(i\lambda)\right|^2 = \frac{g(\lambda)}{h(\lambda)h(-\lambda)} \tag{4.14}$$

Note that in Eq. (4.14) $g_n(\lambda) = b_0\lambda^{2n-2} + b_1\lambda^{2n-4} + \ldots.. + b_{n-1}$ and $h(\lambda) = a_0\lambda^n + a_1\lambda^{n-1} + \ldots + a_n$ are two $2n-2$ and n order polynomials, respectively. As all roots of $h(\lambda)$ lie in the upper half-plane, the integration can be solved using Cauchy residue theorem [21,28,29]. Accordingly, the variance of the response can be express as follows:

$$\bar{\sigma}^2 = \frac{1}{2\pi}\int_{-\infty}^{\infty}\left|H(i\lambda)\right|^2 d\lambda = \frac{1}{2\pi}\int_{-\infty}^{\infty}\frac{g(x)\,d\lambda}{h(\lambda)h(-\lambda)} = \frac{i}{2a_0}\frac{M_n}{\Delta_n} \tag{4.15}$$

where

$$\Delta_n = \begin{vmatrix} a_1 & a_3 & a_5 & & 0 \\ a_0 & a_2 & a_4 & & 0 \\ 0 & a_1 & a_3 & & 0 \\ \vdots & & & \ddots & \\ 0 & 0 & 0 & \cdots & a_n \end{vmatrix} ; M_n = \begin{vmatrix} b_0 & b_1 & b_2 & \cdots & b_{n-1} \\ a_0 & a_2 & a_4 & & 0 \\ 0 & a_1 & a_3 & & 0 \\ \vdots & & & \ddots & \\ 0 & 0 & 0 & \cdots & a_n \end{vmatrix}$$

Note that the detailed and general solution can be found in [100,127].

Eq. (4.15) gives the general exact expression of $\bar{\sigma}^2$. In the case of C1:

$$\bar{\sigma}^2 = 4\left(\mu_1+1\right)\frac{p_1\alpha_2{}^4 + p_2\alpha_2{}^2 + p_3}{\zeta\alpha_2{}^3\mu_1\mu_2} \tag{4.16}$$

where

$$p_1 = \begin{pmatrix} \left(\mu_1+1\right)^4\alpha_1{}^4 - 2\left(\mu_1+1\right)^2\left(\left(\mu_2-1\right)\mu_1+\mu_2+1\right)\alpha_1{}^2 + \ldots \\ \ldots + \left(\mu_2{}^2-\mu_2+1\right)\mu_1{}^2 + \left(2\mu_2{}^2+\mu_2-1\right)\mu_1 + \left(\mu_2+1\right)^2 \end{pmatrix}\zeta^2$$

$$p_2 = \begin{pmatrix} \left(-8\left(\mu_1+1\right)^4\alpha_1{}^4 + 8\left(\mu_1+1\right)^2\left(\left(\mu_2-1\right)\mu_1+\mu_2+2\right)\alpha_1{}^2 - 8\mu_2\mu_1 - 8\mu_2\right)\zeta^2 + \ldots \\ \ldots 1 + \left(\mu_1+1\right)^4\alpha_1{}^4 + \left(\mu_1{}^3 - 3\mu_1 - 2\right)\alpha_1{}^2 \end{pmatrix}$$

$$p_3 = 4\zeta^2\left(1+\left(\mu_1+1\right)^3\alpha_1{}^4 + \left(-2\mu_1-2\right)\alpha_1{}^2\right)$$

In the case of C2:

$$\bar{\sigma}^2 = \frac{p_1\alpha_2{}^4 + p_2\alpha_2{}^2 + p_3}{4\zeta\alpha_1{}^2\alpha_2\mu_2\mu_1} \tag{4.17}$$

where

$$p_1 = \left(\left(\mu_1+1\right)^6\alpha_1{}^6 - 2\left(\mu_1+1\right)^4\left(\left(\mu_2-\frac{3}{2}\right)\mu_1+\mu_2+1\right)\alpha_1{}^4 + \left(\left(2\mu_2{}^2-2\right)\mu_1+\left(\mu_2+1\right)^2\right)\left(\mu_1+1\right)^2\alpha_1{}^2 + \mu_1{}^3\right)$$

$$p_2 = \begin{pmatrix} \left(\mu_1+1\right)^4\left(4\zeta^2\mu_1+4\zeta^2-2\mu_1-2\right)\alpha_1{}^6 - 8\left(\mu_1+1\right)^3\begin{pmatrix} \left(\zeta^2\mu_2-\zeta^2-\frac{1}{4}\mu_2+\frac{1}{2}\right)\mu_1 \\ +\zeta^2\mu_2+\zeta^2-\frac{\mu_2}{4}-\frac{1}{2} \end{pmatrix}\alpha_1{}^4 \\ 4\begin{pmatrix} \left(\zeta^2\mu_2{}^2+\left(-\zeta^2+\frac{1}{4}\right)\mu_2+\zeta^2-\frac{1}{2}\right)\mu_1{}^2+\left(2\zeta^2\mu_2{}^2+\left(\zeta^2-\frac{1}{4}\right)\mu_2-\zeta^2+\frac{1}{2}\right)\mu \\ {}_1+\left(\mu_2+1\right)\left(\zeta^2\mu_2+\zeta^2-\frac{1}{2}\right)\left(\mu_2+1\right)\alpha_1{}^2 \end{pmatrix} \end{pmatrix}$$

$$p_3 = \left(\mu_1+1\right)^4\alpha_1{}^6 - 2\left(\mu_1+1\right)^2\left(-\frac{\mu_1}{2}+1\right)\alpha_1{}^4 + \alpha_1{}^2$$

Finally, in the case of the C3 inerter-based TMD :

$$\bar{\sigma}^2 = \frac{p_0\alpha_2^{\ 6} + p_1\alpha_2^{\ 4} + p_2\alpha_2^{\ 2} + p_3}{4\zeta\alpha_2^{\ 5}\mu_2\mu_1} \tag{4.18}$$

where

$$p_0 = 4\zeta^2\mu_2^{\ 2}\left(\mu_1+1\right)$$
$$p_1 = \left(\mu_1+1\right)^2\alpha_1^{\ 4} + \left(\left(8\zeta\mu_1+8\zeta^2-2\mu_1-2\right)\mu_2-\mu_1-2\right)\alpha_1^{\ 2} - 8\zeta^2\mu_2+\mu_2^{\ 2}+2\mu_2+1$$
$$p_2 = \left(4\zeta^2\mu_1+4\zeta^2-2\mu_1-2\right)\alpha_1^{\ 4} + \left(-8\zeta^2+2\mu_2+4\right)\alpha_1^{\ 2} + \left(\mu_1-2\right)\mu_2+4\zeta^2-2$$
$$p_3 = 1+\alpha_1^{\ 4}+\left(\mu_1-2\right)\alpha_1^{\ 2}$$

Having obtained the algebraic expressions for $\bar{\sigma}^2$, the next step of the optimum design procedure in [101] is calculating the derivatives of $\bar{\sigma}^2$ with respect to the first frequency ratio, second frequency ratio, damping ratio, and inertance mass ratio and then solving them simultaneously as a system of equations. To simplify the optimization procedure in this study, the inertance mass ratio, is not considered at this point in the optimization. Rather, the optimum first frequency ratio, optimum second frequency ratio and optimum damping ratio are calculated as a function of the inertance mass ratio. Then, these optimum values are evaluated over a range of inertance mass ratios and the optimization values, including the inertance mass ratio, that gives the minimum H2 norm are considered as the optimum design values. Taking this into account, the optimum solution for given main and inertance mass ratios can be found by solving the following equations:

$$\frac{\partial\bar{\sigma}^2}{\partial\alpha_1} = \frac{\partial\bar{\sigma}^2}{\partial\alpha_2} = \frac{\partial\bar{\sigma}^2}{\partial\zeta} = 0 \tag{4.19}$$

For any given main mass ratio considered, these equations can be solved for any arbitrary inertance mass ratio. It was found that in all three cases (C1, C2, and C3), there are specific inertance mass ratios that gives the minimum H2 norm. This inertance mass ratio value and its corresponding optimum values are the H2 optimum design values.

H2 optimum design values for the C1, C2, and C3 inerter-based TMDs are presented in Table 2 for several main mass ratios. These design values give the minimum H2 norm of the primary system's displacement response. These results show the optimum design first frequency ratio is decreasing for all cases by increasing the main mass ratio. The optimum design second frequency ratio decreases by increasing the main mass ratio for C1 and C2. However, the optimum design second frequency ratio for C3 is close to 1 for all of the main mass ratios considered and the optimum design damping ratio is decreasing for C1 and increasing for C2 and C3. In addition, the optimum design damping ratio for C1 is significantly larger than the optimum design damping ratio of the C2 and C3. As shown in the last column of Table 2, the optimum design inertance mass ratios increase by increasing the main mass ratio.

Defining R as the ratio of the H2 norm of the inerter-based TMD to a comparably designed TMD, the results show a 7%-8% reduction in the H2 norm for the inerter-based TMDs compared to the TMD.

Figure 4-6 shows how the optimum H2 value varies by increasing the main mass ratio. Results show there is not a noteworthy difference between the C1, C2 and C3 performance. There is good agreement between these results, which considers base excitation, and previous studies, which considered force excitation [10].

Table 2: H2 optimum design values for inerter based tuned mass dampers C1, C2, and C3

	μ_1	α_1	α_2	ζ	μ_2	H2	R
C1	0.01	0.9863	0.9912	2.8691	0.02	2.9621	0.930
	0.02	0.9729	0.9825	2.0168	0.04	2.5069	0.930
	0.03	0.9599	0.9743	1.6639	0.059	2.2798	0.929
	0.04	0.9469	0.9657	1.4271	0.079	2.1350	0.929
	0.05	0.9343	0.9575	1.2785	0.098	2.01317	0.920
C2	0.01	0.9899	0.9811	0.0820	0.019	2.9672	0.931
	0.02	0.9798	0.9624	0.1156	0.038	2.5153	0.933
	0.03	0.9698	0.9450	0.1388	0.056	2.2909	0.934
	0.04	0.9597	0.9307	0.1526	0.071	2.1485	0.935
	0.05	0.9498	0.9135	0.1704	0.089	2.0475	0.936
C3	0.01	0.9828	1.002	0.0845	0.019	2.9612	0.930
	0.02	0.9655	1.005	0.1228	0.038	2.5054	0.929
	0.03	0.9490	1.007	0.1491	0.055	2.2777	0.928
	0.04	0.9329	1.0096	0.1687	0.070	2.1324	0.928
	0.05	0.9177	1.0120	0.1881	0.085	2.0287	0.927

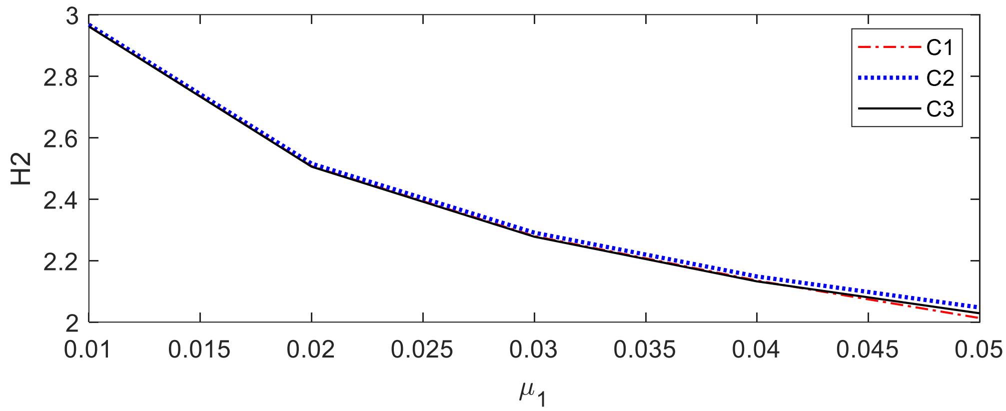

Figure 4-6: H2 optimum values versus main mass ratio

Harmonic Excitation and H-Infinity Optimum Designs

In this section, the numerical optimum design and performance evaluation of the inerter-based TMDs when the primary structure is subjected to a harmonic ground excitation is presented.

The goal of H_infinity optimum design is minimizing the maximum dynamic magnification factor of the primary structure under harmonic load. Minimization of the maximum dynamic magnification factor for TMDs has been studied through approximate, exact, and numerical methods [84,94,104]. For inerter-based TMDs, the numerical H_infinity optimum design when the primary structure is subjected to force excitation is presented in [10]. In addition, the analytical optimization presented in [100] is the extension of the fixed point technique [99], but only considers the force excitation case.

For inerter-based TMDs, the numerical H_infinity optimum design when the primary structure is subjected to force excitation is presented in [94] and extending fixed point technique [99] required rigorous mathematical procedures that can be prohibitively complex, in this work a numerical optimization method is implemented to find the design values.

The maximum amplitude of the transfer function, named as H_infinty norm, is defined as:

$$H_\infty = \left\| H\left(i\lambda\right) \right\|_\infty = \underset{\omega}{Max}\left\{ H\left(i\lambda\right) \right\} \tag{4.20}$$

Consequently, the constrained optimization problem can be expressed as follows:

$$\begin{aligned}
&\text{minimize} \quad \underset{\omega}{Max}\left\{ H\left(i\lambda\right) \right\} \\
&\text{subject to } \left[\alpha_1 \quad \alpha_2 \quad \zeta \quad \mu_2 \right] \\
&\alpha_{1l} \le \alpha_1 \le \alpha_{1u}, \alpha_{2l} \le \alpha_2 \le \alpha_{2u}, \zeta_l \le \zeta \le \zeta_u, \mu_{2l} \le \mu_2 \le \mu_{2u}
\end{aligned} \tag{4.21}$$

Where, subscribe l and u denote the lower and upper bound of the values.

The optimization problem expressed in Eq.(4.21) can be solved by using the fmincon nonlinear programming solver in MATLAB [105]. However, it is more likely to find local optimums instead of the global optimum design if arbitrary bounds and a single initial point are considered. To obtain the global optimum, it is crucial to choose adequate bounds and initial iteration points. That said, this work utilizes a multi-initial point optimization using fmincon and considering the exact H2 norm optimum design values as the first initial points. In addition, 100 random points are considered as alternative initial points between the lower and upper bounds. As the initial points are produced between the upper and lower bounds randomly, it is more beneficial to set these limits reasonably and as small as possible. In this regard, the upper and lower bounds are set to be equal to half and twice the first initial point, respectively. This range of upper and lower bounds is reasonable as the optimum design values of the H2 and Hinfinity designs for TMDs [10] and inerter-based TMDs are close to each other in the case of force excitation loading.

The proposed optimization procedure is conducted for three inerter-based TMDs C1, C2, and C3 considering five main mass ratios. The optimum design values for minimizing the maximum amplitude response for the C1, C2, and C3 inerter-based TMDs are presented in Table 3. The results show the optimum design first frequency ratio is decaying by increasing the main mass ratio in all three cases. The optimum design damping ratio in the cases C1 and C2 is decreasing by increasing the main mass ratio and decreasing by increasing the main mass ratio in the case of C3. It can be seen also by increasing the main mass ratio, a larger optimum inertance mass ratio is needed in all three cases. P is defined as the ratio of the maximum displacement of the structure with an inerter-based TMD to the maximum displacement of the structure with an equivalently designed TMD. From the ratio P shown in Table 3. an approximately 25% reduction in the maximum displacement for each of the inerter-based TMDs considered, compare to the TMD, is observed

.Figure 4-6 shows how the optimum maximum displacement changes by increasing the main mass ratio. Similar to the H2 design performance, Results show there are not significant difference between the C1, C2 and C3 performance in this case.

Table 3: optimum design values of inerter tuned mass dampers for minimizing the maximum amplitude response

	μ_1	α_1	α_2	ζ	μ_2	H_∞	P
C1	0.01	0.9861	0.9906	2.2344	0.0243	11.0637	0.743
	0.02	0.9724	0.9825	1.6253	0.0470	7.8863	0.740
	0.03	0.9591	0.9715	1.2951	0.0719	6.5252	0.741
	0.04	0.9458	0.9639	1.1214	0.0953	5.6966	0.739
	0.05	0.9329	0.9538	0.9791	0.1216	5.1516	0.739
C2	0.01	0.9920	0.9788	0.1093	0.0239	11.1045	0.746
	0.02	0.9833	0.9591	0.1479	0.0457	7.9734	0.748
	0.03	0.9749	0.9395	0.1784	0.0676	6.6134	0.751
	0.04	0.9661	0.9198	0.2004	0.0876	5.8971	0.765
	0.05	0.9574	0.9023	0.2202	0.1076	5.2769	0.757
C3	0.01	0.9801	1.0035	0.1107	0.0235	11.0352	0.739
	0.02	0.9613	1.0062	0.1513	0.0441	7.8817	0.737
	0.03	0.9419	1.0122	0.1893	0.0652	6.4876	0.736
	0.04	0.9234	1.0159	0.2178	0.0840	5.6729	0.736
	0.05	0.9064	1.0186	0.2374	0.0996	5.1201	0.735

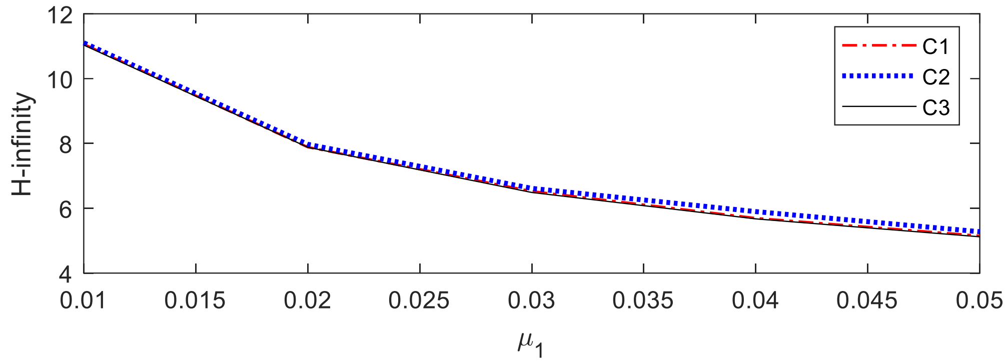

Figure 4-7: H-Infinity optimum values versus main mass ratio

Seismic excitation

In this section, the capacity of the inerter-based TMDs to reduce the RMS and maximum displacement of the primary structure subjected to seismic excitation is studied. While this section is not intended to provide a comprehensive seismic evaluation, it aims to compare the performance of these devices under seismic excitations considering different types of inerter-based TMD, differences in design methodology, and the performance of conventional TMDs.

When evaluating the seismic performance of the inerter-based TMDs considered, the actual loading used in determining the design values is an important consideration. One option is to consider the seismic excitation as white noise and use optimum design values for random white noise excitation [63,72,89]. Another option is to find the optimum design values through numerical optimizations with real earthquake records as the input excitations [106,107]. In this section, both methods are considered and the results are compared to evaluate the differences in their performance.

While the white noise design of these systems has been discussed in the previous section, the design of the inerter-based TMDs considered using earthquake records is described in this section. For this design, 44 earthquake records are considered as the input loads. These records are the FEMA far-field records without scale factors that have been previously used in the design and performance evaluation of TMDs[106] An undamped SDOF structure with frequency equal to 0.8 Hz is considered as the primary structure for this analysis [23].

Considering the minimization of the RMS of the primary structure's displacement response as the objective function, the numerical optimization problem for inerter-based TMDs C1, C2 and C3 can be expressed as follows:

$$\begin{aligned}&\text{minimize} \quad Rms\left(x_s\right)\\&\text{subject to } \left[\alpha_1 \quad \alpha_2 \quad \zeta \quad \mu_2\right]\\&\alpha_{1l} \le \alpha_1 \le \alpha_{1u}, \alpha_{2l} \le \alpha_2 \le \alpha_{2u}, \zeta_l \le \zeta \le \zeta_u, \mu_{2l} \le \mu_2 \le \mu_{2u}\end{aligned} \tag{4.22}$$

In order to avoid local optimum points, the multi-initial point optimization method is considered for each optimization and the H2 optimum design values are considered as the first initial points. Then, for each ground motion, the design values $(\alpha_1, \alpha_2, \zeta, \mu_2)$ are obtained by numerically preforming the optimization defined by Eq. (4.22). In the next step, the average of all 44 optimum design value sets are considered as the possible overall best optimum design values of the specific inerter-based TMD for that structure. In other words, for each type of inerter-based TMD considered, a set of 44 optimum design values are obtained by individually considering 44 earthquakes and then the average seismic optimal design values are obtained from averaging the values in these 44 sets.

Utilizing 44 sets of optimum designs, by definition, the minimum RMS of the response is obtained for each record. The average optimum design and H2 design values were also utilized to calculate the RMS response when subjected to each seismic load. These results and the RMS of the response utilizing the H2 optimum design are presented in Figure 4-8. While the expected large differences in the resulting RMS of the response for different earthquakes is observed, very small differences (typically around 0.1%) are seen in the resulting RMS for the C1, C2, and C3 inerter-based TMD. Furthermore, these results show that by utilizing the individual design values, the RMS of the response is, on average, 10% less than the RMS of the response utilizing the average design and H2 optimum design values. In addition, the response from the H2 optimum design and average design values are approximately 1% different, on average. Having said that, the H2 optimum design values are chosen for the later performance evaluation of the devices compared to TMDs.

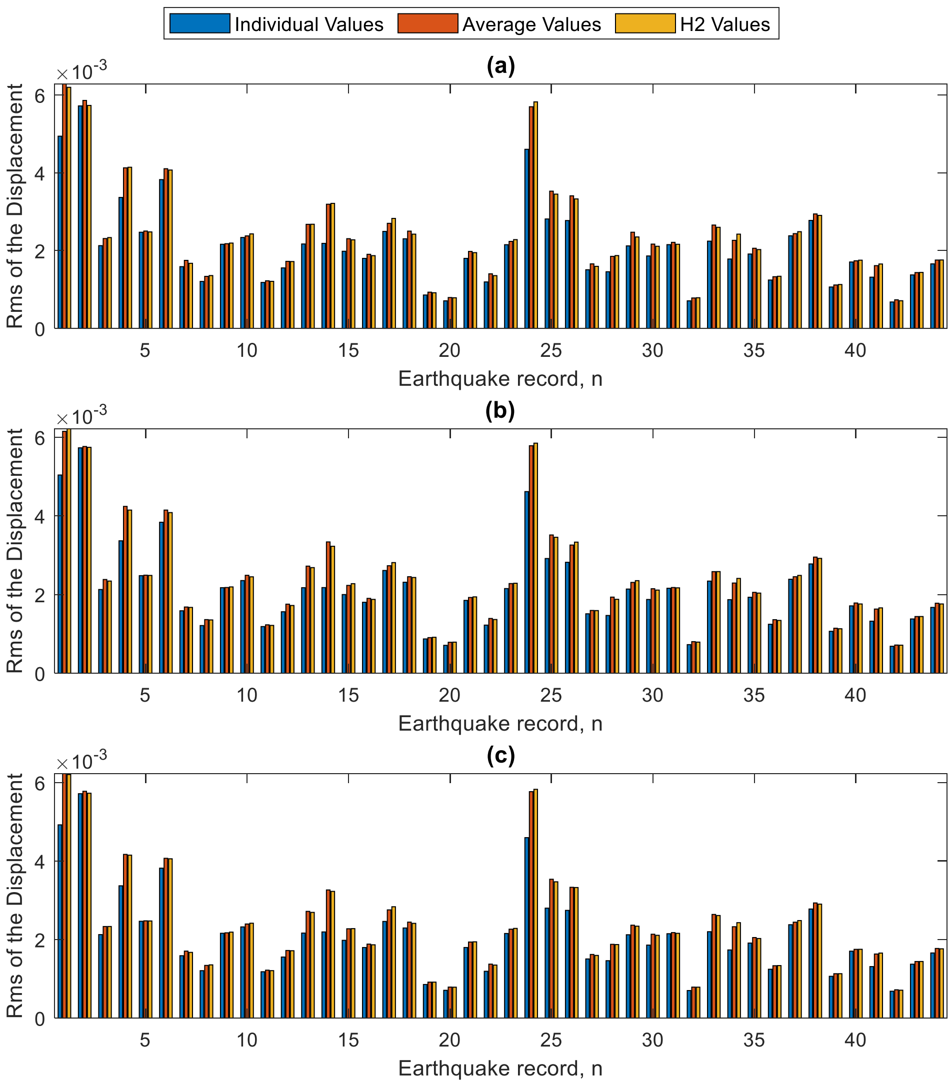

Figure 4-8: RMS of the response in case of individual design values, average deign values and H2 design values. (a) C1, (b) C2, and (c) C3

Having said that, the H2 optimum design values are chosen for the later performance evaluation of the devices compared to TMDs.

Considering the maximum displacement of the primary structure as the objective function, the numerical optimization problem for the C1, C2, and C3 inerter-based TMDs can be expressed as follows:

$$\begin{aligned} &\text{minimize} \quad \text{Max}\{x_s\} \\ &\text{subject to } \left[\alpha_1 \quad \alpha_2 \quad \zeta \quad \mu_2\right] \\ &\alpha_{1l} \le \alpha_1 \le \alpha_{1u}, \alpha_{2l} \le \alpha_2 \le \alpha_{2u}, \zeta_l \le \zeta \le \zeta_u, \mu_{2l} \le \mu_2 \le \mu_{2u} \end{aligned} \tag{4.23}$$

Similar to the optimization minimizing the RMS and to avoid local optimum points, a multi-initial point optimization is considered for each of these optimizations as well. For each case the design values $(\alpha_1, \alpha_2, \zeta, \mu_2)$ are obtained by numerically preforming the optimization defined by Eq.(4.23) . In the next step, the average of all 44 optimum design value sets are considered as the average optimum design values.

For each of the inerter-based TMDs considered, the maximum displacement of the response of the primary structure is obtained for each of the 44 earthquakes with the individual maximum displacement optimum designs for each particular earthquake. Then, utilizing the average maximum displacement optimum design values, the maximum displacement of the primary structure subjected to each of the earthquakes is determined. These results and the maximum displacement response utilizing the H-infinity optimum design values are presented in Figure 4-9. These results again show similar performance between the C1, C2 and C3 inerter-based TMD.

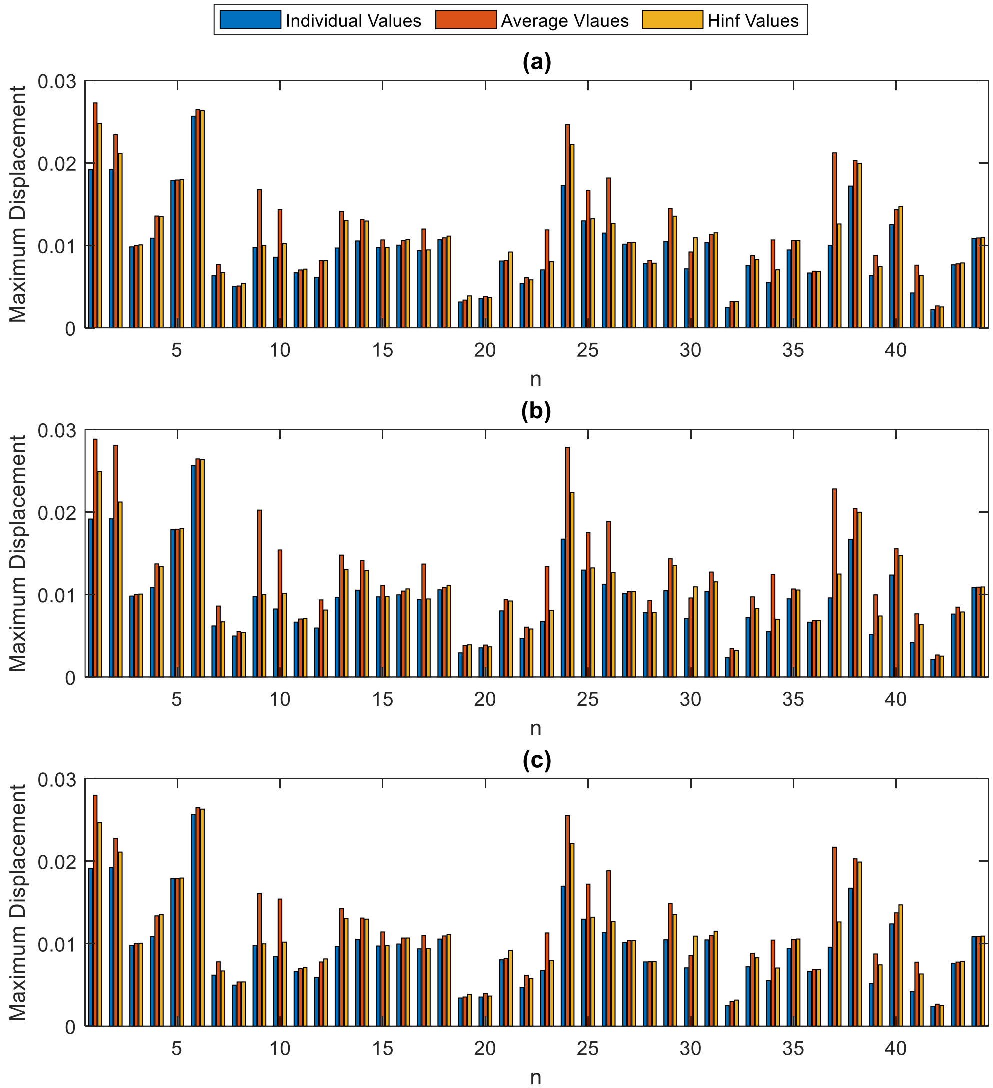

Figure 4-9: Maximum displacement of the response in case of individual design values, average deign values and H-infinity design values. (a) C1, (b) C2, and (c) C3

Additionally, by utilizing the individual design values, the maximum displacement of the response is, on average, 25% less than the maximum of the responses considering the average value designs. This difference indicates these devices are sensitive to detuning when optimally designed for specific seismic records when minimizing the maximum displacement is the goal. In addition, the H-Infinity design provides, on average, a maximum that is 13% less than what results from the average design and 15% higher then what results from the individual design values. Comparing the H-infinity design values and average design values, H-infinity design provide good performance and can be feasibly considered in a seismic design; thus, they are chosen for the later performance evaluation of the devices compared to TMDs.

In order to further evaluate the inerter-based TMDs, comparisons to the effectiveness of the conventional TMD can be made. To make these comparisons, in addition to responses with the inerter-based TMDs, the responses of the considered primary structure with a TMD with the same secondary mass ratio were also calculated when subjected to the same suite of 44 seismic ground motions. For this analysis, H2 optimum design values for the TMD [84] and C1, C2, and C3 inerter-based TMDs were used. The ratio of the RMS of the displacement response of the primary structure with the C1, C2, and C3 inerter-based TMDs to the RMS of the response with the TMD is calculated for each of the 44 earthquakes. The results, which are presented in Figure 4-10, show the generally superior performance of the C1, C2, and C3 inerter-based TMDs in comparison to the TMDs in the reduction of the RMS response subjected to the 44 earthquake records. These results show up to a 15% reduction and an average 7% reduction in the H2 norm of the response by utilizing inerter-based TMDs compared to the conventional TMDs.

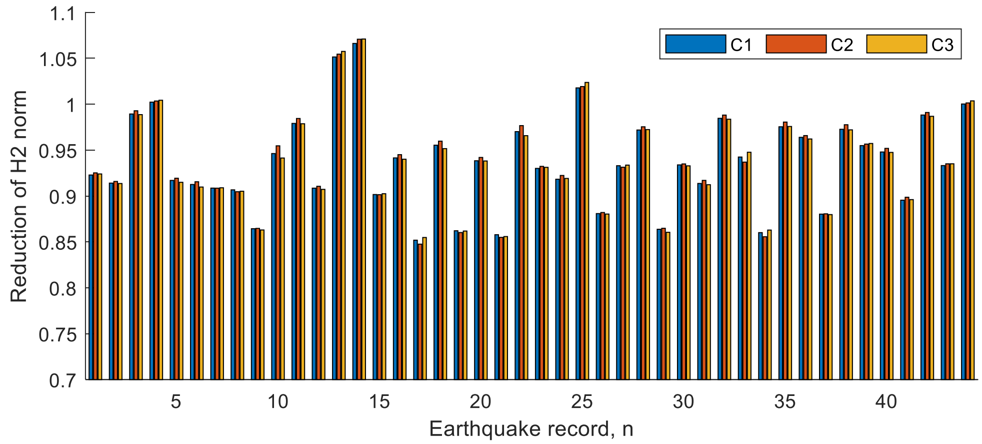

Figure 4-10: Reduction factor of the H2 norm compare to the C1, C2 and C3

This amount of reduction for the C1, C2, and C3 inerter-based TMDs is similar to the results observed in the random excitation case. While there is variability in the performance of the inerter-based TMDs, compared to the TMD, the TMD shows superior performance in only 4 of the 44 records.

Utilizing the H-Infinity optimum design values of the TMDs [84], the maximum response of the primary structure with a TMD are calculated when subjected to the 44 earthquake records. Utilizing H-Infinity values for the C1, C2, and C3 inerter-based TMDs, the maximum response of the structure subjected to the 44 records is also obtained. Then, the ratio of the maximum displacement of the structure with the C1, C2, and C3 inerter-based TMDs to the maximum displacement of the structure with the TMD is calculated. The results, which are presented in Figure 4-11 , show that the average maximum displacement reduction performance of the C1, C2, and C3 inerter-based TMDs in comparison to the TMDs is more minor in this case with an average reduction of only 2%-3%. This amount of reduction is similar for C1, C2, and C3 and less than the reduction when the structure is subjected to harmonic load. While the reduction is up to 15% in a few cases, in the response to 10 earthquake records the maximum response of the inerter-based TMDs is 0.1%-5% higher than the TMD.

In order to evaluate the performance of the inerter-based TMDs compared to the uncontrolled structure, 2% damping was included in the primary structure to account for intrinsic damping in the structure and enable the modeling of realistic responses in the uncontrolled structure.

Figure 4-12 shows the comparison between the RMS of the uncontrolled structure and with the TMD, C1, C2 and C3 inerter-based dampers. For this analysis, the previously considered H2 optimized design values (considering the undamped system) are used in the devices.

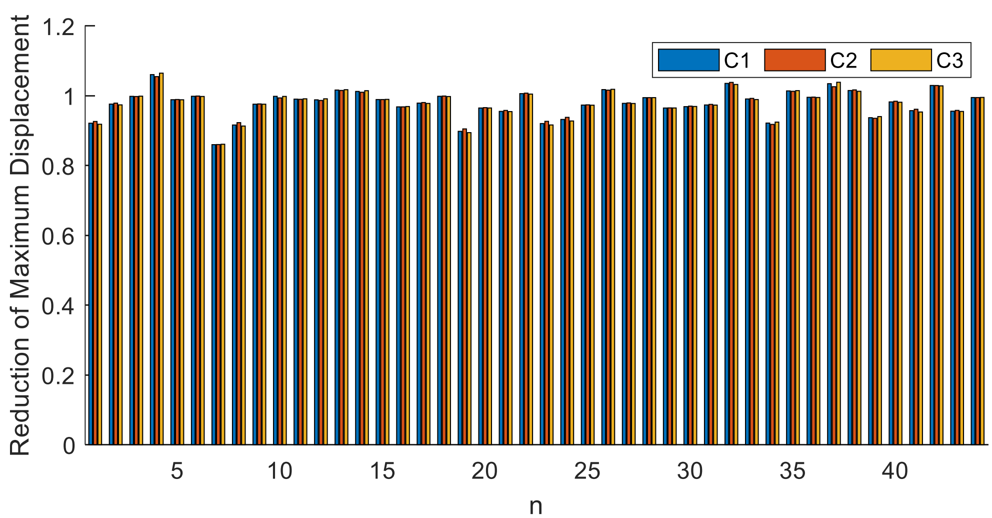

Figure 4-11: Primary structure maximum displacement reduction factor for the C1, C2, and C3 inerter-based TMDs

These results show that the C1, C2, and C3 inerter-based TMDs have similar performance in the reduction of the response RMS compared to the uncontrolled structure. In addition, the TMDs and all of the inerter-based TMDs provide an average RMS response reduction of 23% and 26%, respectively. While the performance of the devices varies, with both the TMD and inerter-based TMDs, only 2 of the records result in a response worse than the uncontrolled structure.

Figure 4-13 shows the comparison between the maximum displacement of the uncontrolled structure, and the structure with the TMD, C1, C2 and C3 inerter-based TMDs. The results in this figure show that, once again, the C1, C2 and C3 inerter-based TMDs have similar performance in the reduction of maximum displacement. In addition, TMDs and all the inerter-based TMDs provide an average reduction in maximum displacement of 9% and 10%, respectively. However, the inerter-based TMD are unable to reduce the maximum displacement of the structure, in comparison to the uncontrolled structure, for 6 of the 44 records.

To illustrate and compare the response of the structure with TMDs and inerter-based TMDs in the time domain, the response of the, once again undamped, structure to the Imperial Valley ground motion 1940 (180 component, recorded at El Centro station) is considered.

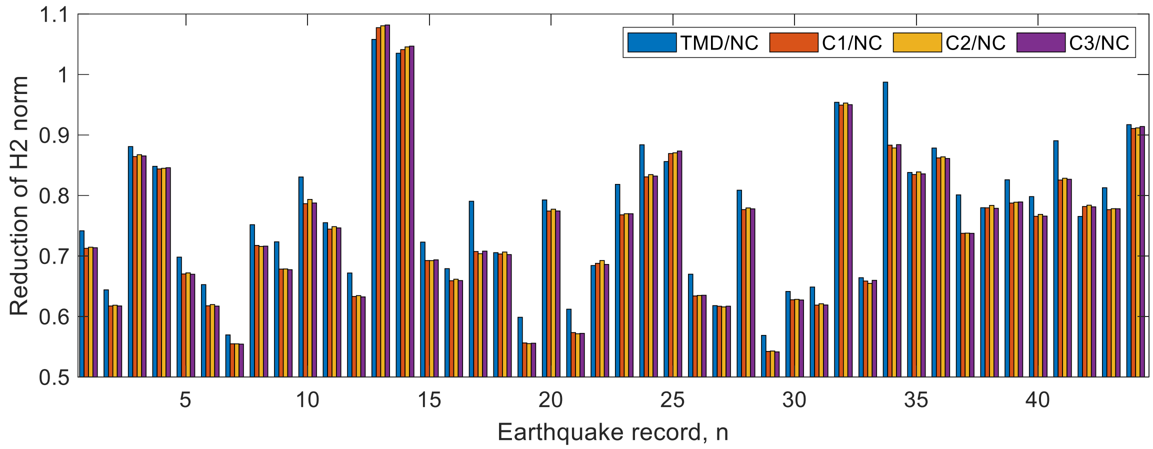

Figure 4-12: Structure displacement RMS reduction factor for the structures with TMDs, C1, C2, and C3 inerter-based TMDs compared to uncontrolled structure (NC)

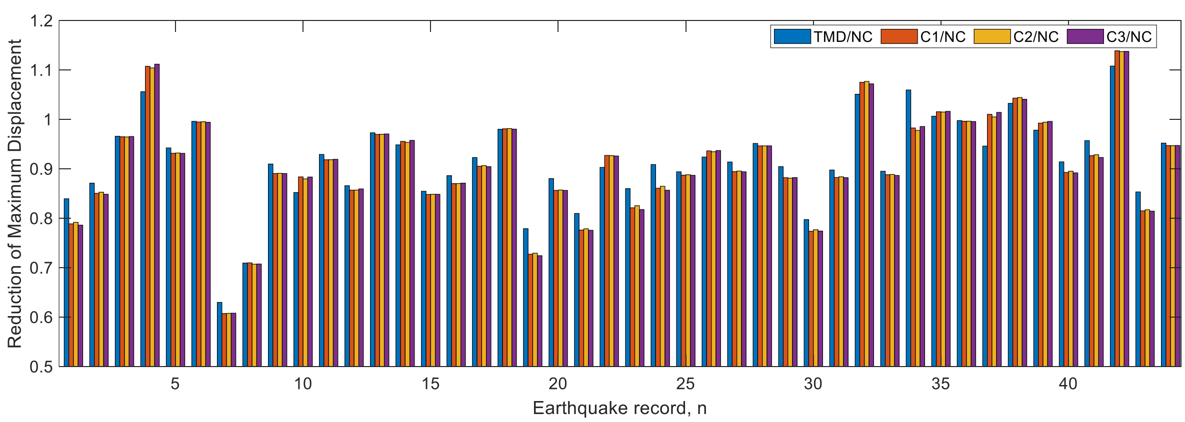

Figure 4-13: Structure maximum displacement reduction factor for the structures with TMDs, C1, C2, and C3 inerter-based TMDs compared to uncontrolled structure (NC)

This record is selected because it has been used before for performance evaluation of TMDs Figure 4-14 shows the comparison of the response of the structure with the TMD and with the C1, C2, and C3 inerter-based TMDs all with the H2 design values. The time history response shows the C1, C2, and C3 inerter-based TMDs have similar performances and provide a 10% reduction in the RMS of the response.

To illustrate the performance when the maximum displacement of the primary structure is used in the optimization, the response of the structure to the Imperial Valley ground motion is shown in Figure 4-15 when the H-infinity optimum designed TMDs and inerter-based TMDs is considered. In this case, all inerter-based TMDs provide similar performance and a 20% reduction in maximum displacement compare to the TMD. This performance is superior to the performance observed in the response to the 44 records previously considered, which illustrates the importance of the frequency content and other specifics of the individual earthquakes. In addition, the maximum response with the TMDs and inerter-based TMDs in this case is a little bit higher than the H2 optimum design, which again shows the sensitivity of the response of these systems to the input characteristics, particularly when considering the maximum displacement.

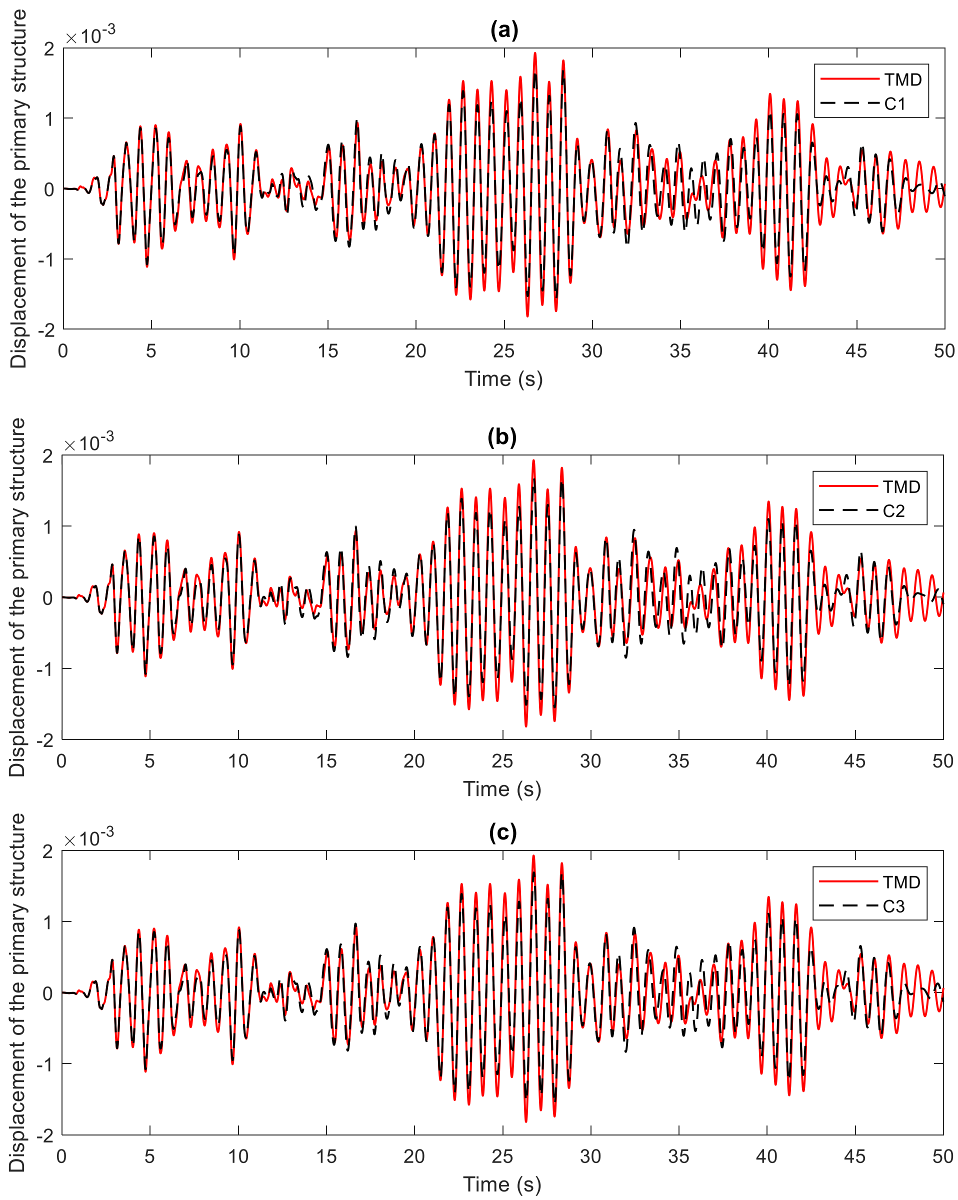

Figure 4-14 : Time history response of the structure when the TMDs and inerter-based TMDs are H2 optimized

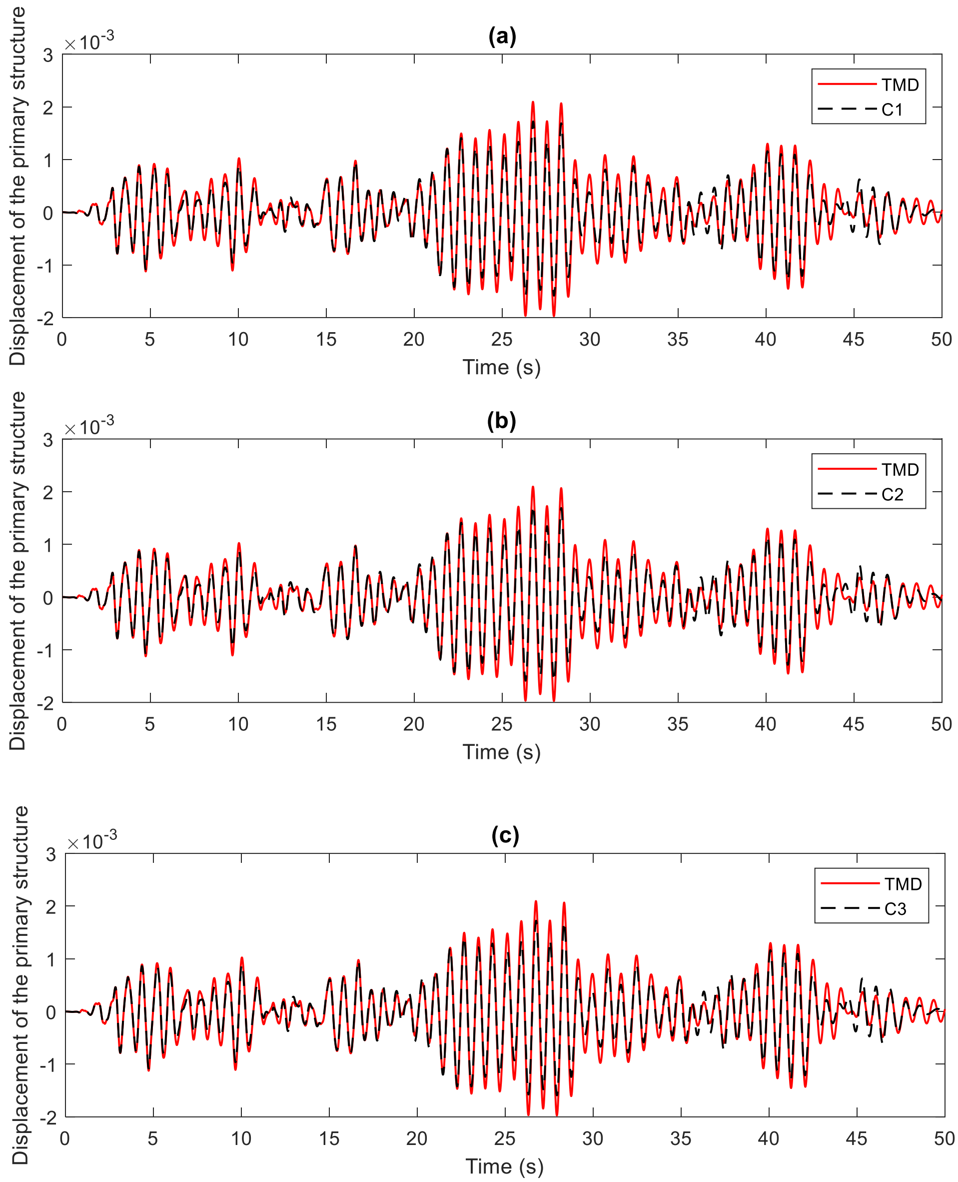

Figure 4-15: Time history response of the structure when the TMDs and inerter-based TMDs are H-Infinity optimized

The results in this section have shown that the performance of both the TMDs and inerter-based TMD vary over the different earthquake records considered. It has been previously found that TMDs can be more effective when the frequency content of the earthquake is close to the structure and when the earthquake has a long duration and broad frequency content [108]. As the TMDs and inerter-based TMDs have similar effects on a structure's frequency response function [9], it is reasonable to predict similar performance trends related to the earthquake parameters for inerter-based TMDs. For example, it can be observed by investigating the records used in the analysis in this paper that the inerter-based TMDs had better performance in the reduction of the H2 norm when the earthquake record has a longer duration. In addition, it can be observed that the inerter-based TMDs provide a more improved reduction of maximum displacement when the structure is subjected to records with its intensity spread over a longer percent of the record rather than concentrated in a short impulse.

While the comprehensive evaluation of the seismic effectiveness of inerter-based TMDs is beyond the scope of this work, this paper has evaluated and compared the effectiveness of different types of inerter-based TMDs and made comparisons to the effectiveness of conventional TMDs. In order to perform a more comprehensive evaluation of these devices for the control of structures subjected to earthquakes, damped multi-degree-of-freedom structures should be considered in future studies as well as the effects of the earthquake parameters.

Conclusions

The optimum design and performance evaluation of three recently developed inerter-based tuned mass dampers (TMDs) considering ground excitation is presented in this paper. The exact analytical solution for the H2 optimum design of inerter-based TMDs when the primary structure is subjected to the random ground excitation is presented. Additionally, considering harmonic ground excitation, a numerical optimum design method is proposed and the performance of inerter-based TMDs in comparison to the TMDs in the reduction of the maximum peak displacement is evaluated. Additionally, the performance of inerter-based TMDs when considering H2 and H_infinity design, design for individual earthquake records, and average design considering multiple earthquake records is studied. The main findings of this study are listed as follows:

It was observed in the response to random ground excitations, harmonic ground excitation, and seismic excitation that the similar optimized C1, C2, and C3 inerter-based TMDs shows similar performance.

When the primary structure is subjected to random ground excitation, the optimum H2 inerter-based TMDs provide an average 7%-8% reduction in the H2 norm compared to TMDs with the same main mass ratio.

Optimum H_Infinity inerter-based TMDs can provide a 25% reduction in the maximum displacement of the primary structure compared to the TMDs in the case of harmonic base excitation.

The exact H_2 optimum design of the inerter-based TMDs can be used when considering seismic excitation and were observed to outperform TMDs by an average of 7% considering the RMS displacement response of the primary structure.

The H_inifity optimum design of the inerter-based TMDs can be used when considering seismic excitation and were observed to outperform TMDs by an average of 2-3% considering the maximum displacement response of the primary structure; however, the resulting maximum displacement was found to be very sensitive to the specific characteristics of the ground motions.

The individual numerical optimization of inerter-based TMDs considering individual ground motions was shown to result in an average improvement of 10% and 15% compared to the H2 optimum and H_infiity optimum designs, respectively.

Inerter-based TMDs show effectiveness in reduction of the maximum displacement and H2 norm compared to no control structure in most cases of seismic excitation.

CHAPTER FIVE:THREE ELEMENT VIBRATION ABSORBER INERTER FOR PASSIVE CONTROL OF SDOF STRUCTURES

A version of this chapter was originally published by Abdollah Javidialesaadi and Nicholas Wierschem:

A. Javidialesaadi, N.E. Wierschem, Three-Element Vibration Absorber–Inerter for Passive Control of Single-Degree-of-Freedom Structures, Journal of Vibration and Acoustics. 140 (2018) 11. https://doi.org/10.1115/1.4040045.

This paper is part of the development of state of the art in inerter-based mass dampers. After background and literature review, formulation, design, and performance evaluation of the proposed inerter-based mass damper is presented and discussed explicitly.

Abstract

In this study, a novel passive vibration control device, the three-element vibration absorber-inerter (TEVAI) is proposed. Inerter-based vibration absorbers, which utilize a mass that rotates due to relative translational motion, have recently been developed to take advantage of the potential high inertial mass (inertance) of a relatively small mass in rotation. In this work, a novel configuration of an inerter-based absorber is proposed and its effectiveness at suppressing the vibration of a single-degree-of-freedom system is investigated. The proposed device is a development of two current passive devices: the tuned mass-damper–inerter (TMDI), which is an inerter-base tuned mass damper, and the three-element dynamic vibration absorber (TEVA). Closed-form optimization solutions for this device connected to a single-degree–of-freedom primary structure and loaded with random base excitation are developed and presented. Furthermore, the effectiveness of this novel device, in comparison to the traditional tuned mass damper (TMD), TEVA, and the TMDI, is also investigated. The results of this study demonstrate that the TEVAI possesses superior performance in the reduction of the maximum and RMS response of the underlying structure in comparison to the TMD, TEVA, and TMDI.

Introduction

Dynamic vibration absorbers (DVAs) can be utilized as effective passive vibration control devices. DVAs were introduced and developed originally as devices for damping the vibration of bodies [13]. One of the most common DVAs is the traditional tuned mass damper (TMD), which consists of a spring parallel to a dashpot connecting a primary system to a, typically small, secondary mass. Different types of TMDs have been successfully installed and utilized for passive control of numerous buildings around the world [5]. It has been demonstrated that the effectiveness of TMDs in the reduction of the maximum amplitude of the primary mass during resonance is highly dependent on the tuning frequency and damping ratio of the TMD [104]. A large number of numerical and analytical studies have been performed in order to find optimal frequency and damping ratios for TMDs [18,23,24,28,84,85,109]. Additionally, because TMDs are sensitive to tuning [2], studies have been conducted to improve the effectiveness and robustness of TMDs by utilizing multiple TMDs in parallel or series [37,41].

Non-traditional configurations of passive mass vibration absorbers have been proposed [110]and optimized for random and harmonic loads [29,93]. The three-element vibration absorber (TEVA), has been proposed, formulated, and optimized [27,28,111]. The configuration of the TEVA is similar to the TMD, except that an additional spring is in series with the device's damper. The TEVA shows superior performance both in the reduction of the maximum amplitude and the RMS of the primary mass compared to the TMD. Unlike the TMD, which adds one degree-of-freedom to the system, the TEVA adds two degrees-of-freedom to the system; therefore, the exact solution for tuning the three parameters of the system is more complicated [27,28,111].

One of the most important properties of traditional and most non-traditional passive vibration absorbers is the ratio of the absorber's mass to the primary system's mass. An option currently being studied to reduce the weight of the secondary mass of the TMD, while aiming to achieve similar performance as a system with higher physical mass, is the addition of “rotational inertial mass”.” Rotational inertial mass” can be provided by a device called an Inerter [54]. An inerter is a two terminal mechanical device which converts relative translational displacement into the localized rotation of an element and produces a resisting force proportional to the relative acceleration of its terminals [54,96]. Rack and pinion [9] or ball-screw [8] mechanisms connected to a flywheel have been used to realize the inerter in inerter-based vibration absorbers.

Inerter-based vibration absorbers have been developed to provide effective passive vibration control while also potentially utilizing less physical mass. In other words, these devices attempt to exploit the capability of the inerter to produce a great deal of effective mass for the absorber by converting the translational motion of a small mass to rotational motion. An example of this capability in one physically realized inerter is a 300 kg effective mass produced by utilizing a 2 kg mass combined with a ball screw mechanism [52].

The performance of multiple configurations of inerter-based vibration absorbers have been investigated. The rotational inertia viscous damper (RIVD), which is a device featuring an inerter, has been proposed for use in a toggle bracing system for passive control [8]. The tuned viscous mass damper (TVMD) has also been proposed and consists of a viscous mass damper, an inerter in parallel with a damper, and a tuning spring connected in series [52]. Substituting the damper in the TMD with a viscous mass damper, once again an inerter in parallel with a damper, the rotational inertia double tuned mass damper (RIDTMD) has been proposed and has been shown to be effective when utilizing an optimum value of rotational mass [9,58] . Inerter-based devices have been also investigated for vibration control of structural cables [73], vehicle suspensions [112,113], and multi-degree of freedom frames where the inerters were designed to utilize inter-story drift [71]

Recently, the tuned mass-damper-inerter (TMDI) has been proposed, developed and optimized [53]. The TMDI consists of a traditional TMD, which has an inerter attached between the TMD mass and the ground. Minimization of the variance (H_2 norm) of the system output of a structure with a TMDI shows better performance in comparison to TMDs with similar secondary mass [53]. Additionally, studies have considered utilizing the TMDI for the control of tall building subjected to wind [59], the transient response of systems with TMDI subject to nonstationary stochastic excitation[60] , and the optimum design and performance evaluation of TMDI in systems subjected to seismic loading [59–61].

This paper proposes the three-element vibration absorber-inerter (TEVAI). This device represents a potential improvement of the TEVA [28] and the TMDI [53], both which have demonstrated superior passive vibration control, in comparison to the traditional TMD. The main differences between the TEVAI and TMD is that, like the TEVA, there is an additional spring which is connected in series to the damper element and main mass and, like the TMDI, there is an inerter attached between the device's mass and the ground.

In the next section, the concept of rotational inertial mass and the inerter mechanism are reviewed. In Section 3, a brief review of the TMDI is presented. In Section 4, the TEVAI is introduced and formulated. Closed-form H_2 optimum design values for the TEVAI subjected to random base excitation are developed and presented in section 5. Then, the effectiveness of the proposed TEVAI, in comparison to the TMDI, in the reduction of the H_2 norm in the case of random base excitation is investigated in section 6. In order to evaluate the effectiveness of the proposed device in reducing the maximum amplitude of the response, H_∞ optimization and performance evaluation are presented in sections 7 and 8, respectively. In section 9, a summary of this work is presented along with the conclusions that were drawn.

Rotational inertial mass

The rotational inertial mass utilized by the TEVAI is a product of the use of a physical device called an inerter. Inerters are mechanical two-terminal devices which produce an equal and opposite force proportional to the relative acceleration between the nodes (terminals) [54], and have been investigated for use in vibration suppression [8,10,52,71,73,112]. In order to exploit the inerter's capacity to provide large inertial mass while utilizing small physical mass, various configurations and applications have been proposed which improve the effectiveness of traditional vibration absorbers. Assuming an ideal linear inerter, the following relationship holds between end forces (F), acceleration of the device's two terminals ($\ddot{u}_1$ and $\ddot{u}_2$), and the inerter mass coefficient (b) which is known as inertance [54,96]:

$$F = b\left(\ddot{u}_1 - \ddot{u}_2\right) \tag{5.1}$$

Figure 5-1 shows the schematic representation of the inerter subjected to two equal forces.

Various mechanical devices can be utilized to satisfy Eq. (5.1) and produce an inerter. Figure. 5-2 shows the ball-screw mechanism [8,52] and the rack and pinion mechanism [9], which are two of the more common mechanisms that have been utilized in literature to produce an inerter.

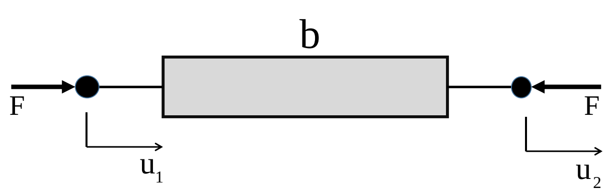

Figure 5-1: Schematic representation of a two-terminal inerter device (b is equivalent rotational mass)

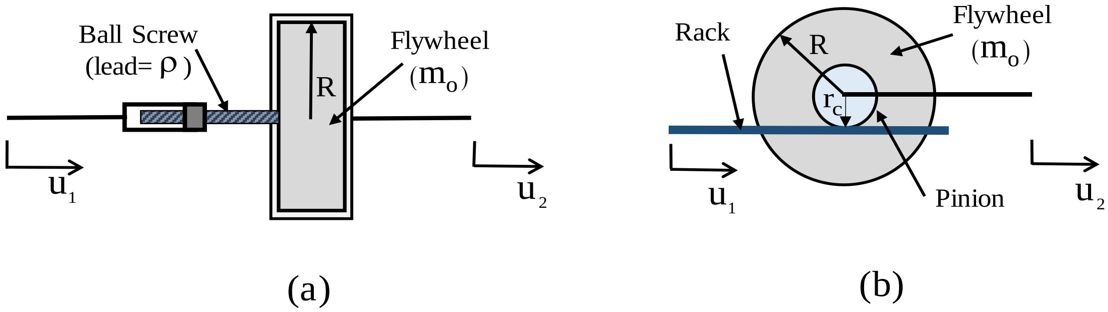

Figure. 5-2: Schematic representation of physical mechanisms used to produce an inerter (a) ball-screw mechanism (b) rack and pinion mechanism

Utilizing these devices, the mechanisms produce inertance (b) by transferring the translational motion of the two terminals into the rotation of a small physical flywheel mass (m_0) and developing the end force (F).The rotational velocity of the inerter's flywheel (ω) is equal to the product of the derivative of the relative displacement between the two terminal ends of the device and α, a coefficient related to the mechanism's geometry.

$$\omega = \alpha\left(\dot{u}_1 - \dot{u}_2\right) \tag{5.2}$$

For the ball screw mechanism,

$$\alpha = 2\pi/\rho \tag{5.3}$$

where ρ is the ball screw lead. For the rack and pinion mechanism,

$$\alpha = 1/r_c \tag{5.4}$$

where r_c is the pinion radius.

Considering the flywheel to be a hollow cylinder, $J = m_0 R^2$, where m_0 and R are the flywheel mass and radius. The kinetic energy of the rotational body can be rewritten as:

$$T = \frac{1}{2} m_0 R^2 \alpha^2 (\dot{u}_1 - \dot{u}_2)^2 \tag{5.5}$$

Based on this kinetic energy, the effective inertial contribution to the system can be written as:

$$\frac{\mathrm{d}}{\mathrm{dt}}(\frac{\partial T}{\partial \dot{u}_i}) = m_0 R^2 \alpha^2 (\ddot{u}_1 - \ddot{u}_2) \tag{5.6}$$

Comparing Eq. (5.1) and Eq. (5.6) and given the assumptions outlined above, the inertance for this device can be written as:

$$b = m_0 R^2 \alpha^2 \tag{5.7}$$

Tuned mass-damper-inerter (TMDI)

One family of inerter-based vibration absorbers are devices utilizing the inerter connected to the absorber and a fixed support [52,53,97]. This type of configuration generally increases the device's effectiveness by increasing the relative motion the inerter is subjected to; however, this configuration requires a fixed support for the connection of the inerter [51,52], which may not be feasible for some configurations. In order to address this issue for large building structures, an outrigger system has been proposed to be utilized as a partially fixed-support for inerter devices positioned in the elevated floors of high-rise buildings [114].

With a goal of improving the effectiveness of the tuned mass damper (TMD) (Figure. 5-3), the tuned mass-damper-inerter (TMDI) (Figure. 5-4), which features the addition of an inerter to the otherwise traditional TMD, has recently been proposed and investigated when attached to a single-degree-of-freedom system [52].

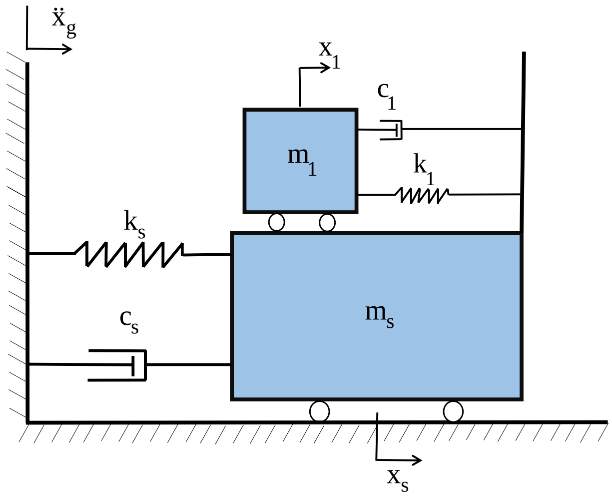

Figure. 5-3: Schematic configuration of a traditional tuned mass damper (TMD) attached to a single-degree-of-freedom structure

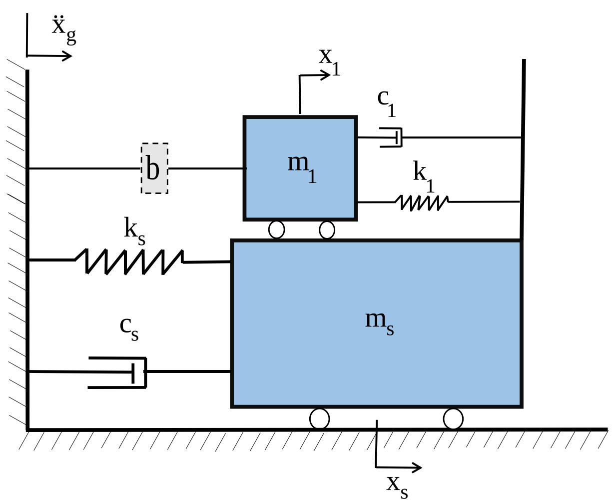

Figure. 5-4: Schematic configuration of a tuned mass-damper-inerter (TMDI) attached to a single-degree-of-freedom structure

The equation of motion of a single-degree-of-freedom structure under random base excitation with a TMDI attached can be express with the following equations of motion:

$$\begin{cases} m_s\ddot{x}_s + c_s\dot{x}_s + c_1(\dot{x}_s - \dot{x}_1) + k_s x_s + k_1(x_s - x_1) = -m_s\ddot{x}_g \\ (m_1 + b)\ddot{x}_1 + c_1(\dot{x}_1 - \dot{x}_s) + k_1(x_1 - x_s) = -m_1\ddot{x}_g \end{cases} \tag{5.8}$$

where m_s is the main structure mass, m_1 is the secondary mass (the physical mass of the TMDI), b is the inertance (inerter effective mass), c_s is the main structure damping, c_1 is the TMDI damping, k_s is the main structure stiffness, k_1 is the TMDI stiffness, and $\ddot{x}_g$ is the support excitation.

Three-element vibration absorber-inerter

The three-element vibration absorber-inerter (TEVAI) (Figure. 5-5) is the novel configuration of an inerter-based vibration absorber that is proposed and investigated in this study. This proposed configuration is a modified version of the TMDI that incorporates aspects of the TEVA in the form of a spring element in series with the device's dashpot. The TEVAI is a two-degree-of-freedom device, one more degree-of-freedom than a TMDI.

The equations of motion of a single-degree-of-freedom structure with the proposed device attached is presented in this section and the transfer function is derived for use in an optimization procedure presented in the next section.

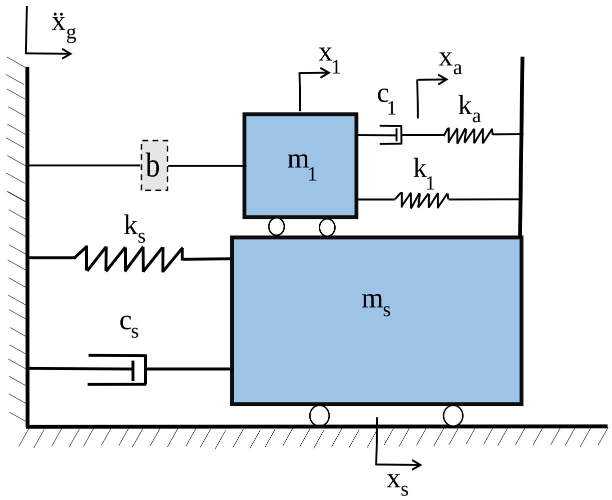

Figure. 5-5: Schematic configuration of a three-element vibration absorber-inerter (TEVAI) attached to a single-degree-of-freedom structure

The equations of motion for this device attached to a single-degree-of-freedom system can be written as:

$$\begin{cases} m_s\ddot{x}_s + c_s\dot{x}_s + k_s x_s + k_1(x_s - x_2) + k_a(x_s - x_a) = -m_s\ddot{x}_g \\ (m_1 + b)\ddot{x}_1 + c_2(\dot{x}_1 - \dot{x}_a) + k_1(x_2 - x_s) = -m_1\ddot{x}_g \\ c_2(\dot{x}_a - \dot{x}_1) + k_a(x_a - x_s) = 0 \end{cases} \qquad (5.9)$$

It is important to note that this device becomes a TEVA as the inertance, b, goes to zero.

To nondimensionalize this system, the following ratios and dimensionless parameters are considered.

$\mu = \dfrac{m_1}{m_s}$: Main mass ratio; $\omega_s = \sqrt{\dfrac{k_s}{m_s}}$: Primary system frequency

$\beta = \dfrac{b}{m_1}$: Inertance mass ratio

$\omega_1 = \sqrt{\dfrac{k_1}{m_1}}$: Secondary system frequency; $\xi = \dfrac{c_1}{2m_1\omega_1}$: Damping ratio

$K = \dfrac{k_a}{k_1}$: Spring ratio

$\lambda = \dfrac{\omega}{\omega_s}$: Input frequency ratio; $\nu = \dfrac{\omega_1}{\omega_s}$: Tuning frequency ratio

When the primary system is subjected to a harmonic ground acceleration at frequency ω, represented as $\ddot{x}_g = Ae^{i\omega t}$, the steady state displacement response of each degree-of-freedom of the system can be represented by $x = Xe^{i\omega t}$. By assuming an undamped primary system $(c_s = 0)$ and substituting $x_s = X_s e^{i\omega t}$ and $\ddot{x}_g = Ae^{i\omega t}$ in Eq. (5.9), a generic transfer function from the ground acceleration to the displacement of the main structure can be written as:

$$H(i\lambda) = \frac{X_s}{A} = \frac{N_3\lambda^3 + N_2\lambda^2 i + N_1\lambda + N_0 i}{D_5\lambda^5 + D_4\lambda^4 i + D_3\lambda^3 + D_2\lambda^2 i + D_1\lambda + D_0 i} \tag{5.10}$$

where

$$N_3 = 2(\beta+1)\xi$$
$$N_2 = -K\nu(\beta+1)$$
$$N_1 = -2(\mu+1)\nu^2(1+K)\xi$$
$$N_0 = (1+\mu)K\nu^3$$
$$D_5 = 2\left(\beta+1\right)\xi$$
$$D_4 = K\left(\beta+1\right)\nu$$
$$D_3 = -2\Big((\beta\mu+1+\mu)(K+1)\nu^2 + \beta+1\Big)\zeta$$
$$D_2 = \Big(\left(\beta\mu+\mu+1\right)\nu^2 + \beta+1\Big)K\nu$$
$$D_1 = 2\nu^2\Big(1+\left(\beta+1\right)K\Big)\beta$$
$$D_0 = -K\nu^3$$

H_2 Optimum Design of the TEVAI

The optimum design of the TEVAI considered in this work consists of the determination of optimal design values for the stiffness and damping elements of the absorber given assumed values for the main mass ratio, μ, and inertance mass ratio, β. H_2 optimization is chosen for this optimization because H_2 optimization is generally considered superior when random excitation is considered [103]. The main goal of the H_2 optimization criterion is minimizing the vibration energy in all frequencies by considering white noise with a uniform power spectrum density as the excitation[18]. In H_2 optimization, optimum values are obtained to minimize the variance of the output [103]. While the optimization of the TEVAI is considered in this study, the closed-form H_2 optimization of the TMDI and TEVA under random base excitation attached to single-degree-of-freedom primary systems have been previously presented in [63] and [28], respectively.

In this section, H_2 optimization of the proposed device, when subjected to random base excitation, is performed in explicit form with exact closed-form formulas for the optimum design values presented.

To begin the optimum design procedure, the variance of the output of the system is written as [84]:

$$\bar{\sigma}^2 = \frac{1}{2\pi}\int_{-\infty}^{\infty} \left|H(i\lambda)\right|^2 d\lambda \tag{5.11}$$

$\left|H(i\lambda)\right|^2$ in Eq. (5.11) represents the square of the transfer function's magnitude in the frequency domain. This complex function can be rewritten as:

$$\left|H(i\lambda)\right|^2 = \frac{\mathrm{Im}\left(H(i\lambda)\right)_n^{\ 2} + \mathrm{Re}(H(i\lambda))_n^{\ 2}}{\mathrm{Im}\left(H(i\lambda)\right)_d^{\ 2} + \mathrm{Re}\left(H(i\lambda)\right)_d^{\ 2}} \tag{5.12}$$

where Im and Re in Eq. (5.12) represents the imaginary and real parts of the transfer function and subscripts n and d denote the numerator and denominator, respectively. This transfer function can also be rewritten as:

$$|H(i\lambda)|^2 = \frac{g(\lambda)}{h(\lambda)h(-\lambda)} \tag{5.13}$$

where $g(\lambda)$ in Eq. (5.13) is a sixth-order odd function.

$$g(\lambda) = a_0\lambda^6 + a_1\lambda^4 + a_2\lambda^2 + a_3 \tag{5.14}$$

where

$$a_0 = 4\xi^2\left(\beta+1\right)^2$$
$$a_1 = \nu^2\left(\beta+1\right)\left(-(8\mu+8)(K+1)\xi^2 + K^2\left(\beta+1\right)\right)$$
$$a_2 = 4\nu^4\left(\left(1+K\right)^2\left(\mu+1\right)\xi^2 - \frac{1}{2}K^2\left(\beta+1\right)\right)\left(\mu+1\right)$$
$$a_3 = K^2\nu^6\left(\nu+1\right)^2$$

$h(\lambda)$ in Eq. (5.13) is a fifth-order complex polynomial.

$$h(\lambda) = b_o\lambda^5 + \mathrm{i}b_1\lambda^4 + b_2\lambda^3 + \mathrm{i}b_3\lambda^2 + b_4\lambda + \mathrm{i}b_6 \tag{5.15}$$

where:

$$b_0 = 2\left(\beta+1\right)\xi$$
$$b_1 = -K\nu\left(\beta+1\right)$$
$$b_2 = -2\left(\left(\beta\mu+\mu+1\right)\left(K+1\right)\nu^2 + \beta+1\right)\xi$$
$$b_3 = \left(\left(\beta\mu+\mu+1\right)\nu^2 + \beta+1\right)K\nu$$
$$b_4 = 2\nu^2\left(1+K\right)\xi$$
$$b_5 = -K\nu^3$$

Writing Eq. (5.11) in the form of Eq. (5.13) provides convenience for developing the closed-form solution. This type of integration can be evaluated directly by factoring the denominator and utilizing complex residual theorem

[18,28].Alternatively, the solution can also be found using integral tables [115] which are also based on residual theorem and can be found in explicit form in [91]. This solution process has been previously used for the optimization of non-traditional TMDs [29]. By performing the integration of Eq. (5.11) utilizing the formula in [115], the resulting variance of the output is:

$$\bar{\sigma}^2 = \frac{q_0\nu^6 + q_1\nu^4 + q_2\nu^2 + q_3}{-2(\beta+1)^2 K^2 \xi \nu^3 \mu} \tag{5.16}$$

where

$$q_0 = K^2\left(1+(\beta+1)\mu\right)^2(\mu+1)^2$$

$$q_1 = 4(\mu+1)\left(\begin{array}{l}\left(\left((\beta+1)\left(\frac{1}{4}+\xi^2(\beta+1)\right)\mu^2+\left(-\frac{1}{4}+(\beta+2)\xi^2\right)(\beta+1)\mu-\frac{1}{2}+\xi^2(\beta+1)\right)(\beta+1)K^2+..\\ 2\left(1+(\beta+1)\mu\right)(\mu+1)(\beta+1)\xi^2 K+\left(1+(\beta+1)\mu\right)(\mu+1)\xi^2\end{array}\right)$$

$$q_2 = (\beta+1)\left(K^2(\beta+1)-8\xi^2(\beta+1)(\mu+1)K-8(\mu+1)\xi^2\right)$$

$$q_3 = 4\xi^2(\beta+1)^2$$

The optimum design values can be obtained by satisfying the following condition:

$$\frac{\partial\bar{\sigma}^2}{\partial\nu} = \frac{\partial\bar{\sigma}^2}{\partial K} = \frac{\partial\bar{\sigma}^2}{\partial\xi} = 0 \tag{5.17}$$

By solving Eq. (5.17) as a set of three parametric equations simultaneously and considering only positive answers, thus ignoring negative stiffness and damping values, the optimum design values can be obtained and presented in an explicit form. Eq. (5.18) shows the optimum tuning frequency ratio, Eq. (5.19) shows the optimum spring ratio, and Eq. (5.20) shows the optimum damping ratio. All three of these expressions are functions of the main mass ratio and inertance mass ratio of the TEVAI.

$$\nu_{opt} = \frac{\sqrt{(\beta+1)(1+(\beta+1)\mu)(\mu+1)^2\left(-\sqrt{\mu(\beta+\mu+1)(\beta\mu+\mu+1)}+1+(\beta+1)\mu\right)}}{\left(1+(\beta+1)\mu\right)(\mu+1)^2} \tag{5.18}$$

$$K_{opt}=-\frac{2\left(-\sqrt{\mu(1+\beta+\mu)(\beta\mu+\mu+1)}\beta+(\beta+\mu+1)\left(1+(\beta+1)\mu\right)\right)\mu}{\left(-1+(-2\beta-1)\mu\right)\sqrt{\mu(\beta+\mu+1)(\beta\mu+\mu+1)}+\mu\left(1+(\beta+1)\mu\right)(2\beta+\mu+1)}$$

(5.19)

(5.20)

$$\xi_{opt}{}^{2}=\frac{\mu(\beta+\mu+1)\begin{pmatrix}2\sqrt{\beta+\mu+1}\left(\left(-\beta^{2}-\frac{3}{2}\beta-\frac{1}{2}\right)\mu^{2.5}+\beta^{2}\mu^{1.5}+\frac{3\sqrt{\mu}\beta}{2}-\frac{\sqrt{\mu}}{2}-\mu^{1.5}\right)\sqrt{\beta\mu+\mu+1}+\ldots\\+\left((2\mu^{2}-2\mu)\beta^{2}+(\mu^{3}+2\mu^{3}-3\mu-2)\beta+\mu^{3}-3\mu-2\right)(\beta\mu+\mu+1)\end{pmatrix}}{2(\beta\mu+\mu+1)(\mu+1)^{4}(\mu-1)}$$

In the specific case of $\beta=0$, Eq. (5.18)-(5.20) will simplify as follows:

$$\nu_{opt}=\frac{\sqrt{1-\sqrt{\mu}}}{1+\mu} \tag{5.21}$$

$$K_{opt}=\frac{2\mu}{-\mu+\sqrt{\mu}} \tag{5.22}$$

$$\zeta=\frac{\sqrt{\dfrac{2\mu\left(\mu^{2}-\mu-\sqrt{(\mu+1)^{2}\mu}-2\right)}{\mu-1}}}{2\mu+2} \tag{5.23}$$

These expressions are consistent with the optimal TEVA parameters previously determined [28].

To examine the variation of the optimum design values versus main mass ratio (μ) and inertance mass ratio (β), graphical representations of Eq. (5.18), Eq. (5.19), and Eq. (5.20) are plotted for μ equal to 0.01, 0.05, 0.1, and 0.2 (1%, 5%, 10%, and 20% mass of the main structure). Variation of the optimum tuning frequency ratio (ν) (see Eq. (5.18)) with respect to inertance mass ratio for different main mass ratios is plotted in Figure 5-6 (a). This figure shows that for any of the main mass ratios considered, the optimum frequency tuning ratio

increases with more inertance mass. However, increasing the main mass ratio, leads to a decrease in the optimal tuning ratio. The variation of the optimum spring ratio (K) (see Eq. (5.19)) with respect to inertance mass ratio (β) for different main mass ratios (μ) is presented in Figure 5-6 (b). Like the optimal tuning frequency, the optimum spring ratio increases with both increases in the inertance mass ratio and the main mass ratio.

Figure 5-6 (c) shows the optimum damping ratio (ζ) (see Eq. (5.20)) with respect to inertance mass ratio (β) for different main mass ratios. These results show that the optimal damping ratio increases with the addition of more inertance mass. It should be noted that the way that the damping ratio is defined ($\xi = \frac{c_1}{2m_1\omega_1}$) does not include any consideration of the inertance mass ratio (β); therefore, even if the optimal damping ratio is over 1, the optimal response will generally not be overdamped.

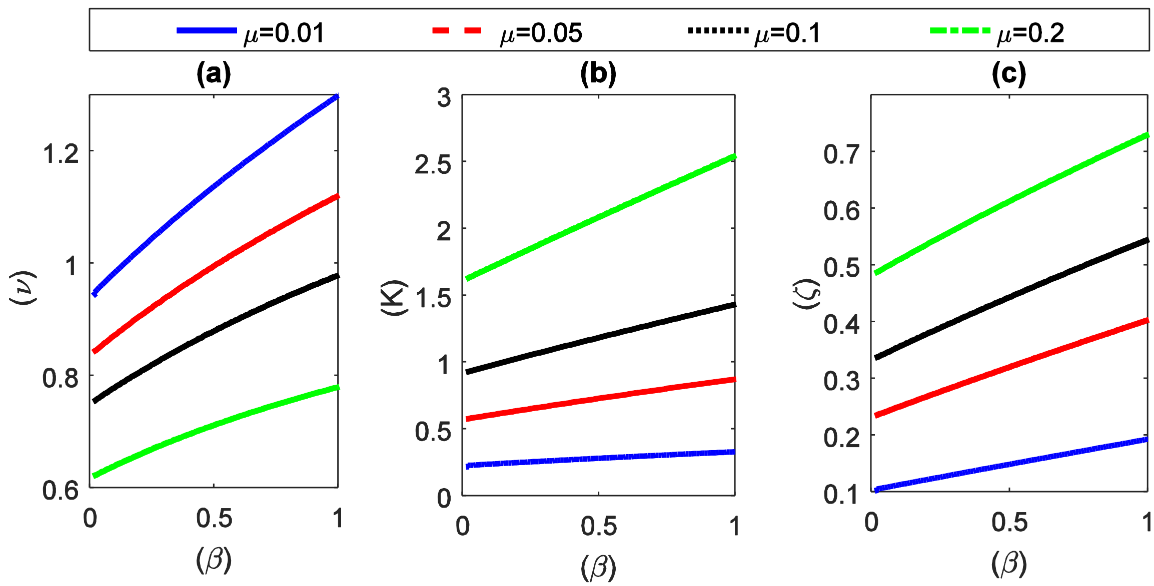

Figure 5-6: Effect of inertance mass ratio on the TEVAI H_2 optimum design values: (a) optimum tuning frequency ratio, (b) optimum spring ratio, (c) optimum damping ratio

H_2 Performance Evaluation of the TEVAI

In this section, an analysis of the performance of the optimum TEVAI, in comparison to the TMDI, is presented. The H_2 performance, which corresponds with the RMS of the system output to a white noise input [103], is calculated for the TEVAI and TMDI in their optimum condition with the same mass ratios. Design values of the TMDI optimized in order to minimize the H_2 norm have been presented in explicit form in [53] and the optimum design values for TEVAI were obtained from the results presented in the previous section.

The resulting H_2 norm of the main structure's displacement response is presented in Figure 5-7 for $\mu =$ 0.01, 0.05, 0.1, and 0.2, with the inertance mass ratio over the range from 0 to 1 $(\beta = 0 \text{ to } 1)$. This figure shows that for both the TMDI and the

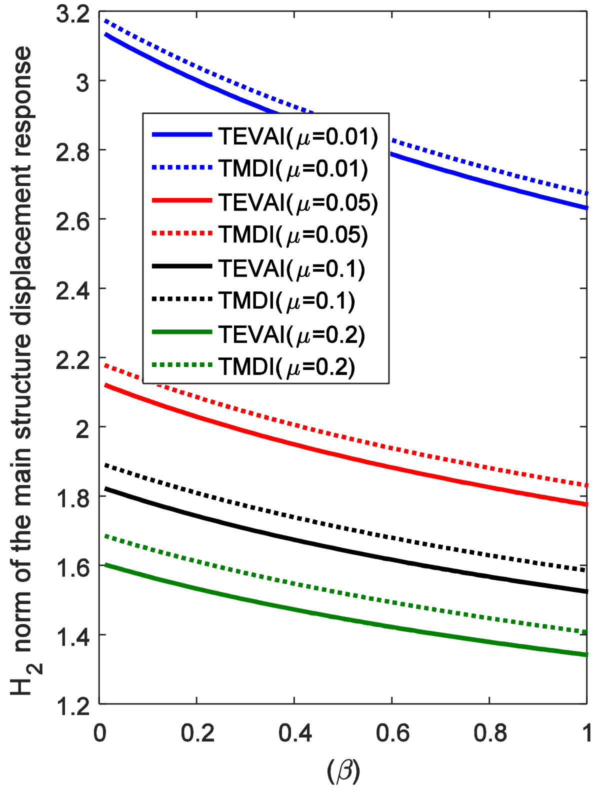

Figure 5-7: H_2 norm vs inertance mass ratio for the H_2 optimal TEVAI and TMDI

TEVAI, the H_2 norm is monotonically decreased with the addition of more inertance. This figure also shows that the TEVAI provides a 1.5%-4% reduction of H_2 norm, in comparison to the TMDI, in the case of 1%, 5%, and 10% main mass ratio and a 2%-5% reduction in the case of a 20% main mass ratio.

In addition to the H_2 norm, the maximum dynamic magnification factor (DMF) of the displacement response of the main structure in the frequency domain is another criterion to evaluate the effectiveness of the device proposed in this study. The H_2 optimization criterion used to design this system does not consider the minimization of the DMF; however, the DMF will be considered herein in order to

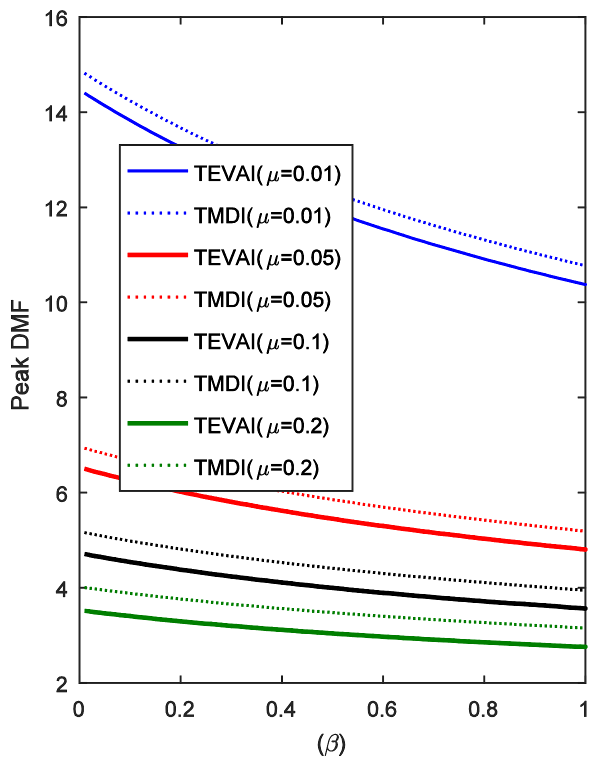

Figure 5-8: Peak dynamic magnification factor (DMF) vs inertance mass ratio for systems with the H_2 optimal TEVAI and TMDI

more fully investigate the performance of the TEVAI and the TMDI. Figure 5-8 shows the peak DMF of the displacement of the main structure with the attached TEVAI and TMDI possessing different mass ratios. This figure shows that the TEVAI provides a 3%-4%, 7%-8%, 9%-10%, and 13%-14% reduction in the peak DMF, in comparison to the TMDI, in the case of the main mass ratio equal to $\mu =$ 0.01, 0.05, 0.1, and 0.2, respectively.

Considering the H_2 optimum systems and a fixed main mass ratio of 10% ($\mu = 0.1$), the frequency domain response, in terms of the DMF, of the TMDI and TEVAI for two inertance mass ratios, $\beta = 0.1$ and $\beta = 1$, is presented in Figure 5-9. Once again, the DMF here is calculated based on the displacement response of the main structure. The results in Figure 5-9 show that, in comparison to the TMDI, the TEVAI achieves a reduction in the DMF of 9% and 11% when $\beta = 0.1$ and $\beta = 1$, respectively. It is observed from this figure that the H_2 optimal frequency response of both the TEVAI and TMDI feature two non-equal peaks. These peaks in the frequency response curves are lower for the TEVAI, compared to the TMDI, but the overall response curve is not significantly widened or narrowed. As the objective of H_2 optimization is the minimization of the total vibration energy across all frequencies, the H_2 optimum TEVAI does not necessarily provide superior performance in the reduction of the DMF at all frequencies. This being said, the results of this study also show that the TEVAI reduces the peak DMF, which is also crucial in vibration control.

It can also be observed in Figure 5-9 that by increasing the inertance ratio (β), both response curves of the TMDI and TEVAI are shifted to the left, which indicates a decrease of the natural frequencies of the system. This is consistent with the results previously found in the literature, in which the natural frequencies of the structure with an inerter decrease with increased inertance [55].

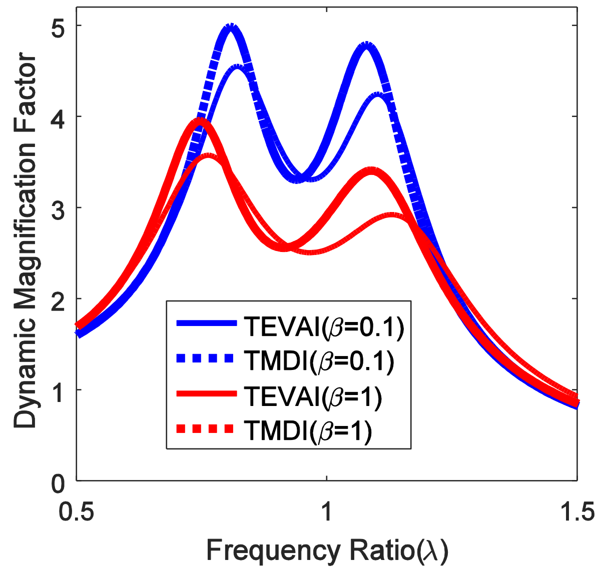

Figure 5-9: : Frequency response function for systems with H_2 optimal TMDI and TEVAI at different inertance mass ratios with a main mass ratio = 10%

The effect of various inertance mass ratios on the DMF is presented in Figure 5-10 This figure shows the frequency response, once again in terms of the DMF of the displacement of the main structure, considering the attachment of a TEVAI with μ equal to 0.1 and β equal to 0, 0.1, 0.5, and 1. Note that a TEVAI with β equal to 0, is in actuality a TEVA. The results show that with increasing inertance mass ratio, there is a substantial reduction in the peak DMF and a small shift in the location of the peaks of the frequency response. By increasing β from 0 to 0.1, 0.5, and 1, a reduction in the peak DMF of 4%, 15% and 25% is achieved, respectively.

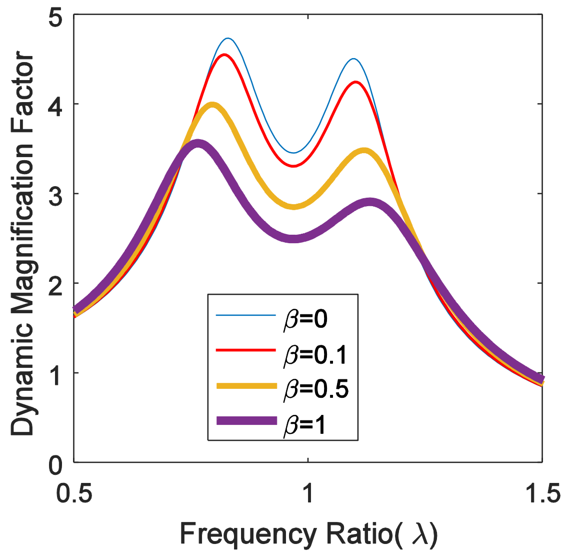

Figure 5-10: Effect of changes to inertance mass ratio on the DMF of a system with an H_2 optimal TEVAI with a main mass ratio = 10

H_∞ Optimum design of the TEVAI

The H_2 optimum design values for the TEVAI presented in Eq. (5.18), Eq. (5.19), and Eq. (5.20) are obtained based on a white noise input to the system and the goal of minimizing the system's H_2 norm, which is a commonly considered optimization criterion given random excitation [103]. Another common criterion for the optimization of mass damper devices is the H_∞ optimization criterion [103]. When the structure is subjected to harmonic excitation across all ranges of frequencies and minimization of the peak response is desired, the H_∞ optimization criterion is often considered to determine design parameters [18,37,93,103].

H_∞ optimum design values of tuned mass dampers attached to an undamped primary system can be obtained utilizing approximate methods like the fixed points method [104] and closed-form exact algebraic solutions [85]. When considering the optimization of base-excited systems with TMDI or TEVAI, the production of closed-form H_∞ optimum algebraic solutions are tedious due to the complexity of the transfer function; therefore, numerical solutions are often pursued in these cases.

In this section, the aim is to evaluate the performance of the proposed TEVAI considering its ability to reduce the peak DMF. To do this, numerical optimization is performed to obtain the optimum values of TMDI and TEVAI given an assumed set of mass ratios.

Considering Eq. (5.8), the equations of motion for the undamped primary structure with an attached TMDI, the objective function for H_∞ optimization of the TMDI is

$$\begin{array}{ll} \text{minimize} & \{J_{TMDI}\} \\ \text{subject to} & \\ \begin{bmatrix} k_1 & c_1 \end{bmatrix} & 0 < k_1 \le k_{1u},\ 0 < c_1 \le c_{1u} \end{array} \tag{5.24}$$

Furthermore, considering Eq. (5.9), the equation of motion for the undamped primary structure with an attached TEVAI, the objective function for H_∞ optimization of the TEVAI is

$$\begin{array}{ll} \text{minimize} & \{J_{TEVAI}\} \\ \text{subject to} & \\ \begin{bmatrix} k_1 & k_a & c_1 \end{bmatrix} & 0 < k_1 \le k_{1u}, 0 < k_a \le k_{au}\ 0 < c_1 \le c_{1u} \end{array} \tag{5.25}$$

In Eq. (5.24) and Eq. (5.25), k_{1u} , k_{au} , and c_{1u} are values utilized as upper bounds for k_1 , k_a , and c_1, respectively and J_{TMDI} and J_{TEVAI} are defined as

$$J_{TMDI} = \max_{\omega\in\Omega} \left\| H(i\omega)_{TMDI} \right\| \tag{5.26}$$

$$J_{TEVAI} = \max_{\omega\in\Omega} \left\| H(i\omega)_{TEVAI} \right\| \tag{5.27}$$

where $\left\| H(i\omega)_{TMDI} \right\|$ and $\left\| H(i\omega)_{TEVAI} \right\|$ represent the absolute values of the transfer functions of the system with the TMDI and TEVAI, respectively. Numerical optimization of the TMDI and TEVAI systems given these objective functions is performed using the numerical optimization solver *fmincon* in MATLAB [92].

Optimum design values of the TMDI are calculated and presented in Figure 5-11. Figure 5-11(a) presents the tuning frequency ratio of the TMDI to provide the minimum H_∞ norm for different main mass ratio (μ) and inertance mass ratio (β) combinations. It can be observed from Figure 5-11 (a) that the optimum tuning frequency of the TMDI increases with increases in the inertance mass ratio and decreases with increases in the main mass ratio.

Figure 5-11 (b) shows the optimum damping ratio of the TMDI for different main mass ratio and inertance mass ratio combinations. This figure shows that the optimal damping increases with increases in both the main mass ratio and the inertance mass ratio. Similar trends in the optimization of the tuning frequency and damping ratio also can be observed for the H_2 optimization of the TMDI [60].

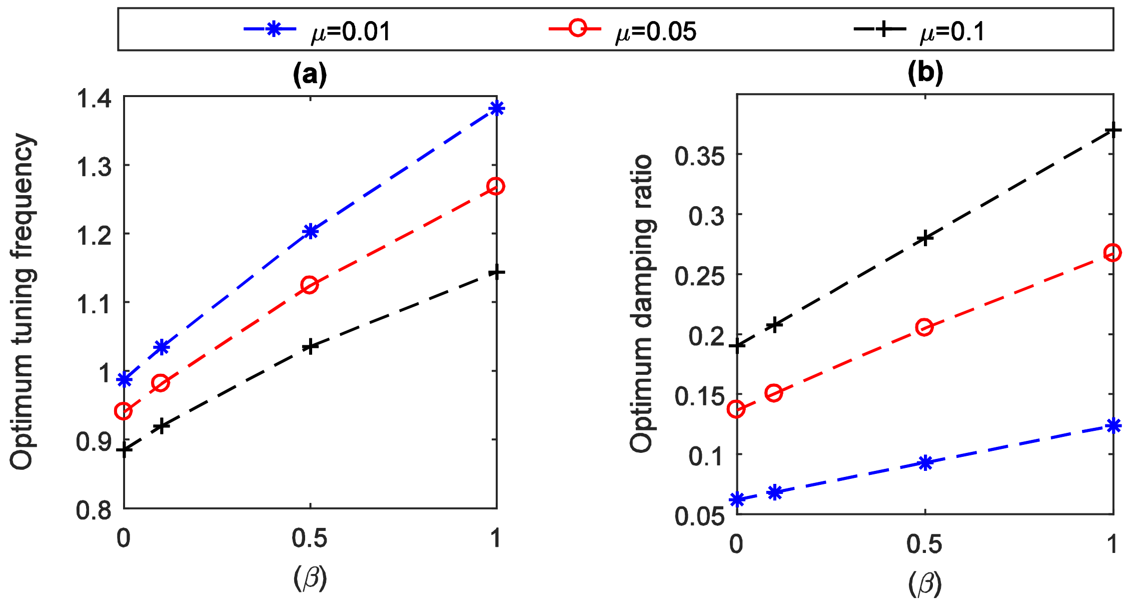

Figure 5-11: H_∞ Optimum design values of TMDI at different mass ratios: (a) optimum tuning frequency ratio, (b) optimum damping ratio

The TEVAI's H_∞ optimum design values were also calculated for several main and inertance mass ratios and are presented in Figure 5-12. Figure 5-12 (a) shows the optimum tuning frequency ratio for different main mass ratios and inertance mass ratios. Like the TMDI, increases in the main mass ratio leads to a reduction of the H_∞ optimum tuning frequency; furthermore, also like the TMDI, increases in the inertance mass ratio to the system lead to increases in the H_∞ optimum tuning frequency.

The optimum damping ratio of the TEVAI is presented in Figure 5-12 (b). The trend observed from this figure is that, in general, the H_∞ optimum damping value increases with increases in the inertance mass ratio and the main mass ratio. Similar behavior was observed for the TMDI.

In addition to the optimum tuning frequency and damping ratio, the optimum spring ratio (K) is presented in Figure 5-12 (c). From this figure, it is found that the H_∞ optimum spring ratio increases with increases in both the main mass ratio and the inertance mass ratio.

H_∞ performance of the TEVAI

Utilizing the H_∞ optimum values, the peak DMF for both the system with the TMDI attached and the system with the TEVAI attached are calculated for μ equal to 0.01, 0.05, and 0.1 and β equal to 0, 0.1, 0.5, and 1 and presented in Figure 5-13.

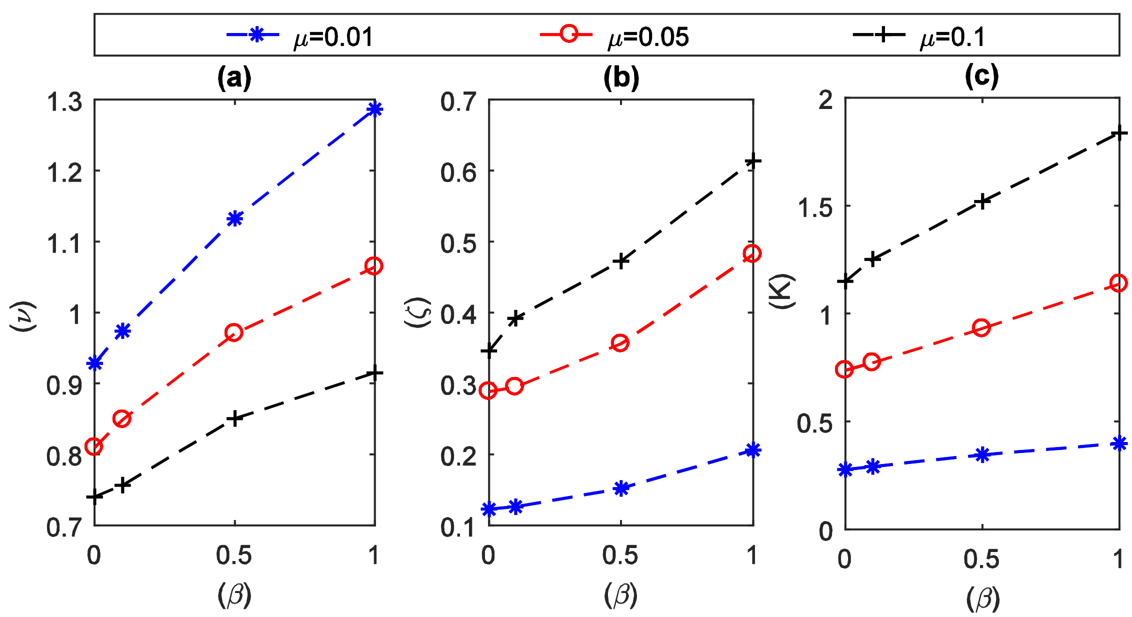

Figure 5-12: H_∞ Optimum design values of TEVAI at different mass ratios: (a) optimum tuning frequency ratio, (b) optimum damping ratio, (c) optimum spring ratio

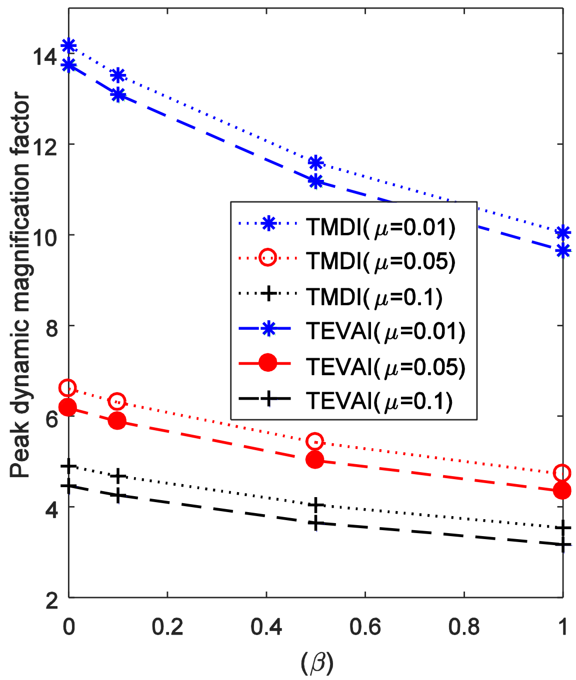

Figure 5-13: Peak dynamic magnification factor (DMF) vs inertance mass ratio for systems with H_∞ optimal TEVAI and TMDI

Note that in the absence of the inertance mass ($\beta = 0$), the TMDI is a traditional TMD and the TEVAI is a TEVA. From Figure 5-13, it is observed that by adding the inertance mass, the peak dynamic magnification factor reduces substantially. In order to investigate the performance of the H_∞ optimum TEVAI in comparison to the H_∞ optimum TMDI, it is beneficial to define the following peak DMF Improvement index, R:

$$R = \left(1 - \frac{\max_{\omega\in\Omega} \mathrm{DMF}_{TEVAI}(i\omega)}{\max_{\omega\in\Omega} \mathrm{DMF}_{TMDI}(i\omega)}\right) \times 100 \ (\%) \tag{5.28}$$

where $\mathrm{DMF}_{TMDI}(i\omega)$ is the DMF of the system with the TMDI attached and $\mathrm{DMF}_{TEVAI}(i\omega)$ is the DMF of the system with the TEVAI attached. Figure 5-14 shows the variation in R for the considered main mass and inertance mass ratios. This figure shows that for the ratios considered herein, compared to the TMDI, the TEVAI can be between about 3% to 10.4% more effective in reducing the peak DMF. The results also indicate that the advantage of the TEVAI performance, in comparison to the TMDI, grows with increases in the main mass ratio. It is also observed that by adding additional inertance with a fixed main mass ratio, the effectiveness of the TEVAI increases.

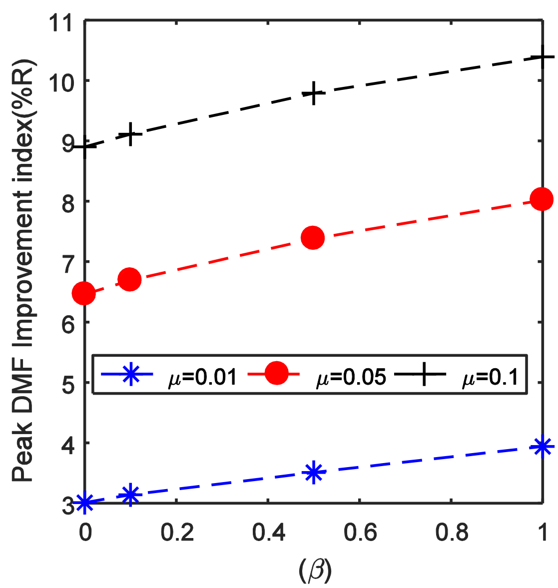

Figure 5-14: Peak DMF Improvement index (R)

Considering a TEVAI with a 10% mass ratio, the effect of the value of the inertance of the device on the DMF is studied. The results show that adding inertial mass in the range of β = 0 to 1 to the absorber can provide a 5% to 29% reduction in DMF. Note that when β is equal to zero, the TEVAI is effectively a TEVA. The frequency domain response of the H_∞ optimum TMDI and TEVAI for $\mu = 0.1$ and $\beta =$ 0.1 and 1 is plotted in Figure 5-16. Figure 5-16 shows that, in these cases, the TEVAI provides about a 10% reduction in peak DMF, in comparison to the TMDI utilizing the same main mass ratio and inertance mass ratio. Furthermore, an overall reduction in the magnitude of the frequency response curve with the TEVAI, in comparison to the TMDI, is observed in this figure.

Regarding the size of the device, practical aspects, and installation, this will vary largely with the type and specifics of the application. In regards to civil engineering applications, many TMDs have been installed in different real structures around the world. The size and practical considerations of utilizing the TMDI have also been studied previously [59], where the benefits of a reduction in the stroke and size of the secondary mass are highlighted. The installation effort of the proposed TEVAI will be similar to the TMDI. Regarding the physical size of the inerter, it is reported in the literature that there is a 2kg inerter which can provide 70 kg of inertance available on the commercial market [116].

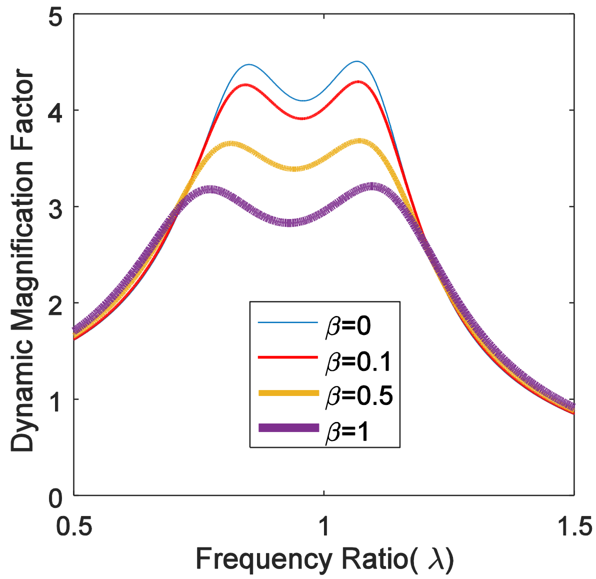

Figure 5-15: Effect of inertance mass ratio on the DMF for H_∞ optimal systems with a TEVAI with a main mass ratio = 10%

Additionally, a 2kg flywheel producing a 350 kg inertance [52] and a 5400 ton inertial mass using 560 kg of actual mass [12] have been studied experimentally. This serves to demonstrate that high inertance values can be created with relatively small masses. As the TEVAI has just one more element than the TMDI, and because large inertance can be provided by utilizing a small physical mass, the size of the device is approximately close to the TMD.

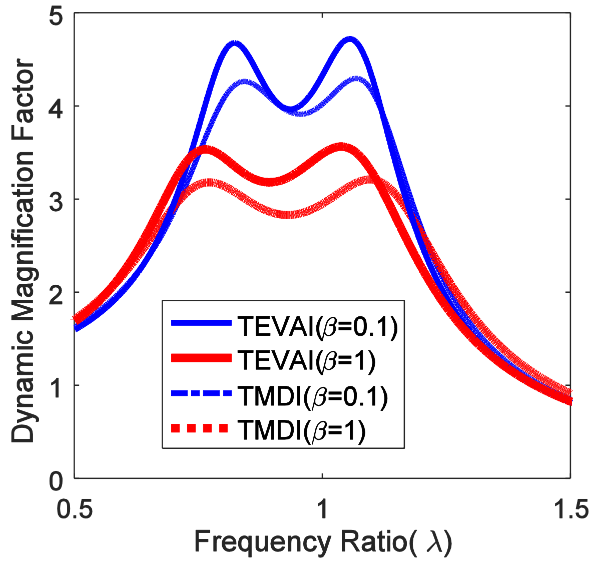

Figure 5-16: Frequency domain response of primary structure with H_∞ optimal TMDI and TEVAI with mass ratio = 10%

It should be noted herein, that the TMDI and TEVAI need a fixed, or approximately fixed, support for the inerter. To provide this fixed support, different practical alternatives can be used such as outrigger systems, which have been proposed for tuned inertia mass electromagnetic transducers [97] and tuned viscous mass dampers [111]. Furthermore, in situations with limited space, the utilization of a large inertance could lead to the reduction of the secondary mass size and, thus, an overall reduction in the size of the installed absorber, compared to the TMD.

Conclusion

In this paper, a new inerter-based passive vibration absorber is proposed. This passive control device, the three-element vibration absorber-inerter (TEVAI), is a development based on the three-element vibration absorber (TEVA) and the tuned mass-damper-inerter (TMDI). In this paper, the TEVAI was introduced, formulated, optimized, and examined in order to evaluate its effectiveness. A closed-form H_2 optimization procedure was performed and expressions for optimal parameters of the device were presented. In addition, numerical optimization was performed to examine the effectiveness of the device given the H_∞ optimization criterion, the reduction of the maximum peak response in the frequency domain. The principle conclusions based on the results of his study are:

The effectiveness of the TEVAI is dependent on the inertance mass ratio. In general, it was observed that the performance of the device increases with increased inertance mass ratio. Similar behavior was observed for the TMDI.

The TEVAI was observed to provide a lower H_2 norm and peak DMF in the case of H_2 optimization and lower peak DMF in the case of H_∞ optimization, compared to the TMDI with the same main mass and inertance mass ratio.

The H_2 optimum TEVAI is able to reduce the H_2 norm of the primary mass by an additional 3% to 5%, in comparison to the H_2 optimal TMDI, over the range of main mass and inertance mass ratios considered.

The H_2 optimum TEVAI is able to provide a 3% to 14% reduction in the peak dynamic magnification factor, in comparison to the H_2 optimal TMDI, over the range of main mass and inertance mass ratios considered.

The H_∞ optimum TEVAI is able to provide a 3% to 10% reduction in the peak dynamic magnification factor, in comparison to the H_∞ optimal TMDI, over the range of main mass and inertance mass ratios considered. It should be noted the peak of the H_∞ optimum system is less than the peak of the H_2 optimum system for both the TMDI and TEVAI.

In comparison to the TEVA, the H_∞ optimum TEVAI was observed to further reduce the maximum dynamic magnification factor by 5% to 29% with inertance mass ratio equal to 0.1 to 1.

In both the H_2 and H_∞ optimum designs, the optimum tuning frequency, damping ratio and spring ratio of the TEVAI all increase with increases in the inertance mass.

The reductions in response, which may be significant for applications in civil engineering, mechanical engineering, and other fields, can be produced with the relatively minor modification of the TMDI needed to produce a TEVAI.

CHAPTER SIX:NONLINEAR ENERGY SINK INERTER

A version of this chapter was originally published by Abdollah Javidialesaadi and Nicholas Wierschem:

A. Javidialesaadi, N.E. Wierschem, An inerter-enhanced nonlinear energy sink, Mechanical Systems and Signal Processing. 129 (2019) 449–454. https://doi.org/10.1016/j.ymssp.2019.04.047.

This paper is part of the development of state of the art in inerter-based mass dampers. Background, formulation, design, and performance evaluation of the proposed inerter-based mass damper is presented in this paper.

Abstract

This short communication proposes a novel nonlinear energy sink (NES) equipped with an inerter for passive vibration control of structures and presents the results related to the performance evaluation of this device. NESs are considered to be robust and effective passive control devices that can resonate in a broadband fashion. The configuration of the proposed nonlinear energy sink-inerter (NESI) is that of a traditional NES with an inerter between the device's physical mass and a fixed point. Through the conversion of relative translational motion to rotational motion, the inerter is capable of providing an effective mass effect to the NESI. The optimum design values of the proposed device are achieved through a numerical search and the effect of the inerter on the response of the primary structure is presented. It was found that the effectiveness of the NESI can be substantially increased, compared to the NES, by using increasingly large values of inertance. As these results can be achieved by utilizing an inerter with a small physical mass, the NESI has potential to provide similar or better structural control performance as a NES that has more physical mass.

Introduction

Nonlinear energy sinks (NESs) have been investigated as passive control devices for the past two decades. NES absorb energy from a structure, irreversibly transfers this energy away, and dissipates it locally [46–48,50]. The traditional NES design, which consists of a small mass connected to a primary structure through a linear dashpot and an essentially nonlinear spring with a cubic stiffness, has been studied for passive structural control and demonstrated robustness and effectiveness [51]. Unlike tuned mass dampers (TMDs), which have a particular resonance frequency, the essential nonlinearity of the NES stiffness element allows the NES to vibrate in a broadband fashion [49,51]. A wide range of activities including the development of steady state periodic solutions of damped NES in the frequency-energy domain [150,151], experimental and theoretical studies on energy pumping of NES under external excitation [117], efficiency of parallel NES for targeted energy transfer [118], and targeted energy transfer from multi-degree-of-freedom-primary structures to the NES [119] have been undertaken in order to study NES.

The structural control effectiveness of mass dampers is generally increased by increasing the secondary mass to main structure mass ratio [6]; however, increasing the amount of secondary mass raises practical concerns and cost considerations. Reducing the physical mass of mass dampers and increasing their effectiveness by utilizing inerters has recently been studied by a number of researchers [8–10,52,53,80].The inerter is a two terminal mechanical device which produces equal and opposite forces across its terminals proportional to the relative acceleration between the terminals [54]. Various different inerter-enhanced TMDs have been proposed wherein the inerter is placed between the device's physical mass and the mass of the primary structure [10,58]. In addition to the enhancement of TMDs with inerters, an improved version of the NES has been proposed recently by utilizing an inerter between the primary structure and the device's physical mass [120]. Despite some improvement in effectiveness, the increase in effectiveness is limited and increases in the device's inertance do not necessarily correspond with increases in the device's effectiveness [9,120].

The tuned mass damper-inerter (TMDI) and the three-element vibration absorber-inerter (TEVAI) are two types of inerter-enhanced TMD that feature an inerter between the device's physical mass and a support [53,98]. The support necessary for the inerter in the TMDI or TEVAI can be provided by the ground [52,121] [53,98]or another degree of freedom of the structure [57,59]. When the TMDI is carefully tuned, the effectiveness of devices with this type of inerter configuration generally increases with increases in inertance [53,59,63,98], which cannot be achieved in devices where the inerter is located between the secondary mass and the primary structure[10,120], such as the rotational inertia double tuned mass damper [9].

Inspired by the effectiveness of the TMDI, this paper proposes the nonlinear energy sink-inerter (NESI). This device features a mass connected to a primary structure with a damping element and a cubic stiffness element along with an inerter placed between the NES mass and a fixed point. In the next section, the equations of motion for this device are presented. After that, the structural control effectiveness of the device, in comparison to a NES, is investigated. Finally, conclusions regarding this device are summarized in the last section.

Nonlinear Energy Sink-inerter (NESI)

Figure 6-1 shows the schematic representation of the inerter. The governing equation of the inerter is given by

$$F = b(\ddot{x}_1 - \ddot{x}_2) \tag{6.1}$$

where F denotes the force at the terminals and b is the inertance or effective rotational inertia mass.

The key benefit of the inerter is its ability to provide a relatively large amount of inertance with a small physical mass. For example, an inerter with a 560 kg physical mass that produces 5,400,000 kg of inertance has been reported in the literature [12].

Figure 6-2 (a) shows the TMDI [53]and Figure 6-2 (b) depicts the proposed NESI device. In this figure, m_1, k_1, and c_2 represent the mass, stiffness, and damping of the primary structure. Furthermore, in Figure 6-2, m_2, b, and c_2 denote the secondary mass, inertance, and the device damping, respectively. The linear stiffness of the TMDI is represented by k_2 and the cubic stiffness coefficient of the NESI is represented by k_{NES}.

The stiffness element in the TMDI is linear and has a restoring force equal to $k_2(x_1 - x_2)$; whereas, the restoring force from the stiffness element in the NESI is essentially nonlinear and equal to $k_{NES}(x_1 - x_2)^3$. Considering Eq.(6.1), the equation of motion of the NESI can be expressed as follows:

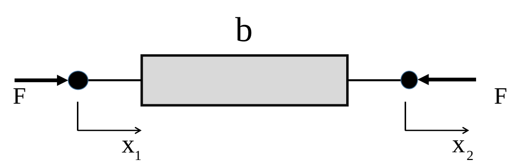

Figure 6-1: Schematic representation of the Inerter

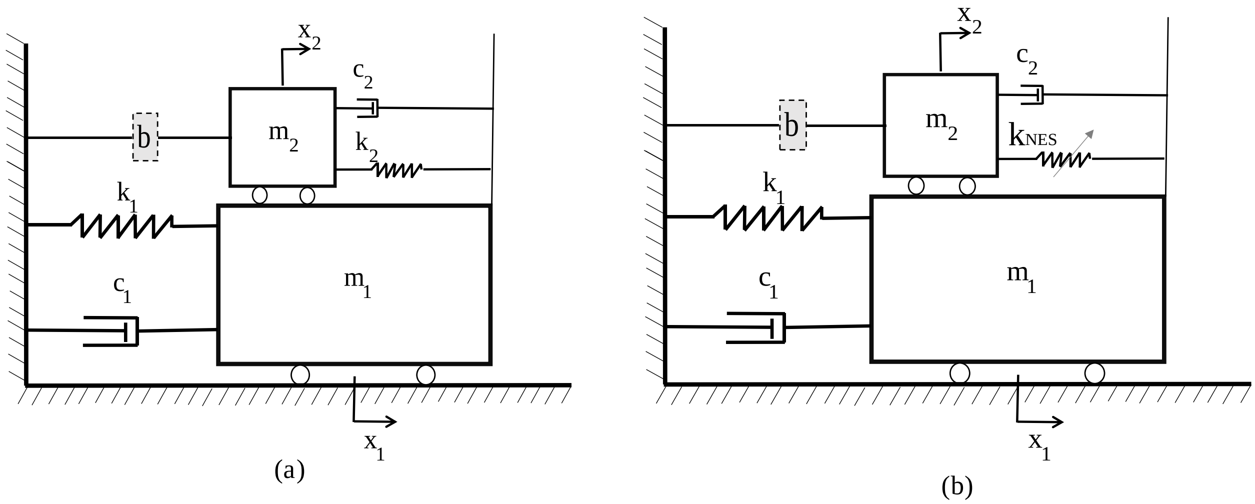

Figure 6-2: The single degree-of-freedom primary structure with attached (a) tuned mass damper-inerter (TMDI) (b) nonlinear energy sink-inerter (NESI)

$$\begin{cases} m_1\ddot{x}_1 + c_1 x_1 + c_2\left(\dot{x}_1 - \dot{x}_2\right) + k_1 x_1 + k_{NES}(x_1 - x_2)^3 = 0 \\ (m_2 + b)\ddot{x}_2 + c_2\left(\dot{x}_2 - \dot{x}_1\right) + k_{NES}(x_2 - x_1)^3 = 0 \end{cases} \tag{6.2}$$

The effect of the inerter on the system is seen in the term $(m_2 + b)$, which shows that the added inertance effectively increases the amount of secondary mass, m_2, by the inertance b.

Analysis and Results

The parameters of the primary structure considered are $m_1 = 24.3\ kg$ and $k_1 = 6820\ N/m$. Additionally, this structure is considered as undamped to allow the effect of the NESI to be better discerned. In this analysis, the primary structure is subjected to an impulsive load that is realized as an initial velocity equal to $\dot{x}_1 = 0.1$ m/s. The displacement of the primary structure is considered as the output and the root mean square (RMS) of the displacement of the primary structure is used in the objective function for the optimization. The goal of the optimization procedure of the NESI is to find the device stiffness value (k_{NES}) and damping value (c_2) to minimize the RMS of the primary structure's displacement given the primary structure properties, the secondary mass ratio ($\mu_1 = m_1/m_s$), and the inertance ratio ($\mu_2 = b/m_2$). The secondary mass considered for this analysis is equal to 5% of the mass of the primary structure ($\mu_1 = 0.05$) and three inertance ratios ($\mu_2 = 0$, $\mu_2 = 0.25$, and $\mu_2 = 1$) are considered. In each case, this optimization is performed by utilizing a numerical search.

The results of this optimization study are presented in Figure 6-3. These results show that by increasing the inertance ratio from zero (see Figure 6-3(a)) to $\mu_2 = 0.25$ (see Figure 6-3(b)), the minimum RMS decreases by 9%. Note that for the zero inertance case, the NESI is an NES. Increasing the inertance ratio to $\mu_2 = 1$ (see Figure 6-3(c)) leads to a decrease in the minimum RMS by 25%, compared to the zero inertance case. In addition to the reduction in the minimum RMS, Figure 6-3 shows that a reduction in RMS is realized with increased inertance at most every combination of device mass and stiffness. Similar behavior has been observed in the TMDI [53] and shows that the addition of the inertance in the device can reduce the response in even the non-optimal cases. Furthermore, the behavior seen in Figure 6-3 also shows some similar trends observed with both the NES and the NESI. At least a minimal level of device damping is required for it to be effective at reducing the response of the structure; with an undamped structure, this device damping is needed for any energy dissipation to occur. Additionally, it is observed that for all damping levels, stiffness in the device above the optimal level leads to a nearly completely ineffective performance [121]; with too high of stiffness, the device cannot achieve the levels of relative motion necessary to be effective. An additional optimization study was also performed to investigate the effect of the inerter on the performance of the NESI when considering different device secondary mass ratios.

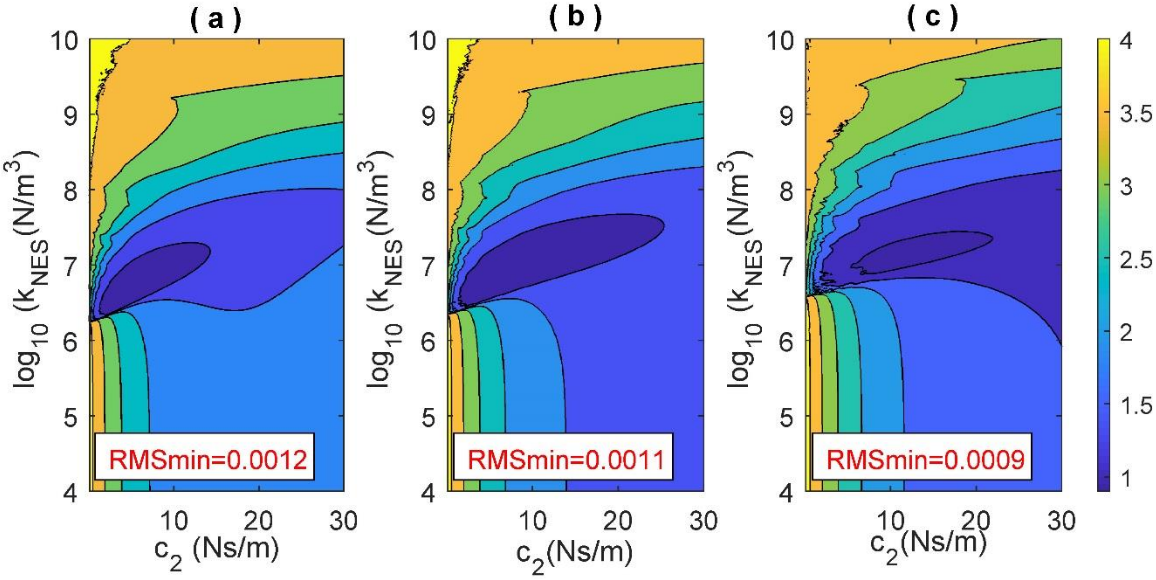

Figure 6-3: Contour plot showing the RMS of the primary structure's displacement versus the damping and stiffness of the NESI (a): $\mu_2 = 0$; (b): $\mu_2 = 0.25$; (c): $\mu_2 = 1$

. For this study, the secondary mass ratios considered are $\mu_1 = 0.01$, $\mu_1 = 0.025$, $\mu_1 = 0.05$, and $\mu_1 = 0.1$ and the range of inertance ratio considered is $0 < \mu_2 < 1$. These secondary mass ratios and inertance mass ratio combinations were selected because they are in-line with the mass ratios commonly considered in the civil engineering application of similar devices [59,63,106]. While not as commonly considered in literature, larger mass and inertance ratios in the device can be used if desired. For each secondary mass ratio and inertance mass ratio combination, an optimization analysis was done to determine the minimum possible RMS of the structure's displacement response to the initial velocity loading. The results of this study are presented in Figure 6-4. These results demonstrate that for all of the NESI secondary mass ratios considered, the reduction in response increases smoothly with increased device inertance. For all of the secondary mass ratios considered, the reduction in RMS was between 25% and 20% when $\mu_2 = 1$, compared to the zero inertance case. From this figure, one can also see, for example, that the performance of the NESI when $\mu_1 = 0.05$ and $\mu_2 = 1$ is approximately equal to the performance when $\mu_1 = 0.1$ and $\mu_2 = 0$. This result demonstrates that, with the effective mass provided by the inerter, it is possible to utilize a device with a smaller secondary mass ratio and inerter to achieve the same performance as a NES with a larger secondary mass ratio. As the effective mass provided by the inerter can be produced with very little physical mass, the total physical mass of the device can be dramatically reduced by using an inerter in this manner, without sacrificing performance.

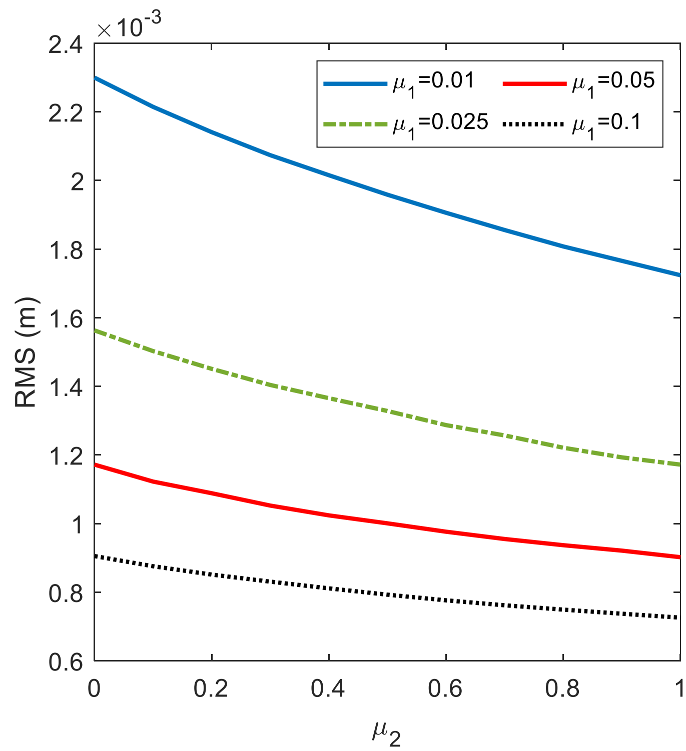

Figure 6-4 RMS of the primary structure's displacement response versus inertance mass ratio

The time history responses of the optimum designed NES (a NESI with $\mu_2 = 0$) and NESI ($\mu_2 = 1$) subjected to the initial velocity are presented in Figure 6-5. This figure shows the effectiveness of the inerter at quickly attenuating the primary structure's response.

To compare the performance of the NESI with the TMDI, a TMDI with a secondary mass ratio of $\mu = 0.05$ and inertance ratio of $\beta = 0.5$ was optimized to reduce the RMS response to an initial velocity. The parameters that result from this optimization are $k_2 = 10^{2.26}\, {}^{N}\!/_{m}$ and $c_2 = 7.7\, {}^{Ns}\!/_{m}$. A comparison of the RMS of the response of this optimized TMDI with the optimized NESI with the same mass ratios shows that the TMDI outperforms the NES by 12%. This result is expected as researchers have found the TMD typically outperforms the NES when only one structural mode is excited, and the system considered has not changed from the system used for optimization [51,122]

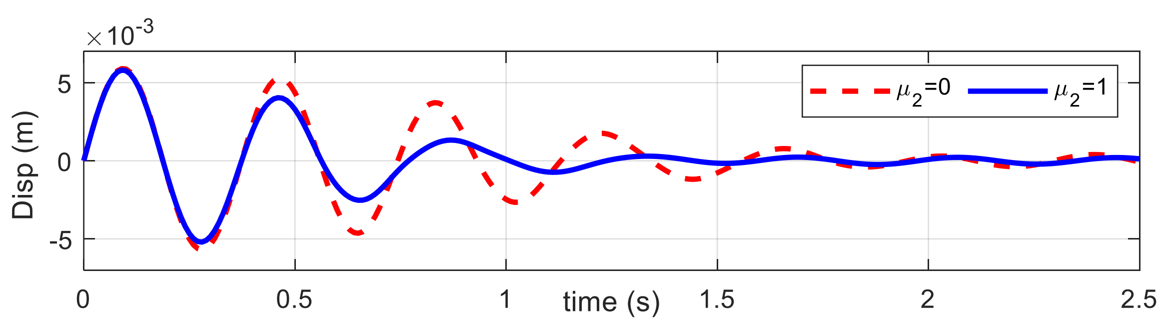

Figure 6-5: Time history response of the primary structure's displacement with NES $(\mu_2 = 0)$ and NESI $(\mu_2 = 1)$

The effectiveness of the TMDI and NESI can be comparatively examined across a range of inertance ratios and secondary mass ratios. For this analysis, a reduction factor, R, comparing the effect of the inerter on the TMDI or the NESI is defined as follows:

$$R=\frac{RMS_{TMDI}}{RMS_{TMD}} \quad \text{or} \quad R=\frac{RMS_{NESI}}{RMS_{NES}} \tag{6.3}$$

Figure 6-6 presents R when it is calculated for both the impulse response of the systems with the optimized NESI and the TMDI. In this analysis inertance ratios

from 0 to 1 and secondary mass ratios equal to 0.01, 0.025, 0.05 are considered. These results show that the RMS of the systems' response reduces with increases in the inertance for both the TMDI, as was seen as well in Figure 5, and for the NESI; however, the effect of the inerter on the NESI is greater than for the TMDI. With an inertance ratio of 1, the results of this analysis showed that the TMDI was up to 17% more effective than the TMD and that the NESI was up to 26% more effective than the NES.

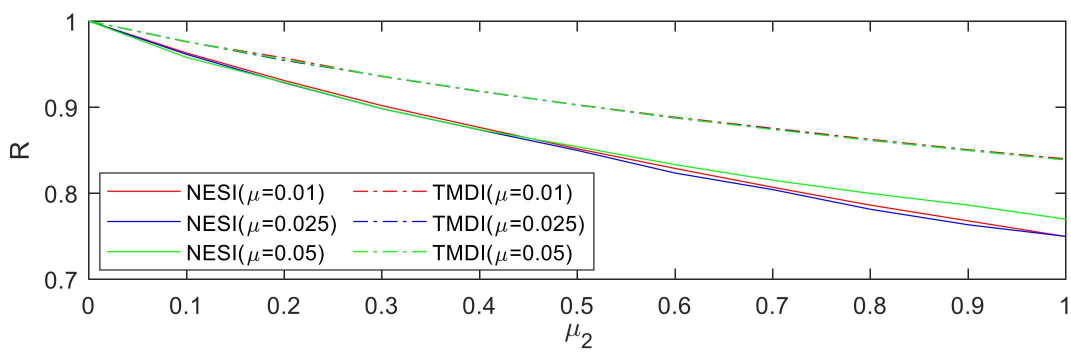

Figure 6-6: Effectiveness of inertance in the TMDI and the NESI

Conclusions

In this short communication, an enhanced nonlinear energy sink (NES) referred to as a nonlinear energy sink-inerter (NESI) is proposed. The NESI is similar to a traditional NES, except an inerter is position between the NES mass and a fixed point. The results of this study demonstrate the superior performance of the proposed device in comparison to the traditional NES. For all of the device secondary mass ratios considered, with increases in the inertance value utilized in the NESI, the reduction in the RMS of the response increases smoothly and monotonically. This type of increase in performance is not observed for inerter configurations in which the inerter is placed between the primary structure and the physical mass of the mass damper. Furthermore, for the different secondary mass ratios considered and an inertance ratio of 1, it was found that the NESI was able to decrease the RMS response by between 20% and 25%, compared to the NES.

As it is possible to configure an inerter to provide a relatively large effective mass, while only having a small physical mass, the use of an inerter in the manner described in this study can be an effective way of increasing the passive structural control performance of an NES without increasing its secondary mass. Alternatively, this configuration could allow for a device with a more effective structural control performance, given an available amount of physical mass.

Future work related to this device will include the design and performance evaluation of the proposed device in MDOF structures subjected to harmonic, random, and earthquake excitation, a study of its robustness, and an experimental validation study.

CHAPTER SEVEN:MULTIPLE TUNED MASS DAMPER INERTER

This paper is part of the development of state of the art in inerter-based mass dampers. In this paper, a new inerter-based mass damper is proposed, formulated, and evaluated. This paper will be submitt for publication in by the end of May202.

Abstract

This paper proposes the multiple tuned mass damper-inerter (MTMDI) as a passive structural control device. The multiple tuned mass damper (MTMD), which features multiple mass-spring-damper attachments, has been widely investigated and can provide more effective performance than the tuned mass damper (TMD). The effectiveness of mass dampers is typically limited by their mass size. Consequently, there is interest in incorporating into mass dampers an inerter, a device that can provide mass effects through the transformation of translation to rotational motion. A prominent example being the tuned mass damper inerter (TMDI), which features an inerter connected between a single mass-spring-damper attachment and the ground. The proposed MTMDI builds on both the TMDI and MTMD. Two MTMDI design philosophies are investigated that both consider the total device mass and the inertance ratio as design choices. In the Type 1 MTMDI, the mass of each attachment is equal and the individual attachment stiffness and damping parameters are obtained via optimization. In the Type 2 MTMDI, the frequencies of the attachments are functionally distributed and the equal attachment stiffness and damping parameters are determined via optimization. The effect of the system parameters and design philosophy on the MTMDI performance are investigated. The results of this study show the proposed device effectiveness is, in general, superior to the TMDI and MTMD; however, this effectiveness depends on the number of absorbers, the mass ratio, and inertance ratio. Additionally, the results demonstrated that the distribution of inertance in the MTMDI does not significantly change its optimized performance.

Introduction

Various types of passive control devices have been proposed and developed in the past decades to protect structures that are subjected to natural and man-made excitations [1]. One of the most prominent passive control devices designed to reduce the dynamic response of structures is the tuned mass damper (TMD) [14]. Traditional TMDs consist of a small mass connected to a main structure through stiffness and damping elements [13,14].The TMD is able to reduce the response of the main structure at its resonance frequency when it is designed well and remains tuned. The goal of the design of TMDs is often to determine the values of the device's stiffness and damping elements that minimize the maximum value or root-mean-square of some response measure. Often studies on the effectiveness and optimum design of TMDs consider structures subjected to harmonic loads or random excitation [18,20,21,84,87,123].

TMDs have been installed in a variety of structures, including a significant number of tall buildings [4]; however, a number of issues exist that limit their more widespread adoption. One of these issues is that TMDs are more effective when the ratio of secondary mass to the main structure's mass is large, particularly when considering the mitigation of seismic excitation [6,7]; however, a large TMD mass may not be practical and would likely be very expensive [34]. Another issue is that TMDs are sensitive to the detuning that might occur due to errors in their design and fabrication [34], because of stiffness changes in the structure that may occur over time, or because of damage to the system [2]. To provide more effective dynamic response reduction and protect against detuning, the multiple tuned mass damper (MTMD) has been proposed and investigated [35,39]

MTMDs consist of two or more interdependently designed TMDs connected to a main structure through spring and damping elements. To date, various types of MTMD design philosophies have been proposed and investigated [124]. One of the most common of these philosophies is one where identical spring and dampers are used for each of the MTMD's TMDs along with different masses to produce a

MTMD with a prescribed distribution of individual TMD frequencies [37,39]. The other most common design philosophy is one where the MTMD's TMDs have equal mass, but nonidentical springs and dampers [37,124]. As the manufacturing of MTMDs with the same damping and stiffness elements is typically simpler, this type of MTMD is often more desirable in structural engineering applications [124]; however, MTMD with nonidentical stiffness and damping can be more effective [40].Despite these differences, for all of the major MTMD design philosophies considered, it has been found that MTMDs can more effectively reduce dynamic responses and are generally more robust against detuning compared to a TMD with the same total mass [37,40,41,43,44,124,125].

While dividing the TMD mass to create the MTMD results in improved performance, the effectiveness of the MTMD is still limited by the total mass of the device. In recent years, great interest related to structural control has been expressed in exploiting the large effective inertia mass produced by a mechanical device called an inerter. The inerter is a two terminal mechanical device that can produce an equal and opposite force proportional to the relative acceleration of two end nodes through the conversion of translational motion into the rotational motion of a flywheel [54]. Utilizing an inerter in combination with stiffness and/or damping elements, the rotational inertia viscous damper (RIVD), tuned viscous mass damper (TVMD), and tuned inerter damper (TID) have been proposed and investigated for single-degree-of-freedom (SDOF) structures as the first generation of inerter-based passive control devices [8,52,71]. Additionally, the clutch inerter damper and one-way rotational inertia damper, devices that utilize rotational mechanisms to transfer energy away from the structure without the possibility of it returning, have been proposed [67,80].

In all of the aforementioned inerter-based devices, only effective mass from the inerter is utilized and no large physical mass in the device itself is present. In addition to these developments, the inerter has been used to improve the TMD's performance and reduce the physical mass of the TMD needed. Replacing the

TMD's dashpot, which is between the TMD mass and the floor the TMD is attached to, with an inerter, damper, and spring in different configurations introduces various types of inerter-based TMD, which have been proposed, designed, and evaluated [9,58,101]. These studies have demonstrated that these kind of inerter-based TMD can show improved performance, but that those improvements are limited and cannot be monotonically increased by increasing the size of the inerter. In contrast, by adding the inerter between the secondary mass of TMDs and a fixed support, the tuned mass damper inerter (TMDI) has been proposed and demonstrated superior performance in comparison to traditional TMDs. It has been found that the effectiveness of the TMDI increases monotonically with larger inerters [53]. Utilizing this same inerter configuration, the three-element vibration absorber inerter (TEVAI) [98]and nonlinear energy sink inerter (NESI) [126] have been proposed recently to improve the TMDI and nonlinear energy sink, respectively.

As a development building on previous work on inerter-based TMD and MTMD, this paper presents a new device called the multiple tuned mass damper inerter (MTMDI) and examines its efficacy for the passive control of SDOF structures. The main contribution of this work is introducing this new device and investigating its performance when designed based on two different design philosophies. In the first design philosophy (Type 1 MTMDI), the individual absorbers have the same physical mass and nonidentical stiffness and damping elements. In the second design philosophy (Type 2 MTMDI), the individual absorbers have identical damping and stiffness elements and nonidentical masses. This study will consider random ground acceleration and investigate the design and performance of the two types of MTMDI, the number of absorbers in the MTMDI, and the level of and distribution of inertance in the MTMDI. Comparisons of the performance of the MTMDI will be made to both the TMDI and MTMD.

This work is presented in the following four sections. The next section (Section 2) presents the formulation of the proposed device. In Section 3, the design procedure and design values for both MTMDI design types is presented. Section

4 covers the performance evaluation of the proposed device with comparisons made to the TMDI and MTMD. Finally, Section 5 presents the summary and conclusions of this work.

Multiple tuned mass damper inerter (MTMDI)

In this section, the equations of motion of the proposed MTMDI is presented as well as the dynamics of the inerter.

The inerter consists of a small physical rotational inertia mass that can provide large effective mass via the transformation of translational motion to rotational motion. Figure 7-1 illustrates the schematic representation of the inerter. Two ways to potentially realize an inerter is with a flywheel connected to a ball-screw mechanism or a flywheel connected to a rack and pinion mechanism. The moment of inertia of the flywheel, physical mass of the flywheel, and geometry of the transformation mechanism all play crucial roles in determining the inertance value, the magnitude of the effective mass. Examples found in literature of the large inertance that can be physically realized with an inerter include 350 kg and 54000×10^{3} kg inertial masses produced using mechanisms with physical masses of 2kg and 560 kg, respectively [12,52].

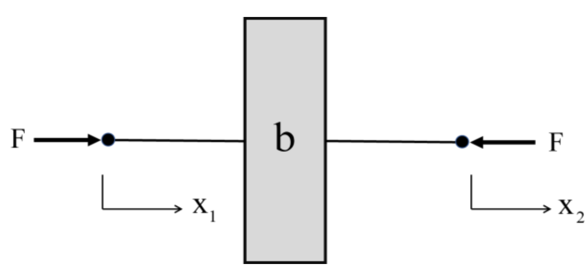

Figure 7-1: Schematic representation of an inerter

The restoring force of the inerter presented in Figure 7-1 can be expressed as

$$F = b(\ddot{x}_2 - \ddot{x}_1) \tag{1.7}$$

where, $\ddot{x}_i$ $(i = 1, 2)$, F, and b are the accelerations at the nodes, the restoring force, and inertance of the inerter, respectively. The specific equation used to calculate the inertance, (b), will vary based on the mechanism and the flywheel type used for the inerter [58].

Figure 7-2 shows the proposed multiple tuned mass damper inerter (MTMDI) connected to a SDOF structure that is subjected to a ground acceleration ($\ddot{x}_g$). In this figure, the MTMDI consists of n mass-spring-damper-inerter systems that are connected to the primary structure. As in the TMDI, the inerters in the MTMDI are connected between the ground and the MTMDI masses.

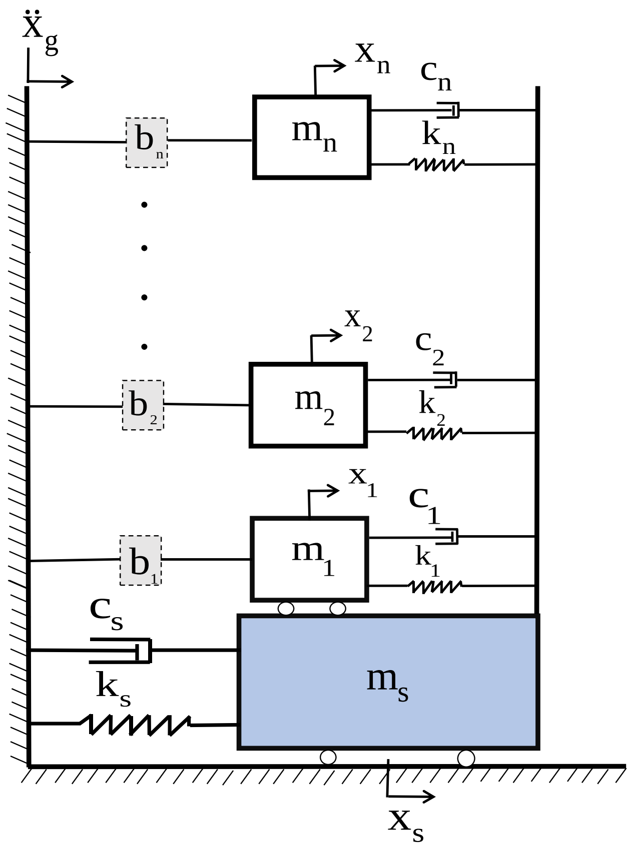

Figure 7-2: Model of a MTMDI connected to a SDOF structure

Considering Eq.)7.1(and utilizing newton's second law, the equations of motion for the system composed of the structure and the connected MTMDI with n absorbers can be expressed as follows:

$$
\begin{cases}
m_s\ddot{x}_s + (c_s + \sum_{i=1}^{n} c_i)\dot{x}_s - \sum_{i=1}^{n} c_i x_i + (k_s + \sum_{i=1}^{n} k_i)x_s - \sum_{i=1}^{n} k_i x_i = -m_s\ddot{x}_g \\
(m_1 + b_1)\ddot{x}_1 + c_1\dot{x}_1 - c_1\dot{x}_s + k_1 x_1 - k_1 x_s = -m_1\ddot{x}_g. \\
. \\
. \\
(m_n + b_n)\ddot{x}_n + c_n\dot{x}_n - c_n\dot{x}_s + k_n x_n - k_n x_s = -m_n\ddot{x}_g
\end{cases}
$$

)7.2(

where m_s, k_s, and c_s are the primary structure's mass, stiffness, and damping, respectively. Additionally, m_i, k_i, c_i, and b_i denote the mass, stiffness, damping, and inertance of the ith absorber, respectively.

In this study, the displacement of the primary structure relative to the ground is used to evaluate the system performance; thus, the equations of motion for this combined system can be rewritten using a state space representation with the relative displacement of the primary structure as the output:

$$
\begin{aligned}
&\dot{\mathbf{X}}(\mathrm{t}) = \mathrm{A}\mathbf{X}(\mathrm{t}) + \mathrm{Bu}(\mathrm{t}) \\
&\mathrm{y}(\mathrm{t}) = \mathrm{C}\mathbf{X}(\mathrm{t})
\end{aligned}
$$

)7.3(

where

$$
\mathbf{X} = [\ \mathrm{x}\ \dot{\mathrm{x}}\ ]\ ;\ \mathrm{x} = [\ m_s \quad m_1 \quad . \quad . \quad m_n\ ]
$$

$$
\mathbf{A} = \begin{bmatrix} \mathbf{0}_{(n+1)\times(n+1)} & \mathbf{I}_{(n+1)\times(n+1)} \\ -\mathbf{M}^{-1}\mathbf{K} & -\mathbf{M}^{-1}\mathbf{C}_{\mathbf{d}} \end{bmatrix}
$$

$$
\mathbf{C} = [1 \quad 0 \quad . \quad . \quad . \quad 0]\ ;\ \mathbf{B} = \begin{bmatrix} \mathbf{0}_{(n+1)\times 1} \\ \mathbf{M}^{-1}\begin{bmatrix} m_s \\ m_1 \\ . \\ . \\ m_n \end{bmatrix} \end{bmatrix}
$$

The mass matrix ($\mathbf{M}$), damping matrix ($\mathbf{C_d}$), and stiffness matrix ($\mathbf{K}$) for the combined system can be written as follows:

$$\mathbf{M}=\begin{bmatrix} m_s & 0 & . & . & 0 \\ 0 & m_1+b_1 & & & \\ . & & . & & \\ . & & & . & \\ 0 & . & . & 0 & m_n+b_n \end{bmatrix};\ \mathbf{K}=\begin{bmatrix} k_s+\sum_{i=1}^{n}k_i & -k_1 & -k_2 & -k_3 & . & -k_n \\ -k_1 & k_1 & 0 & 0 & . & 0 \\ -k_2 & 0 & k_2 & 0 & 0 & . \\ k_3 & 0 & 0 & k_3 & . & . \\ . & . & . & . & . & 0 \\ -k_n & 0 & 0 & 0 & 0 & k_n \end{bmatrix}$$

$$\mathbf{C_d}=\begin{bmatrix} c_s+\sum_{i=1}^{n}c_i & -c_1 & -c_2 & -c_3 & . & -c_n \\ -c_1 & c_1 & 0 & 0 & . & 0 \\ -c_2 & 0 & c_2 & 0 & 0 & . \\ c_3 & 0 & 0 & c_3 & . & . \\ . & . & . & . & . & 0 \\ -c_n & 0 & 0 & 0 & 0 & c_n \end{bmatrix}$$

(7.4)

A generic transfer function for the structure in the frequency domain that considers the displacement of the primary structure as the output can be written as follows:

$$H(i\omega)=\mathbf{C}(i\omega\mathbf{I}_{2(n+1)\times 2(n+1)}-\mathbf{A})\mathbf{B}$$)7.5(

For convenience, the following parameters are defined:

$\mu_1=\dfrac{\sum_{i=1}^{n}m_i}{m_s}$: Mass ratio; $\mu_2=\dfrac{\sum_{i=1}^{n}b_i}{\sum_{i=1}^{n}m_i}$: Inertance ratio; $\omega_s=\sqrt{\dfrac{k_s}{m_s}}$: Primary structure frequency

$\omega_i=\sqrt{\dfrac{k_i}{(m_i+b_i)}}$: Frequency of absorber i;

$\lambda = \dfrac{\omega}{\omega_s}$: Input frequency ratio;

$\zeta_i = \dfrac{c_i}{2(m_i + b_i)\omega_i}$: Damping ratio of absorber i

Similar to the MTMD [18,42,44,53,94], various design philosophies can be considered for the proposed device. However, this work is limited to the following two design philosophies:

Type 1 MTMDI

In this design philosophy, the secondary masses of the MTMDI are all identical and the stiffness and damping of each absorber is nonidentical. Mathematically, the MTMDI parameters in this design philosophy can be expressed as:

$$\begin{aligned} m_1 &= m_2 = ... = m_n \\ k_1 &\neq k_2 \neq ...... \neq k_n \\ c_1 &\neq c_2 \neq ..... \neq c_n \end{aligned} \tag{7.6}$$

In this design philosophy, the mass of the MTMDI and the inertance considered would be chosen by the designer and the stiffness and damping values would be obtain from an optimization procedure, which is discussed in the next section.

Type 2 MTMDI

In this design philosophy, the stiffness and damping of each absorber is identical and the secondary masses of the absorbers are nonidentical. The absorber masses in this design philosophy are distributed such that the individual absorbers have frequencies that are linearly distributed. The equation governing the frequency of each absorber is

$$\omega_i = \omega_c \left(1 + \left(i - \frac{n+1}{2} \right) \frac{\beta}{n-1} \right) \tag{7.7}$$

where ω_c is the central frequency of the MTMDI, β is a measure that controls the spacing of the natural frequencies of the device [34], and n is the number of absorbers in the MTMDI.

Mathematically, the MTMDI parameters in this design philosophy can be expressed as:

$$\begin{aligned} &m_1 \neq m_2 \neq .... \neq m_n \\ &k_1 = k_2 = ... = k_n = k_T \\ &c_1 = c_2 = ... = c_n = c_T \end{aligned} \tag{7.8}$$

where k_T and c_T are the identical stiffness and damping values.

In this design philosophy, the total physical mass of the absorbers ($\mu_1 m_s$) and the inertance considered would be chosen by the designer and c_T , β , and ω_c would be obtained through an optimization. k_T would then be calculated as follows:

$$k_T = \frac{\mu_1 m_s (1 + \mu_2)}{\sum_{i=1}^{n} \frac{1}{\omega_i^2}} \tag{7.9}$$

The mass of the ith absorber of the Type 2 MTMDI can be solved for as follows:

$$m_i = \frac{k_T}{\omega_i^2 \left(1 + \mu_2\right)} \tag{7.10}$$

Optimization Procedure

The goal of this section is to report on the procedure used for obtaining design values of the Type 1 and Type 2 MTMDI. Design values for the MTMDI can be obtained through optimizations that consider a particular objective function. In the literature, the optimization of TMDs, TMDIs, and MTMDs have typically considered the minimization of the maximum or variance of the displacement response of the SDOF structure they are attached to [18,37,44,53,124]. When the main structure is subjected to random excitation, it is typically more desirable to design the absorbers to minimize the variance of the displacement response relative to the ground [18,160]. Given this, the objective function used herein for the optimum design of the proposed devices can be expressed as the minimization of the following:

$$\bar{\sigma}^2 = \frac{1}{2\pi}\int_{-\infty}^{\infty} \left| H(i\lambda) \right| d\lambda \tag{7.11}$$

where, $\bar{\sigma}$ represents the variance of the output and $\bar{\sigma}^2$ represents the H2 norm of the output.

The minimization of Eq. (7.11) can be performed numerically or through an exact solution. With a SDOF primary structure and an absorber that is one or two degrees-of-freedom, obtaining optimal designs through exact solutions is a viable option and has been done for the TMD, TMDI, TEVAI and the double TMD in series and parallel configurations [18,90,98,124]. In the case of the MTMD, when the number of absorbers is more than two, the exact design optimization can be very complicated and tedious; thus, previous efforts that have considered the optimum design of the MTMD have been primarily limited to numerical optimization [42,124,127]. Likewise, the design of the proposed MTMDI investigated herein is based on numerical optimization.

The optimum design problem for the Type 1 MTMDI can be expressed as follows:

$$
\begin{array}{ll}
\text{minimize} & \{\bar{\sigma}^2\} \\
\text{subject to} & \\
\begin{bmatrix} c_i & k_i \end{bmatrix} & 0 < k_i \le k_u,\ 0 < c_i \le c_u \quad (i = 1, n)
\end{array}
\tag{7.12}
$$

where k_u and c_u are values utilized as upper bounds for k_i and c_i, respectively.

As the complexity of the optimization, particularly for the Type 1 MTMDI, increases with increases in the number of absorbers, it is necessary to take steps to avoid local optimums. In order to obtain more reliable optimal design values, the following two-stage procedure was performed for the Type 1 MTMDI optimization. The first stage was to utilize a genetic algorithm considering a wide positive domain for the upper limit values. In the second stage, the optimum values obtained from the genetic algorithm were then utilized to create a set of 100 initial points for the nonlinear constrained optimization with the *fmincon* command in MATLAB [105]. In order to reduce the search domain in this second stage, the lower and upper boundaries of the constrained optimization were set as one tenth and ten times the initial point, respectively.

The optimum design problem for the Type 2 MTMDI can be expressed as follows:

$$
\begin{array}{ll}
\text{minimize} & \{\bar{\sigma}^2\} \\
\text{subject to} & \\
\begin{bmatrix} c_T & \omega_c & \beta \end{bmatrix} & 0 < c_T \le c_u,\ 0 < \omega_c \le \omega_c, 0 < \beta \le \beta_u
\end{array}
\tag{7.13}
$$

where c_u, ω_u, and β_u are values utilized as upper bounds for c_T, ω_c, and β respectively.

In this case, the optimization is less complex as the number of parameters considered in the optimization does not grow with the number of absorbers in the MTMDI. Consequently, the optimization of the Type 2 MTMDI considered in this work was done using the *fmincon* command in MATLAB with multiple initial solution points, but without a first stage featuring a genetic algorithm.

Analysis and Performance Evaluation

This section covers the analysis and performance evaluation of the MTMDI. First, the results and performance evaluation of the Type 1 MTMDI is presented, then the evaluation of the Type 2 MTMDI is presented. As both types of MTMDI are designed for minimizing the variance of the output, the H2 norm of the primary structure considering the displacement relative to the ground as an output is considered as one of the criterions used for evaluating its performance. In addition, even though it is not considered in the optimization, the maximum amplitude of the displacement of the primary structure, as measured by the maximum amplitude of the ground acceleration to structure displacement transfer function, is also considered for evaluating the performance of the MTMDI. The consideration of this criteria is commonly utilized for similar devices also optimized based on minimizing the variance of their response [53].

For all the following analyses, an undamped SDOF structure with $m_s = 1$, $k_s = 1$, and $c_s = 0$ is considered as the primary structure and a random load is considered for the base excitation ($\ddot{x}_g$).

Type 1 MTMDI

For the Type 1 MTMDI, the stiffness and damping of each absorber are values determined from the optimum design procedure and the total physical mass of the MTMDI is a design choice. The inertance ratio is also a design choice, but the distribution of that inertance between the different absorbers of the MTMDI also needs to be considered in the design. In order to evaluate the effect of the distribution of the inertance on the performance of the MTMDI, two subcategories of Type 1 MTMDI have been considered:

Equally Distributed Inertance: In this subcategory, the given total inertance is equally distributed to all of the individual absorbers. Mathematically this can be expressed as:

$$\frac{b_1}{m_1} = \frac{b_2}{m_2} = \ldots = \frac{b_i}{m_i}$$
$$\mu_2 = \frac{nb_1}{\sum_{j=1}^{n} m_j} = \ldots = \frac{nb_n}{\sum_{j=1}^{n} m_j} \qquad (7.14)$$

Concentrated Inertance: In this subcategory, the given total inertance is applied to just one of the absorbers. Mathematically this can be expressed as:

$$\mu_2 = \frac{b_1}{\sum_{i=1}^{n} m_i}$$
$$b_2 = b_3 = \ldots = b_n = 0 \qquad (7.15)$$

As a first step in examining the performance of both the equally distributed and concentrated inertance Type 1 MTMDI, a set of Type 1 MTMDI with a mass ratio equal to 10% ($\mu_1 = 0.1$) and an inertance ratio equal to 100% ($\mu_2 = 1$) is considered. The H2 optimum design procedure that was discussed in Section 3 was implemented for these Type 1 MTMDI with three, five, seven and nine absorbers ($n = 3, 5, 7, \text{ and } 9$). The frequency response curves for all of these optimized Type 1 MTMDI are presented in Figure 7-3. These results show that, regardless of the number of absorbers considered, there are not significant differences in the overall response for the equally distributed and concentrated inertance cases. The primary differences in the frequency response observed are localized to the right-hand side of the curve where a single deeper and wider dip occurs in the frequency response for the concentrated inertance case. This behavior occurs due to the larger impact from the one absorber with the concentrated inertance.

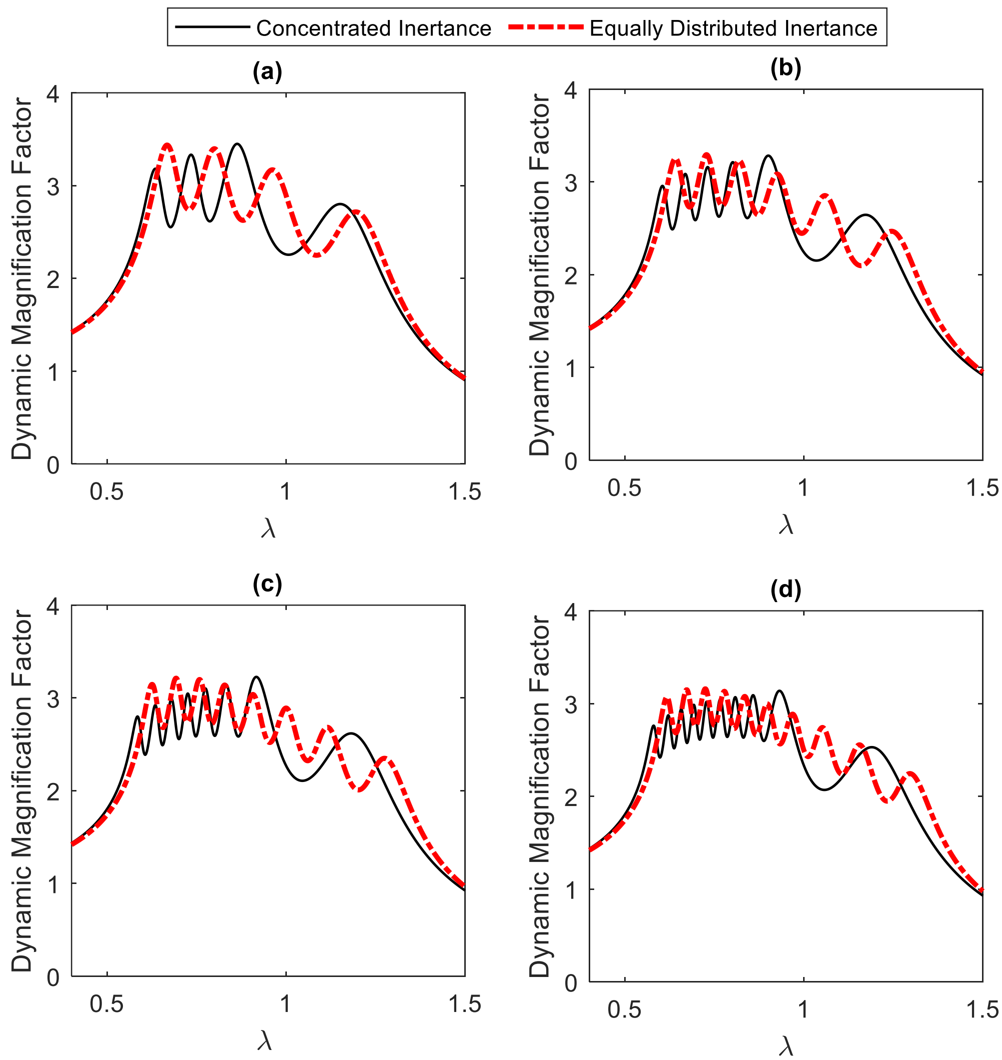

Figure 7-3: Effect of concentrated inertance and equally distributed inertance on the frequency response of a primary structure with a Type 1 MTMDI with a 10% mass ratio, 100% inertance ratio, and (a) $n=3$ (b) $n=5$ (c) $n=7$ and (d) $n=9$

To further examine the performance differences between the concentrated inertance and the equally distributed inertance Type 1 MTMDI, the H2 norm of the displacement response of the optimized systems with different combinations of mass ratio, inertance ratio, and number of absorbers is presented in Figure 7-4. In all the cases examine, the concentrated inertance Type 1 MTMDI displayed better H2 performance compared to the distributed inertance configurations.

The addition of inertance is intended to improve the performance of the MTMDI in comparison with the MTMD; consequently, when the same mass ratio and number of absorbers is considered, a relevant performance index is R_{H_2}, the ratio of the . Additionally, while the differences between the concentrated and equally

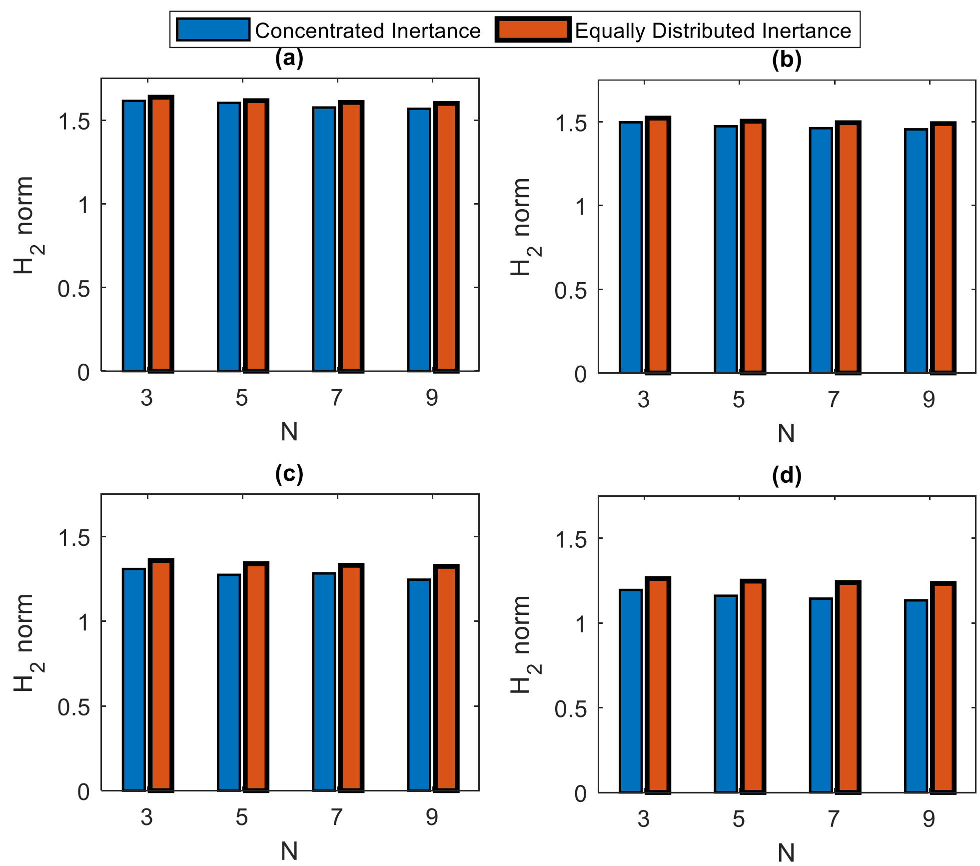

Figure 7-4: Comparison between concentrated inertance and equally distributed inertance (a) $\mu_1 = 0.10$, $\mu_2 = 1.0$; (b) $\mu_1 = 0.10$, $\mu_2 = 0.50$; (c) $\mu_1 = 0.40$, $\mu_2 = 1.0$; and (d) $\mu_1 = 0.40$, $\mu_2 = 0.50$

distributed cases were not particularly large (overall between a 1% and 2% difference was observed between the concentrated and distributed cases when the mass ratio is 0.1), these differences were greater when the mass ratio of the system was bigger and when more absorbers were utilized. Furthermore, Figure 7-4 shows that, as expected, the H2 performance of the system improved with a larger mass ratio and inertance ratio. As superior performance has been observed from the concentrated inertance designs, concentrated inertance will only be used thereafter when considering the Type 1 MTMDI.

H2 norm of the primary structure's displacement response with the MTMDI to the H2 norm with the MTMD.

$$R_{H_2} = \frac{H_2 \text{ norm of structural displacement with MTMDI}}{H_2 \text{ norm of structural displacement with MTMD}} \tag{7.16}$$

Figure 7-5 presents the R_{H_2} index for the Type 1 MTMDI. The MTMD considered to produce these results utilized the design constraints of the Type 1 MTMDI: the stiffness and damping of each absorber are different and the secondary mass is equally distributed among the absorbers. Figure 7-5 shows that the performance advantage of the MTMDI, compared to the MTMD, increases considerably with increases in the inertance ratio and less significantly with increases in the device mass ratio. Furthermore, these results show that increasing the number of absorbers increases the performance advantage of the MTMDI; however, these gains in advantage encounter diminishing returns quickly as the number of absorbers increases.

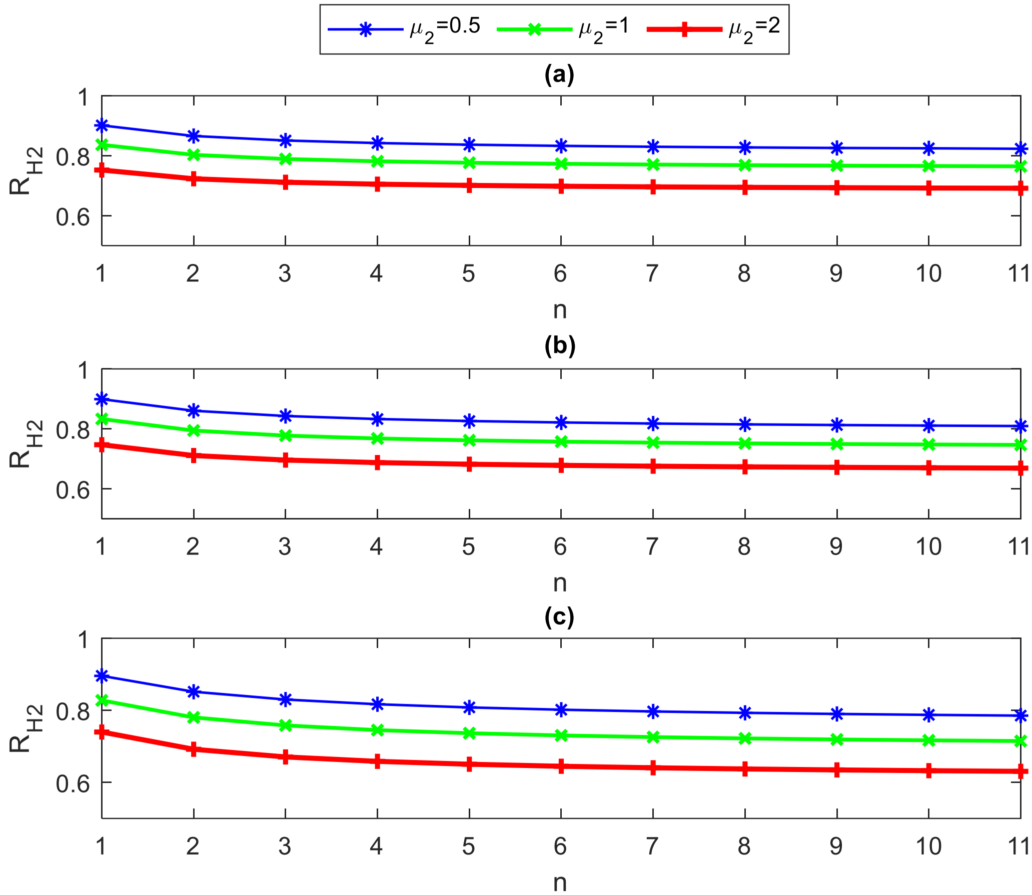

Figure 7-5: R_{H_2} for the Type 1 MTMDI as a function of the inertance ratio and number of absorbers, n, given (a) $\mu_1 = 0.10$ (b) $\mu_1 = 0.20$ and (c) $\mu_1 = 0.40$

The MTMDI is also design to be an improvement on the TMDI; thus, it is important to investigate the performance of the MTMDI in comparison with the TMDI with the same mass ratio and inertance ratio. For this comparison, the following index is defined:

$$P_{H_2} = \frac{H_2 \text{ norm of SDOF structure with MTMDI}}{H_2 \text{ norm of SDOF structure with TMDI}} \tag{7.17}$$

Figure 7-6 shows how the P_{H_2} index for the Type 1 MTMDI varies across a range of mass ratios, inertance ratios, and number of absorbers. In this figure, $P_{H_2} = 1$ when $n = 1$ as a MTMDI with one absorber is a TMDI. In each of the mass ratio and inertance ratio scenarios investigated in this figure, the performance of the MTMDI, compared to the TMDI, improves with an increase in the number of absorbers with a close to 8%, 10%, and 15% reduction possible for $\mu_1 = 0.1$, $\mu_1 = 0.2$, and $\mu_1 = 0.4$, respectively. However, as seen in Figure 7-5, these gains in advantage encounter diminishing returns quickly as the number of absorbers increases with little additional advantage noticeable after $n = 7$. The performance advantage of the MTMDI also increases with increases in the mass ratio. While there is little difference in the performance advantage of the MTMDI with increases in inertance ratio when $\mu_1 = 0.1$ and $\mu_1 = 0.2$, there is a noticeable increase in performance with increased inertance ratio when $\mu_1 = 0.4$.

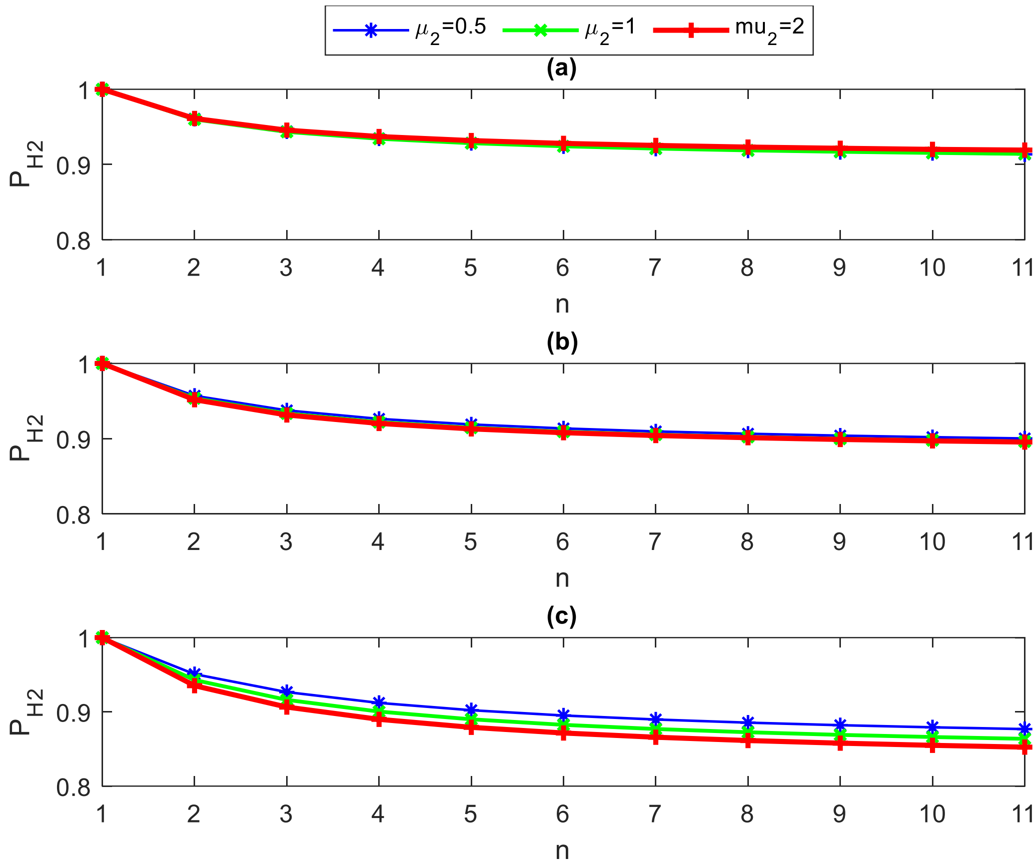

Figure 7-6 : P_{H_2} for the Type 1 MTMDI as a function of the inertance ratio and number of absorbers, n, given (a) $\mu_1 = 0.10$, (b) $\mu_1 = 0.20$, and (c) $\mu_1 = 0.40$

While the H2 of the displacement response is considered in the system optimization, the ability of the device to reduce the peak value on the displacement frequency response function is still relevant. The index used to track the performance of the MTMDI, in comparison to the MTMD, at reducing this peak transfer function value is defined as:

$$R_{H_\infty} = \frac{H_\infty \text{ norm of SDOF structure with MTMDI}}{H_\infty \text{ norm of SDOF structure with MTMD}} \tag{7.18}$$

where the different H_∞ norms represent the corresponding peak displacement frequency response values. Figure 7-7 shows how the index R_{H_∞} for the Type 1 MTMDI varies across a range of mass ratios, inertance ratios, and number of absorbers. These results show that R_{H_∞} decreases with increasing inertance ratio and increases with increasing mass ratio. Furthermore, a decrease in R_{H_∞} is observed with more absorbers, but the performance is relatively insensitive to the number of absorbers.

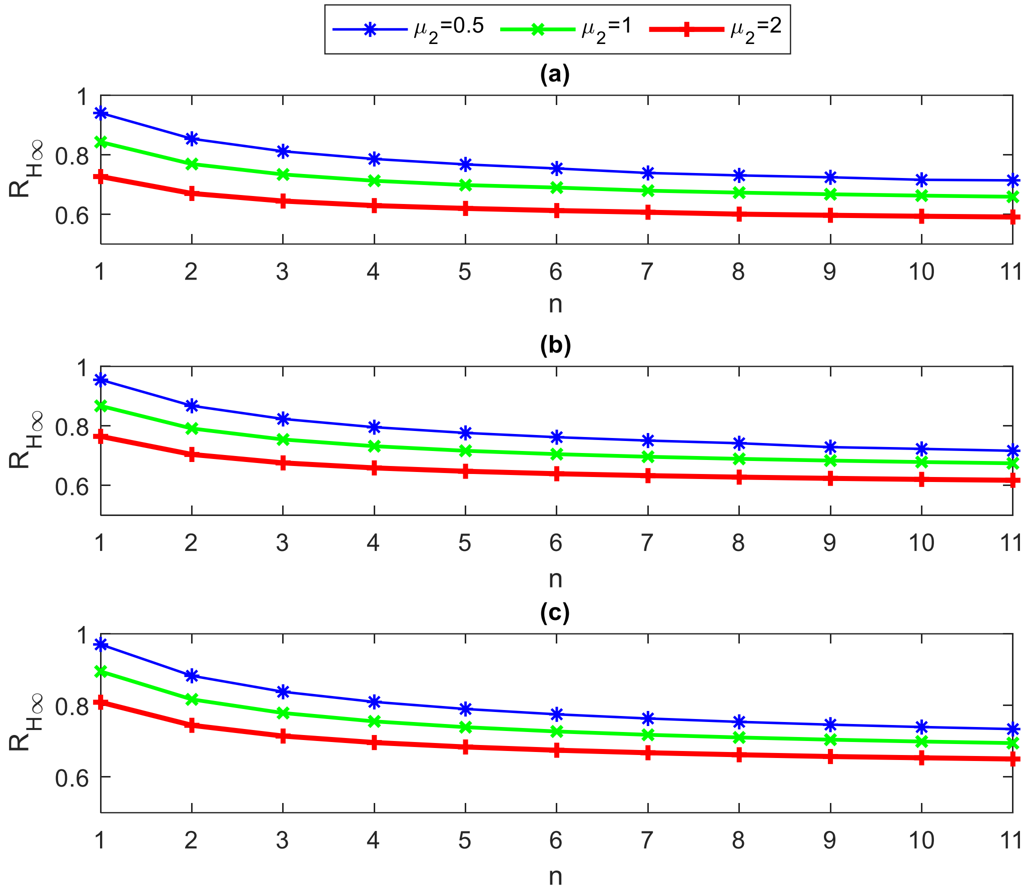

Figure 7-7: $R_{H\infty}$ for the Type 1 MTMDI as a function of the inertance ratio and number of absorbers, n, given (a) $\mu_1 = 0.10$, (b) $\mu_1 = 0.20$, and (c) $\mu_1 = 0.40$

The performance of the device at reducing the maximum transfer function value, in comparison to the TMDI, is also relevant. This performance can be tracked with the index defined as:

$$P_{H_\infty} = \frac{H_\infty \text{ norm of SDOF structure with MTMDI}}{H_\infty \text{ norm of SDOF structure with TMDI}} \tag{7.19}$$

Figure 7-8 shows how the P_{H_∞} index for the Type 1 MTMDI varies across a range of mass ratios, inertance ratios, and number of absorbers. This figure shows that

P_{H_∞} is relatively insensitive to the mass ratio, but decreases with increased inertance ratio. This figure also shows the decreases in P_{H_∞} with increases in the number of absorbers considered, with an up to a 24%, 23%, and 20% reduction in P_{H_∞} observed when $\mu_2 = 0.5$, $\mu_2 = 1.0$, and $\mu_2 = 2.0$, respectively.

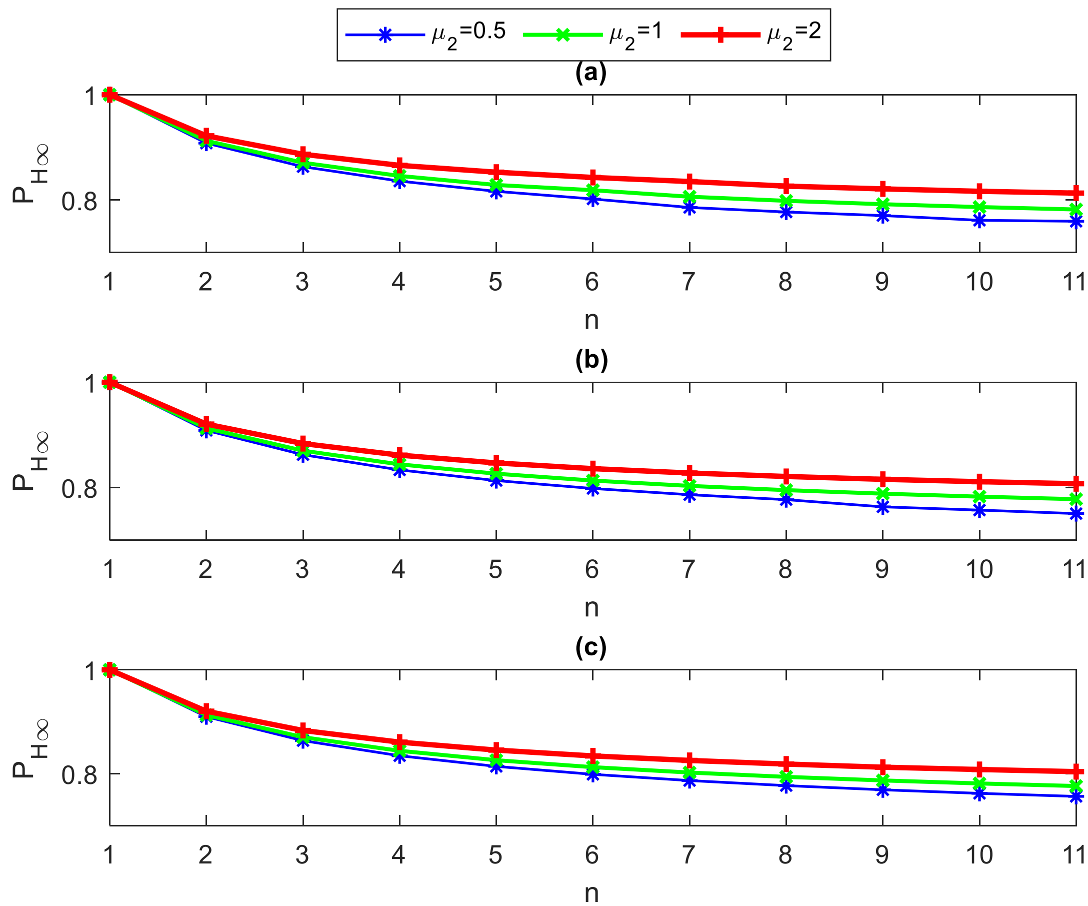

Figure 7-8: $P_{H\infty}$ for the Type 1 MTMDI as a function of the inertance ratio and number of absorbers, n, given (a) $\mu_1 = 0.10$, (b) $\mu_1 = 0.20$, and (c) $\mu_1 = 0.40$

To evaluate the behavior of a system with the Type 1 MTMDI, and compare this behavior to the TMDI, it is informative to examine the complete frequency response of the system. Considering a 10% mass ratio ($\mu_1 = 0.10$) and a 100% inertance ratio ($\mu_2 = 1.0$), Figure 7-9 presents the frequency response functions for the optimized TMDI and the Type 1 MTMDI with $n = 3,\ 5,\ 7,\ \text{and}\ 9$. These results show that, as expected based on the number of degrees-of-freedom, the frequency response curve for the TMDI has two peaks, while the curve for the MTMDI has $n+1$ peaks. Furthermore, the MTMDI frequency response has a large valley as one of its dominant features, which is in contrast to its series of nearly uniform peaks and valleys. This feature is present because the inertance is concentrated in one absorber of the MTMDI. In addition, even in the case when the MTMDI has a small number of absorbers, these frequency response curves show a meaningful reduction for the MTMD, in comparison to the TMDI, in the overall area under the curve as well as the maximum value of the curve.

To present the influence of the inertance ratio on the frequency response curve of the Type 1 MTMDI, Figure 7-10 shows the frequency response curves for the Type 1 MTMDI with 11 absorbers, a mass ratio of 10%, and a range of inertance ratios. This figure shows that the optimized Type 1 MTMDI produces the same deep valley in the frequency response also seen in Figure 7-9 and that this valley grows with increased inertance ratio. Furthermore, in addition to decreasing the amplitude and area under the frequency response curve, increasing the inertance ratio also shifts the peaks of the system to the left, which represents a reduction in the dominant natural frequencies of the system with increased inertance ratio.

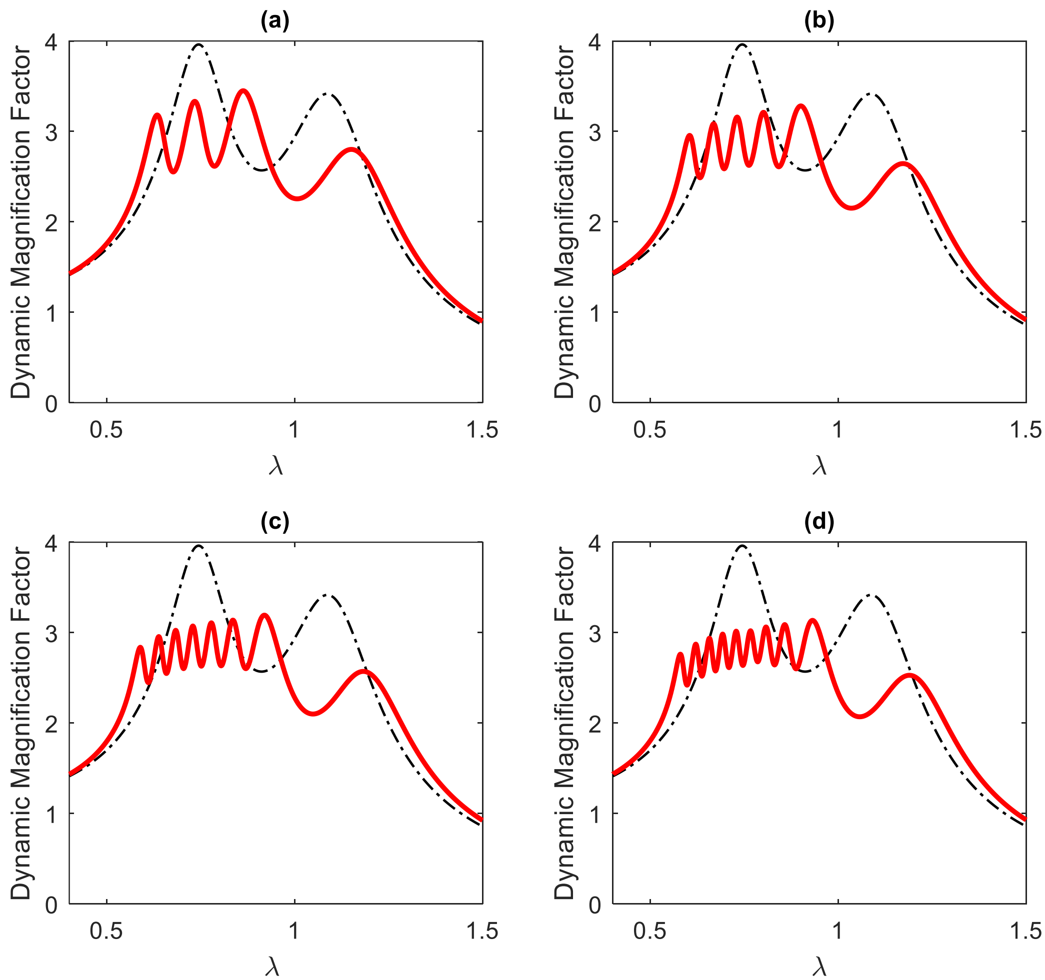

Figure 7-9: Frequency response comparison of the TMDI and Type 1 MTMDI with $\mu_1 = 0.10$, $\mu_2 = 1.0$, and (a) $n = 3$, (b) $n = 5$, (c) $n = 7$, and (d) $n = 9$

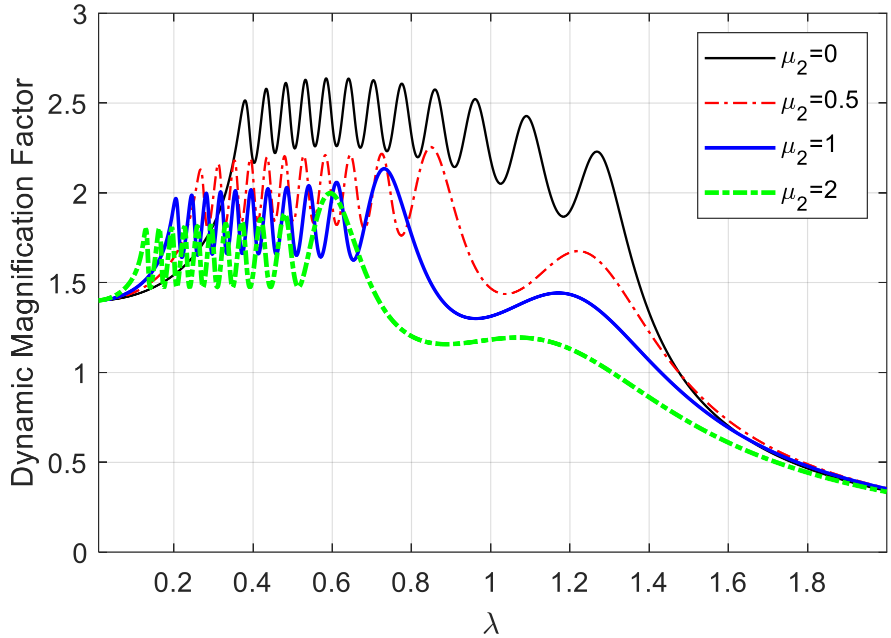

Figure 7-10: Effect of the inertance ratio on the frequency response of the Type 1 MTMDI ($n=11$) with $\mu_1=0.10$

Type 2 MTMDI

The Type 2 MTMDI features an alternative design philosophy for the MTMDI that considers that the individual absorbers have different size masses, but the same stiffness and damping values. This type of MTMDI may be more practical and easier to install in some situations due to the ability to use identical stiffness and damping elements for each absorber. While the individual absorber masses are different, in this work, the frequencies of the absorbers are linearly distributed.

As indicated by Eq. (7.8), the inertance ratio of each absorber of a Type 2 MTMDI is the same, but, as the mass of each absorber is different, the inertance of each absorber varies. Based on the constraints provided by the relationships in the design of the Type 2 MTMDI that have been described, only 3 variables need to be considered in the optimization of a design: the identical damping values (c_T), the central frequency (ω_c), and the frequency space measure (β). Once again, in this work, these values are solved for by numerical optimization.

To evaluate the performance of the Type 2 MTMDI in comparison to the MTMD, which is also designed given the same constraints and with $\mu_2 = 0$, the R_{H_2} index is calculated and presented in Figure 7-11. These results show that the relative performance advantage of the MTMDI is rather insensitive to the mass ratio and increases with increased inertance ratio; R_{H_2} is roughly 0.90, 0.80, and 0.75 when $\mu_2 = 0.5$, $\mu_2 = 1.0$, and $\mu_2 = 2.0$, respectively. The performance advantage of the MTMDI is also relatively insensitive to the number of absorbers considered; however, a small, but noticeable, decrease in the performance advantage of the MTMDI, relative to the MTMD, can be observed when the number of absorbers increases.

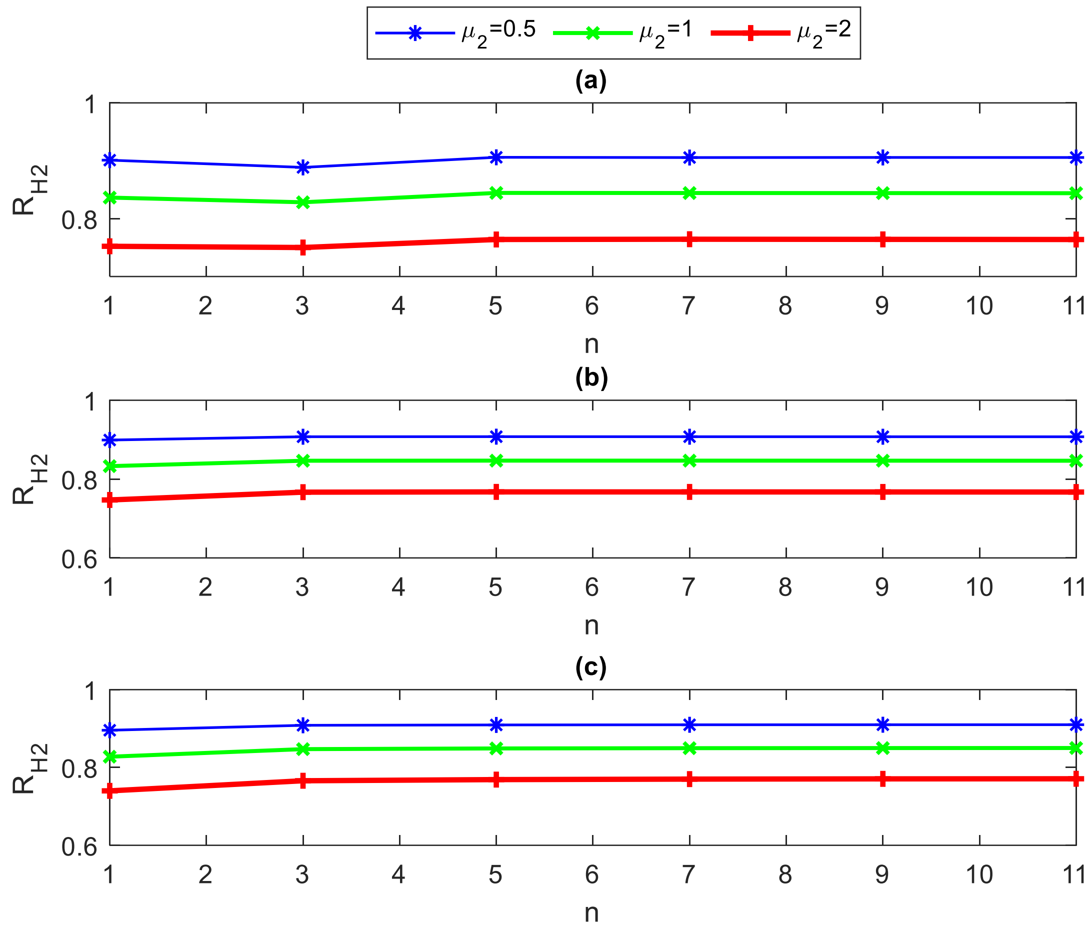

Figure 7-11: R_{H_2} for the Type 2 MTMDI as a function of the inertance ratio and number of absorbers, n, given (a) $\mu_1 = 0.10$, (b) $\mu_1 = 0.20$, and (c) $\mu_1 = 0.40$

The performance of the Type 2 MTMDI, in comparison to the TMDI, for the reduction of the H2 norm of the primary structure's displacement is calculated with the P_{H_2} index and presented in Figure 7-12. This figure shows that the H2 performance advantage of the Type 2 MTMDI, relative to the TMDI, is reduced with increases in both the inertance ratio and mass ratio. Furthermore, the Type 2

MTMDI shows an up to 5% improvement, compared to the TMDI, with increases in the number of absorbers in the MTMDI.

The performance of the H2 optimized Type 2 MTMDI, in comparison to the MTMD, in the reduction of the peak value on the displacement frequency response function, $R_{H\infty}$, is calculated and presented in Figure 7-13.

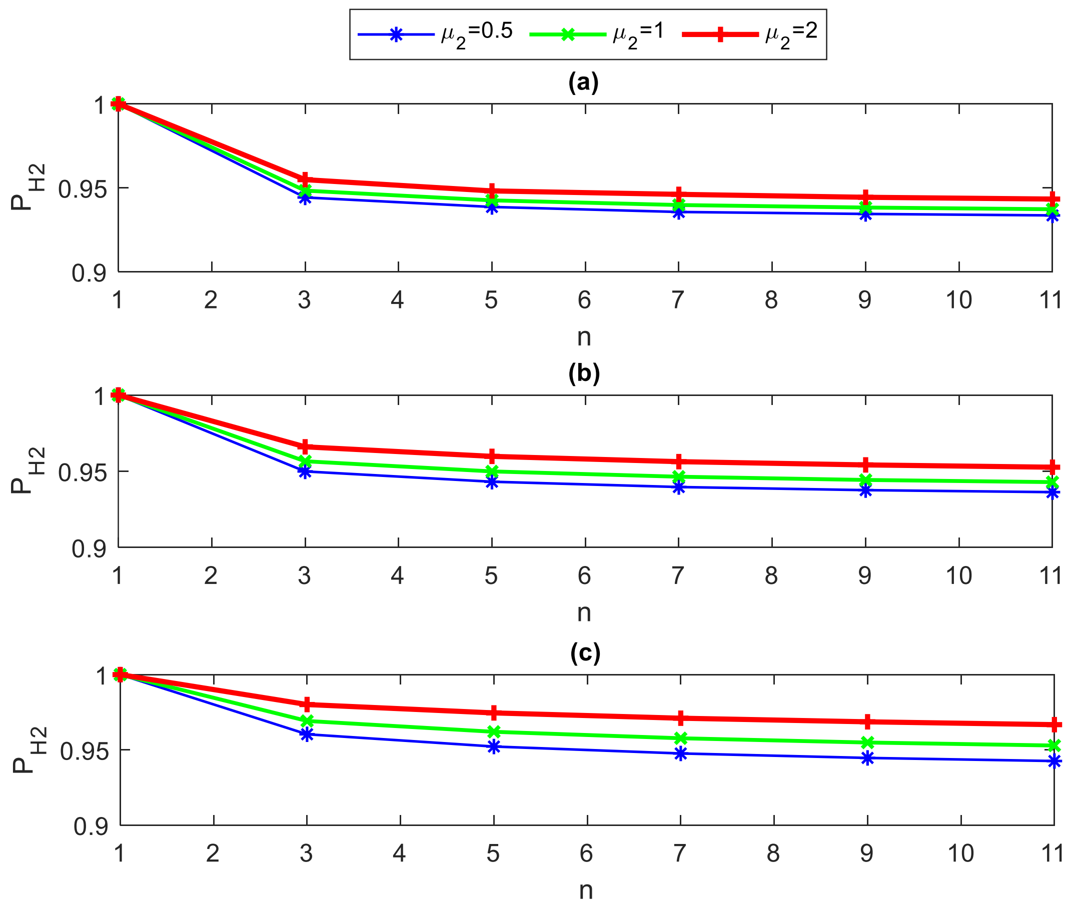

Figure 7-12: P_{H_2} for the Type 2 MTMDI as a function of the inertance ratio and the number of absorbers, n, given (a) $\mu_1 = 0.10$, (b) $\mu_1 = 0.20$, and (c) $\mu_1 = 0.40$

These results are similar to the R_{H2} results for the Type 2 MTMD and show the MTMDI is relatively insensitive to the mass ratio and the performance advantage decreases slightly with increases in the number of absorbers. Furthermore, considering inertance ratios $\mu_2 = 0.5$, $\mu_2 = 1.0$, and $\mu_2 = 2.0$, the Type 2 MTMDI shows a roughly 10%, 20%, and 30% improvement compared to the MTMD, respectively.

The performance of the H2 optimized Type 2 MTMDI, in comparison to the TMDI, in the reduction of the peak value on the displacement frequency response function, $P_{H\infty}$, is calculated and presented in Figure 7-14. Unlike its performance in comparison to the MTMD, in comparison to the TMDI, the MTMDI shows only limited performance advantage and performs worse in many scenarios. The $P_{H\infty}$ performance of the MTMDI particularly degrades when the number of absorbers and the mass ratio are high.

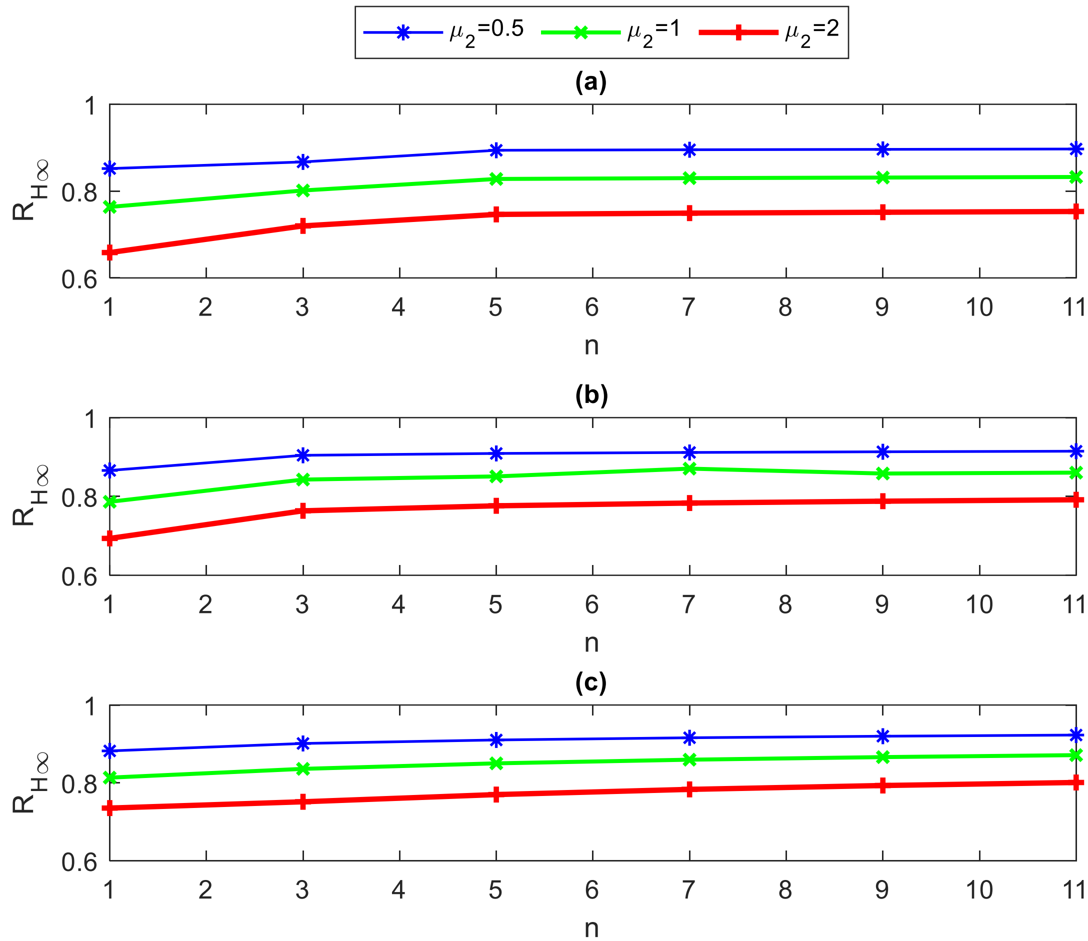

Figure 7-13: $R_{H\infty}$ for the Type 2 MTMDI as a function of the inertance ratio and number of absorbers, n, given (a) $\mu_1 = 0.10$, (b) $\mu_1 = 0.20$, and (c) $\mu_1 = 0.40$

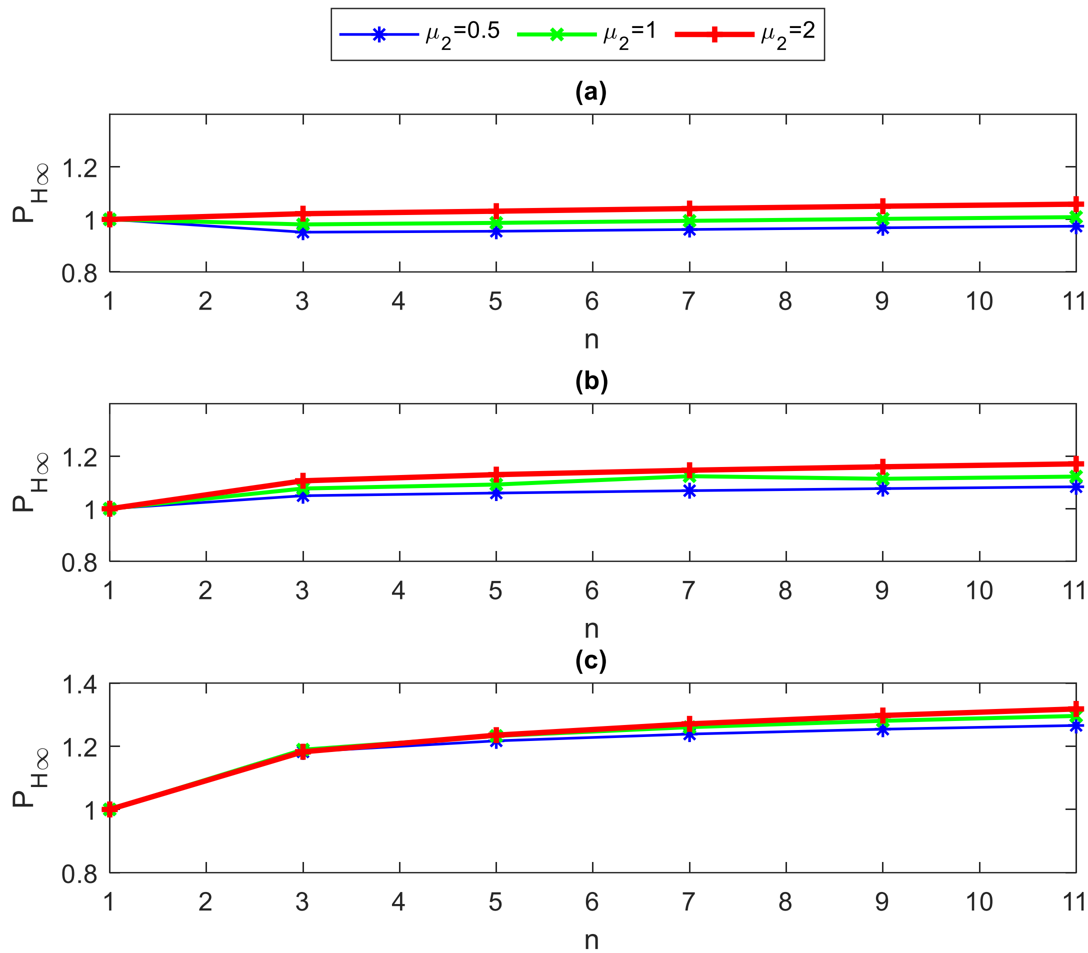

Figure 7-14: $P_{H\infty}$ for the Type 2 MTMDI as a function of the inertance ratio and number of absorbers, n, given (a) $\mu_1 = 0.10$, (b) $\mu_1 = 0.20$, and (c) $\mu_1 = 0.40$

It is informative to show the effect of the number of Type 2 MTMDI absorbers on the full frequency response of the displacement of the primary structure; thus, Figure 7-15 compares the frequency response of the Type 2 MTMDI and the TMDI considering a 10% mass ratio, 100% inertance ratio, and a range of the number of absorbers. A key feature in these results is that the lowest frequency peak on the frequency response curve is the highest amplitude. The results in this figure align with the results shown in Figure 7-12 and Figure 7-14 in that increasing the number of absorbers in the Type 2 MTMDI does not reduce the maximum response value, but decreases the overall area under the curve. This decrease primarily occurs because the added peaks that come with more absorbers results in a reduction in the width of the dominant peak in the frequency response curve for the MTMDI.

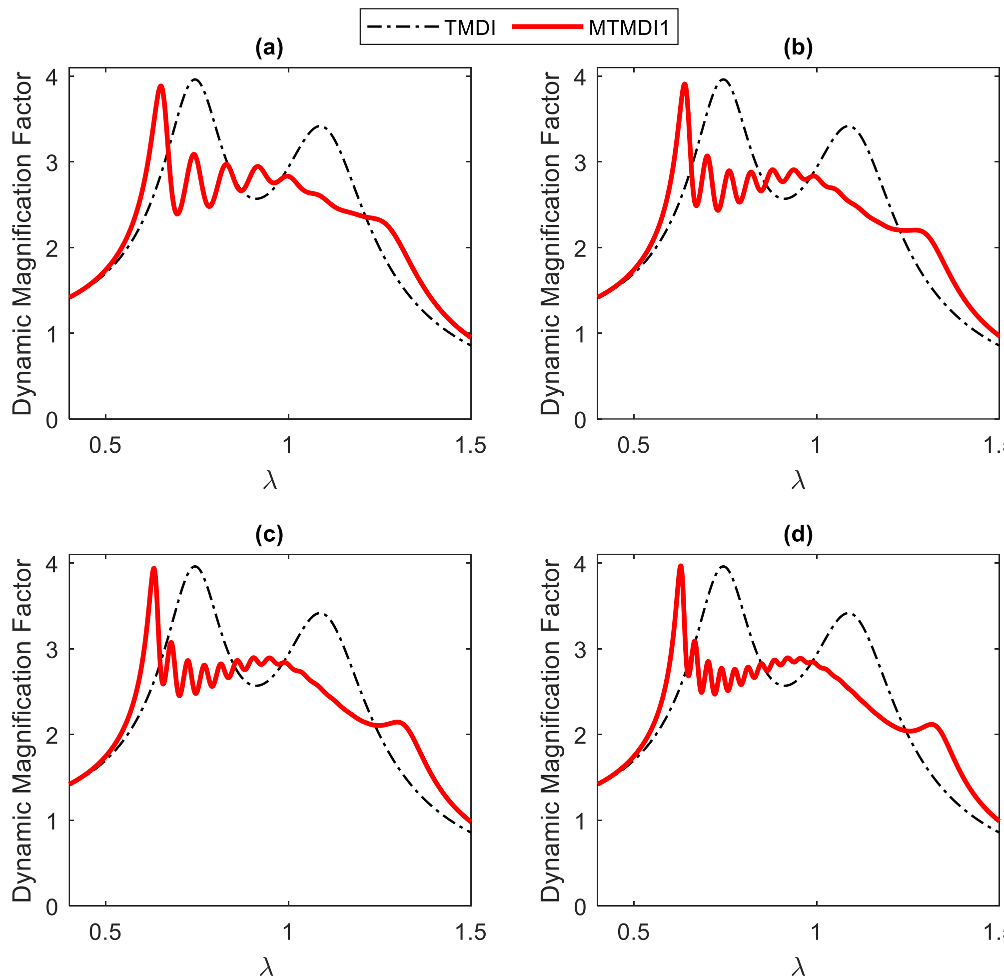

Figure 7-15: Frequency response comparison of the TMDI and Type 2 MTMDI with $\mu_1 = 0.10$, $\mu_2 = 1.0$, and (a) $n = 3$ (b) $n = 5$ (c) $n = 7$ and (d) $n = 9$

The effect of the inertance ratio on the frequency response of the Type 2 MTMDI with a 10% mass ratio and 11 absorbers is presented in Figure 7-16. It can be observed that by increasing the inertance ratio, the dynamic response is smoother and the overall curve is lower. Additionally, by increasing the inertance ratio, the dominant peak in the frequency response shifts to the left and reduces.

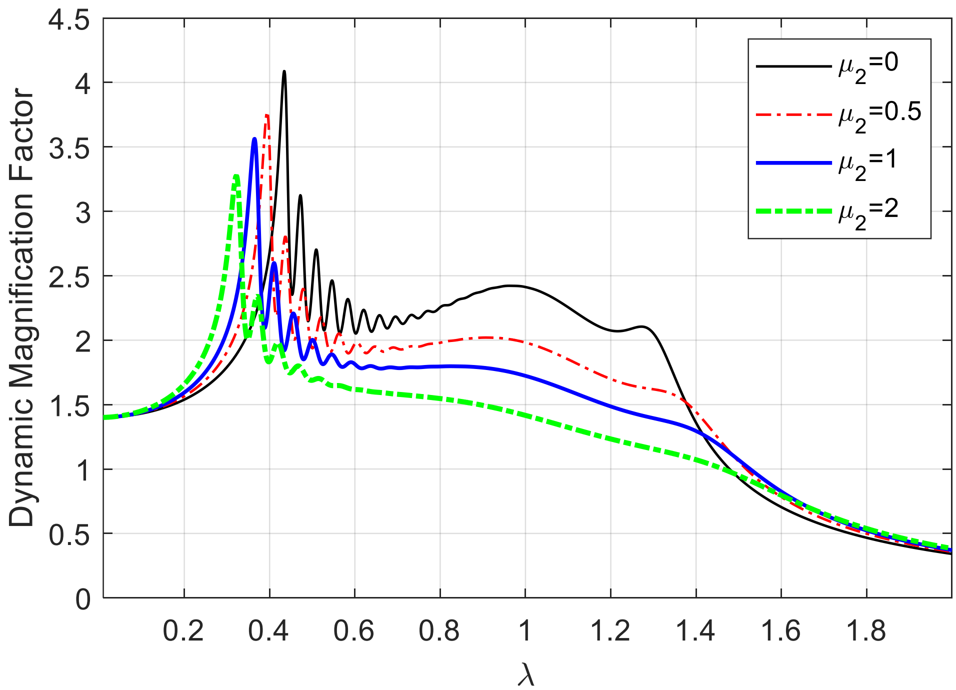

Figure 7-16: Effect of the inertance ratio on the frequency response of the Type 2 MTMDI with $\mu_1 = 0.10$ and $n = 11$ over a range of inertance ratios

Conclusions

This study proposed a new inerter-base vibration absorber for the passive control of structures subjected to random ground acceleration. The proposed device is the multiple tuned mass damper inerter (MTMDI), which can be considered as an advancement that is based on the tuned mass damper inerter (TMDI), but features multiple absorbers, like the multiple tuned mass damper (MTMD). The Type 1 MTMD is a type of MTMDI in which the physical secondary mass of each absorber is the same and each absorber is designed with different damping and stiffness parameters. The Type 2 MTMDI is another type of MTMDI that is designed with identical stiffness and damping, but absorber masses that are different and distributed based on a functional expression. Considering an excitation that is random, optimized parameters of the TMDI were obtained through the minimization of the H2 norm of the displacement of the primary structure. These optimal values, which were obtained numerically, were then use to evaluate the performance of the MTMDI, in comparison to both the TMDI and MTMD, considering multiple mass ratios, inertance ratios, and number of absorbers. The main conclusions of this study can be summarized as follows:

The Type 1 MTMDI shows superior effectiveness compared to the MTMD and the TMDI in the reduction of the H2 norm and peak value on the frequency response curve for the displacement of the primary structure and this effectiveness increases by increasing the inertance ratio.

The Type 2 MTMDI shows superior effectiveness compared to the MTMD in the reduction of the H2 norm and peak value on the frequency response curve for the displacement of the primary structure.

The Type 2 MTMDI shows superior effectiveness compared to the TMDI in the reduction of the H2 norm of the displacement of the primary structure, but cannot significantly improve the reduction of the peak value on the frequency response curve.

The distribution of the inertance in the Type 1 MTMDI was shown to have little effect on its performance as the Type 1 MTMDI with inertance concentrated on one absorber only slightly outperformed the Type 1 MTMDI with inertance distributed to each absorber.

For both types of MTMDI, most of the response indices examined showed improved performance of the primary structure when the number of absorbers in the MTMDI increases; however, most of the improvement in performance is realized with the addition of the first few absorbers and there are significantly diminished returns with higher numbers of absorbers.

CHAPTER EIGHT:ENERGY TRANSFER AND PASSIVE CONTROL OF SINGLE-DEGREE-OF-FREEDOM STRUCTURES USING A ONE-DIRECTIONAL ROTATIONAL INERTIA VISCOUS DAMPER

A version of this chapter was originally published by Abdollah Javidialesaadi and Nicholas Wierschem:

A. Javidialesaadi, N.E. Wierschem, Energy transfer and passive control of single-degree-of-freedom structures using a one-directional rotational inertia viscous damper, Engineering Structures. 196 (2019) 109339. https://doi.org/10.1016/j.engstruct.2019.109339.

This paper proposing innovative inerter-based passive control device in order to improve states of the art in passive control of structures. Background, motivation, description of the device, and performance evaluation are presented in this paper.

Abstract

In this paper, a novel rotational inertia device known as a one-directional rotational inertia viscous damper (ODRIVD) is proposed for the passive control of structures and studied as an attachment to single-degree-of-freedom (SDOF) systems. The ODRIVD allows for energy to be passively transferred from a primary structure to a rotational flywheel in a one-directional fashion. This one-directional transfer allows energy to be transferred to this flywheel, where it can be locally dissipated, but does not allow energy to be transferred back to the primary structure. This behavior is in contrast to traditional rotational inertia dampers, which utilize an inerter that allows for the two-way transfer of energy back and forth between the inerter and the primary structure. The proposed ODRIVD shows the ability for the passive control of SDOF systems without changing its natural frequency significantly, which typically occurs when using inerters. The mechanism of the proposed device and a model of its dynamics are presented in this paper and its behavior and effectiveness are investigated. The results of this study show that the ODRIVD has the potential for superior effectiveness at passive vibration control, in comparison to traditional rotational inertia dampers with the same rotational inertia mass and damping.

Introduction

Various vibration control strategies and supplemental devices have been proposed and developed in the last decades with the goal of controlling structural vibrations that result from disturbances such as wind, seismic ground motions, and machinery loads [1,2,128,129]. Recently, rotational inertia supplements have been proposed and investigated as passive control devices. While these rotational inertia supplements have taken various forms, their common feature is a mechanical device called an inerter. The inerter is a two terminal mechanical device which produces a rotational inertia mass proportional to the relative acceleration between its two terminals [54,96].

The rotational inertia viscous damper (RIVD), which has been investigated as part of a toggle bracing system [8], is one of the first generation of inerter-based devices proposed for the passive control of SDOF systems. The RIVD can provide a large inertial mass and is designed for the control of structures by coupling the structure's motion to the rotational motion of a rotary mass and transferring kinetic energy to that rotary mass. By adding a tuning spring to the RIVD, the tuned viscous mass damper (TVMD) has been proposed [52]. While the RIVD and the TVMD are passive control devices, converting linear to rotational motion utilizing a semi-active control system has also been studied [130].

Investigations on the control of structures with rotational inertia dampers also includes inerter-based vibration absorbers that have been developed with the goal of improving mass dampers [9,10,53,58,98,100,112,126]. Substituting the viscous damper in a tuned mass damper (TMD) with a tuned rotational inertia viscous mass, the rotational inertia double tuned mass damper (RIDTMD) has been proposed and has demonstrated effectiveness in the reduction of the dynamic response of SDOF structures [9,58,99]. The tuned-mass-damper-inerter (TMDI), which features an inerter attached between a fixed support and the secondary mass of a TMD, has also been proposed for this purpose [53]. The TMDI shows significant improvement, compared to the TMD, in the suppression of the vibration of structures subjected to seismic and wind loads [59,63]. As a further improvement of the TMDI, the three-element vibration absorber-interter (TEVAI) has recently been proposed [98].

An inerter alone, such as an RIVD with no damping, can be utilized for the control of a SDOF system by increasing the system’s effective mass and reducing the effect of a ground motion input [70].However, the use of an inerter, alone or as a part of a more complex configuration, can also lead to some unintended side effects. These unintended side effects include the fact that adding an inerter to a SDOF structure reduces the natural frequency of that structure [55], which may be undesirable in some cases. This reduction in natural frequency is due to the addition of the effective rotational inertia mass into the system, which can also be interpreted as a negative stiffness element [70]. Furthermore, when the inerter is subjected to relative motion, it will rotate and accumulate a substantial amount of kinetic energy. When the relative motion across the inerter slows down, the rotation of the flywheel attached to the inerter will slow down as well; however, the kinetic energy in the flywheel will resist this change in velocity leading to a situation where the inerter then drives the displacement of the system [80].

With the goal of improving rotational inertia mass dampers, a new type of passive rotational inertia mass device featuring state switching has been proposed [69]. This proposed device consists of two flywheels and a passive clutch system. With this clutch, the rotational inertia mass is engaged with the SDOF system it is attached to when the velocity and acceleration of the structural mass have the same sign. When the acceleration and velocity don’t have the same sign, the device is not engaged with the primary system. In other words, the inerter is engaged while the absolute value of the velocity of the system is increasing and after this absolute velocity peaks, when the acceleration of the system reverses, the device is no longer engaged. The benefit of this state switching configuration is that the kinetic energy contained within the device cannot be transferred back and drive the system. The displacement reduction effectiveness of this clutch inerter for SDOF systems has been investigated and evaluated recently [81].

While the device proposed by [80] does consider one-directional behavior, the energy in the flywheel is assumed to be completely dissipated or harvested after the flywheels stop being engaged. This assumption allows this device to always be able to be engaged with a flywheel after a change in the sign of the device's velocity; therefore, this assumption has a significant effect on the device's dynamics and has the potential to increase its apparent effectiveness.

In this paper, a novel rotational inertia supplement, the one-directional rotational inertia viscous damper (ODRIVD) is proposed as a development based on the rotational inertia viscous damper (RIVD) [8]. In devices with inerters, like the RIVD, the translational motion of a structure can be converted to the rotational motion of a flywheel; however, the rotational kinetic energy of the device can be again transferred back to the structure. The ODRIVD features a one-way rotational mechanism in which translational motion can be converted into rotational motion, but the device's rotational kinetic energy cannot be transferred back to the structure. A similar one-way clutch mechanism has been proposed for harvesting energy on a rectifier-based shock absorber, but the investigation of this device has been limited to the energy harvesting in shock absorbers and aspects related to the passive control of structures have not been studied [131]. In contrast to other one-way mechanisms studied [80,81], the kinetic energy in the device considered in this paper is not entirely dissipated or harvested when the device is disengaged. Rather, the mechanics of this one-way transfer mechanism are formulated such that the kinetic energy of the device's flywheel is considered when it is not engaged and also considered in the determination of if the flywheel can be engaged.

To control the response of the structure in both directions of motion equally, the proposed implementation of the damper studied consists of two ODRIVD orientated in opposite directions (the 2ODRIVD). This device will function as a passive state-switching device going in and out of states where the flywheels are engaged and states when they are not engaged. Comparisons in this paper will be made with a RIVD with equal damping and the same total amount of rotational inertia mass.

In the next two sections of this paper, the basic concept of the inerter and the RIVD are presented. In the fourth section, the model and formulation are presented for the 2ODRIVD. The performance assessment of the proposed device is performed in the fifth section. The sixth section covers the energy analysis and the conclusions of this study are presented in the seventh section.

Inerter

An inerter is a two terminal mechanical device with the property that the relative acceleration between the terminals is proportional to the equal and opposite forces at the terminals [54]. The governing equation of an inerter subjected to equal and opposite forces F at terminals 1 and 2 with accelerations $\ddot{u}_1$ and $\ddot{u}_2$ is

$$F = b(\ddot{u}_2 - \ddot{u}_1) \tag{8.1}$$

where, b is a constant term, called the “inertance” or “inertia mass”.

Figure 8-1 shows the ball screw and the rack and pinion, which are two different common mechanisms that have been proposed for use as an inerter,[8,9]. Despite the differences in these two mechanisms, both are capable of producing large effective inertia mass while utilizing a flywheel with a relatively small physical mass. The views of the mechanisms in Figure 1 are cross-sectional views. The flywheels in Figure 8-1 (a) and (b) are both envisioned as cylinders; however, they appear differently in the figures due to the way that the flywheels are oriented in the mechanisms. This difference in the orientation of the flywheels does not influence the modeled dynamics of the system.

For both inerter mechanisms considered, the rotational velocity of the flywheel ($\dot{\theta}$) is proportionally related to the relative velocity of the terminals

$$\dot{\theta} = \alpha(\dot{u}_2 - \dot{u}_1) \tag{8.2}$$

The coefficient governing this relationship, α, is equal to $\frac{2\pi}{\rho}$ and $\frac{1}{r}$ for the ball screw and rack and pinion, respectively. The resulting inertia mass of the inerter, the inertance, is a function of this mechanism and the properties of the attached flywheel [98]. With appropriate combinations of the device's parameters, large mass amplification factors can be achieved. For example, mass amplification factors equal to 175 and 3300 were achieved with inerters being experimentally investigated [52,102].

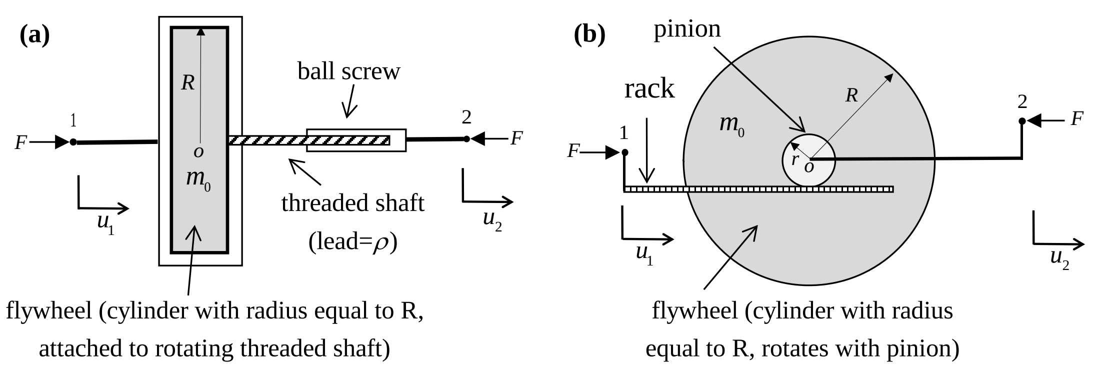

Figure 8-1: Common mechanisms considered for inerters (a): cross section view of ball screw (b): cross section view of the rack and pinion

Rotational inertia viscous damper

The rotational inertia viscous damper (RIVD) is an inerter with viscous damping. This can be practically achieved by surrounding the rotational inertia mass (flywheel) by a viscous material with the ball and screw mechanism as a motion amplifier [8]. In the RIVD, the flywheel provides effective rotational inertia mass to the structure and the dissipation of energy occurs through the rotation of the flywheel within the viscous fluid. Figure 8-2 shows a single-degree-of-freedom (SDOF) structure passively controlled with a RIVD. In this configuration, the motion of the SDOF structure drives the motion of the RIVD, including the rotation of the flywheel.

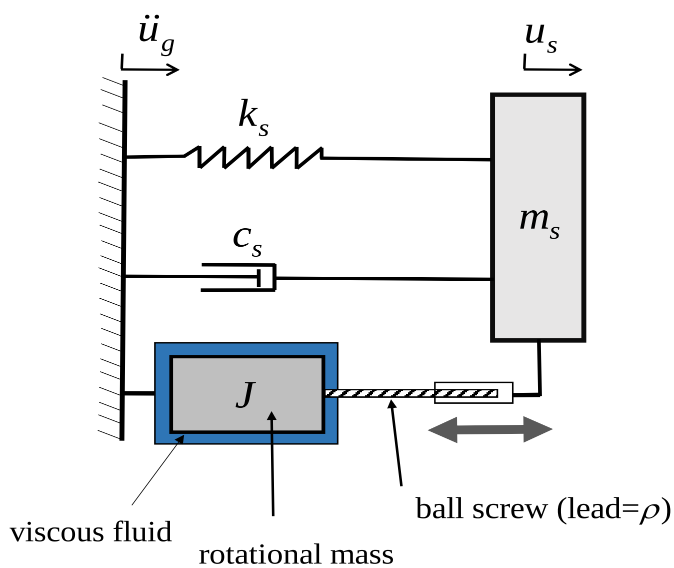

Figure 8-2: SDOF system with a RIVD

Whereas the ball screw mechanism converts linear motion to the rotational motion of the flywheel, the displacement of the SDOF system, relative to its base, and the flywheel's rotation has the following relationship

$$\theta = \frac{2\pi}{\rho} u_s \tag{8.3}$$

Where, θ is the rotation angle of the flywheel. Assuming an undamped SDOF $(c_s = 0)$, the equation of motion of the RIVD controlled SDOF structure can be expressed as follows:

$$(m_s + J\frac{4\pi^2}{\rho^2})\ddot{u}_s + D\frac{4\pi^2}{\rho^2}\dot{u}_s + k_s u_s = -m_s \ddot{u}_g \tag{8.4}$$

where D represents the damping coefficient, m_s is the mass of the main structure, J is the inertia of the rotational inertia mass (with m_o physical mass), u_s is the displacement of the main structure relative to the ground, u_g is the ground displacement, k_s is the stiffness of the structure.

Eq. (8.4) demonstrates that the inertia mass of the RIVD will have the effect of reducing the system's natural frequency as it will cause the effective mass of the system to increase.

One-directional rotational inertia viscous damper

The RIVD can passively control a SDOF system by increasing the system's effective mass and dissipating energy through the motion of the rotational inertia mass within a viscous material. With the RIVD, kinetic energy is transferred to the RIVD and stored in the flywheel when the structure starts moving and is contained there until the structure reaches its maximum velocity, relative to the base. After this point, the structure slows down and the energy stored in the flywheel is transferred back to the structure. From a physical perspective, the structure drives the flywheel of the RIVD to rotate with this rotation resulting in kinetic energy contained in the flywheel, then the flywheel drives the structure and returns the remaining kinetic energy from the flywheel back to the structure. In literature, this behavior has drawn an analogy between the inerter and a capacitor [113]. In other words, while the RIVD may dissipate energy through viscous damping, the flywheel itself does not permanently absorb energy.

In an attempt to provide a device in which energy is irreversibly transferred away from the main structure and to a flywheel, this paper proposes the one-directional rotational inertia viscous damper (ODRIVD), which is introduced in this section.

The general idea of the ODRIVD is similar to a spinning top toy or some types of push-down salad spinners (see Figure 8-3). In the spinning top toy, by pushing down on the handle on the top, the top starts spinning. This spinning then continues until it naturally decays or is interrupted. The main characteristics of this mechanism are as follows:

In the first step, pushing down on the handle on the top moves a screw and then the screw drives the flywheel to rotate in one direction. In this step, the flywheel performs like an inerter with a ball and screw or lead screw mechanism.

When the handle moves up, unlike the inerter, the screw does not engage with the rotational inertia mass, which means the flywheel spins freely. The mechanism of the rotation of the inertia mass is similar to ratchetting, which allows the flywheel to rotate only in one direction.

Subsequent times when the handle is pushed down, the screw moves down and drives the flywheel mass only if the linear velocity of the rotating screw contacts are equal to or larger than the linear velocity of the surface at the contact point with the flywheel. The equivalent rotational velocity can be determined by the relationship between the linear and rotational motion (see Eq. (8.3)).

As the ODRIVD can only be engaged in one direction, a device with two ODRIVD (the 2ODRIVD) is primarily considered in this paper hereafter. The 2ODRIVD has one ODRIVD that can be engaged with the positive velocity of the structure and a second for negative velocity. A diagram of a SDOF system controlled with the 2ODRIVD and subjected to base excitation is presented in Figure 8-4. In this figure, D_1 and D_2 are the device's damping coefficients and ρ_1 and ρ_2 are the leads of the ball screws connected to the SDOF system mass. J_1 and J_2 are the moment of inertia of the device's flywheels, which can be calculated as follows:

$$J_1 = \frac{1}{2} m_{01} R_1^{\,2} \tag{8.5}$$

$$J_2 = \frac{1}{2} m_{02} R_2^{\,2} \tag{8.6}$$

In Eq. (8.5) and Eq. (8.6), m_{01} and m_{02} are the flywheel physical masses and R_1 and R_2 are the radii of the flywheels.

Considering the ODRIVD mechanism described above, the SDOF system with the 2ODRIVD can be described as vibrating with the three following states:

State One (S_1): The 2ODRIVD is in S_1 if the structure is moving left (negative velocity relative to the base, $\dot{u}_s \leq 0$) and the relative velocity of the structure is equal to or larger than the linear velocity of the first flywheel at the contact point ($\left|\dot{u}_s(t)\right| \geq \frac{\rho_1}{2\pi}\left|\dot{\theta}_1(t)\right|$). In this state, the first ODRIVD is engaged and the flywheel of the other ODRIVD spins freely.

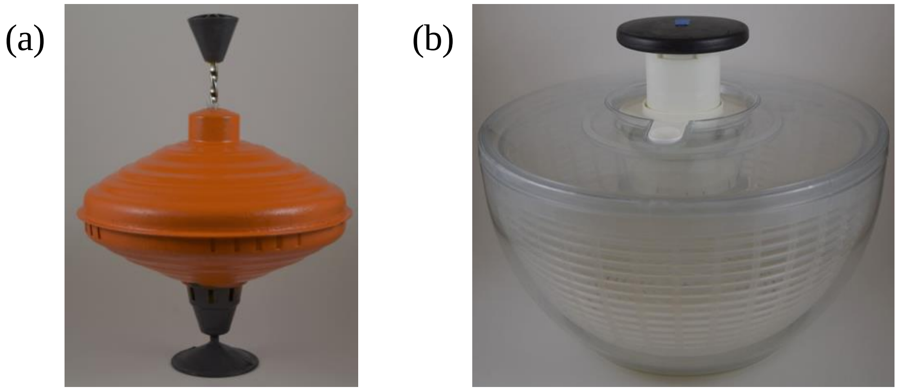

Figure 8-3: Examples of physical realizations of one-way rotational devices (a) spinning top toy (b) salad spinner device

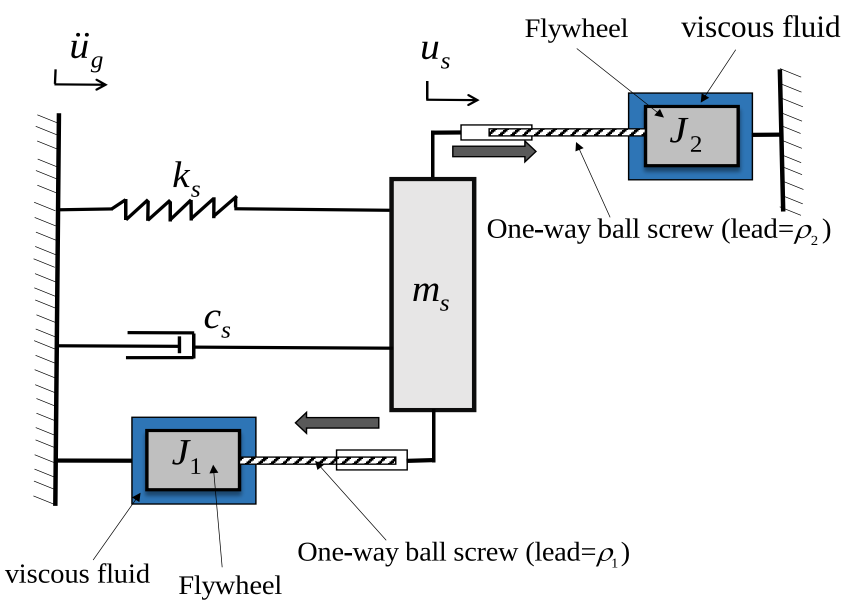

Figure 8-4: SDOF system with a 2ODRIVD

State Two (S_2): The 2ODRIVD is in S_2 if the structure is moving right (positive velocity relative to the base, $\dot{u}_s \geq 0$) and the relative velocity of the structure is equal to or larger than the linear velocity of the second flywheel at the contact point ($|\dot{u}_s(t)| \geq \frac{\rho_2}{2\pi}|\dot{\theta}_2(t)|$). In this state, the second ODRIVD is engaged and the flywheel of the other ODRIVD spins freely.

State Three (S_3): The 2ODRIVD is in S_3 if none of the above conditions for S_1 or S_2 are satisfied. The SDOF system oscillates without being engaged with either ODRIVD. In this state the flywheels of both ODRIVDs spin freely.

The kinetic energy (T), potential energy (U), and dissipative function of the system $(\Im)$ are as follows:

$$T = \frac{1}{2} m_s (\dot{u}_s - \dot{u}_g)^2 + \frac{1}{2} J_1 \dot{\theta}_1^2 + \frac{1}{2} J_2 \dot{\theta}_2^2 \tag{8.7}$$

$$U = \frac{1}{2} k_s u_s^2 \tag{8.8}$$

$$\Im = -D_1 \dot{\theta}_1 \delta\theta_1 - D_2 \dot{\theta}_2 \delta\theta_2 \tag{8.9}$$

When the first ODRIVD is engaged (S_1), the displacement of the structure relative to its base (u_s) and the rotation of the ODRIVD flywheel (θ_1) are related as follows:

$$\theta_1 = \frac{2\pi}{\rho_i} u_s \tag{8.10}$$

When the second ODRIVD is engaged (S_2), the displacement of the structure relative to its base (u_s) and the rotation of the ODRIVD flywheel (θ_2) are related as follows:

$$\theta_2 = \frac{2\pi}{\rho_i} u_s \tag{8.11}$$

When neither ODRIVD is engaged (S_3), there is not a relationship between the rotations of the flywheels and the displacement of the structure.

Substituting Eq. (8.10) and Eq. (8.11) into Eq. (8.7) to (8.9) and using Lagrange's equations leads to the equation of motions for the three different states.

State S_1: The SDOF system is engaged with the 2ODRIVD's first ODRIVD.

$$(m_s + J_1 \frac{4\pi^2}{\rho_1^{\ 2}})\ddot{u}_s + D_1 \frac{4\pi^2}{\rho_1^{\ 2}} \dot{u}_s + k_s u_s = -m_s \ddot{u}_g \tag{8.12}$$

As the second ODRIVD is not engaged, its flywheel spins with the following equation of motion:

$$J_2 \ddot{\theta} + D_2 \dot{\theta} = 0 \tag{8.13}$$

State S_2: The SDOF system is engaged with the 2ODRIVD's second ODRIVD

$$(m_s + J_2 \frac{4\pi^2}{\rho_2^{\ 2}})\ddot{u}_s + D_2 \frac{4\pi^2}{\rho_2^{\ 2}} \dot{u}_s + k_s u_s = -m_s \ddot{u}_g \tag{8.14}$$

As the first ODRIVD is not engaged, its flywheel spins with the following equation of motion:

$$J_1 \ddot{\theta} + D_1 \dot{\theta} = 0 \tag{8.15}$$

State S_3: The SDOF system is not engaged with either of the 2ODRIVD's ODRIVDs. The primary structure is then undamped with the following equation of motion:

$$m_s \ddot{u}_s + k_s u_s = -m_s \ddot{u}_g \tag{8.16}$$

As both ODRIVDs are not engaged, their flywheels spin with the following equations of motion.

$$J_1 \ddot{\theta} + D_1 \dot{\theta} = 0 \tag{8.17}$$

$$J_2\ddot{\theta} + D_2\dot{\theta} = 0 \tag{8.18}$$

In order to accommodate changes in the state of the system, a numerical analysis of this system must be performed in an incremental way in which the conditions defining the states are checked at every step. As mentioned above, the state of the system is dependent on the velocity of the structure and the linear velocities of the contact points on the flywheels. When the conditions for a state change are detected, the simulation must be interrupted and the system must be modified based on the new state and the new set of equations of motion, listed in Eqs. (8.12) thru (8.18), before the analysis is restarted.

During these state changes, the kinetic energy in the system must be accounted for. If flywheel i is disengaged at time t_{sw}, the rotational velocity of the flywheel when the analysis is restarted, $\dot{\theta}_i(t_{sw}^+)$, is defined as

$$\dot{\theta}_i(t_{sw}^+) = \frac{2\pi}{\rho_i}\dot{u}_s(t_{sw}^-) \tag{8.19}$$

where t_{sw}^- and t_{sw}^+ are the times immediately before and after engaging the flywheel, respectively. The velocity of the flywheel when it is disengaged is governed by Eq. (8.13), Eq. (8.15), Eq. (8.17) or Eq. (8.18). Solving this first order differential equation with any arbitrary initial rotation results in the following equation for the velocity of the flywheel

$$\dot{\theta}_i(t + \Delta t) = \dot{\theta}_i(t)e^{-\frac{D_i}{J_i}\Delta t} \tag{8.20}$$

In this equation, Δt represents the duration of time that the flywheel has been disengaged.

The potential for feasible implementation of the proposed device for civil engineering applications has been demonstrated by the large-scale testing and application of related devices. Included in this is the full-scale dynamic testing of a tuned viscous mass damper (TVMD) installed in a steel frame [11]. Additionally, a working TVMD with 5400 ton of inertia mass has been installed in a multistory steel structure located in Tokyo Japan [12]. While the 2ODRIVD utilizes two flywheels and a modified mechanism for converting translational motion to the rotation of those flywheels, the TVMD is similar enough to suggest that the full-scale implementation of the 2ODRIVD is feasible. Furthermore, while the connection of the proposed device to a SDOF system is considered in this paper, realistic implementations of this device in civil engineering structures may include the device connected between stories [59], as part of advanced isolation systems [132], or as part of a damped outrigger system [97]. As this paper serves as an introduction to this proposed device, the detailed consideration of this device in these specific configurations is beyond the scope of the paper.

Performance Evaluation

To examine the performance of the proposed device, the responses of the SDOF system with the RIVD and with the 2ODRIVD are examined under harmonic loadings with different input frequencies. In this analysis, a unit linear undamped SDOF system ($m_s = 1$ and $k_s = 1$) is considered and the same level of damping and rotational inertia mass are utilized for the RIVD and 2ODRIVD devices being compared. The rotational inertia mass of the RIVD's flywheel (m_r) and 2ODRIVD's flywheels (m_{r1}, m_{r2}) are defined as follows:

$$m_r = \frac{4\pi^2}{\rho^2} J = \frac{4\pi^2}{\rho^2}\left(\frac{1}{2} m_0 R^2\right) = \frac{2\pi^2 m_0 R^2}{\rho^2} \tag{8.21}$$

$$m_{r1} = \frac{4\pi^2}{\rho_1^2} J_1 = \frac{4\pi^2}{\rho_1^2}\left(\frac{1}{2} m_{01} R_1^2\right) = \frac{2\pi^2 m_{01} R_1^2}{\rho_1^2} \tag{8.22}$$

$$m_{r2} = \frac{4\pi^2}{\rho_2^2} J_2 = \frac{4\pi^2}{\rho_2^2}\left(\frac{1}{2} m_{02} R_2^2\right) = \frac{2\pi^2 m_{02} R_2^2}{\rho_2^2} \tag{8.23}$$

Considering the physical flywheel masses $m_{01} = m_{02} = \frac{m_0}{2}$, the flywheel radii $R_1 = R_2 = R$, and screw lead $\rho_1 = \rho_2 = \rho$, the total resulting rotational inertia mass of the 2ODRIVD can be considered equal to the rotational inertia mass of the RIVD ($m_{r1} = m_{r2} = \frac{m_r}{2}$). In other words, the physical mass and resulting rotational inertia mass of each of the components of the 2ODRIVD are half of that of the RIVD such that the total physical and rotational inertia mass of the 2ODRIVD and the RIVD are equal.

In the following sections, the total physical mass of the devices is considered as 1% of the SDOF mass ($2m_{01} = 2m_{02} = m_0 = 0.01m_s$), unit SDOF mass will be considered ($m_s = 1$), and the radii of the flywheels are considered equal to $\sqrt{10}$ ($R_1 = R_2 = R = \sqrt{10}$). Various amplitudes of rotational inertia mass can be produced by considering the screw lead as a variable. For example, $\rho_1 = \rho_2 = \rho = 2\pi$ produces $m_r = 0.1$ and $m_{r1} = m_{r2} = 0.05$ while $\rho_1 = \rho_2 = \rho = \pi$ produces $m_r = 0.4$ and $m_{r1} = m_{r2} = 0.2$. It should be noted herein that different values of the physical masses, radii of the flywheels, and screw leads can be utilized to produce the same rotational inertia mass.

For the following analysis, equal total damping is considered for both devices. With twice the physical mass and the same radius, the surface area of the RIVD's flywheel is equal to twice that of one of the 2ODRIVD's flywheels. Assuming the same viscous material in both the RIVD and the 2ODRIVD, the damping coefficient of the RIVD should be twice the damping coefficient of each ODRIVD in the 2ODRIVD $(D_1 = D_2 = \frac{D}{2})$; thus, providing the same level of total damping for both devices. It should be noted herein that various damping coefficients can be produced by considering differences in the kinematic viscosity of the fluid and the gap between the rotational inertia mass and tube it is contained in [52].

To evaluate the performance of the proposed device, the response of an undamped linear SDOF system with an RIVD and 2ODRIVD subjected to a harmonic load over a range of different frequencies will be primarily considered. As the SDOF system with a RIVD is a linear time-invariant system, its frequency domain response can be obtained utilizing Laplace transforms; however, the SDOF system controlled with the 2ODRIVD is a variant system with multiple possible system states. Consequently, the response of the system with the 2ODRIVD will be obtained utilizing multiple numerical time-domain analyses with harmonic loads over the range of frequencies considered. For consistency, the analysis of the system with an RIVD will also be performed numerically in a similar manner. A time step size equal to 0.01 sec will be used in the analysis of both devices.

For these analyses, a harmonic base excitation $(\ddot{u}_g = A\sin(\omega t))$ will be considered and the system's displacement relative to the base (u_s) will be solved for. As the RIVD and 2ODRIVD are not amplitude depended systems, an arbitrary value for A can be selected. For the purposes of this study $A = 10^{-3}$ is chosen. From the displacement response, the maximum absolute amplitude of the displacement will be determined and considered as the displacement response factor (DRF),

$$DRF(\omega_i) = \max_{\omega=\omega_i} |u_s(t)| \tag{8.24}$$

where ω_i are the individual loading frequencies in the range considered ($0.5 \text{ rad/sec} \le \omega \le 1.2 \text{ rad/sec}$).

Undamped Response (D=0)

The response of the SDOF system with an attached undamped RIVD and undamped 2ODRIVD $(D = 2D_1 = 2D_2 = 0)$ is considered first. For this analysis, total rotational inertia masses of the devices equal to 0.1 $(m_r = 2m_{r1} = 2m_{r2} = 0.1)$ and 0.4 $(m_r = 2m_{r1} = 2m_{r2} = 0.4)$ are considered.

The DRF of the SDOF systems with the undamped RIVD and 2ODRIVD attached are presented in Figure 8-5. As shown by the response of the SDOF system with the RIVD in Figure 8-5, the frequency at which resonance appears to occur at is shifted to the left of the natural frequency of the uncontrolled system $(\omega = 1 \text{ rad/sec})$, indicating the reduction of the natural frequency of the system. This agrees with the natural frequency for the system with the RIVD calculated using Eq (8.4).

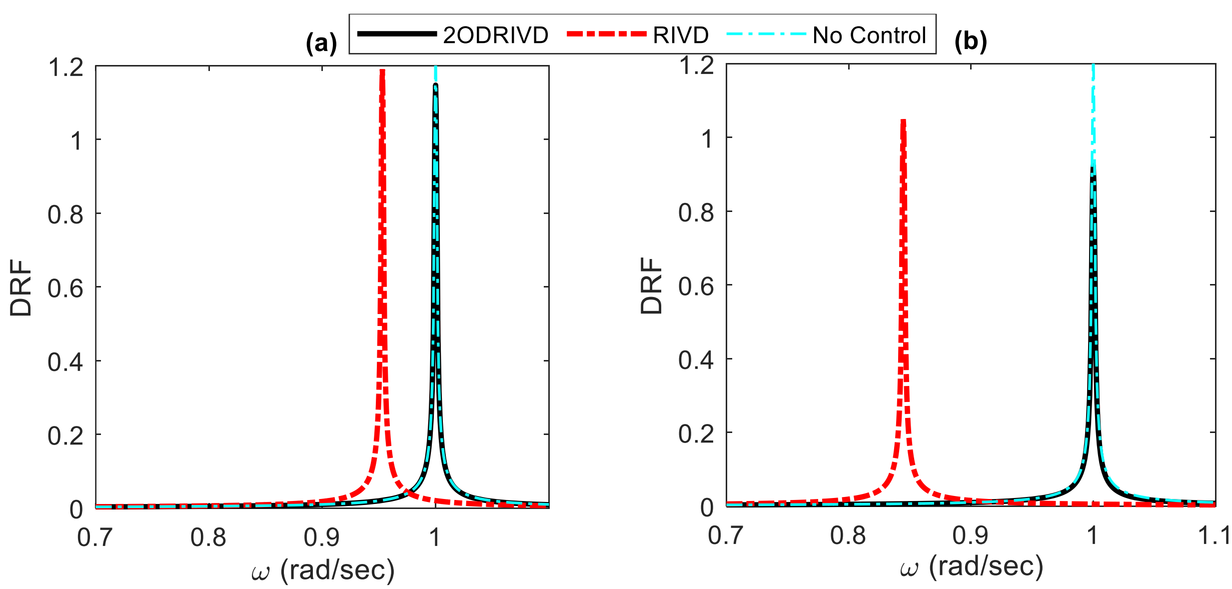

Figure 8-5: DRF of the systems with the RIVD and the 2ODRIVD over a range of frequencies when $D = 0$ and (a): $m_r = 2m_{r1} = 2m_{r2} = 0.1$ (b): $m_r = 2m_{r1} = 2m_{r2} = 0.4$

In contrast with the RIVD, the frequency at which resonance appears to occur at for the SDOF system with the 2ODRIVD, in both the $m_r = 0.1$ and $m_r = 0.4$ cases, does not significantly change. The lack of a shift in the apparent resonance frequency of the SDOF system with the 2ODRIVD is possible because the SDOF system controlled with the 2ODRIVD contains multiple natural frequencies due of the state switching nature of the device. When either flywheel is engaged with the main mass of the structure, the effective vibrating mass is equal to the structural mass plus the effective inertia mass of the flywheel engaged. One of these natural frequencies is the natural frequency when the SDOF system is engaged with the first ODRIVD (associated with state S_1). Another natural frequency is the natural frequency when the SDOF system is engaged with the second ODRIVD (associated with state S_2); however, due to the symmetry of the 2ODRIVD considered in this paper, this is the same as the frequency associated with state S_1. When neither flywheel is engaged, state S_3, the effective vibrating mass is equal to only the structural mass; thus, there is another natural frequency associated with this state. Despite the states of the system having different natural frequencies, only one peak occurs in the frequency response of the 2ODRIVD. The reason for this is that the system does not persist in one of the states with a flywheel engaged, but rather is only temporarily in one of these states when the amplitude of the response increases.

As the zero damping case is considered here, the steady-state response of both systems at their apparent resonance frequencies is unbounded; however, given the time limitation in these numerical analyses, the responses are limited to a large amplitude. As shown in Figure 8-5, over the duration of the vibration considered in the calculation of the DRF in this analysis (2500 sec), the maximum response of the SDOF system with the RIVD is larger than the SDOF system with the 2ODRIVD, which indicates the rate of growth of the resonant response with the 2ODRIVD is less than with the RIVD. The superior performance at resonance of the 2ODRIVD can be attributed to the 2ODRIVD's ability to transfer energy to its flywheels without that energy being able to be transferred back to the primary structure. Furthermore, this is noteworthy as, with everything else being equal, slower growth would be observed in the resonant response of the system with the smaller natural frequency, the system with the RIVD in this case.

In order to evaluate the behavior and performance of the proposed device at its apparent resonance frequency, the time history responses of the SDOF system with the 2ODRIVD and the RIVD are also investigated. The response of the SDOF system with the 2ODRIVD and the RIVD with zero damping coefficient $(D=0)$ and rotational inertia mass equal to 0.4 $\left(m_r = 2m_{r1} = 2m_{r2} = 0.4\right)$ is presented in Figure 8-6. The resonance frequency of the system with the RIVD can be calculated directly utilizing Eq. (8.4) and the apparent resonance frequency of the system with the 2ODRIVD can be determined from the D plot shown in Figure 8-5. As there is no damping in the system, both resonant responses will grow unbounded; however, a limited time window from zero to 300 seconds was selected for this analysis. As shown in Figure 8-6, the maximum displacement is equal to 0.125 m in the case of the RIVD, while the 2ODRIVD provides a maximum displacement equal to 0.107 m. These results again demonstrate the decreased rate of the growth of the response under resonant conditions with the 2ODRIVD.

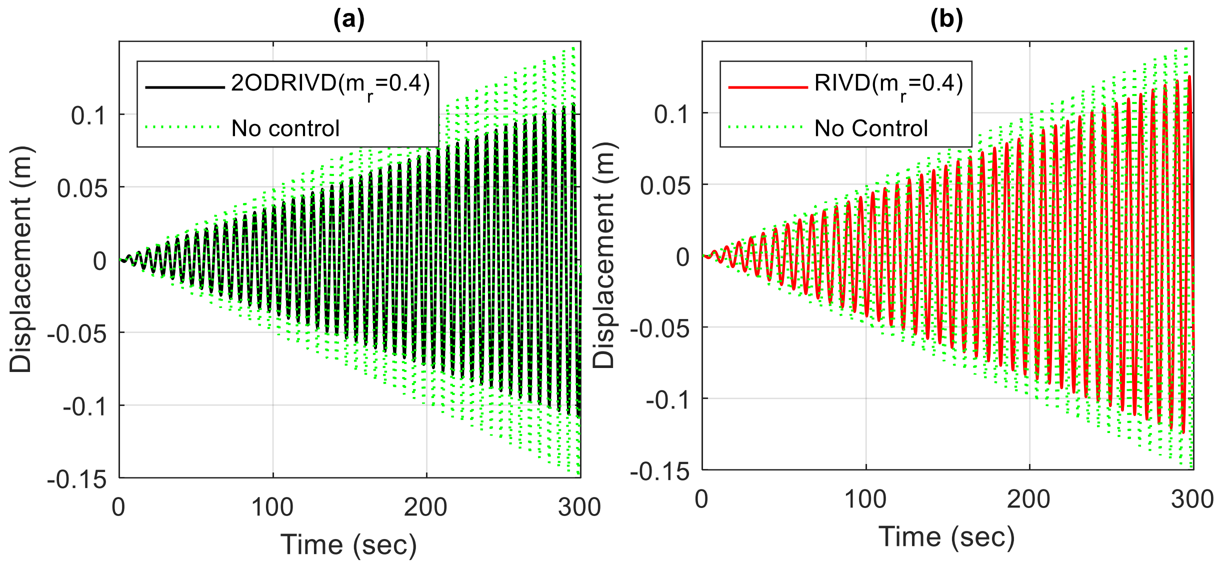

Figure 8-6: Time domain response given $m_r = 2m_{r1} = 2m_{r2} = 0.4$ and $D = 0$ for the (a) SDOF system with the 2ODRIVD excited at its apparent resonance frequency (b) SDOF system with the RIVD excited at its resonance frequency

Damped Response (D>0)

In order to assess the damped behavior of the 2ODRIVD, the response of the SDOF system with the RIVD and the 2ODRIVD with two rotational inertia masses ($m_r = 2m_{r1} = 2m_{r2} = 0.1$ and $m_r = 2m_{r1} = 2m_{r2} = 0.4$) and two levels of device damping ($D = 2D_1 = 2D_2 = 0.01$ and $D = 2D_1 = 2D_2 = 0.02$) are considered in this section. For each case, the DRF is calculated over a range of input ground motion frequencies from the time-domain responses, as described previously. Because of the inclusion of damping in the devices, the time-domain response converges to the steady state response for all input frequencies by the end of the time duration considered in the analysis. The DRF, calculated with the steady state values, is shown in Figure 8-7 for the rotational inertia masses and the device damping levels considered.

In Figure 8-7, it is once again observed that the resonant frequency of the system with the RIVD is significantly shifted lower, while the apparent resonant frequency of the system with the 2ODRIVD only moves slightly lower. This small shift in the apparent resonant frequency of the system with the 2ODRIVD is larger in the cases when the device's damping is higher. This result is logical because larger damping would slow the 2ODRIVD's flywheels more quickly and result in more time when either of the 2ODRIVD's flywheels are engaged.

It is also observed from Figure 8-7 that, in the case of $m_r = 2m_{r1} = 2m_{r2} = 0.1$ and $D = 2D_1 = 2D_2 = 0.01$, the 2ODRIVD provides a 20% reduction in the maximum response compared to the RIVD. This reduction value is 10% in the case of $m_r = 2m_{r1} = 2m_{r2} = 0.4$ and $D = 2D_1 = 2D_2 = 0.01$, -2.6% for $m_r = 2m_{r1} = 2m_{r2} = 0.1$ and $D = 2D_1 = 2D_2 = 0.02$, and 5.8% for $m_r = 2m_{r1} = 2m_{r2} = 0.4$ and $D = 2D_1 = 2D_2 = 0.02$. These results demonstrate that the combination of rotational inertia mass and damping coefficient plays a crucial role in the performance of the 2ODRIVD in comparison to the RIVD.

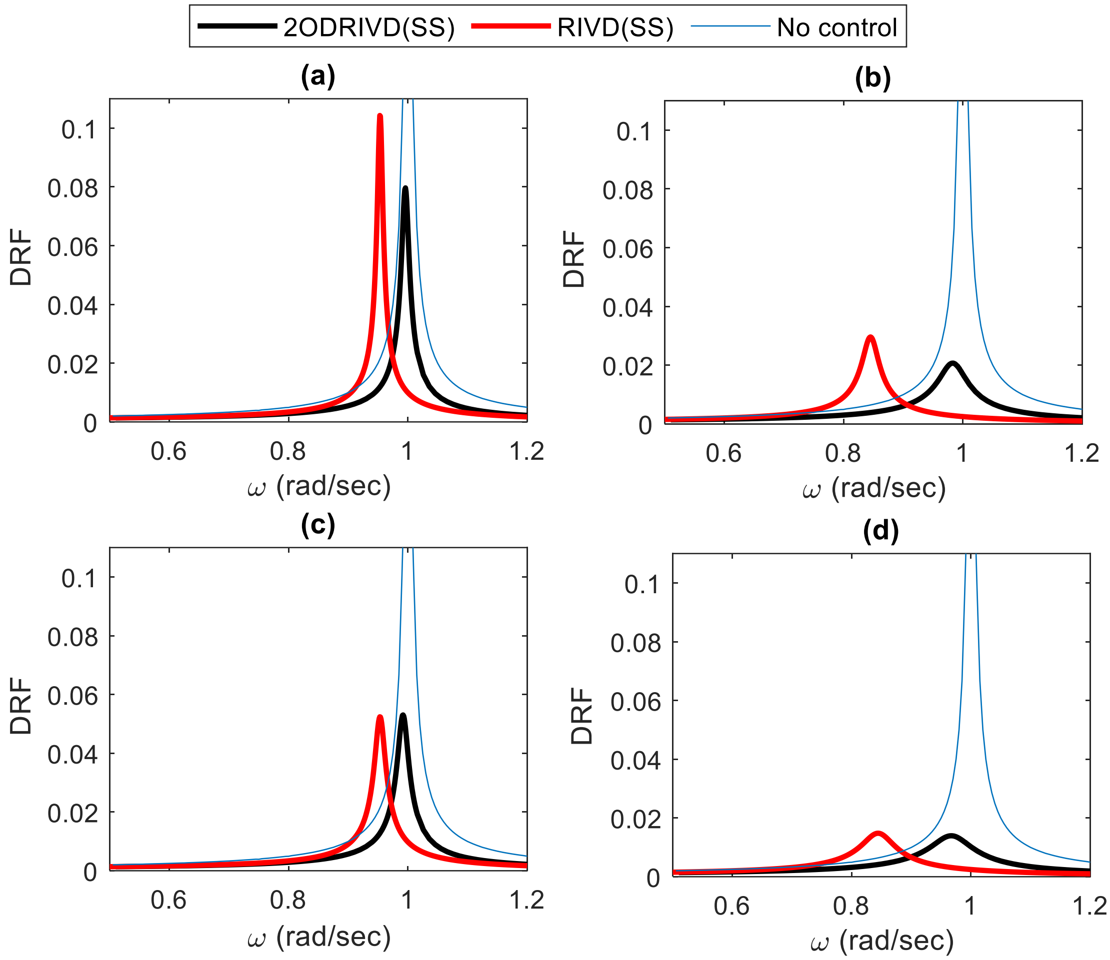

Figure 8-7: DRF of the systems with the RIVD and the 2ODRIVD over a range of frequencies when (a): $m_r = 2m_{r1} = 2m_{r2} = 0.1$ and $D = 2D_1 = 2D_2 = 0.01$ (b): $m_r = 2m_{r1} = 2m_{r2} = 0.4$ and $D = 2D_1 = 2D_2 = 0.01$ (c): $m_r = 2m_{r1} = 2m_{r2} = 0.1$ and $D = 2D_1 = 2D_2 = 0.02$, and (d): $m_r = 2m_{r1} = 2m_{r2} = 0.4$ and $D = 2D_1 = 2D_2 = 0.02$

For some applications of this device, the lack of a significant shift in natural frequency observed in the 2ODRIVD response could be advantageous. However, this shift in the natural frequency will provide some advantage to the RIVD if considering the acceleration response as the acceleration response to a harmonic loading is equivalent to the displacement response times the square of the loading frequency.

To investigate the effect of the device's damping coefficient and the amount of rotational inertia mass on the performance of the 2ODRIVD and the RIVD, the maximum DRF for different combinations of damping and rotational inertia mass are calculated and presented in Figure 8-8.

It can be observed from Figure 8-8 that for an arbitrary amount of rotational inertia mass, the 2ODRIVD reduces the maximum DRF more than the RIVD when the device damping is low. For both the RIVD and the 2ODRIVD, the maximum DRF decreases with increases in device damping. This decrease in maximum DRF with increased damping is faster for the RIVD; thus, the RIVD eventually outperforms the 2ODRIVD when the device damping is increased. The explanation for this is that at lower levels of damping, the flywheels of the 2ODRIVD rotate at a higher average speed than the RIVD, thus it is more effective at dissipating energy. However, when the damping increases, the flywheels of the 2ODRIVD slow down quickly when not engaged. The result is a lower average flywheel speed, which makes the 2ODRIVD less efficient at dissipating energy, compared to the RIVD, when the level of device damping is high.

Figure 8-8 shows that superior system performance is realized for both the 2ODRIVD and the RIVD with increases in both rotational inertia mass and device damping. Furthermore, Figure 8-8 shows that, for every level of device rotational inertia mass, there exists a value of damping at which the 2ODRIVD and RIVD have equivalent performance, in terms of DRF. The value of damping that results in equivalent performance is observed to increase with increases in the level of the device rotational inertia mass. At values of damping under the value where equivalent performance is observed, the 2ODRIVD has superior performance. In particular, this includes the undamped case. At levels of damping above this value, the RIVD has superior performance. From a design perspective, the best device to use would depend on the relative values of rotational inertia mass and damping that could feasibly be provided. To this end, changes in the flywheel moment arm or other mechanics of the rotational device can potentially provide increases in the effective mass provided by the device in a low-cost manner.

In contrast, adding damping to these systems can be complicated and increases in the level of damping provided can be costly, as damping can be a major source of expense in structural control devices [34,133,134]. Therefore, it may be advantageous, that the 2ODRIVD provides a structural control option that requires less damping to be effective.

Figure 8-9 presents the time history responses of the SDOF system with the RIVD and with the 2ODRIVD both with non-zero damping and loaded at their resonance frequencies.

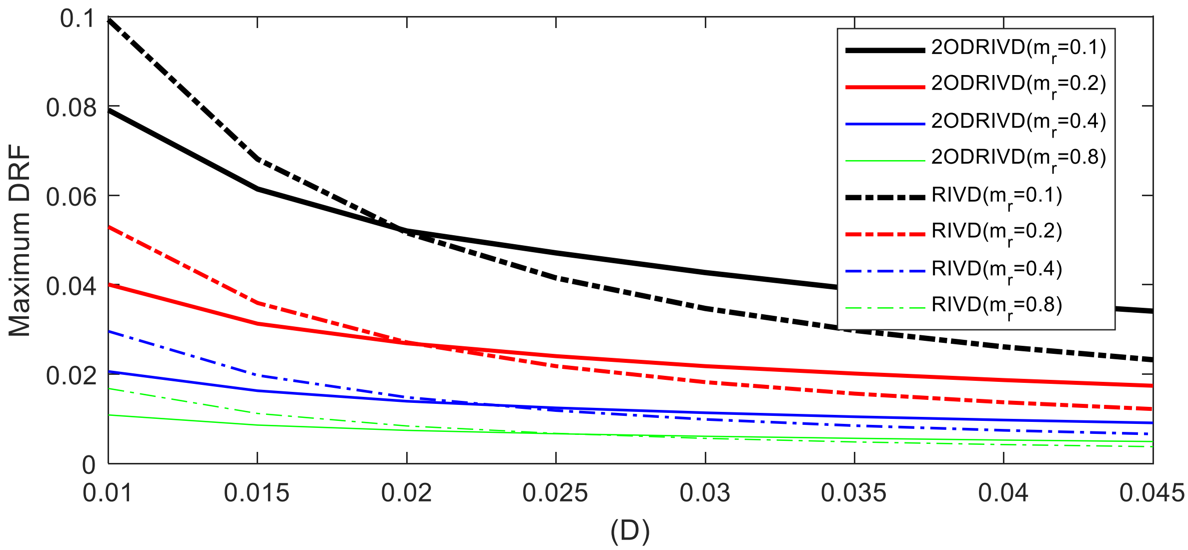

Figure 8-8: Effect of rotational inertia mass and device damping coefficient on the maximum DRF of a SDOF system with a RIVD and a 2ODRIVD

Both time history responses are based on the same amount of rotational inertia mass ($m_r = 2m_{r1} = 2m_{r2} = 0.1$) and the same level of damping ($D = 2D_1 = 2D_2 = 0.01$). As shown in Figure 8-9, the time history response of the SDOF system with the 2ODRIVD indicates superior performance, in terms of both the transient and steady state behavior, in comparison to the response of the SDOF system with the RIVD. In the transient part of the response, the growth of the response with the 2ODRIVD is slower than with the RIVD. Additionally, the steady state response of the system with the RIVD is approximately 20% higher than the response with the 2ODRIVD.

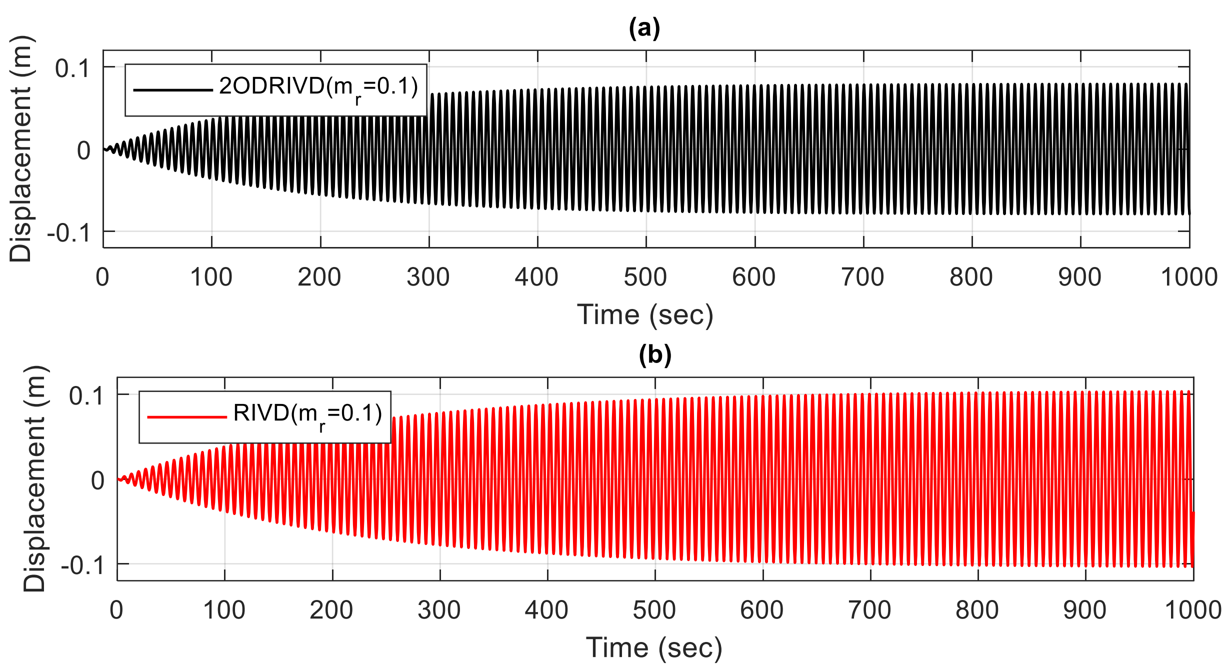

Figure 8-9: Time domain response given $m_r = 2m_{r1} = 2m_{r2} = 0.1$ and $D = 2D_1 = 2D_2 = 0.01$ for the (a) SDOF system with the 2ODRIVD excited at its apparent resonance frequency (b) SDOF system with the RIVD excited at its resonance frequency

The response of the system when subjected to a pulse-like load can also be examined. The loading used for this investigation is a single half-cycle of a sine function beginning at 0 secs with a frequency of 10 rad/sec and an amplitude of 1 N. The response of the system with the 2ODRIVD and the RIVD was then calculated with a range of combinations of inertia mass and damping properties. The resulting root mean square of the displacement response and the maximum displacement over this range are then shown in Figure 8-10 and Figure 8-11 , respectively.

As seen in Figure 8-10, increasing the inertia mass ratio decreases the RMS response for both the RIVD and 2ODRIVD at every level of damping. When comparing the 2ODRIVD and the RIVD with the same level of damping, at all inertia mass ratios investigated, the 2ODRIVD device has superior performance in reducing the RMS at relatively low levels of damping. However, these results show that by increasing the damping, the performance of the RIVD and 2ODRIVD get closer and then the RIVD eventually outperforms the 2ODRIVD. These results are similar to the results calculated from the response to harmonic loads that is shown in Figure 8-8.

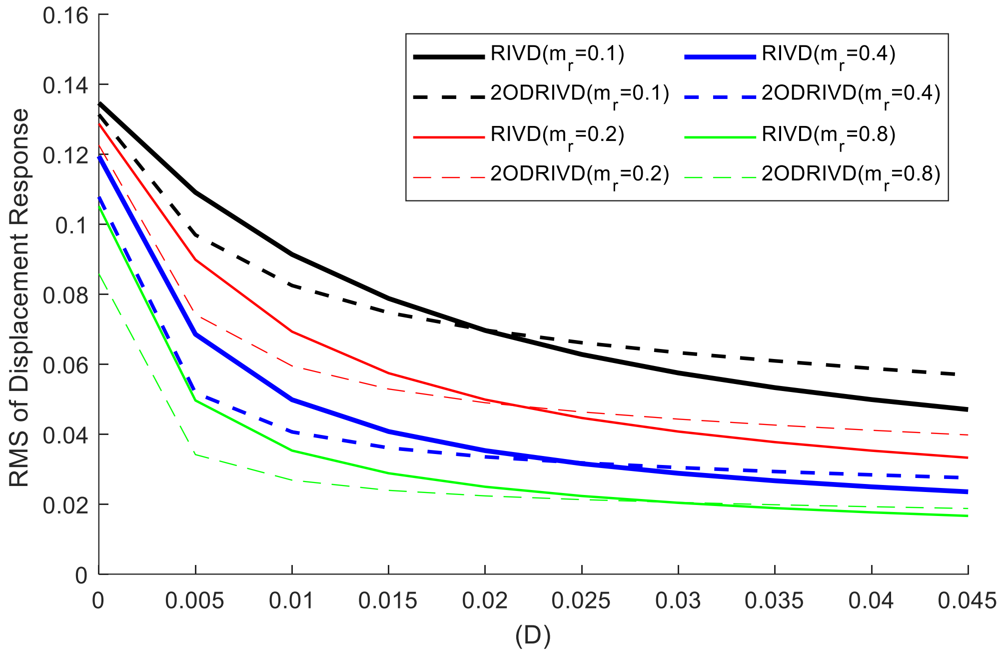

Figure 8-10: Effect of rotational inertia mass and device damping coefficient on the RMS response of a SDOF system subjected to impulsive load with a RIVD and a 2ODRIVD

Figure 8-11 shows the effect of the rotational inertia mass and device damping on the maximum response of the system when subjected to the pulse-like load considered. Once again, increasing the inertia mass ratio reduces this response in all cases, the 2ODRIVD outperforms the RIVD at low damping levels, and the RIVD outperforms the 2ODRIVD at high damping levels. However, unlike the response to harmonic loading and the RMS response to this pulse-like load, the maximum response of the system with the RIVD and 2ODRIVD is relatively insensitive to changes in damping.

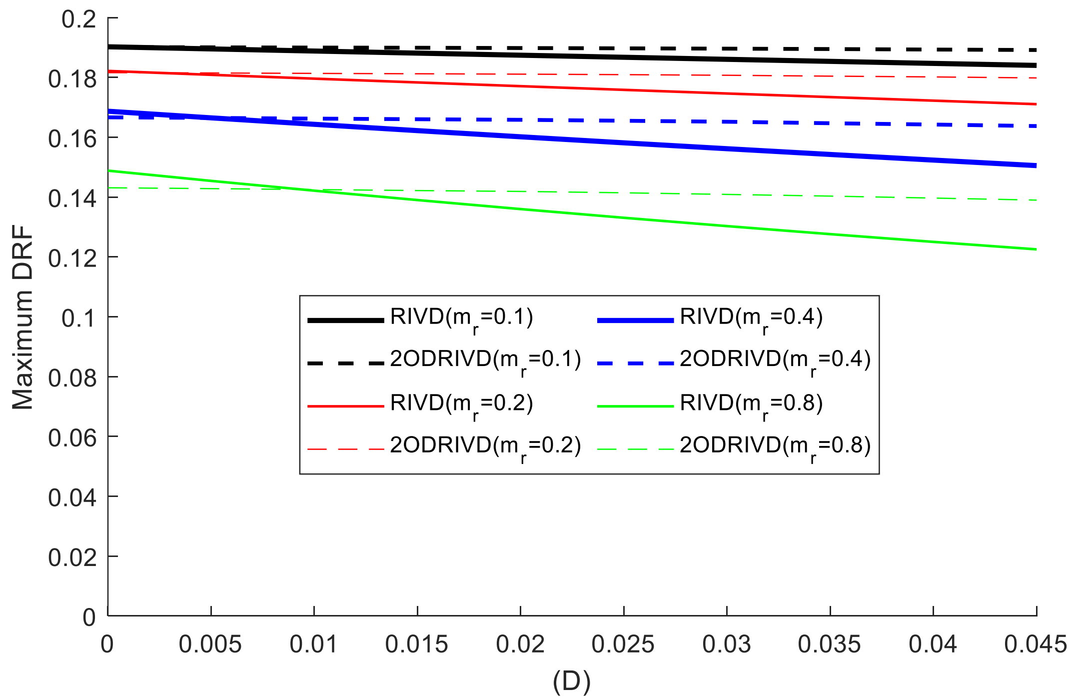

Figure 8-11: Effect of rotational inertia mass and device damping coefficient on the maximum DRF of a SDOF system subjected to the pulse-like load with a RIVD and a 2ODRIVD

Figure 8-12 shows time history responses of the structure with an RIVD and 2ODRIVD subjected to the pulse-like load with $m_r = 2m_{r1} = 2m_{r2} = 0.8$ and two different levels of damping. As shown in this figure, in the case of low damping, the 2ODRIVD provides a lower maximum amplitude and quicker attenuation of the response compared to the RIVD. However, with the increased level of damping, the performance of the RIVD and 2ODRIVD are more comparable in terms of maximum response and overall attenuation.

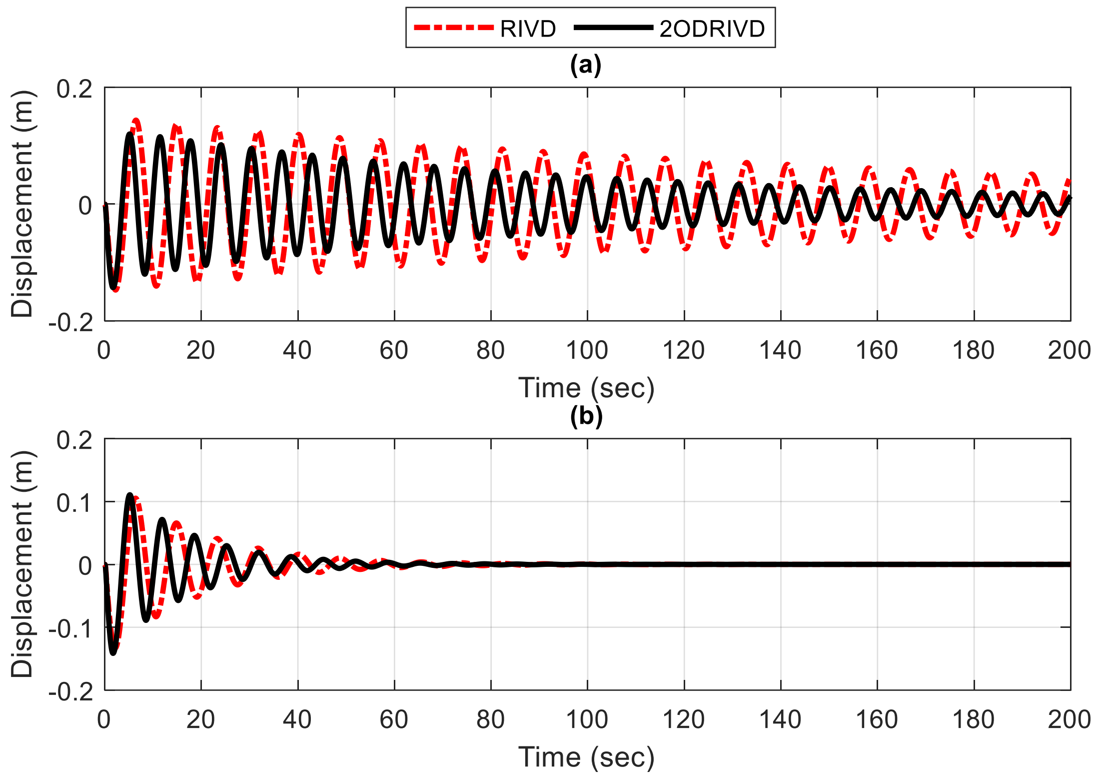

Figure 8-12: Time history response of RIVD and 2ODRIVD subjected to impulse load (a) $m_r = 2m_{r1} = 2m_{r2} = 0.8$ and $D = 2D_1 = 2D_2 = 0.0025$ (b) $m_r = 2m_{r1} = 2m_{r2} = 0.8$ and $D = 2D_1 = 2D_2 = 0.025$

Energy Analysis

An examination of the energy in the structure and contained as kinetic energy in the control devices during its response can provide more insight about the roles of energy redirection and dissipation in the 2ODRIVD and the RIVD. Consequently, time-histories of the kinetic and potential energy of the structure, kinetic energy of the devices' flywheels, and the total energy, which is the sum of these kinetic and potential energies, are considered in this section. Additionally, the relationship between the state of the 2ODRIVD and the energy in the system will be considered in this section.

The energy time-history response of the SDOF system with a RIVD and with a 2ODRIVD with the same rotational inertia mass and both with zero damping ($m_r = 2m_{r1} = 2m_{r2} = 0.4$ and $D = 2D_1 = 2D_2 = 0$) is presented in Figure 8-13. The input excitation in this analysis is a harmonic ground motion ($\omega = 0.9$ rad/sec); therefore, the potential and kinetic energy time-history responses of the SDOF system are also harmonic functions. The frequency of this loading was chosen so as to investigate the behavior of the device during a non-resonant loading. In this figure, the systems with the RIVD and the 2ODRIVD possess different maximum levels of total energy; however, this is expected due to the different values of DRF for the SDOF system with the devices at this input frequency observed in Figure 8-5.

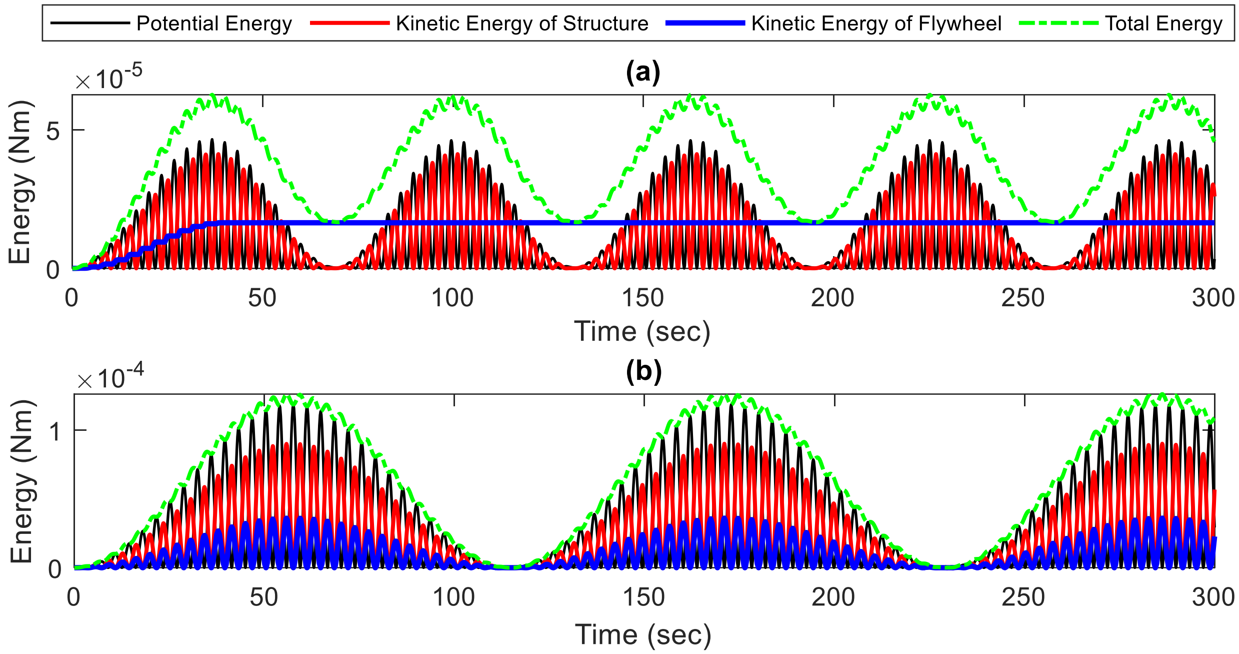

Figure 8-13: Response in terms of energy given $m_r = 2m_{r1} = 2m_{r2} = 0.4$, $D = 2D_1 = 2D_2 = 0$, and a harmonic input ($\omega = 0.9$ rad/sec) for the SDOF system with the (a) 2ODRIVD (b) RIVD

As shown in Figure 8-13, when the kinetic energy of the structure has reached a peak, the potential energy is equal to zero and vice versa. The rotational velocity of the flywheel of the RIVD is always linearly proportional to the velocity of the structure; therefore, the kinetic energy in the RIVD will always be proportional to the kinetic energy of the structure. This behavior is seen in Figure 8-13 (b) where the kinetic energy of the flywheel increases with the velocity of the structure, reaches a maximum point, goes down to zero, and then the cycle repeats itself. As no device damping is considered, all of the energy transferred to the RIVD is transferred back to the structure when the structure's velocity is equal to zero (at the maximum and minimum displacement points of the harmonic response).

The key difference between the RIVD and the 2ODRIVD is how the kinetic energy is transferred between the structure and the flywheel(s). The rotational velocity of the flywheels in the 2ODRIVD is linearly related to the velocity of the structure when the correct conditions are met and the flywheels are engaged with the structure. However, when they are not engaged, the flywheels spin freely with a constant velocity and the kinetic energy of the flywheels remain constant, as no device damping is considered. It can be observed in Figure 8-13 (a), that when the velocity of the structure increases, the structure engages with the flywheels and their kinetic energy increases. This continues until the structure reaches its maximum velocity. When the structure reaches this maximum velocity, the flywheels spin with their maximum velocity; therefore, the 2ODRIVD will not be engaged to the structure anymore. This behavior is the key benefit of the 2ODRIVD; the energy transferred to the 2ODRIVD stays in the flywheels and cannot be transferred back to the structure. This is observed in Figure 8-13 (a) where the potential energy of the structure never equals the total energy in the system.

The kinetic energy of the flywheels of the 2ODRIVD and the RIVD for this response are shown by themselves in Figure 8-14 (a) and the state of the 2ODRIVD during this response is presented in Figure 8-14 (b). As seen in this figure, the kinetic energy of the RIVD harmonically oscillates. However, the kinetic energy of the flywheel in the 2ODRIVD increases step by step when the device is in states S1 and S2, and stays constant when both flywheels are spinning freely (S3). After increasing in energy in the first part of the response, the 2ODRIVD is predominantly in S3 in the later parts of the response when the input is no longer meaningfully adding energy to the system. Note that there are several jumps from S3 to S2 after 50 seconds.

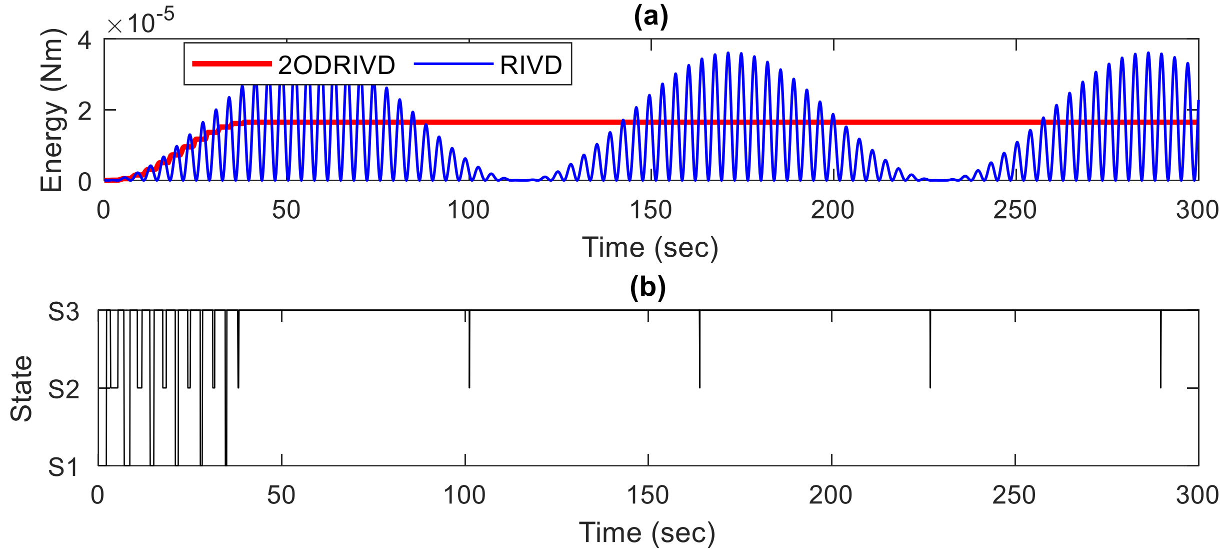

Figure 8-14: (a): Kinetic energy of flywheels in the RIVD and the 2ODRIVD ($m_r = 2m_{r1} = 2m_{r2} = 0.4$, $D = 2D_1 = 2D_2 = 0$, and $\omega = 0.9\ \text{rad/sec}$) (b): state of the 2ODRIVD

These jumps occur because the conditions momentarily exist for the flywheels of the 2ODRIVD to be engaged, but do not represent a significant increase in the energy of the flywheels.

In order to show the effect of damping on the system, the response to a harmonic excitation ($\omega = 0.9$) in terms of the energy of the system given 2ODRIVD and RIVD properties of $m_r = 2m_{r1} = 2m_{r2} = 0.4$ and $D = 2D_1 = 2D_2 = 0.01$ is presented in Figure 8-15. In these responses the viscous damping of the flywheels leads to the dissipation of energy which causes the amplitude of the response to decrease as it moves away from the initial transient portion to the steady state portion of the response.

The kinetic energy of the flywheels of the 2ODRIVD and the RIVD for this response are shown by themselves in Figure 8-16 (a) and the state of the 2ODRIVD during this response is presented in Figure 8-16 (b). Similar to the zero-damping case, the kinetic energy of the flywheel in the RIVD is harmonic, which means part of the kinetic energy in the flywheel is discharged back to the structure when the structure's velocity decreases. As damping is present, part of this kinetic energy is dissipated too. In contrast, the rotational velocity of the flywheel in the 2ODRIVD increases when driven by the structure and only decreases due to energy dissipation. Compared to the no damping case, the 2ODRIVD is more often engaged with the structure (S1 and S2) in this damped case. The reason for this is that the damping reduces the flywheel velocities, which means that the conditions for the flywheels to become engaged exist more often.

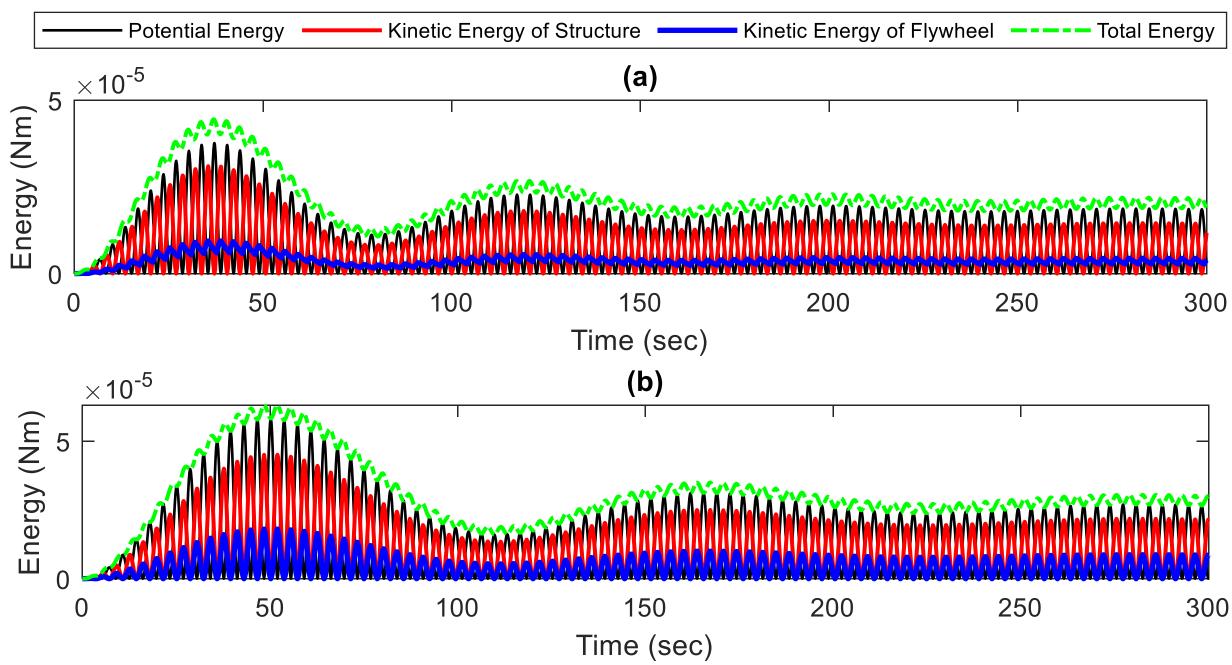

Figure 8-15: Response in terms of energy given $m_r = 2m_{r1} = 2m_{r2} = 0.4$, $D = 2D_1 = 2D_2 = 0.01$, and a harmonic input ($\omega = 0.9$ rad/sec) for the SDOF system with the (a) 2ODRIVD (b) RIVD

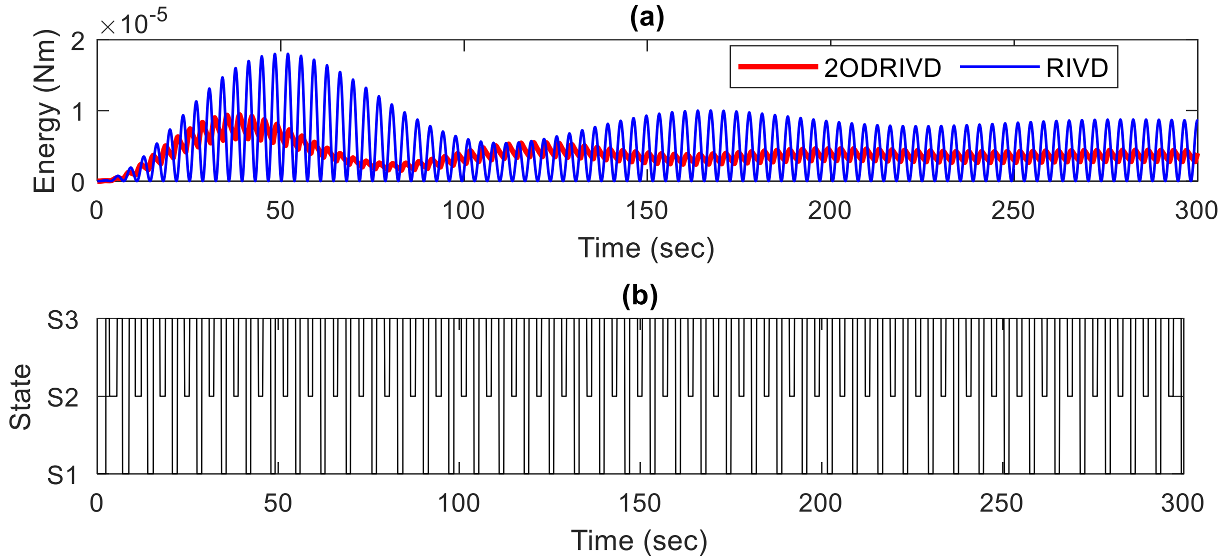

Figure 8-16: (a) Kinetic energy of flywheels in RIVD and 2ODRIVD ($m_r = 2m_{r1} = 2m_{r2} = 0.4$, $D = 2D_1 = 2D_2 = 0.01$, and $\omega = 0.9$ rad/sec) (b): state of the 2ODRIVD

Examining the kinetic energy in the flywheels helps to explain the results in Figure 8-8. The flywheels of the 2ODRIVD slow only due to damping in the device; therefore, when there is a small amount of damping, the flywheels remain at relatively high velocities longer then if the damping in the device is large. As a result, the average flywheel velocity of the 2ODRID decreases rapidly with increases in flywheel damping. In contrast, the flywheel of the RIVD will have a velocity that is always proportional to the velocity of the primary mass of the

system; thus, the velocity of the RIVD flywheel will cycle and include significant portions where the flywheel velocity is low. At low damping levels, the 2ODRIVD's higher average flywheel velocity enables it to, compared to the RIVD with the same damping level, more effectively dissipate energy through this viscous damping.

With increases in the damping levels, the 2ODRIVD's average flywheel velocity decreases and the damping in the RIVD is eventually more effective.

To further illustrate the behavior of the devices and their energy dissipation mechanisms, the response to a harmonic excitation ($\omega = 0.9$) in terms of the damping mechanism of the system is presented in Figure 8-17. For this analysis, the properties of the 2ODRIVD and the RIVD were $m_r = 2m_{r1} = 2m_{r2} = 0.4$ and $D = 2D_1 = 2D_2 = 0.01$. In both cases, the damping moment provided to the device flywheels is the rotational velocity of the flywheel multiplied by the assumed damping coefficient of the viscous material. As shown in Figure 8-17, the rotational behavior of the two devices is very different. The rotation of the RIVD is proportional to the relative displacement; thus, it is bounded and cycles between clockwise and counterclockwise rotation. On the other hand, each flywheel of the 2ODRIVD only spins in one direction; thus, the rotation of that flywheel is only increasing (or decreasing). The energy dissipation by the RIVD can be determined by calculating the hysteretic area represented by this curve, while the energy dissipated by the 2ODRIVD can be found by considering the area under the curve

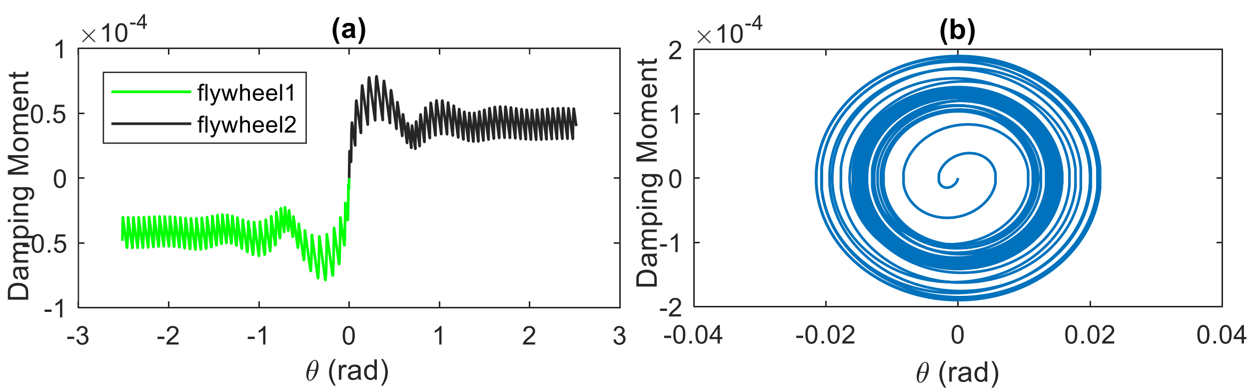

Figure 8-17 : Damping moment versus flywheel rotation for the (a) 2ODRIVD and (b) RIVD

Conclusions

An innovative rotational inertia damper known as the one-directional rotational inertia viscous damper (ODRIVD) is proposed, formulated, and investigated in this paper. The proposed damper consists of a one-directional ball screw and flywheel, which is engaged in and converts relative motion in one direction to the rotation of the flywheel, but is not affected by relative motion in the other direction. Furthermore, once this flywheel is put into motion, it can only be engaged again if subsequent motion in the same direction has a velocity high enough to allow the one-directional ball screw to engage. In order to maintain symmetry, this paper primarily investigates the performance of two ODRIVD combined, referred to as the 2ODRIVD, which allows a portion of the device to become engaged with motion in either direction. The full accounting of the velocity of the flywheels of the 2ODRIVD, and their corresponding kinetic energy, once they are not engaged is what separates this device from the limited number of similar devices previously introduced.

A SDOF controlled with a 2ODRIVD will respond in a combination of three states: 1) the first flywheel engaged and the second spinning freely; 2) the first flywheel spinning freely and the second engaged; 3) both flywheels spinning freely.

Comparisons in this paper are made to the rotational inertia viscous damper (RIVD), a device similar to the ODRIVD but utilizing an inerter which keeps the device always engaged to the structure with a flywheel rotational velocity proportional to the structure's velocity.

The performance of the 2ODRIVD was primarily investigated in this paper by calculating the displacement response factor from the response of a SDOF system with the 2ODRIVD and the RIVD subjected to harmonic excitations over a range of frequencies. In both zero and nonzero device damping cases, while the RIVD changes the resonant frequency of the system significantly, the change in the apparent resonant frequency of the SDOF controlled with the 2ODRIVD is not significant. Additionally, it was observed that the performance of the 2ODRIVD and the RIVD are dependent on the level of device damping and rotational inertia mass. For both devices, it was found that the performance, in terms of decreasing the peak displacement response factor, increases with increases in device damping and rotational inertial mass. Comparing the performance of the RIVD and the 2ODRIVD, it was found that when subject to the harmonic load or a pulse-like load and at each level of rotational inertia mass considered, the RIVD had superior performance at relatively high device damping levels and the 2ODRIVD had superior performance at lower device damping levels.

Time history responses are also used to investigate the behavior of the proposed device. In the case of zero damping, the growth of the resonant response of an SDOF system with a 2ODRIVD is significantly slower than the growth of the resonant response of an SDOF system with a RIVD. When considering device damping, it is observed that the 2ODRIVD can provide a resonant response with significantly lower amplitude compared to the RIVD.

An analysis of the energy time histories of both systems shows that the potential for superior performance of the 2ODRIVD can be attributed to the 2ODRIVD's one-directional energy mechanism. This mechanism allows for energy to be transferred to the device's flywheels where it can be locally contained without being transferred back to the primary structure. When damping in the 2ODRIVD is considered, this energy can be locally dissipated by the device. Due to this damping, the rotational velocity of the flywheels of the 2ODRIVD is reduced, which enables the device to be more often engaged with the structure it is attached to. However, at high levels of damping, better performance is generally observed from the RIVD.

CHAPTER NINE:CONCLUSIONS

Summary and Conclusions

Inerter-based passive control devices have the potential to be highly effective for the passive control of structures. Through the transformation of translational motion to the rotational motion of a physically small mass, an inerter can provide large effective inertia mass. This phenomenon has been used to develop ideas on a new generation of passive control devices. Recently, inerter-based passive control devices have been investigated as a part of mass dampers and in structural control devices without a physical mass component. The goals of this dissertation are to extend the state of the art in this field by developing optimum design methods for these systems, evaluating the performance of different inerter-based passive control devices, proposing new and innovative linear and nonlinear configurations.

The comprehensive literature review on inerter-based passive control devices is presented and the gaps in the literature is discussed in Chapter 2. Then, in order to fulfill the objective of this dissertation, the investigation on inerter-based passive control devices is presented and divided into the six following chapters (Ch 3 to Ch 9).

In an effort to improve the state of the art related to the optimum design of inerter-based mass dampers, an optimal design of the rotational inertial double tuned mass damper (RIDTMD) presented in Chapter 3. This chapter presents an exact solution for the design of the optimum values of stiffness and damping for RIDTMD devices attached to an undamped SDOF system subjected to random force and base excitation. Expressions for the variance in the displacement response of the structure the RIDTMD is attached to for both force and base excitation are derived in closed-form and conditions for optimization of this response are satisfied mathematically. The proposed method provides a set of closed-form equations for the optimal design values for an arbitrary main and secondary mass ratio. While these results show that the value of the optimum parameters have substantial differences for the force and base excitation cases, the trends observed with changes in the mass ratios are the same for each loading case.

In this chapter, the optimum secondary mass ratio and the effectiveness of the RIDTMD in comparison to the TMD was investigated. It was found, for both force and base excitation, the optimum RIDTMD with optimal secondary mass ratios shows a more effective performance in reducing the response of the primary structure, as measured by the dynamic magnification factor and H_2 norm, in comparison to the optimal TMD with the same main mass ratio. In addition, the RIDTMD's performance advantage, compared to the TMD, is substantial when the secondary mass is optimum; around a 7% reduction in H_2 norm and 16%-30% reduction of the DMF observed by utilizing optimum secondary mass.

In continuation of the optimum design and performance evaluation of inerter-based mass dampers, the optimum design and performance evaluation of three recently developed inerter-based mass dampers is investigated in Chapter 4. In previous works, numerical optimum design methods considering harmonic ground excitation were proposed and the performance of inerter-based tuned mass dampers in comparison to the TMD in the reduction of the maximum peak was evaluated. In this work, the exact analytical solutions for the optimum design of inerter-based mass dampers when the primary structure is subjected to random ground excitation was presented. Furthermore, numerical optimal designs for these devices were presented considering seismic ground motions.

In this work, it was found that when the primary structure is subjected to random ground excitation, the optimum H_2 inerter based tuned mass dampers can provide a 7%-8% reduction of the H_2 norm compared to TMDs with the same main mass ratio. In addition, H_∞ optimum design inerter-based mass dampers can provide a 25% reduction of the maximum displacement of the primary structure compared to the TMDs in the case of random base excitation. For seismic evaluation, the exact H_2 optimum design of inerter-mass dampers show, on average, a 6% reduction in the RMS displacement response. As the numerical optimization considering a suite of ground motions is more difficult to perform and only provides a 7% average improvement in performance, the H_2 optimum design is likely more practical in many cases than a design considering a suite of ground motions. The H_2 optimum designed inerter-mass damper provides a 7% improvement in the reduction of the RMS displacement response of the primary structure in comparison to TMDs. Furthermore, compared to the TMDs, the inerter-based mass dampers cannot be effective in the reduction of the maximum displacement.

As the improvement of existing passive vibration absorbers that have yet to be studied considering inerters was another goal of this dissertation, a new inerter-based mass damper is proposed in Chapter 5. This vibration absorber is called the "three element vibration absorber-inerter" (TEVAI). This device is similar to the three-element vibration absorber, which is like a TMD except, it has an inerter attached between the secondary mass and a fixed support. The TEVAI, which is an improvement of both the three-element vibration absorber and tuned mass damper inerter (TMDI) was introduced, formulated, optimized, and examined. A closed-form H_2 optimization procedure was performed and expressions for optimal parameters of the device were presented. In addition, a numerical optimization was performed to examine the effectiveness of the device given the H_∞ optimization criterion, which corresponds to the reduction of the maximum peak response in the frequency domain.

From the results of this study, it was observed that the performance of the TEVAI increases with increased inertance mass ratio. This behavior is unlike devices where the inerter is placed between the mass of the device and the primary structure, such as the RIDTMD. In addition, in comparison to the TMDI with the same mass ratio, the TEVAI provides a lower H_2 norm and peak dynamic magnification factor in the case of H_2 optimization and a lower peak dynamic magnification factor in the case of H_∞. The TEVAI is able to reduce the H_2 norm of the primary mass by an additional 3% to 5%, in comparison to the H_2 optimal TMDI, over the range of main mass and inertance mass ratios considered. In addition, the H_2 optimum TEVAI is able to provide a 3% to 14% reduction in the peak dynamic magnification factor, in comparison to the H_2 optimal TMDI, over the range of main mass and inertance mass ratios considered. Furthermore, the H_∞ optimum TEVAI provides a 3%-10% reduction in the peak dynamic magnification factor, in comparison to the H_∞ optimal TMDI.

In continuation of the objective of improving existing passive vibration absorbers that have yet to be studied considering inerters, a nonlinear inerter-based mass damper was proposed in Chapter 6. This inerter-based mass damper is called the nonlinear energy sink inerter (NESI). The difference between the NESI and nonlinear energy sink (NES) is an inerter which is attached to the secondary mass of NES and a fixed point. The performance evaluation of the NESI demonstrates the superior performance of the proposed device in comparison to the traditional NES. The reduction in the RMS of the response increases smoothly and monotonically with increases in the inertance value utilized in the NESI, for all of the device secondary mass ratios considered. Furthermore, for the different secondary mass ratios considered and an inertance ratio of 1, it was found that the NESI was able to reduce the RMS response by between 20% and 25%, compared to the NES. As the inertance mass can be provided by utilizing a small physical mass, the use of an inerter in the manner used in this device can be an effective way of increasing the passive structural control performance of an NES without increasing its physical secondary mass.

Another improved passive control device using an inerter was proposed and investigated in Chapter 7. The proposed device is the multiple tuned mass damper inerter (MTDMI), which can be considered as an advancement that is based on the tuned mass damper inerter (TMDI) and multiple tuned mass damper (MTMD). This device consists of multiple masses connected to the primary structure through springs and dashpots, and multiple inerters connected to the masses and fixed support. The device was proposed in two types: 1) Type 1 MTMD where the physical secondary mass of each absorber is the same and each absorber is designed with different damping and stiffness parameters and 2) Type 2 MTMDI where the stiffness and damping are considered identical, but the masses of each absorber are different and distributed based on a functional expression.

The Type 1 MTMDI was observed to provide superior effectiveness compared to the MTMD and the TMDI in the reduction of the H_2 norm and peak value on the frequency response curve for the displacement of the primary structure. The Type 2 MTMDI, has increased effectiveness in the reduction of the H_2 norm and peak value on the frequency response curve for the displacement of the primary structure in comparison to the TMDI; however, the Type 2 MTMDI cannot significantly improve the reduction of the peak value on the frequency response curve. If desired, the inertance of the Type1 MTMDI can be provided as a concentrated inertance to one of the absorbers as the results of this study revealed no significant difference between the effectiveness when the inertance is concentrated or distributed.

In Chapter 8, an innovative inerter-based passive control device called the "one-directional rotational inertia viscous damper (ODRIVD)" for the passive control of SDOF structures was proposed and investigated. This device is fundamentally different from the other devices studied in this work because this device is not linear time invariant, rather this is a nonlinear inerter-based passive damper that switches between different linear states. The proposed damper consists of a one-directional ball screw and flywheel, which is engaged in and converts relative motion in one direction to the rotation of the flywheel, but is not affected by relative motion in the other direction. Furthermore, once this flywheel is put into motion, it can only be engaged again if subsequent motion in the same direction has a velocity high enough to allow the one-directional ball screw to engage. In order to maintain symmetry, the performance of two ODRIVD combined, referred to as the

2ODRIVD, which allows a portion of the device to become engaged with motion in either direction, is primarily investigated in this chapter.

The performance of the 2ODRIVD was investigated by calculating the amplitude of the dynamic response of a SDOF system with the 2ODRIVD and the RIVD subjected to harmonic excitations over a range of frequencies. In both zero and nonzero device damping cases, while the RIVD changes the resonant frequency of the system significantly, the change in the apparent resonant frequency of the system controlled with the 2ODRIVD is not significant. Additionally, it was observed that the performance of the 2ODRIVD and the RIVD are dependent on the level of device damping and rotational inertia mass. For both devices, it was found that the performance, in terms of decreasing the peak displacement response factor, improves with increases in device damping and rotational inertial mass. Comparing the performance of the RIVD and the 2ODRIVD, it was found that when subject to the harmonic load or a pulse-like load and at each level of rotational inertia mass considered, the RIVD had superior performance at relatively high device damping levels and the 2ODRIVD had superior performance at lower device damping levels. Time history responses were also used to investigate the behavior of the proposed device. In the case of zero damping, the growth of the resonant response of an SDOF system with a 2ODRIVD is significantly slower than the growth of the resonant response of an SDOF system with a RIVD. When considering device damping, it is observed that the 2ODRIVD can provide a resonant response with significantly lower amplitude compared to the RIVD.

Table 4 presents a brief summary of all the passive control devices discussed in the different chapters of this dissertation. This table provides some of the most important information about the devices including the name, type, configuration, application, and the key advancements of the device. Additionally, a diagram of each of these devices is presented in this table.

The state of the art in passive control and inerter-based passive control devices has been further developed in this dissertation. Exact optimum design methods for previously proposed inerter-based mass dampers have been introduced and the performance of these devices have been evaluated in loading conditions not previously considered. Additionally, three new inerter-based mass dampers have been proposed, formulated and evaluated. Finally, an innovative nonlinear inerter-based passive control device was proposed in this dissertation. This work serves to demonstrate the potential and promise of inerter-base passive control devices and methods to outperform and enhance current passive control devices and methods.

Table 4:Traditonal and inerter-based passive control devices

Passive Control Device	Type	Proposed in this thesis?	Physical mass needed?	Advancements	Application note	Configuration	Linear / Nonlinear System	Kinetic Energy Returned to System
Tuned mass damper (TMD)	Mass damper	No	Yes	Classical way to reduce the dynamic response of structures	Primarily considered as installed at the top of a structure	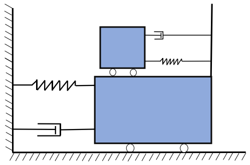	Linear	Yes
Three element vibration absorber (TEVA)	Mass damper	No	Yes	Improvement to the TMD through an additional DOF	Primarily considered as installed at the top of a structure	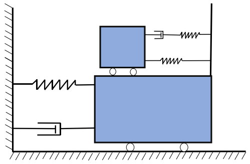	Linear	Yes
Tuned mass damper (TMDI)	Inerter-based mass damper	No	Yes	Improvement to the TMD through added effective mass	Primarily considered as installed at the top of a structure with a ground connection (such as an outrigger)	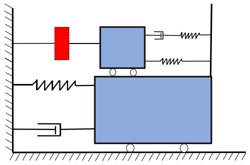	Linear	Yes

Table 4 Continued

Three element vibration absorber Inerter (TEVAI)	Inerter-based mass damper	Yes	Yes	Improvement to the TMDI and TEVA through combining their benefits	Primarily considered as installed at the top of a structure with a ground connection (such as an outrigger)	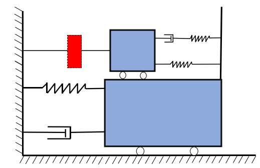	Linear	Yes
Nonlinear energy sink Inerter (NESI)	Inerter-based mass damper	Yes	Yes	Improvement to the NES through added effective mass	Primarily considered as installed at the top of a structure with a ground connection (such as an outrigger)	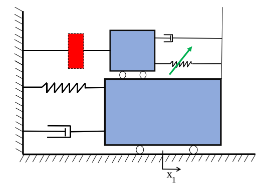	Strongly nonlinear due to essentially nonlinear stiffness element	Yes
Multiple tuned mass damper (MTMD)	Mass damper	No	Yes	Improvement to the TMD through multiple additional DOFs	Primarily considered as installed at the top of a structure, but can be distributed	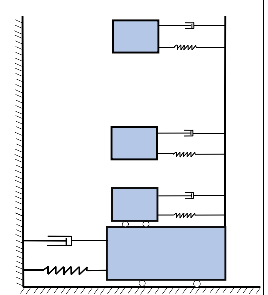	Linear	Yes

Table 4 Continued

Multiple tuned mass damper inerter (MTMDI)	Inerter-based mass damper	Yes	Yes	Improvement to the TMDI and MTMD through combining their benefits	Primarily considered as installed at the top of a structure with a ground connection (such as an outrigger), but can be distributed	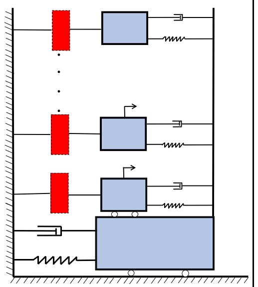	Linear	Yes
Rotational inertia double tuned mass damper (RIDTMD)	Inerter-based mass damper	No	Yes	Improvement to the TMD through an additional DOF with effective mass	Primarily considered as installed at top of the MDOF structure	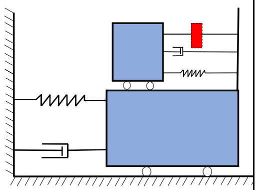	Linear	Yes
Viscous Damper (VD)	Damper	No	No	Classical damper without mass effects	Primarily considered as installed between stories of a structure or in isolation layer		Typically modeled as linear. Physical dampers often have significant nonlinearities	N/A

Table4 Continued

Rotational inertia viscous damper (RIVD)	Inerter-based damper	No	No	Reduces the dynamic response of structures utilizing small inertia mass	Primarily considered as installed between stories of a structure	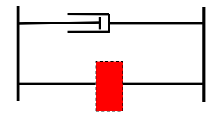	Linear	Yes
Tuned inerter damper (TID)	Inerter-based damper	No	No	Damper with mass effects and an additional DOF, behaves like a TMD	Primarily considered as installed between stories of a structure	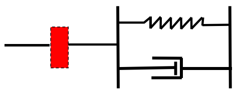	Linear	Yes
Tuned viscous mass damper (TVMD)	Inerter-based damper	No	No	Damper with mass effects and an additional DOF, behaves like a TMD	Primarily considered as installed between stories of a structure	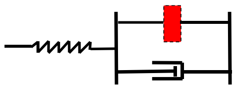	Linear	Yes
Clutch inerter damper	Inerter-based damper	No	No	Improvement on the RIVD through only allowing one-way transfer of energy	Primarily considered as installed between stories of a structure	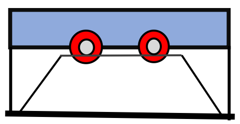	Overall nonlinear, system jumps between different linear states	No

Table 4 Continued

One-way rotational inertia viscous damper (ODRIVD)	Inerter-based damper	Yes	No	Improvement on the RIVD through only allowing one-way transfer of energy. Physics of flywheel energy considered more fully than in clutch inerter damper formulation	Primarily considered as installed between stories of a structure or in isolation layer	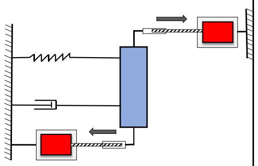	Overall nonlinear, system jumps between different linear states	No

Future works

Despite the recent development of inerter-based passive control devices, there are still many aspects of these devices and their usage where potential for improvement exists. In this section, some key areas of potential improvements for this field are described.

First, the optimum design and performance evaluation of inerter-based mass dampers has mostly been limited to random and harmonic excitations. However, structures are subjected to a variety of different type of loads in reality. Future work can be design and evaluation of inerter-based mass dampers for control of structure subjected to wind, blast and impulsive loads. In addition, design and optimization of inerter-mass dampers in this work has been limited to linear primary structures. Therefore, design of inerter-based mass dampers when the primary structure is nonlinear, performance-based design, and robust design can be considered as other developments. Furthermore, the design and performance evaluation of MTMDI and distributed inerter-based tuned mass dampers considering an underlying MDOF structure that is subjected to wind and seismic load has also not been studied yet.

Second, the inerter can be used to improve nonlinear vibration absorbers as seen by the nonlinear energy sink inerter (NESI) proposed in this dissertation. However, many aspects of this proposed device should be studied in the future to extend this initial work. Analytical solutions for NESI, can provide more insight about the performance and behavior of the proposed device. NESI for MDOF structures under various excitations is another option to introduce this device as a passive control device in structural engineering. Improvement using inerters to these nonlinear passive control devices can reduce their physical mass and increase their performance. Pendulum dampers and nonlinear tuned mass dampers are two examples of nonlinear devices which can be improved by utilizing an inerter.

Third, the ODRIVD was proposed and investigated numerically in this dissertation, but much work remains. Linearization of the equation of motion or otherwise providing a solution for estimating the effective system resonance frequency and response function would be a significant contribution. Furthermore, the performance of the ODRIVD in the reduction of the response of MDOF structures subjected to random or harmonic loads is also another option for development. In order to validate the proposed device, an experimental investigation for control of SDOF and then MDOF structures would be impactful.

Finally, improvement to the passive control of structures through the introduction of innovative nonlinear inerter-based dampers will be an important contribution to this field. Traditional inerter-based dampers provide constant increases in effective mass that result in constant shifts in the dynamics of structures, including their natural frequencies. Variable inertia rotational dampers would instead provide added mass effects that change with the response of the structure. These devices could help avoid resonance by continuously shifting the natural frequencies of a structure. In addition, the particle rotational inertia damper is an idea to increase the chance of avoiding resonance by vibration in different phases due to changing the effective mass. In this type of device, the inertia mass changes based on the acceleration and velocity during the vibration, which is desirable for avoiding resonance.

References

[1] Gw. Housner, L.A. Bergman, T.K. Caughey, A.G. Chassiakos, R.O. Claus, S.F. Masri, R.E. Skelton, T.T. Soong, B.F. Spencer, J.T. Yao, Structural control: past, present, and future, Journal of Engineering Mechanics. 123 (1997) 897–971. https://doi.org/10.1061/(ASCE)0733-9399(1997)123:9(897).

[2] B.F. Spencer Jr., S. Nagarajaiah, State of the Art of Structural Control, JOURNAL OF STRUCTURAL ENGINEERING. 129(7) (2003) 845–856. https://doi.org/10.1061/(ASCE)0733-9445(2003)129:7(845).

[3] S. Nagarajaiah, E. Sonmez, Structures with semiactive variable stiffness single/multiple tuned mass dampers, Journal of Structural Engineering. 133 (2007) 67–77.

[4] J.D. Holmes, Listing of installations, Engineering Structures. 17 (1995) 676–678. https://doi.org/10.1016/0141-0296(95)90027-6.

[5] M. Gutierrez Soto, H. Adeli, Tuned Mass Dampers, Archives of Computational Methods in Engineering. 20 (2013) 419–431. https://doi.org/10.1007/s11831-013-9091-7.

[6] F. Sadek, B. Mohraz, A.W. Taylor, R.M. Chung, A method of estimating the parameters of tuned mass dampers for seismic applications, Earthquake Engineering and Structural Dynamics. 26 (1997) 617–636. https://doi.org/10.1002/(SICI)1096-9845(199706)26:6%3C617::AID-EQE664%3E3.0.CO;2-Z.

[7] E. Matta, Effectiveness of Tuned Mass Dampers against Ground Motion Pulses, Journal of Structural Engineering. 139 (2013) 188–198. https://doi.org/10.1061/(ASCE)ST.1943-541X.0000629.

[8] J.-S. Hwang, J. Kim, Y.-M. Kim, Rotational inertia dampers with toggle bracing for vibration control of a building structure, Engineering Structures. 29 (2007) 1201–1208. https://doi.org/10.1016/j.engstruct.2006.08.005.

[9] H. Garrido, O. Curadelli, D. Ambrosini, Improvement of tuned mass damper by using rotational inertia through tuned viscous mass damper, Engineering Structures. 56 (2013) 2149–2153. https://doi.org/10.1016/j.engstruct.2013.08.044.

[10] Y. Hu, M.Z.Q. Chen, Performance evaluation for inerter-based dynamic vibration absorbers, International Journal of Mechanical Sciences. 99 (2015) 297–307. https://doi.org/10.1016/j.ijmecsci.2015.06.003.

[11] Y. Watanabe, K. Ikago, N. Inoue, H. Kida, S. Nakaminami, H. Tanaka, Y. Sugimura, K. Saito, Full-scale dynamic tests and analytical verification of a force-restricted tuned viscous mass damper, in: Proceedings of the 15th World Conference on Earthquake Engineering, Lisbon, Portugal, Paper ID, 2012. http://www.iitk.ac.in/nicee/wcee/article/WCEE2012_1206.pdf (accessed June 19, 2016).

[12] Y. Sugimura, W. Goto, H. Tanizawa, K. Saito, T. Nimomiya, Response control effect of steel building structure using tuned viscous mass damper, in: 15th World Conference on Earthquake Engineering, 2012.

[13] H. Frahm, Device for Damping Vibrations of Bodies, 1909.

[14] J. Den Hartog, Mechanical vibrations, 4th ed., McGraw-Hill, NY, 1956.

[15] W.O. Wong, Optimal design of a hysteretic vibration absorber using fixed-points theory, The Journal of the Acoustical Society of America. 139 (2016) 3110–3115.

[16] Y.L. Cheung, W.O. Wong, H-infinity optimization of a variant design of the dynamic vibration absorber—Revisited and new results, Journal of Sound and Vibration. 330 (2011) 3901–3912. https://doi.org/10.1016/j.jsv.2011.03.027.

[17] J. Dayou, Fixed-points theory for global vibration control using vibration neutralizer, Journal of Sound and Vibration. 292 (2006) 765–776. https://doi.org/10.1016/j.jsv.2005.08.032.

[18] T. Asami, O. Nishihara, A.M. Baz, Analytical Solutions to H[sub ∞] and H[sub 2] Optimization of Dynamic Vibration Absorbers Attached to Damped Linear Systems, Journal of Vibration and Acoustics. 124 (2002) 284. https://doi.org/10.1115/1.1456458.

[19] L. Zuo, S.A. Nayfeh, Minimax optimization of multi-degree-of-freedom tuned-mass dampers, Journal of Sound and Vibration. 272 (2004) 893–908.

[20] Crandall, Mark, Random vibration in mechanical systems, Academic Press, 1963.

[21] O.F. Tigli, Optimum vibration absorber (tuned mass damper) design for linear damped systems subjected to random loads, Journal of Sound and Vibration. 331 (2012) 3035–3049. https://doi.org/10.1016/j.jsv.2012.02.017.

[22] O.F. Tigli, Optimum vibration absorber (tuned mass damper) design for linear damped systems subjected to random loads, Journal of Sound and Vibration. 331 (2012) 3035–3049. https://doi.org/10.1016/j.jsv.2012.02.017.

[23] A.Y.T. Leung, H. Zhang, C.C. Cheng, Y.Y. Lee, Particle swarm optimization of TMD by non-stationary base excitation during earthquake, Earthquake Engineering & Structural Dynamics. 37 (2008) 1223–1246. https://doi.org/10.1002/eqe.811.

[24] G. Bekdaş, S.M. Nigdeli, Estimating optimum parameters of tuned mass dampers using harmony search, Engineering Structures. 33 (2011) 2716–2723. https://doi.org/10.1016/j.engstruct.2011.05.024.

[25] N. Hoang, Y. Fujino, P. Warnitchai, Optimal tuned mass damper for seismic applications and practical design formulas, Engineering Structures. 30 (2008) 707–715. https://doi.org/10.1016/j.engstruct.2007.05.007.

[26] J.R. Sladek, R.E. Klingner, Effect of Tuned-Mass Dampers on Seismic Response, Journal of Structural Engineering. 109 (1983) 2004–2009. https://doi.org/10.1061/(ASCE)0733-9445(1983)109:8(2004).

[27] N.D. Anh, N.X. Nguyen, L.T. Hoa, Design of three-element dynamic vibration absorber for damped linear structures, Journal of Sound and Vibration. 332 (2013) 4482–4495. https://doi.org/10.1016/j.jsv.2013.03.032.

[28] T. Asami, O. Nishihara, H[sub 2] Optimization of the Three-Element Type Dynamic Vibration Absorbers, Journal of Vibration and Acoustics. 124 (2002) 583. https://doi.org/10.1115/1.1501286.

[29] Y.L. Cheung, W.O. Wong, H2 optimization of a non-traditional dynamic vibration absorber for vibration control of structures under random force excitation, Journal of Sound and Vibration. 330 (2011) 1039–1044. https://doi.org/10.1016/j.jsv.2010.10.031.

[30] P. Xiang, A. Nishitani, Optimum design and application of non-traditional tuned mass damper toward seismic response control with experimental test verification: Optimum Design and Application of Non-traditional TMD, Earthquake Engineering & Structural Dynamics. 44 (2015) 2199–2220. https://doi.org/10.1002/eqe.2579.

[31] N.A. Alexander, F. Schilder, Exploring the performance of a nonlinear tuned mass damper, Journal of Sound and Vibration. 319 (2009) 445–462. https://doi.org/10.1016/j.jsv.2008.05.018.

[32] P. Lukkunaprasit, A. Wanitkorkul, Inelastic buildings with tuned mass dampers under moderate ground motions from distant earthquakes, Earthquake Engineering & Structural Dynamics. 30 (2001) 537–551.

[33] K.K. Wong, Seismic energy dissipation of inelastic structures with tuned mass dampers, Journal of Engineering Mechanics. 134 (2008) 163–172.

[34] R. Greco, G.C. Marano, A. Fiore, Performance-cost optimization of tuned mass damper under low-moderate seismic actions: Tuned Mass Damper Optimization, The Structural Design of Tall and Special Buildings. 25 (2016) 1103–1122. https://doi.org/10.1002/tal.1300.

[35] T. Igusa, K. Xu, Wide-Band Response of Multiple Subsystems with High Modal Density, in: Y.K. Lin, I. Elishakoff (Eds.), Stochastic Structural Dynamics 1, Springer Berlin Heidelberg, Berlin, Heidelberg, 1991: pp. 131–145. https://doi.org/10.1007/978-3-642-84531-4_7.

[36] A.S. Joshi, R.S. Jangid, Optimum parameters of multiple tuned mass dampers for base-excited damped systems, Journal of Sound and Vibration. 202 (1997) 657–667.

[37] M. Abe, Y. Fujino, Dynamic characterization of multiple tuned mass dampers and some design formulas, Earthquake Engineering & Structural Dynamics. 23 (1994) 813–835. https://doi.org/10.1002/eqe.4290230802.

[38] C. Li, Y. Liu, Optimum multiple tuned mass dampers for structures under the ground acceleration based on the uniform distribution of system parameters, Earthquake Engineering & Structural Dynamics. 32 (2003) 671–690.

[39] K. Xu, T. Igusa, Dynamic characteristics of multiple substructures with closely spaced frequencies, Earthquake Engng. Struct. Dyn. 21 (1992) 1059–1070. https://doi.org/10.1002/eqe.4290211203.

[40] J. Park, D. Reed, Analysis of uniformly and linearly distributed mass dampers under harmonic and earthquake excitation, Engineering Structures. 23 (2001) 802–814. https://doi.org/10.1016/S0141-0296(00)00095-X.

[41] L. Zuo, Effective and Robust Vibration Control Using Series Multiple Tuned-Mass Dampers, Journal of Vibration and Acoustics. 131 (2009) 031003. https://doi.org/10.1115/1.3085879.

[42] L. Zuo, S.A. Nayfeh, Optimization of the Individual Stiffness and Damping Parameters in Multiple-Tuned-Mass-Damper Systems, Journal of Vibration and Acoustics. 127 (2005) 77. https://doi.org/10.1115/1.1855929.

[43] C. Li, Y. Liu, Further characteristics for multiple tuned mass dampers, Journal of Structural Engineering. 128 (2002) 1362–1365. https://doi.org/10.1061/(ASCE)0733-9445(2002)128:10(1362).

[44] T. Bandivadekar, R. Jangid, Optimization of multiple tuned mass dampers for vibration control of system under external excitation, Journal of Vibration and Control. 19 (2013) 1854–1871. https://doi.org/10.1177/1077546312449849.

[45] O.V. Gendelman, Transition of Energy to a Nonlinear Localized Mode in a Highly Asymmetric System of Two Oscillators, in: A.F. Vakakis (Ed.), Normal Modes and Localization in Nonlinear Systems, Springer Netherlands, Dordrecht, 2001: pp. 237–253. https://doi.org/10.1007/978-94-017-2452-4_13.

[46] O. Gendelman, L.I. Manevitch, A.F. Vakakis, R. M'Closkey, Energy Pumping in Nonlinear Mechanical Oscillators: Part I—Dynamics of the Underlying Hamiltonian Systems, Journal of Applied Mechanics. 68 (2001) 34. https://doi.org/10.1115/1.1345524.

[47] A.F. Vakakis, O. Gendelman, Energy Pumping in Nonlinear Mechanical Oscillators: Part II—Resonance Capture, Journal of Applied Mechanics. 68 (2001) 42. https://doi.org/10.1115/1.1345525.

[48] A.F. Vakakis, Inducing Passive Nonlinear Energy Sinks in Vibrating Systems, Journal of Vibration and Acoustics. 123 (2001) 324. https://doi.org/10.1115/1.1368883.

[49] P.N. Panagopoulos, O. Gendelman, A.F. Vakakis, Robustness of nonlinear targeted energy transfer in coupled oscillators to changes of initial conditions, Nonlinear Dynamics. 47 (2007) 377–387. https://doi.org/10.1007/s11071-006-9037-9.

[50] G. Kerschen, Y.S. Lee, A.F. Vakakis, D.M. McFarland, L.A. Bergman, Irreversible Passive Energy Transfer in Coupled Oscillators with Essential Nonlinearity, SIAM Journal on Applied Mathematics. 66 (2005) 648–679. https://doi.org/10.1137/040613706.

[51] N.E. Wierschem, B.F. Spencer Jr, L.A. Bergman, A.F. Vakakis, Numerical study of nonlinear energy sinks for seismic response reduction, in: Proceedings of the 6 Th International Workshop on Advanced Smart Materials and Smart Structures Technology (ANCRiSST 2011), 2011: pp. 25–26. https://www.researchgate.net/profile/Lawrence_Bergman2/publication/266012200_Numerical_Study_of_Nonlinear_Energy_Sinks_for_Seismic_Response_Reduction/links/54bd23790cf218da93919056.pdf (accessed October 8, 2016).

[52] K. Ikago, K. Saito, N. Inoue, Seismic control of single-degree-of-freedom structure using tuned viscous mass damper: THE TUNED VISCOUS MASS DAMPER, Earthquake Engineering & Structural Dynamics. 41 (2012) 453–474. https://doi.org/10.1002/eqe.1138.

[53] L. Marian, A. Giaralis, Optimal design of a novel tuned mass-damper–inerter (TMDI) passive vibration control configuration for stochastically support-excited structural systems, Probabilistic Engineering Mechanics. 38 (2014) 156–164. https://doi.org/10.1016/j.probengmech.2014.03.007.

[54] M.C. Smith, Synthesis of mechanical networks: the inerter, IEEE Transactions on Automatic Control. 47 (2002) 1648–1662. https://doi.org/10.1109/TAC.2002.803532.

[55] M.Z.Q. Chen, Y. Hu, L. Huang, G. Chen, Influence of inerter on natural frequencies of vibration systems, Journal of Sound and Vibration. 333 (2014) 1874–1887. https://doi.org/10.1016/j.jsv.2013.11.025.

[56] S.J. Swift, M.C. Smith, A.R. Glover, C. Papageorgiou, B. Gartner, N.E. Houghton, Design and modelling of a fluid inerter, International Journal of Control. 86 (2013) 2035–2051. https://doi.org/10.1080/00207179.2013.842263.

[57] D. De Domenico, P. Deastra, G. Ricciardi, N.D. Sims, D.J. Wagg, Novel fluid inerter based tuned mass dampers for optimised structural control of base-isolated buildings, Journal of the Franklin Institute. 356 (2019) 7626–7649. https://doi.org/10.1016/j.jfranklin.2018.11.012.

[58] A. Javidialesaadi, N.E. Wierschem, Optimal design of rotational inertial double tuned mass dampers under random excitation, Engineering Structures. 165 (2018) 412–421. https://doi.org/10.1016/j.engstruct.2018.03.033.

[59] A. Giaralis, F. Petrini, Wind-Induced Vibration Mitigation in Tall Buildings Using the Tuned Mass-Damper-Inerter, Journal of Structural Engineering. 143 (2017) 04017127. https://doi.org/10.1061/(ASCE)ST.1943-541X.0001863.

[60] S.F. Masri, J.P. Caffrey, Transient Response of a SDOF System With an Inerter to Nonstationary Stochastic Excitation, Journal of Applied Mechanics. 84 (2017) 041005.

[61] S.F. Masri, J.P. Caffrey, H. Li, Transient Response of MDOF Systems With Inerters to Nonstationary Stochastic Excitation, Journal of Applied Mechanics. 84 (2017) 101003.

[62] A.A. Taflanidis, A. Giaralis, D. Patsialis, Multi-objective optimal design of inerter-based vibration absorbers for earthquake protection of multi-storey building structures, Journal of the Franklin Institute. 356 (2019) 7754–7784. https://doi.org/10.1016/j.jfranklin.2019.02.022.

[63] D. Pietrosanti, M. De Angelis, M. Basili, Optimal design and performance evaluation of systems with Tuned Mass Damper Inerter (TMDI): Optimal Design and Performance of Tuned Mass Damper Inerter Systems, Earthquake Engineering & Structural Dynamics. (2017). https://doi.org/10.1002/eqe.2861.

[64] A. Javidialesaadi, N. Wierschem, Seismic Performance Evaluation of Inerter-Based Tuned Mass Dampers Dampers, in: 3RD Huixian International Forum on Earthquake Engineering for Young Researchers, University of Illinois, Urbana-Champaign, 2017.

[65] J. Dai, Z.-D. Xu, P.-P. Gai, Tuned mass-damper-inerter control of wind-induced vibration of flexible structures based on inerter location, Engineering Structures. 199 (2019) 109585. https://doi.org/10.1016/j.engstruct.2019.109585.

[66] Y. Hu, M.Z.Q. Chen, Z. Shu, L. Huang, Analysis and optimisation for inerter-based isolators via fixed-point theory and algebraic solution, Journal of Sound and Vibration. 346 (2015) 17–36. https://doi.org/10.1016/j.jsv.2015.02.041.

[67] A. Javidialesaadi, N.E. Wierschem, Energy transfer and passive control of single-degree-of-freedom structures using a one-directional rotational inertia viscous damper, Engineering Structures. 196 (2019) 109339. https://doi.org/10.1016/j.engstruct.2019.109339.

[68] R. Mirza Hessabi, O. Mercan, Investigations of the application of gyro-mass dampers with various types of supplemental dampers for vibration control of building structures, Engineering Structures. 126 (2016) 174–186. https://doi.org/10.1016/j.engstruct.2016.07.045.

[69] M. Saitoh, On the performance of gyro-mass devices for displacement mitigation in base isolation systems, Structural Control and Health Monitoring. 19 (2012) 246–259. https://doi.org/10.1002/stc.419.

[70] I. Takewaki, S. Murakami, S. Yoshitomi, M. Tsuji, Fundamental mechanism of earthquake response reduction in building structures with inertial dampers, Structural Control and Health Monitoring. 19 (2012) 590–608. https://doi.org/10.1002/stc.457.

[71] I.F. Lazar, S.A. Neild, D.J. Wagg, Using an inerter-based device for structural vibration suppression: USING AN INERTER-BASED DEVICE FOR STRUCTURAL VIBRATION SUPPRESSION, Earthquake Engineering & Structural Dynamics. 43 (2014) 1129–1147. https://doi.org/10.1002/eqe.2390.

[72] Y. Wen, Z. Chen, X. Hua, Design and Evaluation of Tuned Inerter-Based Dampers for the Seismic Control of MDOF Structures, Journal of Structural Engineering. 143 (2017) 04016207. https://doi.org/10.1061/(ASCE)ST.1943-541X.0001680.

[73] I.F. Lazar, S.A. Neild, D.J. Wagg, Vibration suppression of cables using tuned inerter dampers, Engineering Structures. 122 (2016) 62–71. https://doi.org/10.1016/j.engstruct.2016.04.017.

[74] I.F. Lazar, S.A. Neild, D.J. Wagg, Performance Analysis of Cables with Attached Tuned-Inerter-Dampers, in: J. Caicedo, S. Pakzad (Eds.), Dynamics of Civil Structures, Volume 2, Springer International Publishing, Cham, 2015: pp. 433–441. http://link.springer.com/10.1007/978-3-319-15248-6_44 (accessed June 19, 2016).

[75] L. Lu, Y.-F. Duan, B.F. Spencer, X. Lu, Y. Zhou, Inertial mass damper for mitigating cable vibration, Structural Control and Health Monitoring. 24 (2017) e1986. https://doi.org/10.1002/stc.1986.

[76] F. Qian, Y. Luo, H. Sun, W.C. Tai, L. Zuo, Optimal tuned inerter dampers for performance enhancement of vibration isolation, Engineering Structures. 198 (2019) 109464. https://doi.org/10.1016/j.engstruct.2019.109464.

[77] Z. Huang, X. Hua, Z. Chen, H. Niu, Optimal design of TVMD with linear and nonlinear viscous damping for SDOF systems subjected to harmonic excitation, Struct Control Health Monit. 26 (2019). https://doi.org/10.1002/stc.2413.

[78] S.Y. Zhang, J.Z. Jiang, S. Neild, Optimal configurations for a linear vibration suppression device in a multi-storey building: Optimal Configurations for a Linear Vibration Suppression Device, Structural Control and Health Monitoring. (2016). https://doi.org/10.1002/stc.1887.

[79] S.Y. Zhang, S. Neild, J.Z. Jiang, Optimal design of a pair of vibration suppression devices for a multi-storey building, Struct Control Health Monit. (2019). https://doi.org/10.1002/stc.2498.

[80] N. Makris, G. Kampas, Seismic Protection of Structures with Supplemental Rotational Inertia, Journal of Engineering Mechanics. 142 (2016) 04016089. https://doi.org/10.1061/(ASCE)EM.1943-7889.0001152.

[81] M. Wang, F. Sun, Displacement reduction effect and simplified evaluation method for SDOF systems using a clutching inerter damper, Earthquake Engineering & Structural Dynamics. 47 (2018) 1651–1672. https://doi.org/10.1002/eqe.3034.

[82] L. Li, Q. Liang, Seismic Assessment and Optimal Design for Structures with Clutching Inerter Dampers, J. Eng. Mech. 146 (2020) 04020016. https://doi.org/10.1061/(ASCE)EM.1943-7889.0001732.

[83] C. Málaga-Chuquitaype, C. Menendez-Vicente, R. Thiers-Moggia, Experimental and numerical assessment of the seismic response of steel structures with clutched inerters, Soil Dynamics and Earthquake Engineering. 121 (2019) 200–211. https://doi.org/10.1016/j.soildyn.2019.03.016.

[84] G.B. Warburton, Optimum absorber parameters for various combinations of response and excitation parameters, Earthquake Engineering & Structural Dynamics. 10 (1982) 381–401. https://doi.org/10.1002/eqe.4290100304.

[85] T. Asami, O. Nishihara, Closed-Form Exact Solution to H[sub ∞] Optimization of Dynamic Vibration Absorbers (Application to Different Transfer Functions and Damping Systems), Journal of Vibration and Acoustics. 125 (2003) 398. https://doi.org/10.1115/1.1569514.

[86] G.C. Marano, S. Sgobba, R. Greco, M. Mezzina, Robust optimum design of tuned mass dampers devices in random vibrations mitigation, Journal of Sound and Vibration. 313 (2008) 472–492. https://doi.org/10.1016/j.jsv.2007.12.020.

[87] S.V. Bakre, R.S. Jangid, Optimum parameters of tuned mass damper for damped main system, Structural Control and Health Monitoring. 14 (2007) 448–470. https://doi.org/10.1002/stc.166.

[88] J.S. Issa, Optimal design of a new vibration absorber setup for randomly forced systems, Journal of Vibration and Control. 19 (2013) 2335–2346. https://doi.org/10.1177/1077546312455082.

[89] C.-L. Lee, Y.-T. Chen, L.-L. Chung, Y.-P. Wang, Optimal design theories and applications of tuned mass dampers, Engineering Structures. 28 (2006) 43–53. https://doi.org/10.1016/j.engstruct.2005.06.023.

[90] T. Asami, Optimal Design of Double-Mass Dynamic Vibration Absorbers Arranged in Series or in Parallel, Journal of Vibration and Acoustics. 139 (2017) 011015. https://doi.org/10.1115/1.4034776.

[91] J. Hubert M, N. Nathaniel B, P. Raphel S, Theory of Servomechanisms, McGraw-Hill, New York, 1947.

[92] Maple 2016.1, Maplesoft, a devision of Waterloo Maple Inc, n.d.

[93] Y.L. Cheung, W.O. Wong, H∞ and H2 optimizations of a dynamic vibration absorber for suppressing vibrations in plates, Journal of Sound and Vibration. 320 (2009) 29–42. https://doi.org/10.1016/j.jsv.2008.07.024.

[94] O. Nishihara, T. Asami, Closed-Form Solutions to the Exact Optimizations of Dynamic Vibration Absorbers (Minimizations of the Maximum Amplitude Magnification Factors), Journal of Vibration and Acoustics. 124 (2002) 576. https://doi.org/10.1115/1.1500335.

[95] G. Chen, J. Wu, Optimal placement of multiple tune mass dampers for seismic structures, Journal of Structural Engineering. 127 (2001) 1054–1062.

[96] C. Papageorgiou, N.E. Houghton, M.C. Smith, Experimental Testing and Analysis of Inerter Devices, Journal of Dynamic Systems, Measurement, and Control. 131 (2009) 011001. https://doi.org/10.1115/1.3023120.

[97] T. Asai, Y. Watanabe, Outrigger tuned inertial mass electromagnetic transducers for high-rise buildings subject to long period earthquakes, Engineering Structures. 153 (2017) 404–410. https://doi.org/10.1016/j.engstruct.2017.10.040.

[98] A. Javidialesaadi, N.E. Wierschem, Three-Element Vibration Absorber–Inerter for Passive Control of Single-Degree-of-Freedom Structures, Journal of Vibration and Acoustics. 140 (2018) 11. https://doi.org/10.1115/1.4040045.

[99] A. Javidialesaadi, N. Wierschem, Extending the Fixed-Points Technique for Optimum Design of Rotational Inertial Tuned Mass Dampers, in: J. Caicedo, S. Pakzad (Eds.), Dynamics of Civil Structures, Volume 2, Springer International Publishing, 2017: pp. 83–86.

[100] E. Barredo, A. Blanco, J. Colín, V.M. Penagos, A. Abúndez, L.G. Vela, V. Meza, R.H. Cruz, J. Mayén, Closed-form solutions for the optimal design of inerter-based dynamic vibration absorbers, International Journal of Mechanical Sciences. 144 (2018) 41–53. https://doi.org/10.1016/j.ijmecsci.2018.05.025.

[101] E. Barredo, J.G. Mendoza Larios, J. Mayén, A.A. Flores-Hernández, J. Colín, M. Arias Montiel, Optimal design for high-performance passive dynamic vibration absorbers under random vibration, Engineering Structures. 195 (2019) 469–489. https://doi.org/10.1016/j.engstruct.2019.05.105.

[102] Y. Nakamura, A. Fukukita, K. Tamura, I. Yamazaki, T. Matsuoka, K. Hiramoto, K. Sunakoda, Seismic response control using electromagnetic inertial mass dampers: Seismic response control using EIMD, Earthquake Engineering & Structural Dynamics. 43 (2014) 507–527. https://doi.org/10.1002/eqe.2355.

[103] L. Zuo, S.A. Nayfeh, The Two-Degree-of-Freedom Tuned-Mass Damper for Suppression of Single-Mode Vibration Under Random and Harmonic Excitation, Journal of Vibration and Acoustics. 128 (2006) 56. https://doi.org/10.1115/1.2128639.

[104] J.P. Den Hartog, J. Ormondroyd, The theory of the dynamic vibration absorber, J. Appl. Mech, n.d.

[105] MATLAB R2019b-academic use, Mathwork, Natick, Massachusettes, n.d.

[106] J. Salvi, E. Rizzi, Optimum tuning of Tuned Mass Dampers for frame structures under earthquake excitation: OPTIMUM TUNING OF TMDs FOR FRAME STRUCTURES UNDER EARTHQUAKE EXCITATION, Structural Control and Health Monitoring. 22 (2015) 707–725. https://doi.org/10.1002/stc.1710.

[107] J. Salvi, E. Rizzi, Optimum earthquake-tuned TMDs: Seismic performance and new design concept of balance of split effective modal masses, Soil Dynamics and Earthquake Engineering. 101 (2017) 67–80. https://doi.org/10.1016/j.soildyn.2017.05.029.

[108] M. Mane, Seismic Effectiveness of Tuned Mass Damper (TMD) for Different Ground Motion Parameters, (n.d.) 8.

[109] G.B. Warburton, Optimum absorber parameters for minimizing vibration response, Earthquake Engineering & Structural Dynamics. 9 (1981) 251–262.

[110] M.Z. Ren, A VARIANT DESIGN OF THE DYNAMIC VIBRATION ABSORBER, Journal of Sound and Vibration. 245 (2001) 762–770. https://doi.org/10.1006/jsvi.2001.3564.

[111] T. Asami, O. Nishihara, Analytical and experimental evaluation of an air damped dynamic vibration absorber: design optimizations of the three-element type model, Journal of Vibration and Acoustics. 121 (1999) 334–342.

[112] Y. Hu, M.Z.Q. Chen, Z. Shu, Passive vehicle suspensions employing inerters with multiple performance requirements, Journal of Sound and Vibration. 333 (2014) 2212–2225. https://doi.org/10.1016/j.jsv.2013.12.016.

[113] M.Z.Q. Chen, Y. Hu, C. Li, G. Chen, Application of Semi-Active Inerter in Semi-Active Suspensions Via Force Tracking, Journal of Vibration and Acoustics. 138 (2016) 041014. https://doi.org/10.1115/1.4033357.

[114] T. Asai, K. Ikago, Y. Araki, Outrigger Tuned Viscous Mass Damping System for High-rise Buildings Subject to Earthquake Loadings, in: University of Illinois, Urbana-Champaign, United States, 2015.

[115] I. Gradshteyn, M. Ryzhik, Table of Integrals Series, and Products, Academic Press Inc, 1994.

[116] A. Gonzalez-Buelga, I.F. Lazar, J.Z. Jiang, S.A. Neild, D.J. Inman, Assessing the effect of nonlinearities on the performance of a tuned inerter damper: Effect of Nonlinearities on a Tuned Inerter Damper Performance, Structural Control and Health Monitoring. 24 (2017) e1879. https://doi.org/10.1002/stc.1879.

[117] E. Gourdon, N.A. Alexander, C.A. Taylor, C.H. Lamarque, S. Pernot, Nonlinear energy pumping under transient forcing with strongly nonlinear coupling: Theoretical and experimental results, Journal of Sound and Vibration. 300 (2007) 522–551. https://doi.org/10.1016/j.jsv.2006.06.074.

[118] B. Vaurigaud, A. Ture Savadkoohi, C.-H. Lamarque, Targeted energy transfer with parallel nonlinear energy sinks. Part I: Design theory and numerical results, Nonlinear Dynamics. 66 (2011) 763–780. https://doi.org/10.1007/s11071-011-9949-x.

[119] G. Kerschen, J.J. Kowtko, D.M. Mcfarland, L.A. Bergman, A.F. Vakakis, Theoretical and Experimental Study of Multimodal Targeted Energy Transfer in a System of Coupled Oscillators, Nonlinear Dynamics. 47 (2006) 285–309. https://doi.org/10.1007/s11071-006-9073-5.

[120] Y.-W. Zhang, Y.-N. Lu, W. Zhang, Y.-Y. Teng, H.-X. Yang, T.-Z. Yang, L.-Q. Chen, Nonlinear energy sink with inerter, Mechanical Systems and Signal Processing. (2018). https://doi.org/10.1016/j.ymssp.2018.08.026.

[121] M. Oliva, G. Barone, G. Navarra, Optimal design of Nonlinear Energy Sinks for SDOF structures subjected to white noise base excitations, Engineering Structures. 145 (2017) 135–152. https://doi.org/10.1016/j.engstruct.2017.03.027.

[122] E. Gourc, L.D. Elce, G. Kerschen, G. Michon, G. Aridon, A. Hot, Performance Comparison Between a Nonlinear Energy Sink and a Linear Tuned Vibration Absorber for Broadband Control, in: G. Kerschen (Ed.), Nonlinear Dynamics, Volume 1, Springer International Publishing, 2016: pp. 83–95.

[123] G.B. Warburton, E.O. Ayorinde, Optimum absorber parameters for simple systems, Earthquake Engineering & Structural Dynamics. 8 (1980) 197–217. https://doi.org/10.1002/eqe.4290080302.

[124] C. Li, Optimum multiple tuned mass dampers for structures under the ground acceleration based on DDMF and ADMF, Earthquake Engineering & Structural Dynamics. 31 (2002) 897–919. https://doi.org/10.1002/eqe.128.

[125] C. Li, B. Zhu, Estimating double tuned mass dampers for structures under ground acceleration using a novel optimum criterion, Journal of Sound and Vibration. 298 (2006) 280–297. https://doi.org/10.1016/j.jsv.2006.05.018.

[126] A. Javidialesaadi, N.E. Wierschem, An inerter-enhanced nonlinear energy sink, Mechanical Systems and Signal Processing. 129 (2019) 449–454. https://doi.org/10.1016/j.ymssp.2019.04.047.

[127] H.-N. Li, X.-L. Ni, Optimization of non-uniformly distributed multiple tuned mass damper, Journal of Sound and Vibration. 308 (2007) 80–97. https://doi.org/10.1016/j.jsv.2007.07.014.

[128] S.J. Calhoun, M.H. Tehrani, P.S. Harvey, On the performance of double rolling isolation systems, Journal of Sound and Vibration. 449 (2019) 330–348. https://doi.org/10.1016/j.jsv.2019.02.030.

[129] M.C. Constantinou, M.D. Symans, Experimental study of seismic response of buildings with supplemental fluid dampers, The Structural Design of Tall Buildings. 2 (1993) 93–132. https://doi.org/10.1002/tal.4320020203.

[130] J.T. Scruggs, W.D. Iwan, Control of a Civil Structure Using an Electric Machine with Semiactive Capability, Journal of Structural Engineering. 129 (2003) 951–959. https://doi.org/10.1061/(ASCE)0733-9445(2003)129:7(951).

[131] Y. Liu, L. Xu, L. Zuo, Design, Modeling, Lab, and Field Tests of a Mechanical-Motion-Rectifier-Based Energy Harvester Using a Ball-Screw Mechanism, IEEE/ASME Transactions on Mechatronics. 22 (2017) 1933–1943. https://doi.org/10.1109/TMECH.2017.2700485.

[132] D. De Domenico, G. Ricciardi, An enhanced base isolation system equipped with optimal tuned mass damper inerter (TMDI): An enhanced base-isolation system equipped with optimal tuned mass damper inerter (TMDI), Earthquake Engineering & Structural Dynamics. (2017). https://doi.org/10.1002/eqe.3011.

[133] E. Matta, Lifecycle cost optimization of tuned mass dampers for the seismic improvement of inelastic structures, Earthquake Engineering & Structural Dynamics. 47 (2018) 714–737. https://doi.org/10.1002/eqe.2987.

[134] D. Wang, T.K.T. Tse, Y. Zhou, Q. Li, Structural performance and cost analysis of wind-induced vibration control schemes for a real super-tall building, Structure and Infrastructure Engineering. 11 (2015) 990–1011. https://doi.org/10.1080/15732479.2014.925941.

VITA

Abdollah Javidialesaadi was born in Shiraz, Iran. After obtaining his diploma from National Organization for Development of Exceptional Talents, he started his Bachelor of Science in Civil Engineering at Shiraz University. After completing his BSc, in the same year he admitted to Iran University of Science and Technology for his Master of Science program in Civil Engineering- Structures and finished his study in 2011. After completing his master thesis titled “Nonlinear large deformation analysis of steel structures with semi-rigid connections”, Mr. Javidialesaadi started working as structural engineer for 4 years in industry.

In 2014, Mr. Javidialessadi moved the United States to pursue his PhD in Civil Engineering-Structures at The University of Tennessee, Knoxville.

His research covers a wide range of topics related to structural dynamics, structural control, passive protection of structures, and optimization of dynamic systems Specifically, Specifically, his research interests is Inerter-based passive control devices and its application in structural control and earthquake engineering. To date, Mr. Javidialessadi has authored 4 journal articles and 7 conference papers. In addition, Mr. Javidialessadi is reviewing papers for several academic journals as a volunteer service.

As a doctoral student, Mr. Javidialesaadi received top-off chancellor fellowship, Graduate Student Senate Travel Award, and Extraordinary Professional Promise award. Mr. Javidialesaadi was teaching assistant and teaching associate for five years in Civil and Environmental Engineering Department.